1

"Investigating Hydrogeological-Hydrogeochemical Processes during Bank Filtration and Artificial Ground Water Recharge Using a Multi Tracer Approach"

"hydrogeo" group, Freie Universität Berlin

Responsible project leader: Prof. Dr. Asaf Pekdeger

Contents:

List of Tables

List of Figures

1 INVESTIGATING HYDROGEOLOGICAL-HYDROGEOCHEMICAL PROCESSES DURING BANK FILTRATION AND ARTIFICIAL GROUND WATER RECHARGE USING A MULTI TRACER APPROACH

1.1 Objectives

The main objective of this subproject was the detailed hydrogeological analysis of the bank filtration system at the target transects at Lake Tegel, Lake Wannsee and the artificial recharge pond 3 in Tegel (GWA) as well as at the semi-technical facilities in Marienfelde. The investigations aim for the general description of the hydrogeological, hydraulic, hydrogeochemical and hydrochemical conditions at the surface water/sediment/groundwater interface as well as within the aquifer at all sites studied on the basis of knowledge gained during previous investigations. Altogether, this will help to improve the knowledge on chemical processes accompanying infiltration including the retention of inorganic and organic compounds in both the saturated and the unsaturated zone close to the surface water source.

A major focus of the study is on the evaluation of spatial and temporal changes in water chemistry and quality depending on water flow paths and velocities which are extremely transient due to continuously changing pumping regimes of the production wells at all sites. The use of a combination of different tracers helped to derive travel times from the surface water to the productions wells, validate flow models and enable the calculation of the fraction of treated sewage in the bank-filtrate. Correlation between tracers and chemical parameters allows the subsequent estimation the retention and degradation of the (sewage bound) chemical compounds in the sediments.

Besides others, the main objective of the project phase was to get an overview on travel times, mixing proportions and the hydrochemical situation at the field-sites studied.

The key questions dealt with were:

- What are the travel times from the surface water to observation and production wells?
- What is the proportion of bank-filtrate (and likewise deeper and landside groundwater) in the production wells?
- What is the proportion of treated wastewater in the surface water and production wells?

- What are the hydrochemical conditions at the sites, in particular with regard to redox conditions?

This is important because:

- Only with the knowledge of the time-scales of the processes studied, a definition of rates is possible.
- It is important to differentiate between dilution and real removal of potential contaminants during bank filtration.
- In order to understand the behaviour of specific substances studied by all working groups, the hydrochemistry, in particular the redox-state of the systems has to be known.

1.2 Methods

1.2.1 Drilling of observation wells and recovery of sediment cores

The installation of additional groundwater observation wells was done in co-operation with the Zalf e.V. Müncheberg (Centre for Agricultural Landscape and Land Use Management) using a 1.5 ton drill with a hollow helical auger of the company NORDMEYER (figure 1), into which the wells were lowered after the drill had reached the desired depth. The observation wells are made of high density polyethylen (HDPE) pipes with a diameter of two inches (2”), topped by a 2“ Cap („Seba-Kappe“). The HDPE filter screens at the bottom have a length of two metres and a slit width of 0.3 mm and are usually followed by a 1 metre long unscreened “swamp” end and a 2“ HDPE cone end. Using HDPE enables undistorted sampling of inorganic and organic water constituents.

Sediment cores were generally taken with vibrocoring rods containing a plastic liner, which were driven into the ground with the same NORDMEYER machine that was used for the well construction. The cores were stored in a deep freezer for subsequent analysis.

Figure 1: Snap shot of NORDMEYER drill (left) and recovered plastic liner containing aquifer sediment (right).

1.2.2 Sampling

From November 2001 to August 2005, groundwater sampling campaigns were conducted by BWB with initial support of the Free University of Berlin. Measurements for redox potential (E_h), pH, O_2, temperature (T) and electric conductivity were carried out in the field in a flow-through cell. Filtration with 0.45 µm membrane filters was done immediately after sample retrieval for analyses of cations and anions. Samples for cation analysis were preserved with concentrated nitric acid (HNO_3) to avoid the precipitation of Fe- and Mn-(hydr)oxides. Alkalinity samples were collected in glass bottles that were carefully filled without any air entrapment. Samples were stored at 4° C and full water analysis was generally performed one day after sampling.

1.2.3 Sediment analysis

Grain-size distribution, hydraulic conductivities

Sediment samples were sieved wet according to DIN 4022 using sieves of a mesh size of 8, 4, 2, 1, 0.500, 0.250, 0.125 and 0.063 mm. Prior to sieving, they were batched over night with sodium-hydrogen-phosphate as a dispersion agent.

Hydraulic conductivities (k_f-values) where calculated with the empirical formulas by HAZEN (1893) and BEYER (1964) using the kvs software (BUß, 1994).

After Hazen, the hydraulic conductivity, k_f, is:

$k_f = C^*(d_{10})^2$

with: C = proportional factor = (0,7+0,03*t)/86,4=0,0116 at 10 °C (~groundwater temperature)

t = temperature [°C]

d_{10} = grain size of a sediment at the intersection with the 10% line of the sum curve [mm]

The formula is only valid when d_{60}/d_{10} is smaller than 5 (d_{60} is the grain size of a sediment at the intersection with the 60% line of the sum curve [mm]). BEYER (1964) modified the HAZEN formula by introducing different proportional factors for different d_{60}/d_{10} values. These formulas are only valid for sands with $0,06 < d_{10} < 0,6$.

Table 1: Proportional factors used for k_f estimation after BEYER.

d_{60}/d_{10}	C (range)	C (average)
1.0 ... 1.9	$(120 ... 105) \cdot 10^{-4}$	$110 \cdot 10^{-4}$
2.0 ... 2.9	$(105 ... 95) \cdot 10^{-4}$	$100 \cdot 10^{-4}$
3.0 ... 4.9	$(95 ... 85) \cdot 10^{-4}$	$90 \cdot 10^{-4}$
5.0 ... 9.9	$(85 ... 75) \cdot 10^{-4}$	$80 \cdot 10^{-4}$
10.0 ... 19.9	$(75 ... 65) \cdot 10^{-4}$	$70 \cdot 10^{-4}$
> 20.0	$< 65 \cdot 10^{-4}$	$60 \cdot 10^{-4}$

Iron- and manganese oxides and hydroxides

Fe(III)- and Mn(IV)-oxyhydroxides in the sediment were measured using ICP-AES (Jobin Yvon) after selective extraction with dithionite-citrate-hydrogencarbonate as a reducing agent (MEHRA & JACKSON, 1960). Both amorphous and crystalline Fe(III) and Mn(IV) minerals are dissolved by dithionite-citrate-hydrogen-carbonate, which is a strong reducing agent.

Two grams of freeze-dried sample were placed in a 100 ml centrifugal glass with 40 ml of 0.3 molar sodium-citrate-solution, 5 ml of 1 molar sodium-hydrogen-carbonate solution ($NaHCO_3$) for pH buffering and 1 g of solid dithionite ($Na_2S_2O_4$) as a reducing agent. The solution was pre-heated at 80°C in a water bath to prevent oxidation prior to adding the solids. The solution was then stirred with a glass rod, centrifuged and decanted into a 100 ml graduated flask. This procedure was repeated once, thereby preheating the required additional solution in a beaker in the water bath and also adding it to the sediment in the water bath. The sediment was flushed afterwards with 10 ml 0.1 molar $MgSO_4$ solution. Before measuring the solution by AAS, it was acidified with 5 ml of 65 % HNO_3 (required because of strong citrate buffering). The remaining insoluble solid residue was flushed into the disintegration apparatus with nitric acid to obtain the total iron content of the sediment by summing both fractions. It was placed into the cabinet drier at 100 °C over night and replenished to 50 ml in a graduated flask.

Total cation contents

For total acid soluble solid phase contents of the cations Na, K, Ca, Mg, Fe, Mn and Al sediments were extracted by HNO_3 pressure elution (HEINRICHS,1989).

Two gram of dried sediment were dissolved with 10 ml of nitric acid (HNO_3) and stored in a disintegration bomb over night. After leaching several times with distilled water, the sample was replenished to 50 ml in a graduated flask. The cations were then analysed by AAS. Those samples previously analysed for Mn(IV) and Fe(II) underwent HNO_3 pressure elution after dithionite-citrate-hydrogencarbonate reduction in order to get both Fe- and Mn-Oxides as well as the remaining fractions (adding up to total contents) from one sample.

Cation exchange capacity (CEC)

Cations are bound to ion exchanger in the soil and sediment. They can only go into solution via exchange with other cations present in the water. An ion exchanger is a substance with a positively or negatively charged surface. The charge is neutralised by ions with the opposite charge. The adsorbed ions form an ion coating. These ions are free to move and exchangeable. During exchange, ions on the surface of the exchanger are exchanged with ions in solution. This is usually reversible and happens fast and stoichiometric. The process can be described by the laws of mass action. Ion exchanger can have a positive or negative surface charge. Clay minerals and humic substances are mainly negatively charged and are cation exchanger. The negative charge of clay minerals is caused by the partial isomorphic substitution of Si^{4+} by Al^{3+} in the crystal lattice. This is only partly balanced by the inclusion of positive ions in the crystal lattice. The charge of humic substances is depending on the pH. At a pH common in soils and sediments, they are negatively charged (LEWANDOWSKI et al., 1997 and therein). The CEC depends mainly on the amount and type of clay minerals, the amount and type of the organic material. The amount of silt and oxides has a minor influence on the CEC. The potential CEC_{pot} is measured at a constant pH of 8.1 (for example after MEHLICH), while the effective CEC_{eff} is the CEC at the actual soil pH. CEC_{eff} and CEC_{pot} are equal at a pH above 7-7.5. According to FÖRSTER & WITTMANN (1979), the CEC is 3-120 mmol(eq)/100g for different clay minerals, 10-24 mmol(eq)/100g for freshly precipitated Fe-Hydroxides, 11-34 mmol(eq)/100g for amorphous silica and 170-590 mmol(eq)/100g for humic acids in soils. Values for calcite are not given.

Cation exchange capacity was measured with the percolation method as CEC_{eff}. The exchange solution was produced by adding 25 g of $BaCl_2$*2 H_2O into a flask and filling it up to 1 l with distilled water. The re-exchange solution was made with 50 g $CaCl_2$ dissolved in 1 l of distilled water. Ten gram of quartz sand (p.a. annealed) were filled into a small PE column as a filter. Ten grams of mildly pounded sample sediment (only the fraction with a grain size <

2mm) were placed on top of the quartz sand. For replacement of the exchangeable cations by Ba^{2+} 75 ml of the exchange solution were added to the column in 5 portions of 15 ml and collected in a 250 ml flask. Afterwards, the column was flushed with distilled water and the flask was filled up to 250 ml. The displaced cations were measured by AAS. The pH has to be determined, because H^+ is accounted for in the budget calculations. For the re-exchange of the Ba^{2+} by Ca^{2+}, 100 ml of the re-exchange solution were added to the column in 4 portions of 25 ml each. The solution was collected in a 100 ml flask and filled to the marker with distilled water. The Ba^{2+} was analysed by ICP. The CEC_{eff} is the amount of Ba^{2+} re-exchanged in mmol(eq)/100g of sediment. Theoretically, the sum of the cations exchanged in the first run should be equal to the CEC. However, it is usually smaller because not all of the cations are measured (for example trace metals or NH_4^+ are missing). In sediments containing calcite the sum of the cations is often larger than the CEC, because some of the calcite is dissolved (KRETSCHMAR, 1991)

Pyrite and mono-sulphide content

Sulphide was extracted as acid volatile sulphide (AVS) using HCl and as pyrite (or CRS) using a Cr(II)Cl solution as extraction agent. AVS-sulphide includes mineral phases such as Fe(II)-monosulphide (FeS), mackinawite ($Fe_{1-x}S$) and greigite (Fe_3S_4) (CORNWELL and MORSE, 1987; HSIEH and YANG, 1989; GAGNON et al., 1995). The extraction with Cr(II)Cl includes pyritebound S as well as AVS phases and elemental S (CANFIELD et al., 1986). In contrast to conventional methods the H_2S degassing in the acid environment was not blown out but transported into the Zn-acetate trap by passive diffusion over 48 h (HSIEH and YANG, 1989). After the precipitation of ZnS in the alkaline solution (pH 13), the amount of sulphide was measured iodometrically (HSIEH and YANG, 1989; GAGNON et al., 1995).

Organic and inorganic carbon content, total sulphur content

Organic and inorganic C as well as total S were determined with a C-N-S Analyser (CS-225, Leco Instruments GmbH). The sediment sample was crushed with an agate mortar and metallic aggregates (zinc, pure iron and wolfram chips) were added in a clay pan and placed in a burning chamber in an oxygen stream. The carbon or sulphur content was analysed via Infra-red (IR) detection.

To differentiate between organic and inorganic carbon, pre-treatment of the sample was necessary. The samples are weighted with the clay pans. 1 N HCl was added in order to destroy the carbonate fraction. After ablation of the excess acid, the remaining carbon can be analysed as before but with a chloride trap for the flue gas cleaning. It is equivalent to the organic carbon fraction of the sample. The inorganic carbon fractions, i.e. the carbonates are

calculated by subtraction of the two values. The results are always averages of 3 measurements.

1.2.4 Water analysis

Standard chemistry

Both ions after sediment extraction as well as water samples from column or batch experiments and the suction cubs at the artificial recharge pond were analysed at the laboratories of the Free University of Berlin, using equipment listed in table 2.

Table 2: Overview on analytical instruments at the hydrogeology laboratory of the Free University of Berlin.

Parameter	Method	Type	Detection limit	Norm
B	ICP	Leemans	0.05 mg/l	
Ba^{2+}	ICP	Leemans	0.5 mg/l	
Br^-	IC	DX 100	0.5 mg/l	DEV (1986)
NO_3^-	IC	DX-100	0.5 mg/l	
Ca^{2+}	AAS/Flame	Perkin Elmer 5000	0.1 mg/l	DIN 38046-E3-1
Cl^-	IC	DX 100	1.0 mg/l	
Cu^{2+}	AAS/ Flame	Perkin Elmer 5000	0.05 mg/l	DIN 38046-E7/E21
Fe^{2+}	AAS/ Flame	Perkin Elmer 5000	0.1 mg/l	
HCO_3^-	Titration	DIN (1979)	1.0 mg/l	DIN 38409
I^-	Titration			DEV (1986)
K^+	Flame photometric	Eppendorf Elex 6361r	0.1 mg/l	DIN 38046-E3-14
Li^+	AAS/flame	Perkin Elmer 5000	0.05 mg/l	
Mg^{2+}	AAS/ flame	Perkin Elmer 5000	0.02 mg/l	DIN 38046-E3-1
Mn^{2+}	AAS/ flame	Perkin Elmer 5000	0.02 mg/l	
Na^+	Flame photometric	Eppendorf Elex 6361r	1.0 mg/l	DIN 38046-E3-14
NH_4^+	Quick test Colorimetric / Photometric	Dr. Lange/ MN / Merck	0.04 mg/l	
NO_2^-	Quick test Colorimetric / Photometric	Dr. Lange / MN / Merck	0.005 mg/l	
SiO_2	Photometric	Technicon Autoanalyser		DIN 38045-D21
SO_4^{2-}	IC	DX-100	1.0 mg/l	
Sr^{2+}	AAS/flame	Perkin Elmer 5000	0.02 mg/l	DIN 38046-E3-22
Zn^{2+}	AAS	Perkin Elmer 5000	0.05 mg/l	
DOC	Photometric	Technicon Autoanalyser	0.5 mg/l	

Stable isotopes

The stable isotope measurements of deuterium (D) and 18-oxygen (^{18}O) were carried out at the Alfred Wegener Institute, Research Unit Potsdam with a H_2 equilibration method for D/H ratios and a CO_2 equilibration method for $^{18}O/^{16}O$ ratios with a Finnigan MAT Delta-S mass spectrometer. After equilibration ten measurements were carried out for each sample. δD and $\delta^{18}O$ values were calculated using the commercial software ISODAT and reported in the standard δ notation representing per mil deviation relative to V-SMOW. The internal 1σ error is generally better than 0.8 ‰ for δD and better than 0.1 ‰ for $\delta^{18}O$. Details on the instrumentation, calibration and the measurement routine are described in (Meyer et al., 2000).

1.2.5 Tracer evaluation methods

Wastewater indicators and environmental tracers can be used to estimate either travel times from lake to production well or the proportion of bank filtrate in the production wells. For both purposes, conservative tracers (non-reactive and non-retarding) were used.

For studying the water movement, an appropriate tracer should show clear seasonality in the surface water or at least clear peaks at certain times of the year. Evaluating the peak shift from the surface water to a groundwater observation well yields travel times to the respective well. Oxygen and hydrogen isotopes show a typical seasonality in the surface water of Berlin with more negative values in winter. Tracers originating from wastewater show seasonality mainly because of dilution effects: The release of wastewater from the treatment plants is relatively constant throughout the year, while the natural discharge is much higher in winter. Therefore, the concentration of wastewater indicators is generally higher during summer. Locally, other effects may play a role too.

The fraction of treated wastewater at a sampling point in the surface water or in a production well is estimated from tracers in the well and in the end-members (for example the surface water and the background groundwater inland of a production well). The differences in concentration of the two end-members should ideally be large and concentrations should be stable with time. If the abstracted water is a mixture of surface water and background groundwater only, the percentage of bank filtrate in the well (*X*, given in %) is estimated by the following equation:

$$X[\%] = \frac{C_w - C_{GW}}{C_{SW} - C_{GW}} * 100$$

With C as the concentration of a suitable tracer in the groundwater (C_{GW}), well (C_w) or surface water (C_{SW}). If several filter screens exist in different aquifers the calculation is more difficult (for example at Wannsee).

Table 3 gives an overview on tracers used within this study, their origin, purpose of use and the difficulties associated with the use their use.

Table 3:Overview on most important major tracer applicable in Berlin.

Tracer:	Origin:	Useful for the interpretation of:	Difficulties:
δD, $\delta^{18}O$	surface water with seasonal variations (precipitation)	water movement, proportion of bank filtrate in raw water	none, conservative tracer
Temperature	surface water with seasonal variations	water movement	retarding
Cl^-, B	surface water with seasonal variations (WWTP)	water movement, proportion of bank filtrate in raw water	only if influence of saline groundwater can be excluded
Cl^-, Na^+, B	saline deeper groundwater	proportion of deeper saline groundwater	may vary strongly locally
SO_4^{2-}	dissolution of gypsum derived from building rubble in the shallow aquifer	proportion of shallow "native" groundwater	may vary strongly locally
Gd-DTPA	surface water with seasonal variations (WWTP)	water movement, proportion of bank filtrate in raw water	degradable
EDTA	surface water, effluent	water movement, proportion of bank filtrate in raw water	sometimes the background groundwater has also got very high concentrations
K	surface water with seasonal variations (WWTP)	water movement	Only if sorption on sediment can be excluded, Generally not behaving conservative
T/He	Surface water, through atmospheric input	groundwater "age"	minimum age required is 6 months

The boxplots were done with available data from May 2002 to May 2005. Because some of the observation wells had only been sampled since January 2003 or had fallen dry in summer, the number of the samples varies and for some wells, only very few samples were analysed. When the concentrations analysed were below the detection limit, 0 was used in figures and for the boxplots.

1.2.6 Age dating

Samples were taken from selected wells for T/^{3}He analysis. The analysis and data evaluation of the groundwater samples was carried out at the noble gas laboratory at the University of Bremen. The method uses the ratio of the concentration of radioactive tritium (^{3}H or T) and its decay product ^{3}He in the groundwater to determine the groundwater age. The "age" τ is the time passed since the water had its last contact with the atmosphere, in the present case, since the water infiltrated into the aquifer. It is defined as (TOLSTIKHIN & KAMENSKIY, 1969):

$$\tau = \frac{t_{1/2}}{\ln 2} \ln(1 + \frac{^3He_{tri}}{^3H})$$

with: τ = age [a]

$t_{1/2}$ = half-life of ^3H (12.43 years)

$^3He_{tri}$ = fraction of total ^3He produced by ^3H decay [TU]

^3H = tritium concentration [TU]

Tritium is expressed in tritium units [TU]. One TU corresponds to a $T/^3H$ ratio of 10^{-18}. The natural ^3H concentration in the atmosphere is low (about 10 TU). In the 1950s and early 1960s the ^3H content in the atmosphere increased several orders of magnitude due to nuclear bomb testing. The concentrations have since been decreasing (figure2). The method has been used in many groundwater studies but only in STUTE et al. (1997), BEYERLE et al. (1999) and SÜLTENFUß & MASSMANN (2004) did the groundwater originate from bank-filtration.

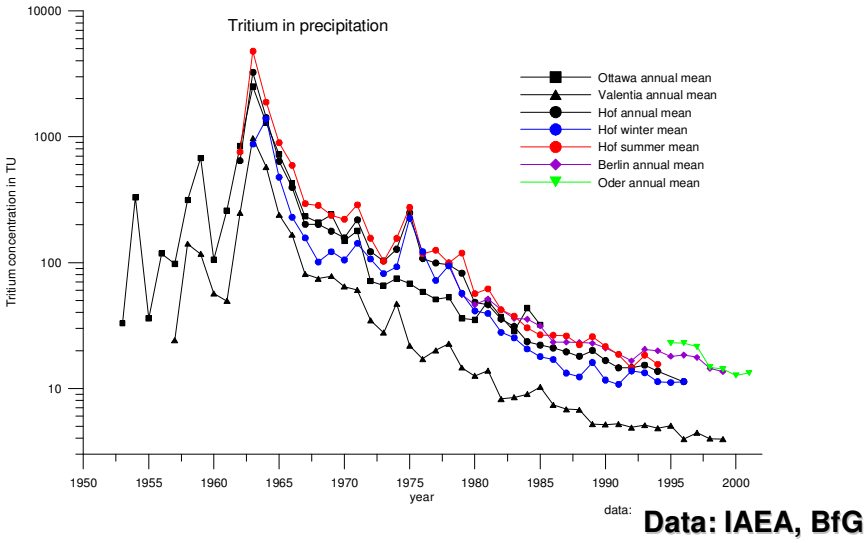

Figure 2: Tritium in the precipitation of several sites in the world (data source: IAEA, BfG).

1.2.7 Stable isotopes of dissolved sulfate

Samples for $\delta^{18}O$ and $\delta^{34}S$ of sulfate were collected in July 2004 and filtered with 0.45 µm membrane filters to avoid impurities. 2–3 ml of HCl were added and SO_4^{2-} was precipitated as $BaSO_4$ in the laboratory of the Free University of Berlin using the reagent $BaCl_2$. The $BaSO_4$ was caught on a filter and freed of the chloride content by rinsing with warm water. The filtered $BaSO_4$ was split in samples for $\delta^{18}O$ and $\delta^{34}S$ analysis and subsequently dried at 30 and 80 °C, respectively. All isotope results are reported as $\delta^{34}S$ and $\delta^{18}O$ values in per mil (‰), where:

$$\delta(‰) = [(R_{sample}/R_{standard}) - 1] * 1000$$

for $\delta^{34}S$ or $\delta^{18}O$, R = $^{34}S/^{32}S$ or $^{18}O/^{16}O$, respectively (Hoefs, 1997). $\delta^{34}S$ analyses of $BaSO_4$ and sulfides were performed after conversion to SO_2 in the presence of V_2O_5 and SiO_2 (YA-

NAGISAWA & SAKAI, 1983) and subsequent determination of the sulfur isotope composition using a Finnigan MAT Delta E mass spectrometer at the isotope laboratory of the Institute of Mineralogy in Freiberg. For routine measurements an internal standard (SO_2), which is calibrated against the international IAEA-standard NBS 127, was used. Isotope values are reported relative to the international standard CDT. $\delta^{18}O$ values of $BaSO_4$ were determined on CO_2 derived through reaction of $BaSO_4$ with graphite at a high temperature (RAFTER, 1967). Simultaneously generated CO was converted to CO_2 on a Ni-catalyst at 350 ^{O}C. After the complete conversion of CO to CO_2 all CO_2 gas was collected and analysed on a Finnigan MAT Delta plus mass spectrometer. As internal standard a synthetic $BaSO_4$ with a $\delta^{18}O$ value of 12.95‰ calibrated against the international IAEA standard NBS 19 was used. The reproducibility of the $\delta^{18}O$ analysis of $BaSO_4$ is usually better than ±0.2‰. $\delta^{34}S$ isotope values are reported relative to the international standard SMOW.

1.3 General Field Site Description

Transsects (TS: groups of observation wells between the surface water and production wells) were installed at three different field sites (Figure 3) and sampled at monthly interval:

- Transsect Lake Tegel , BF-site (TS Tegeler See),
- Transsect Tegel, AR pond (GWA Tegel),
- Transsect Wannsee, BF site (TS Wannsee).

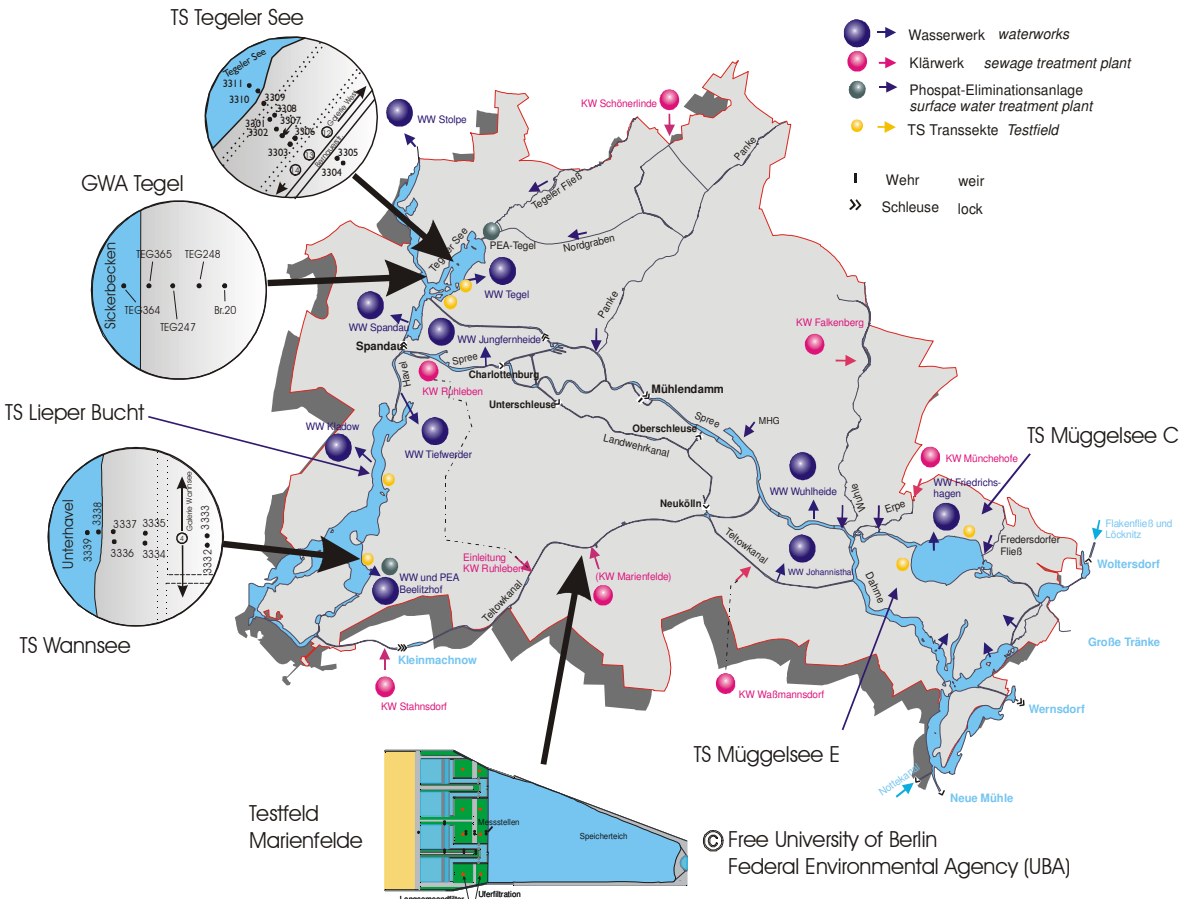

Figure 3: Location of the 3 transsects and the UBA testfield Marienfelde investigated during the NASRI project.

Transsect Lake Tegel , BF-site (TS Tegeler See) is situated on the eastern bank of Lake Tegel (Figure 3) and consists of 15 observation wells screened in different depths (Figure 4).

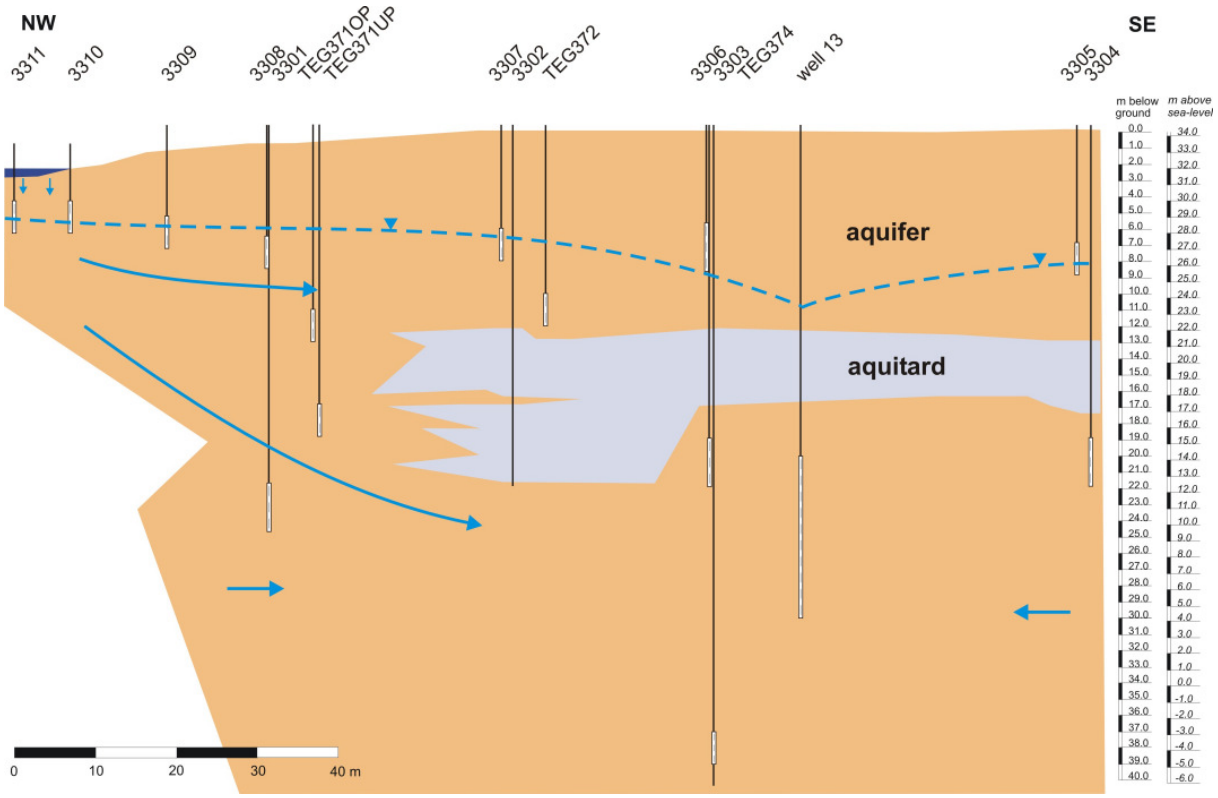

Figure 4: Schematic cross section of NASRI field site TS Lake Tegel, BF-site (arrows indicate flow paths derived from tracer and hydrochemical investigations).

Transsect Tegel , AR-pond (GWA Tegel) is situated east of infiltration pond #3, off the eastern bank of Lake Tegel (Figure 3) and consists of 14 observation wells screened in different depths (Figure 5).

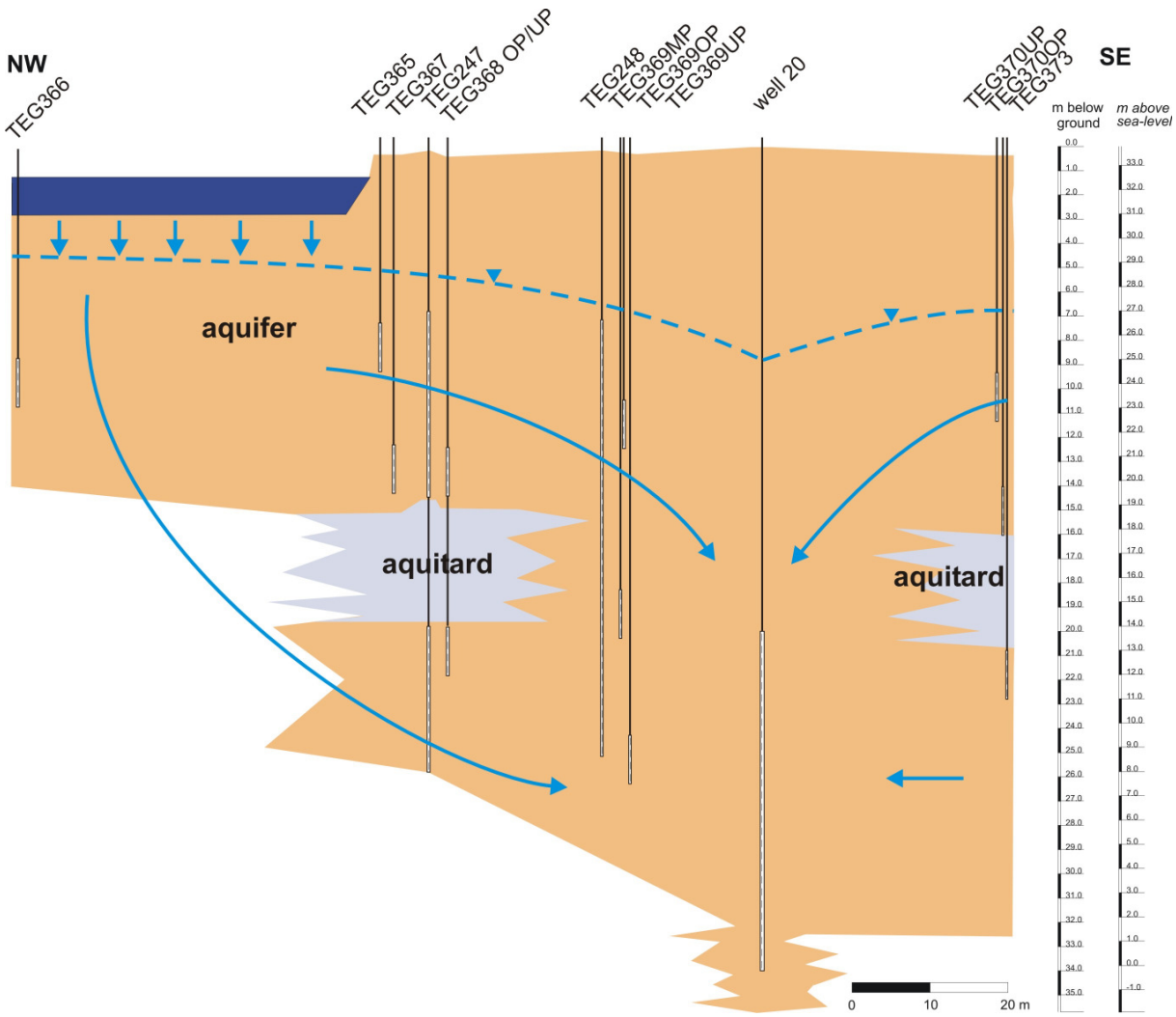

Figure 5: Schematic cross section of NASRI field site GWA Tegel, (arrows indicate flow paths derived from tracer and hydrochemical investigations).

At the Lake Wannsee field site situated on the eastern bank of Lake Wannsee (Figure 3), 2 transsects were constructed, after first investigations had shown that the production well at transsect 1 was not receiving water in the uppermost aquifer, mainly influenced by bank filtrate. The two transsects Wannsee-1 and Wannsee-2 consist of 11 and 9 observation wells, respectively, screened in different depths of the aquifer.

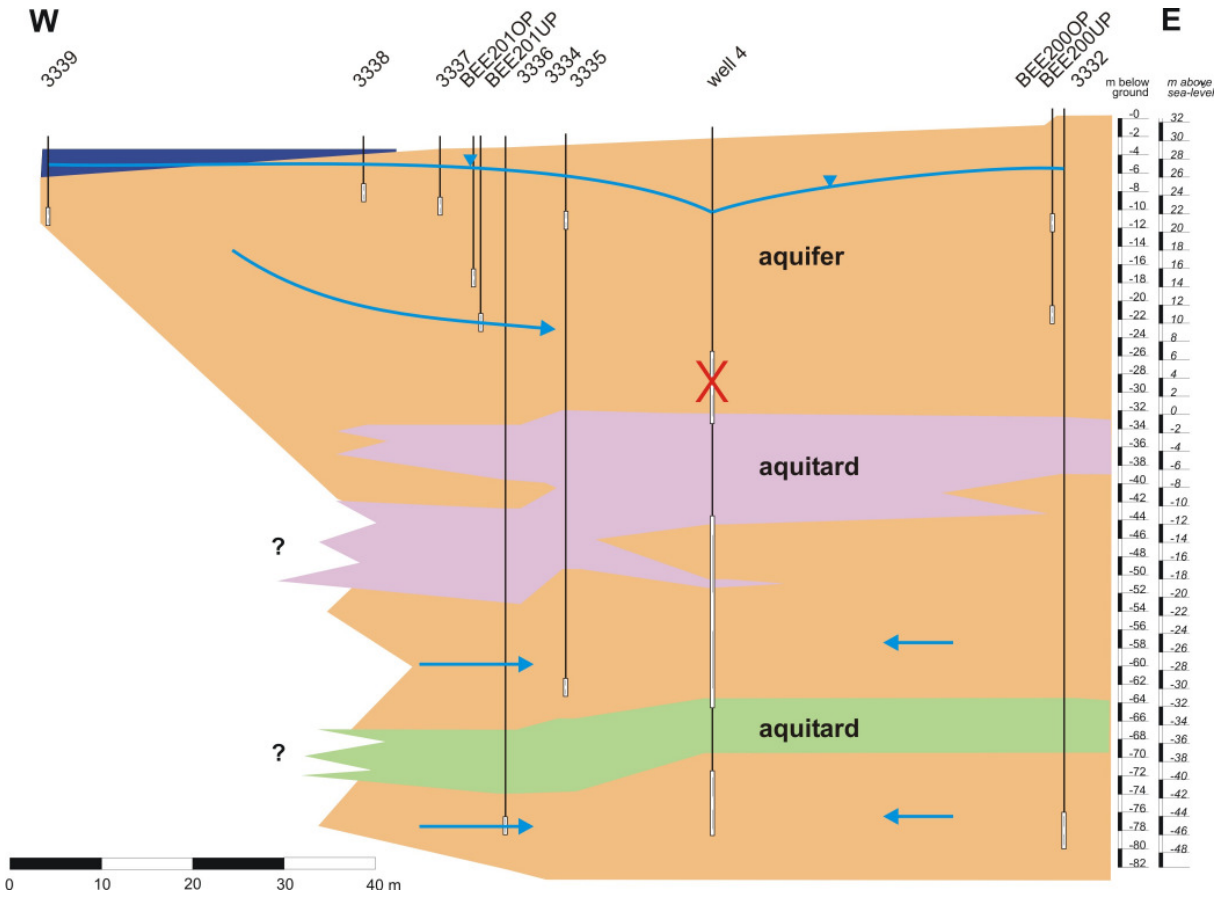

Figure 6: Schematic cross section of NASRI field site TS Wannsee 1, (arrows indicate flow paths derived from tracer and hydrochemical investigations).

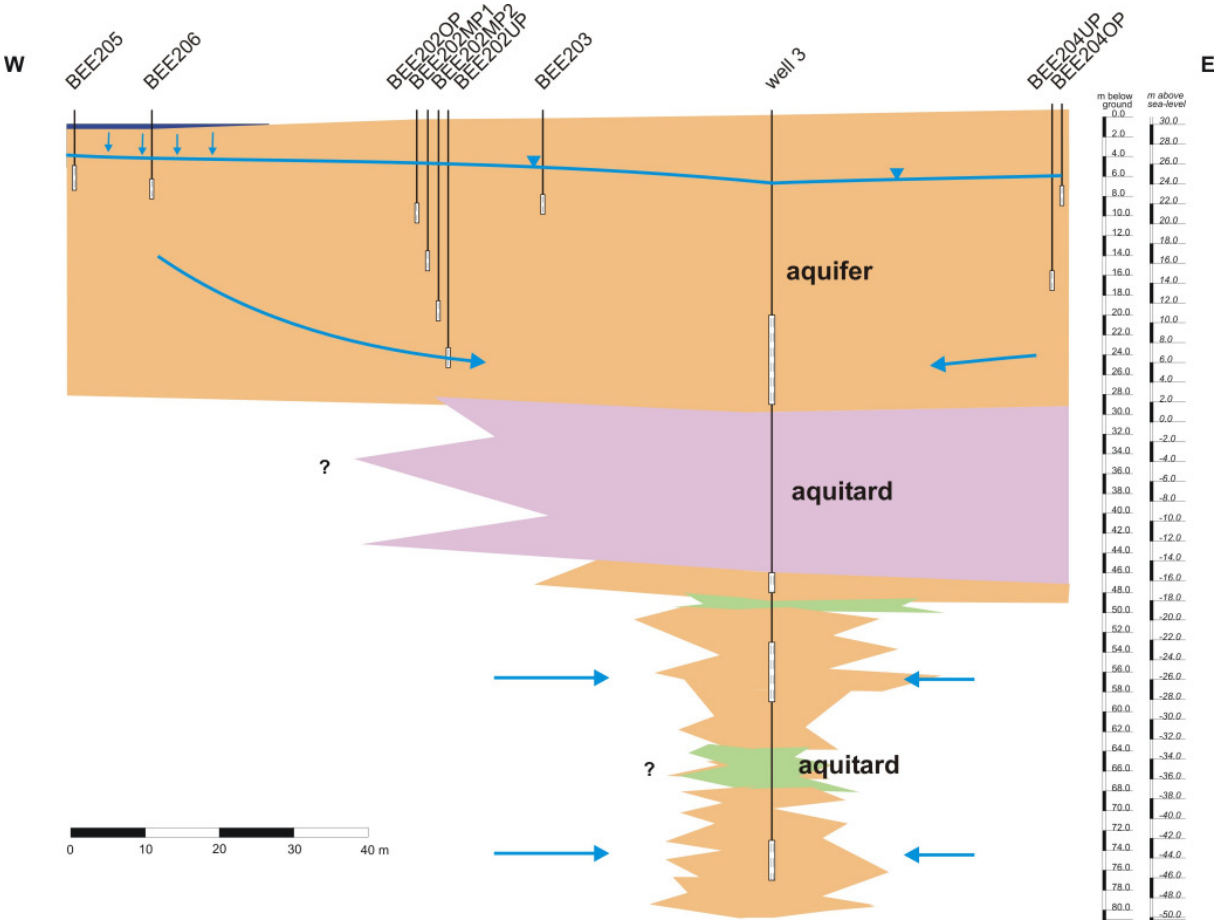

Figure 7: Schematic cross section of NASRI field site TS Wannsee 2, (arrows indicate flow paths derived from tracer and hydrochemical investigations).

1.4 Hydrogeological Results Lake Tegel Bank Filtration Site

1.4.1 Surface Water Investigations

Surface water investigations in the western part of the city were done within a student project (Doreen Richter, in cooperation with DFG project A. Knappe) in 2001 and 2002. Previous detailed surface water investigations at Lake Tegel had been performed by HEIM et al. (2002) and FRITZ (2002). The necessity to take the surface water into consideration when investigating the bank filtration system arises from the fact that it is the source of the bank filtrate and therefore, hydrochemical variations have a large impact on the quality of the bank filtrate itself. Although the surface water was sampled within NASRI in front of the respective transects on a monthly basis, results only give very selective information for one particular point whereas results of the additional surface water investigations helped to understand the proc-

esses influencing the surface water quality and give an additional idea on its temporal and spatial variations.

The surface water contains a considerable amount of treated wastewater, since the natural base flow is low and 6 wastewater treatment plants (WWTP) are in operation. Indications of wastewater influence in the surface water are high concentrations of wastewater indicators such as Cl^-, Na^+, SO_4^{2-}, B, DOC or Gd-DTPA, high temperatures (in winter) and more negative isotopic signatures, because of the groundwater share (more negative isotopic signature) in the drinking water (KNAPPE et al., 2002, HEIM et al., 2002, MASSMANN et al., 2004)

Figure 3 shows maps of Cl^-, B and Gd concentrations and $\delta^{18}O$ values and in the surface water in July 2001 and December 2001 as two examples for the tracer distribution in summer and winter. In July, the base flow was the lowest in 2001/2002. Therefore, the spatial differences and absolute concentrations of wastewater indicators are larger in July 2001 as compared to winter months. The concentrations are highest (darkest colours) at the northern end of Lake Tegel, where the Nordgraben meets Lake Tegel and in the Teltowkanal, hence the proportions of WW are highest at these locations. It becomes clear that the transect Lake Wannsee is located in an transition area between Teltowkanal water flowing northwards into Lake Wannsee and water of the Lower Havel, resembling the Spree water with lower proportions of treated wastewater (compare chapter Wannsee). Figure 4 illustrates the approximate proportions of treated wastewater calculated as percentage of WWTP discharge of the total discharge at the respective gauging station (evaporation and abstraction disregarded). More detailed calculations for previous years were done by SCHUHMACHER & SKRIPALLE (1999).

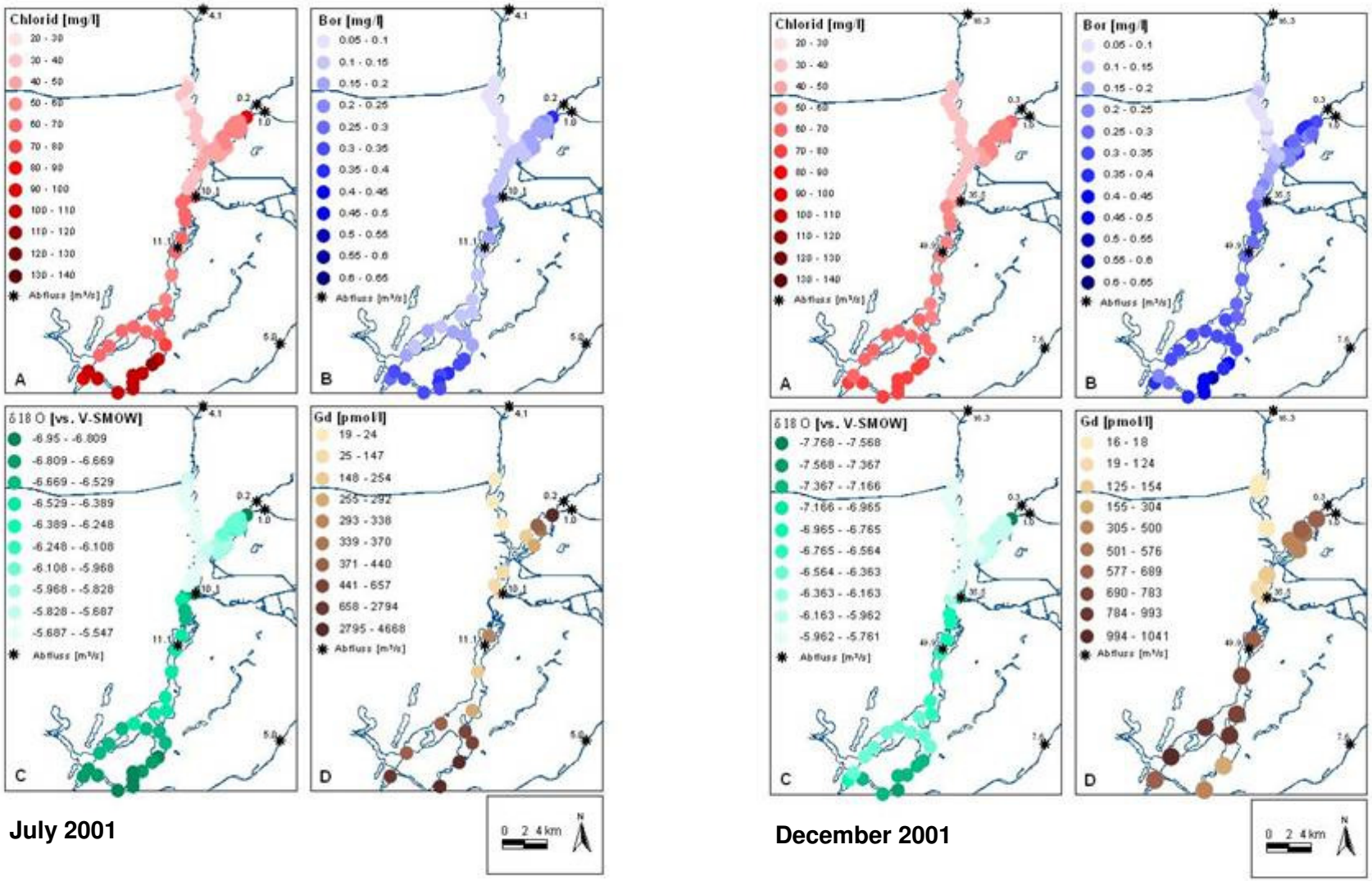

Figure 8: Exemplary comparison of distribution of wastewater indicators in the surface water system in summer and winter (RICHTER, 2003).

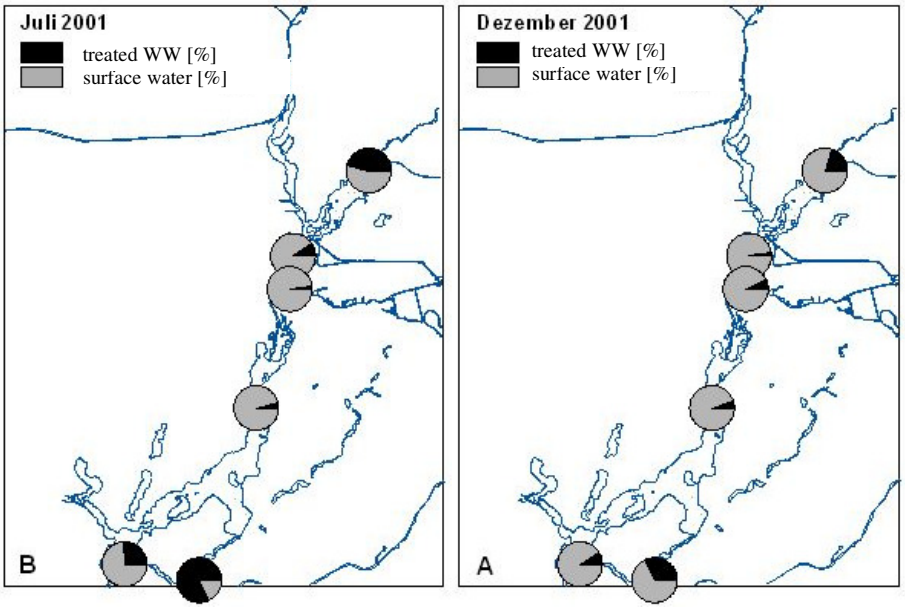

Figure 9: Exemplary proportion of treated wastewater in the surface water for summer and winter (RICHTER, 2003).

The Nordgraben and the Tegeler Fließ (both small ditches) discharge into Lake Tegel after passing through the OWA phosphate elimination plant. The Tegeler Fließ water is only partly (but largely) flowing through the OWA and partly discharging directly into the lake. The Nordgraben carries a high load of treated WW from the WWTP Schönerlinde. A pipeline started operating in October 2001, pumping Upper Havel (Oberhavel) water into the OWA (in particular during summer months) to dilute the treated WW when the base flow is low in order to improve the surface water quality. The pipeline caused the proportion of WW in the OWA discharge to temporarily decrease from October 2001 onwards (figure 5). However, the total discharge of the WWTP Schönerlinde increased as well in the beginning of 2003, which is why the proportion of WW now resembles the original situation before October 2001 again (40 % WW). The components discharging into lake Tegel from the north (natural discharge Tegeler Fließ and Nordgraben, discharge WWTP Schönerlinde and added Oberhavel water share) as well as the percentage of WW in the total OWA discharge are shown in Figure 5. The sum of these components is not always perfectly equal to the values given for the total OWA discharge (black line), probably due to measurement errors and because the Tegeler Fließ only partly passes through the OWA. It can be seen that due to the higher share of Upper Havel water in summer, the proportion of treated WW in the OWA discharge in 2003 and 2004 was lower than in winter, which is the opposite of the “normal” situation (more dilution in winter), further complicating the evaluation of the tracer data.

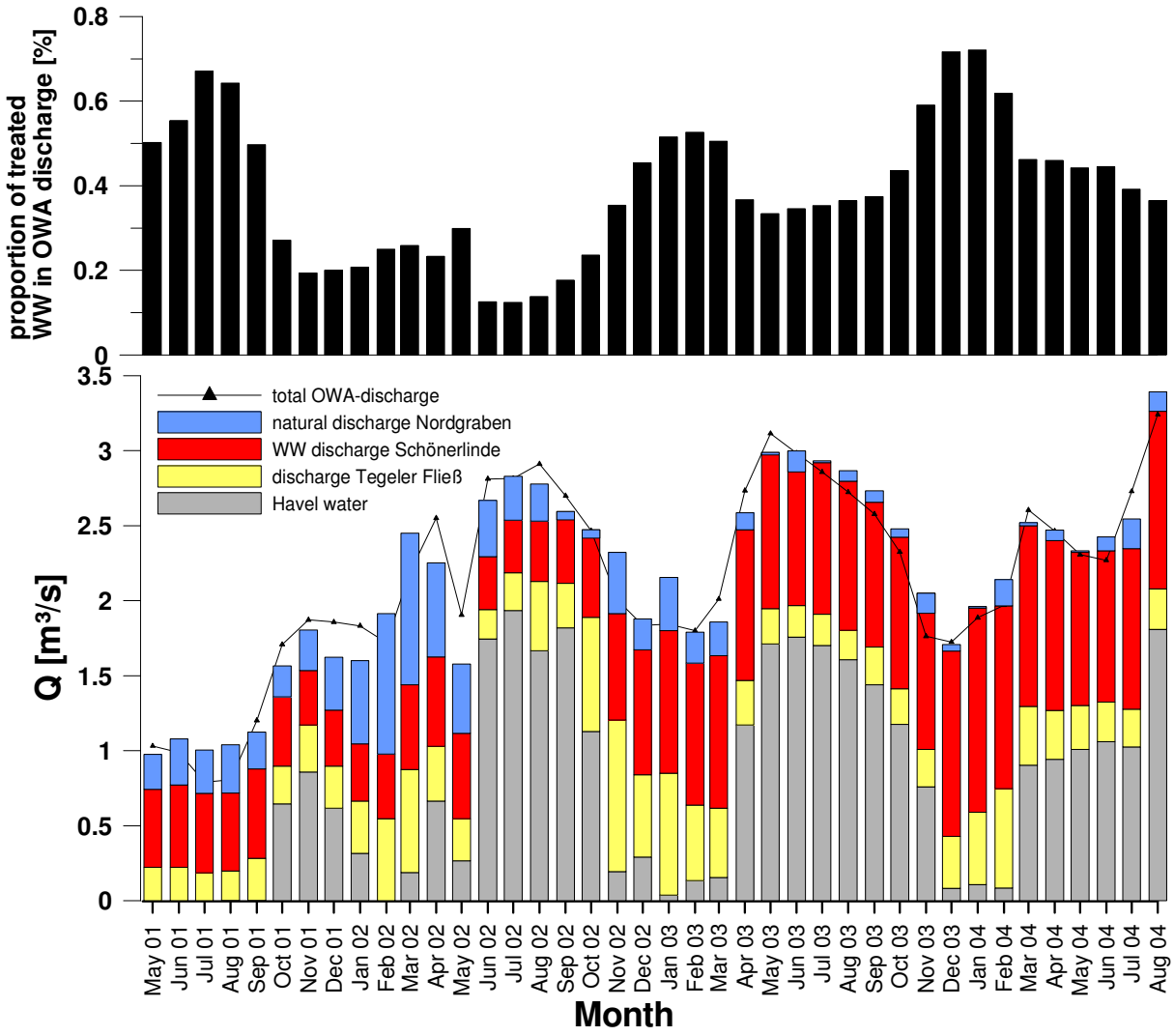

Figure 10: Total discharge of the OWA (black line) and discharge of components WWTP Schönerlinde (red bars), total discharge of Tegeler Fließ (yellow bars), calculated "natural" discharge of Nordgraben (blue bars, natural discharge Nordgraben = OWA inflow Nordgraben – discharge WWTP Schönerlinde) and Oberhavel input via pipe line). Data source: SENSTADT, 2001-2004 and BWB. Values are monthly averages.

Compared to Lake Wannsee, the conditions within the lake itself around the transect are more stable in terms of spatial distribution of the WW. The WW influence diminished with increasing distance from the OWA outlet (point 800, figure 6, right) but around the transect (point 310), the spatial variation at a certain time is small (figure 6, left).

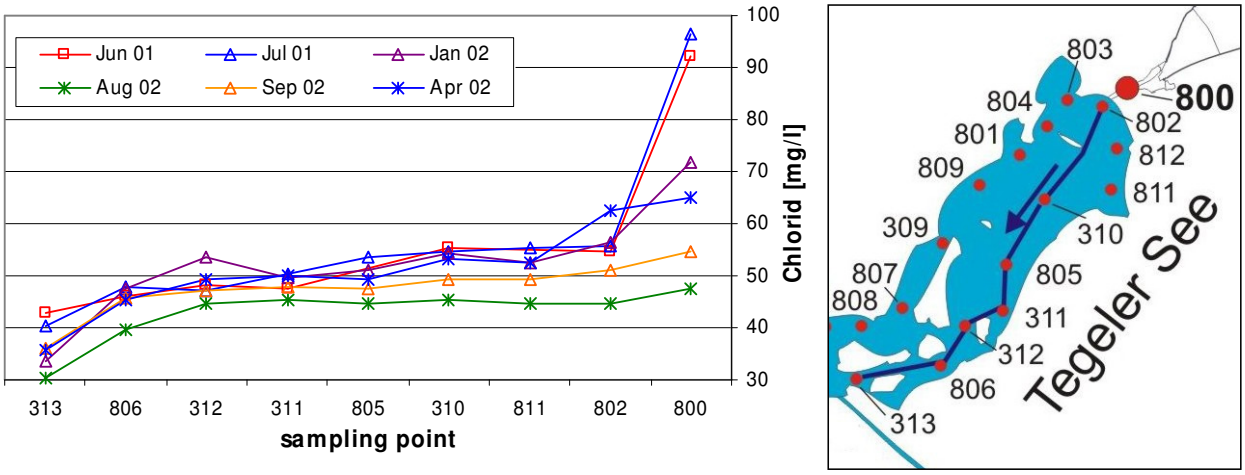

Figure 11: Chloride profiles throughout Lake Tegel during 6 sampling campaigns, sampling locations are given in the map to the right (RICHTER, 2003).

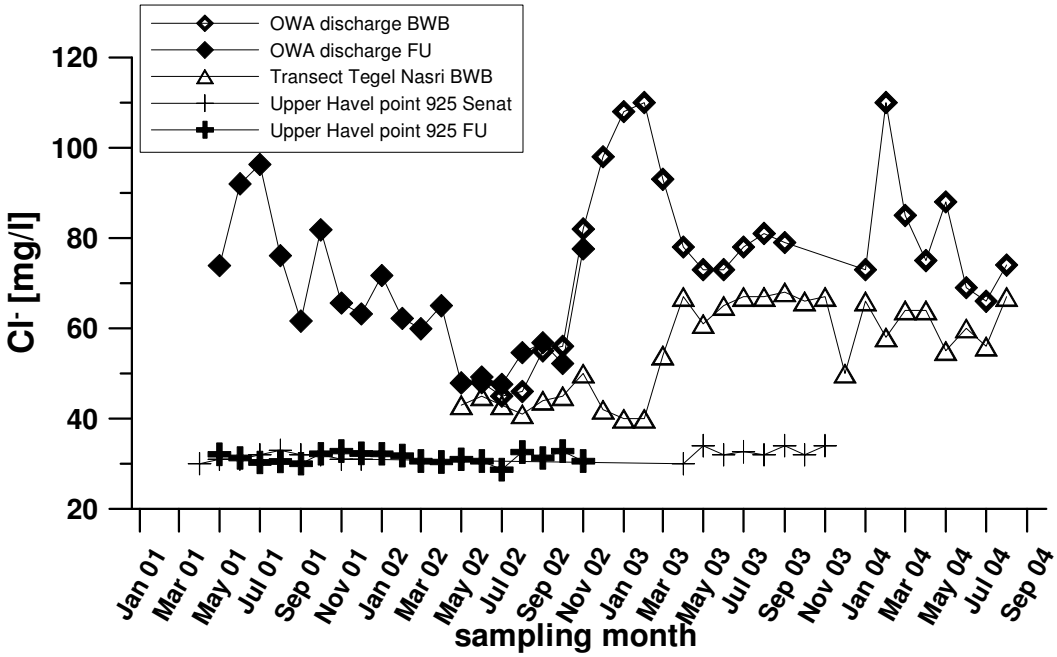

Figure 12: Cloride concentration in the surface water of the Upper Havel, Lake Tegel in front of the transect Tegel and Lake Tegel directly after the OWA outlet.

Figure 7 shows the chloride concentration in the Upper Havel (point 925), which is constantly low (~31 mg L^{-1}), Lake Tegel right after the OWA outlet (point 800, figure 6) and right in front of the transect Tegel. The sudden increase at the OWA outlet around December 2002 which coincides with the increased WW loads from Schönerlinde (figure 5) may be related to the increase in front of the transect about 4 months later. Using averages of this data-set, the proportion of treated WW in the surface water in front of the transect Tegel from May 2002 to August 2004 was ~21 % in average.

Principally, the concentrations of WW constituents are lower in winter, due to dilution with the larger natural discharge. The discharge of the WWTP's varies on a daily basis but does not show any seasonal fluctuations. The concentrations of wastewater bound substances in the effluent, for example chloride, do generally not show clear seasonalities (this is not true for specific substances, for example drug residues, which may be prescribed more often during certain times of the year). In contrast, the natural discharge is much higher in winter than it is in summer. However, as explained above, the changing conditions at Lake Tegel (figure 5) made the situations somewhat more complicated. In addition, the climatic situation was very different in 2002 compared to 2003. The combination of a very wet summer 2002 with lesser WW in the OWA discharge eliminated the typical summer peaks for most WW indicators, which were therefore of no use for the interpretation of travel time. Fortunately for the bank-filtration study, a clear minimum in February 2003 and a clear maximum in summer 2003 could be seen for most WW indicators which enables to define travel times at the transect.

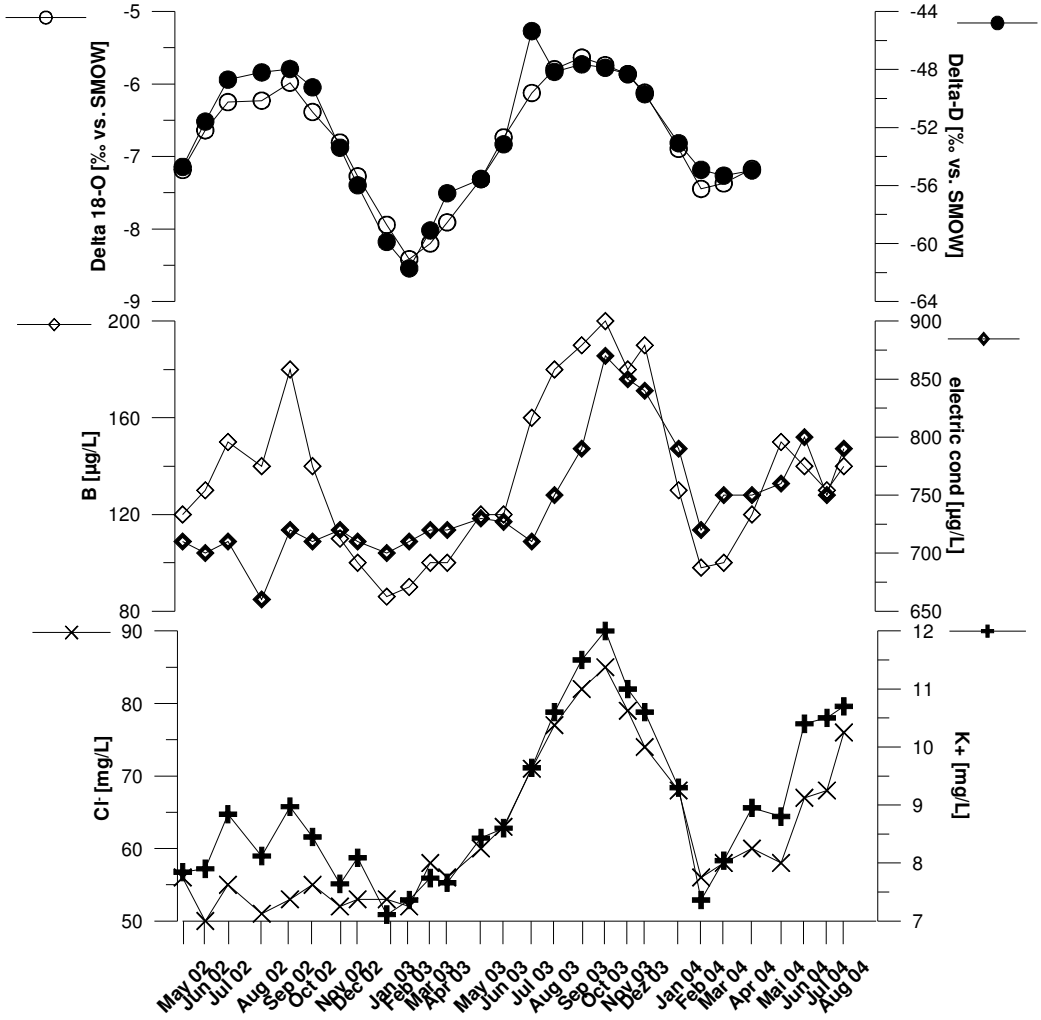

Figure 13: Stable isotopes, electric conductivity, B, Cl^- and K^+ in Lake Tegel (data source: AWI + BWB).

1.4.2 Clogging layer

The bottom of Lake Tegel is covered with very thick layers of lacustrine sapropel. These mud sediments are characterized by low hydraulic conductivity (2.1E-07 to 2.8E-09 m/s; FRITZ et al., 2002). At the lake borders, adjacent to the shores, the lake bottom is free of these sediments. However, the sands present in these areas are still heavily clogged, resulting in a hydraulic conductivity of 5.4E-06 m/s (FRITZ et al., 2002). Despite decreasing infiltration capacity, the presence of the low conductivity sediments has two positive effects. First, their relatively low permeability slows down travel times from the lake to the production wells. Second, they are far more effective in removing contaminants than unclogged aquifer sands, as the high proportions of organic matter and the finer grained material increase the adsorption and reduction capacities of the sediments (e.g. HISCOCK & GRISCHEK, 2002). Several authors have found that the most significant chemical changes related to organic matter degradation take place during the first few meters of flow (e.g. JACOBS ET AL., 1988; BOURG & BERTIN, 1993; DOUSSAN et al, 1997).

Analysis of mud sediment cores, taken from Lake Tegel, (SIEVERS, 2001) revealed that at the upper parts of the mud profile, the organic carbon content exceeds 22 % and at a depth of 80 cm below the mud surface, the organic carbon content exceeds 17 % (figure 9). This extremely high organic content is expected to have a positive influence on the removal of certain undesirable contaminants by microbial activity.

One species, undesired in high concentrations in the drinking water and detected in the water resources of Berlin, is sulfate. Relatively high concentrations of sulfate have been sampled in the surface water systems of Berlin in the past. A maximum concentration of 175 mg/l was detected during the period between February 1998 and October 1999 in the main pond of Lake Tegel, and a maximum concentration of 184 mg/l was detected during the period between May 1998 and June 1999 in Lake Müggelsee (FRITZ, 2002). There is also a big concern that sulfate concentrations in the river Spree may strongly increase in the future since open pit mining upstream of Berlin was largely abandoned after 1990. The former open mines are currently flooded and will be used as storage ponds for the Spree in order to discharge water into the Spree when the base flow is low. Sulfate concentrations within the ponds are extremely high with up to 60 meq/l in 2000 (KOHFAHL, 2004) In the case of future Spree concentrations exceeding the drinking water limit, these cannot be diluted with groundwater because the groundwater itself (from first and second aquifer) contains sulfate in concentrations higher than drinking water limits over large areas of Berlin (SOMMER VON-JARMERSTEDT et al. 1998; PEKDEGER et al. 1998).

Reduction of sulfate during bank filtration is a natural process with the positive effect of reducing sulfate concentrations. Therefore, the study of sulfate reduction during bank filtration in the lake sediments around Berlin is of great interest. While SIEVERS (2001) could show

that sulfate disappears within a few decimetres within the mud (figure 9), sulfate concentrations in the groundwater are in the same order of magnitude as the surface water, indicating that only little water passes through the impermeable lacustrine sapropels.

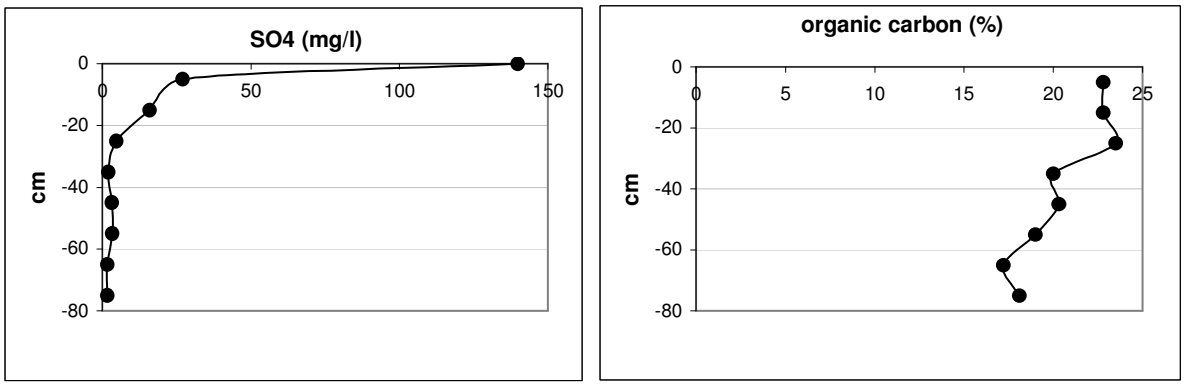

Figure 14: Sulfate in the pore water and organic carbon in the sediment of the mud sediment cores (SIEVERS, 2001).

Excursus: Modeling of sulfate reduction kinetics through a mud profile in Lake Tegel

Sulfate concentrations in the pore water of a 80 cm long mud core drilled in the bottom of Lake Tegel (SIEVERS, 2001, figure 9) were used to model sulfate reduction. Assuming that sulfate transport through the profile could be derived by diffusion and that the depletion in sulfate concentration was a consequence of redox reactions only, the geochemical computer program PHREEQC was used to fit first-order kinetic coefficients to the reduction process rates. The first-order coefficients obtained were 1.49×10^{-7} s^{-1} and 2.0×10^{-8} s^{-1} for the sections 0-10 and 10-40 cm below the mud surface, respectively. In the lowest 40 cm of the mud profile, 40-80 cm below the mud surface, steady-state concentrations were observed. The variation in the reduction rate constants in the upper 40 cm were suggested to be a consequence of the different types of organic compounds along the profile, rather than the total organic matter content. The steady-state concentrations at the lowest part of the profile are thought to be the consequence of either competition with other microbial populations or sulfide toxicity, a product of the sulfate reduction (figure 10).

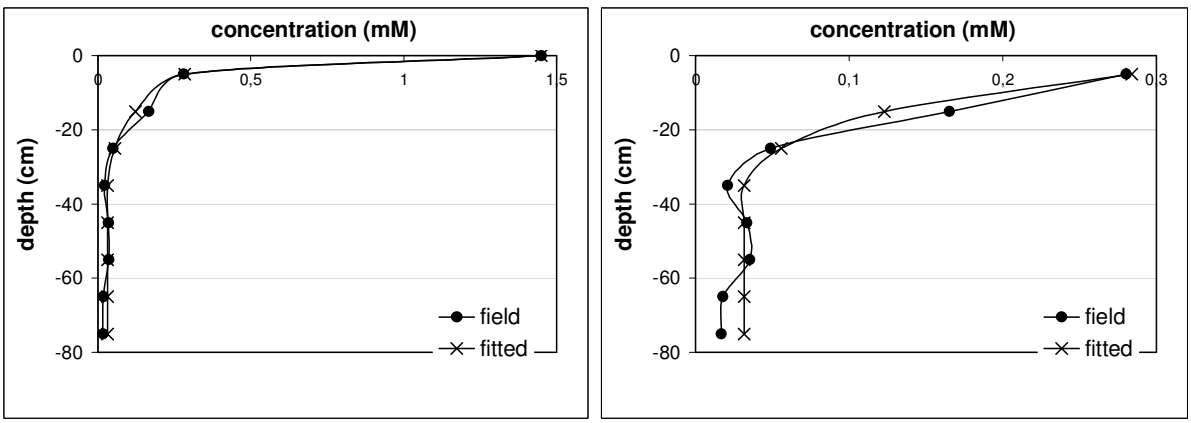

Figure 15: Sulfate concentration profile (full dots) and the fitted profile (crosses) using first-order kinetics. In the right figure the lake water concentrations were taken out in order toincrease the scale.

1.4.3 Aquifer sediments

The porous glaciofluvial sediments in the area are of Quaternary age (Saale glaciation; HANNAPPEL & ASBRAND, 2002). They consist of fine to coarse grained, but mainly medium sized sands. According to the Berlin terminology by LIMBERG AND THIERBACH (2002), both aquifers are part of the hydrogeological unit GWL 2 (qhol-qw). The aquifer is underlain by an aquitard of the Holstein interglacial at approximately 5 m below sea-level at both sites (HANNAPPEL & ASBRAND, 2002). A local aquitard, a glacial till of Saale age (local denotation qsWA) divides the aquifer in two (figure 11). The production well filter screens have been placed below the aquitard. However, the till is only partly present and was not encountered in drillings near the lake shore and below the pond. Therefore, the infiltration below the till is possible. The lithological cross section of FRITZ (2002) has been complemented with the new information (figures 11 and 14). Results from sieving analysis of samples taken at each lithological change (or at least every metre) of core TEG371UP) were added to figure 11. A relatively small variation from 1.5E-4 to 1.1E-03 m/s was observed, which is similar to hydraulic conductivities at the GWA Tegel.

Grain size distribution and hydraulic conductivities of core TEG371UP are shown in figure 12. In terms of the geochemical properties of the sediment, the unsaturated sediment zone (or, more precisely what was the unsaturated zone over a long period of time) differs from the sands below. At present, the unsaturated zone is much larger than it would be without pumping, at a water-table depth of 7-12 m below ground, depending on the pumping regime. Carbonate (inorganic carbon) appears from a depth of around 5.6 m onwards (figure 13) with a content of 0.16 to 1.3 weight %. The organic carbon content is low with 0.02-0.08 weight % (figure 13). With a few exceptions, the total iron content is 1-2 g/kg Fe (figure 13). The share of the reducible manganese fraction (Mn(hydr)oxides) seems to be getting slightly less with depth. In terms of total ion concentrations (HNO_3 extraction, figure 13), aluminium and iron are the main minor cations in the unsaturated sands, while calcium dominates within the saturated zone (figure 13).

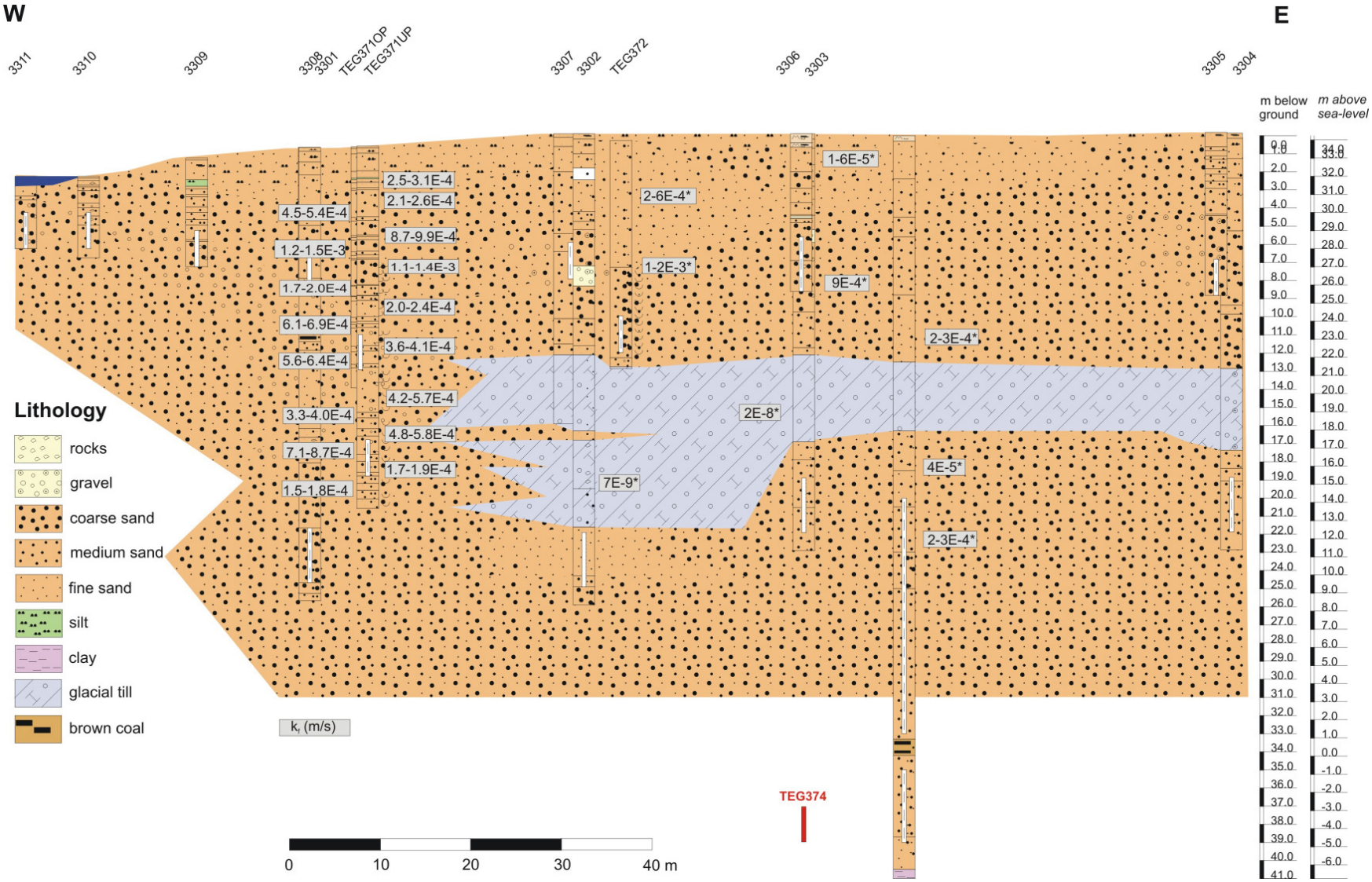

Figure 16: Geological cross-section of the transect Tegel with hydraulic conductivities from sieving of core TEG371UP. Values with* from Fritz (2002).

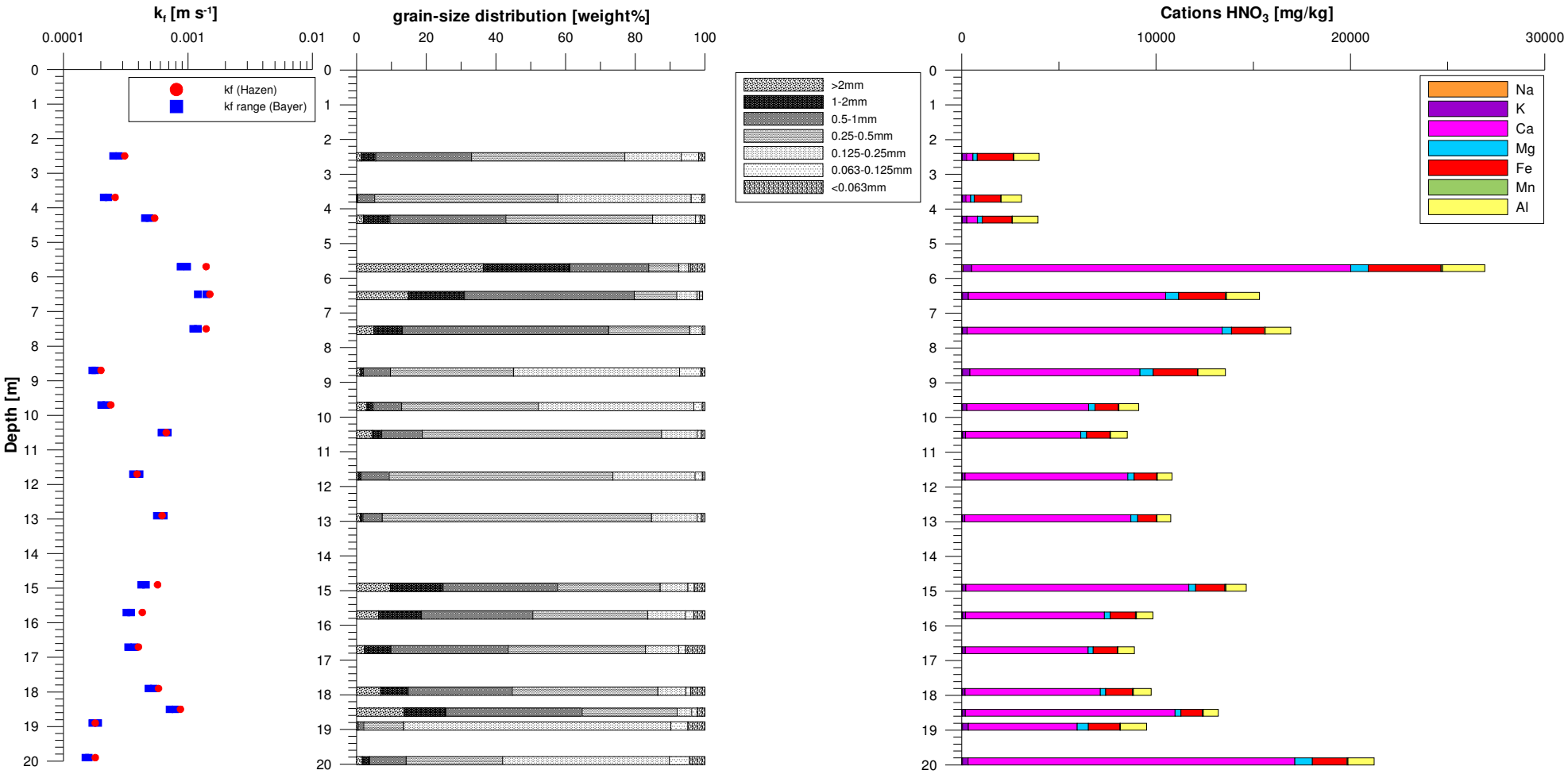

Figure 17: Hydraulic conductivities (k_f), grain-size distribution and cations from HNO_3 extraction in core TEG371UP.

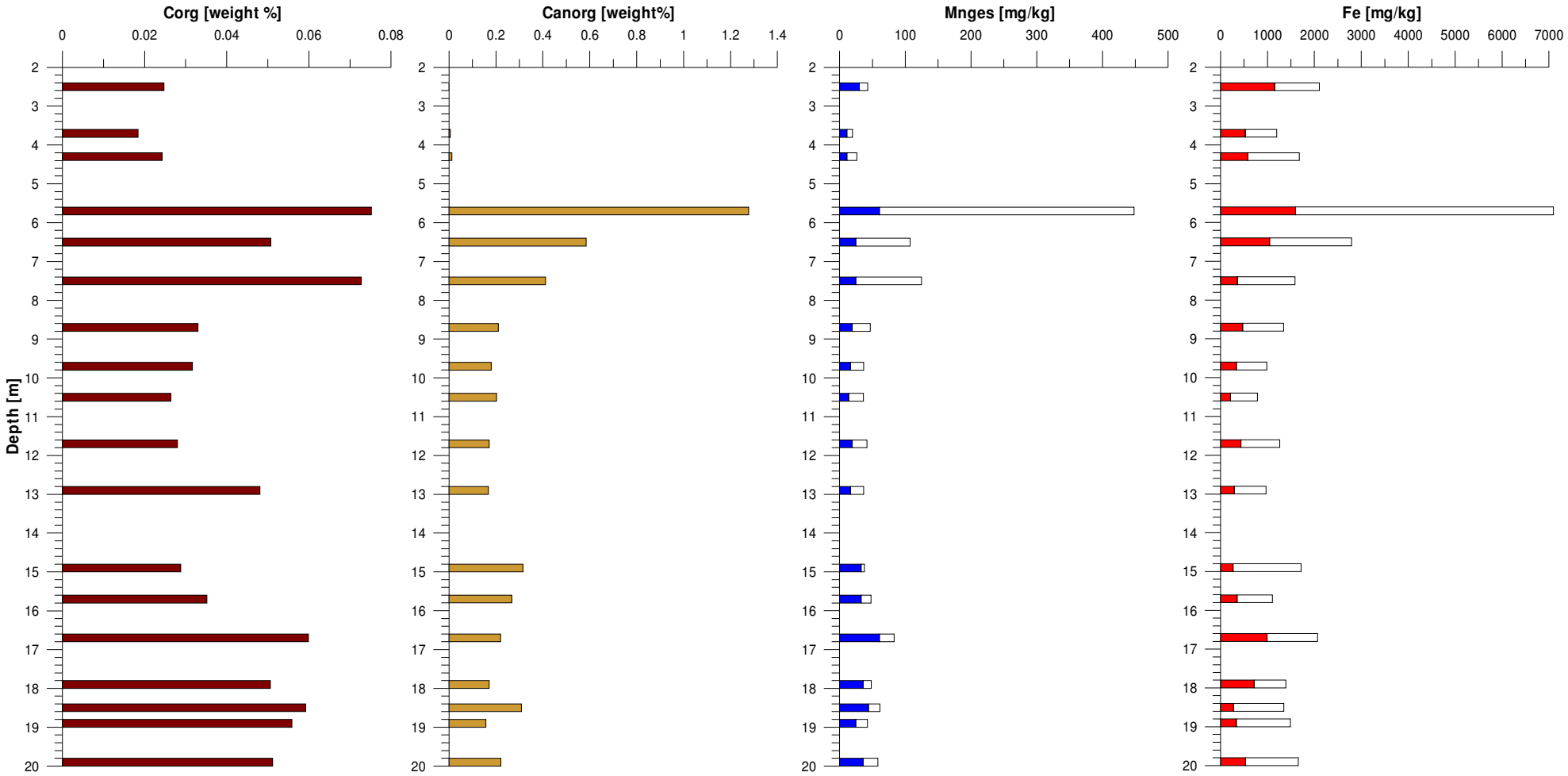

Figure 18: Organic and inorganic carbon content, Fe(III, red) and Fe(II, white), Mn(IV, blue) and Mn(II, white) content in core TEG371UP.

1.4.4 Hydraulic situation

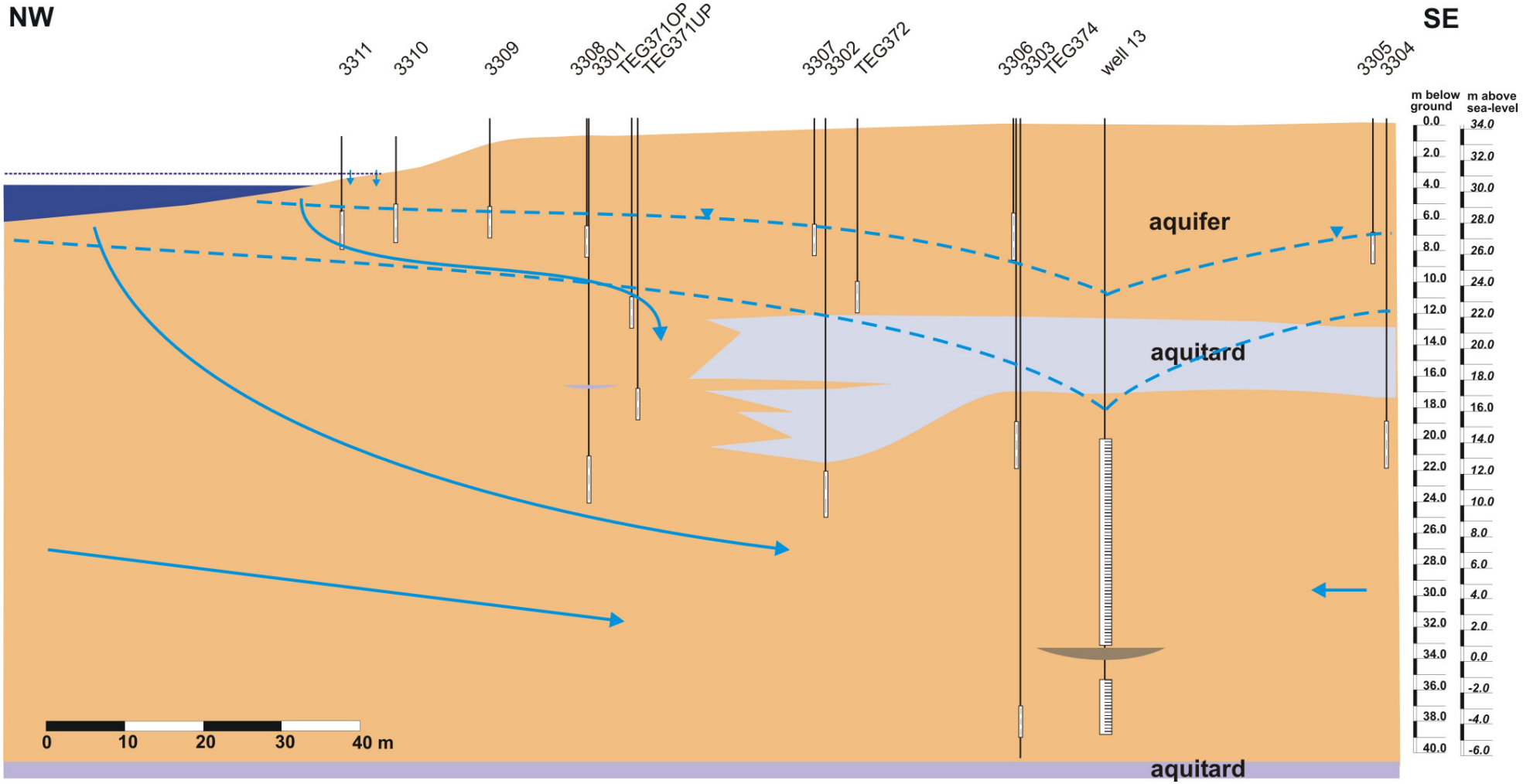

Figure 19: Simplified hydrogeological cross-section of transect Tegel, including the approximate location of the minimum and maximum surface and groundwater-level and exemplary flow-paths.

Figure 14 shows a simplified hydrogeological cross-section with approximate minimum and maximum surface- and groundwater levels as given by logger data between 2002 and 2004 (when well is in operation). All logger data available is presented in figure 15 for a first hydraulic overview. It reflects the fact that the summer 2003 was extraordinary dry and hot, causing a much larger groundwater drawdown and lower surface water level. In summer 2003, even the “deeper” shallow wells TEG372 and TEG371OP fell dry which means, since they have filter screens just above the till, that there was virtually almost no water above the till in the upper aquifer anymore.

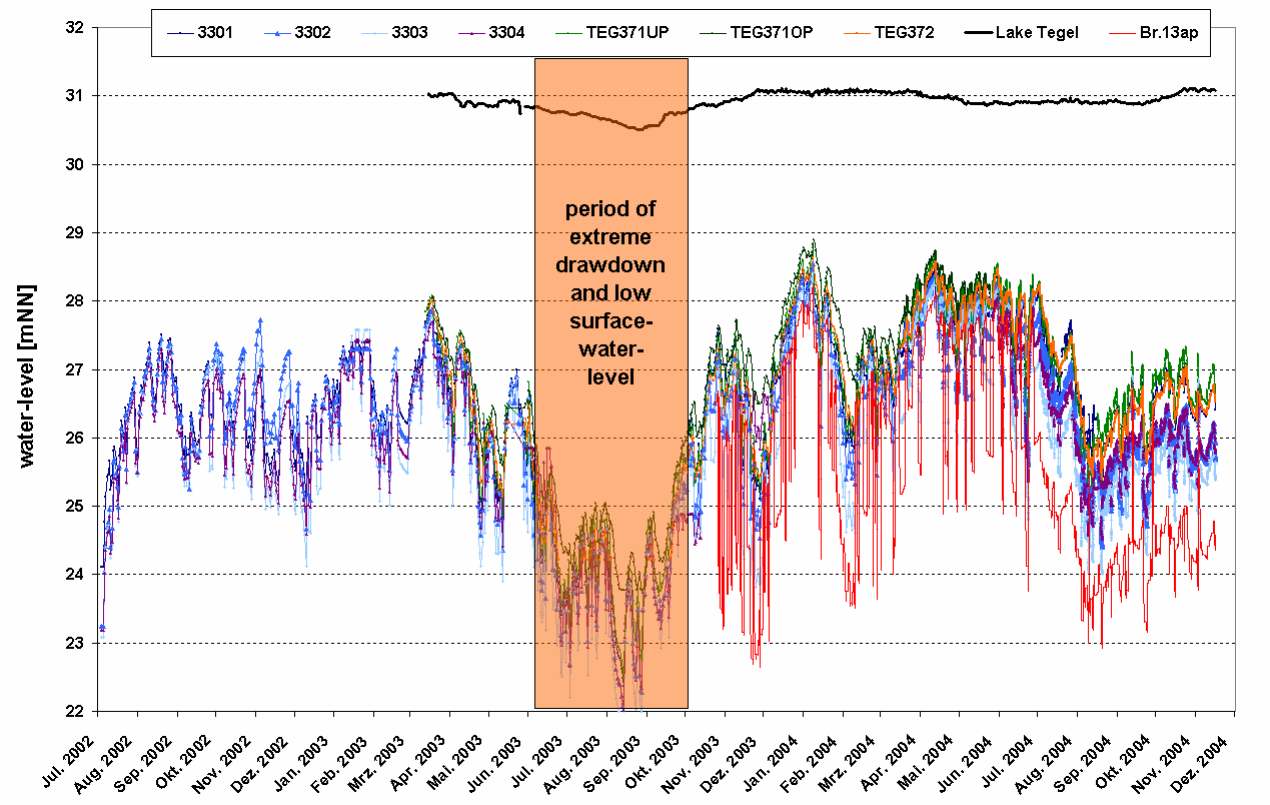

Figure 20: Available water-level data from data loggers at the transect Tegel. Lake Tegel is given in black at the top, while the red line is data from the piezometers in the gravel pack around the production well.

A steady-state 3-dimensional model of the site was constructed in the previous projects (FRITZ, 2002; EICHHORN, 2000). A simplified transient 2-dimensional model, simulating a number of pumping scenarios was developed by RÜMMLER (2003) in joint co-operation between the IGB and the FU on the basis of pumping test data from EICHHORN (2000). The aim was to understand how flow-paths, travel times and proportions of bank-filtrate vary depending on pumping rates and well regimes. Figure 16 shows the flow-paths of one scenario and is meant to give an idea on how flow-paths show a zigzag pattern due to alternating operation of the productions wells. But however strongly flow-paths may move, the following tracer evaluation still gives reasonable average values for residence times. But it has to be taken into account that the actual flow-path length may be larger than expected.

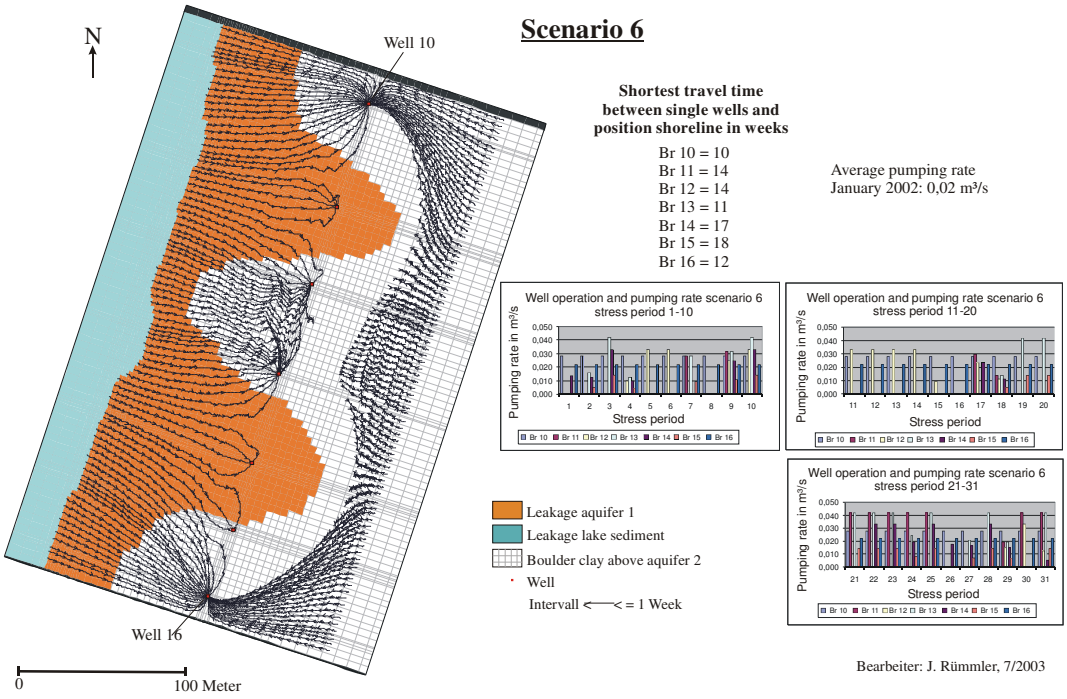

Figure 21: Flow-paths in a transient simulation with monthly alternation of wells 10, 12, 14, 16 and 10, 11, 15, 16 (RÜMMLER, 2003).

1.4.5 Tracer evaluation: Travel times/groundwater age

Breakthrough curves of potential tracers were sighted and a selection of the more suitable ones is shown below, divided into figures of the deeper (figures 17, 18) wells and a succession from shallower to deep (figures 19, 20) observation wells on one spot. Missing data is due to the fact that observation wells fell dry during summer months. For the approximation of travel times the shift of peaks or the shift of the increase or decrease of the concentration was used and estimated visually. Potassium, which appeared to be a suitable tracer at first, showed some retardation and was disregarded. Chloride breakthrough curves are also not shown, because they seem to fluctuate too strongly. The temperature, although not a conservative tracer, proved to be very useful and using a retardation factor of 2 seemed appropriate for the site. The stable isotopes, which are the most useful tracer for the determination of travel times since they are less vulnerable towards side-effects and are perfectly conservative, clearly show that the travel times have overall decreased, i.e. the flow velocities have increased within the time period of sampling. Therefore, rather then given just one value for travel time to a certain well, a range of travel times is given in the summary in figure 23, which is not due to uncertainty of the method but rather due to the fact that travel times did vary over the 2 years of sampling.

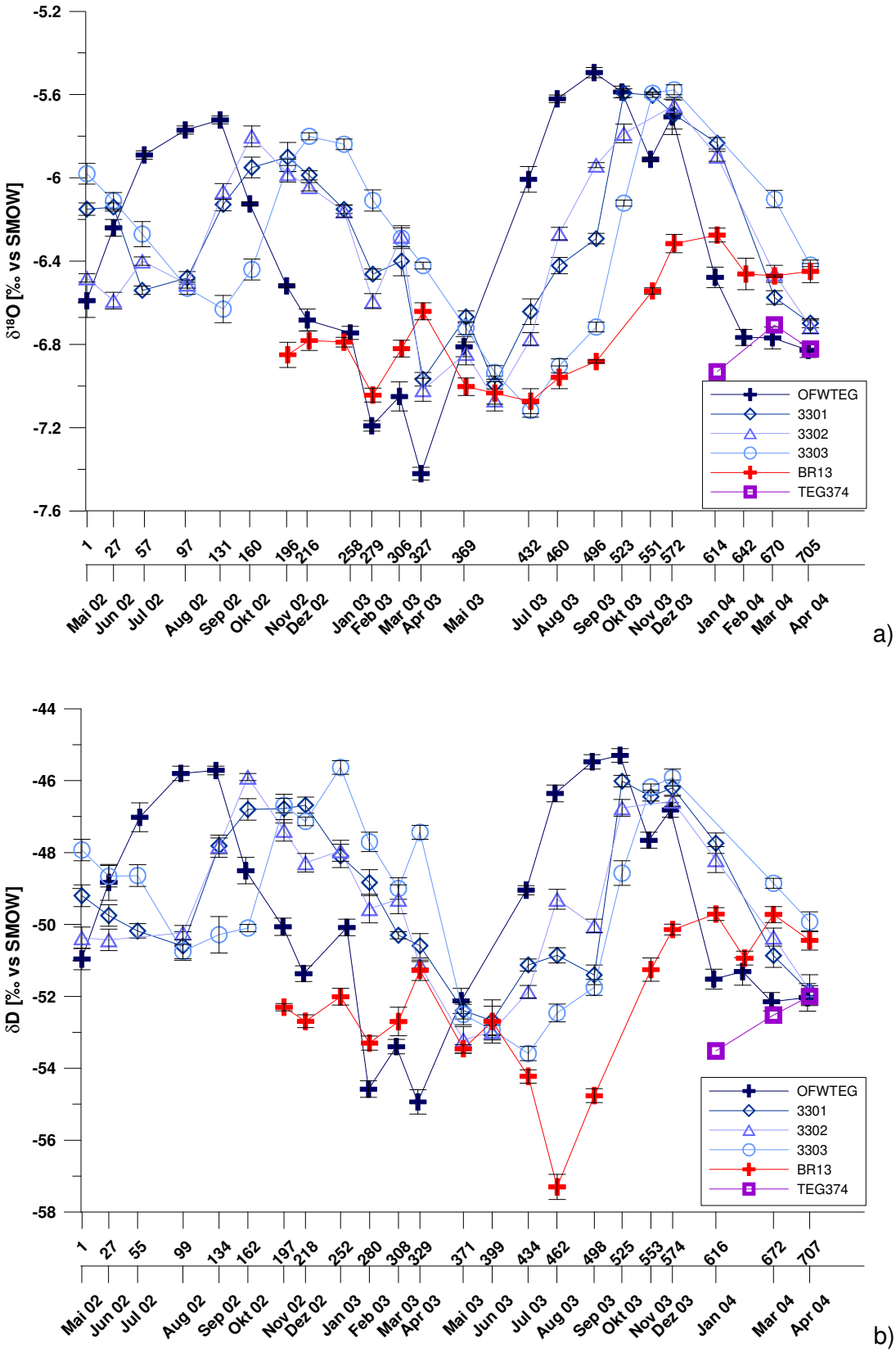

Figure 22: Breakthrough curves of $\delta^{18}O$ (a) and δD (b) in production well 13 (red symbols) and observation wells 3301, 3302, 3303 and TEG374 (compare figure 14). Data source: AWI. Month of sampling and days since start of NASRI are given on x-axis.

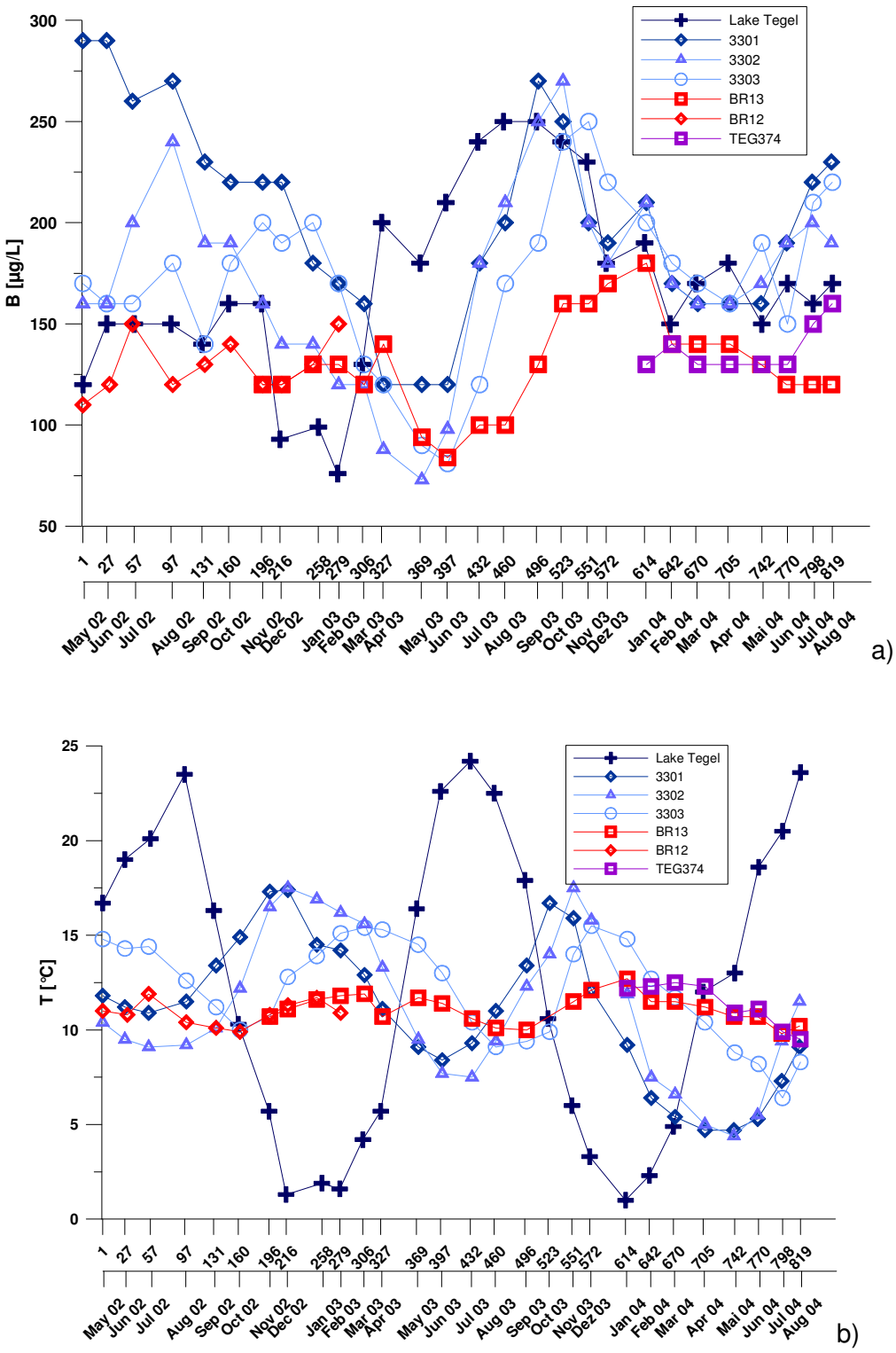

Figure 23: Breakthrough curves of B (a) and temperature (b) in production well 13 (red symbols) and observation wells 3301, 3302, 3303 and TEG374 (compare figure 14). Data source: BWB. Month of sampling and days since start of NASRI are given on x-axis.

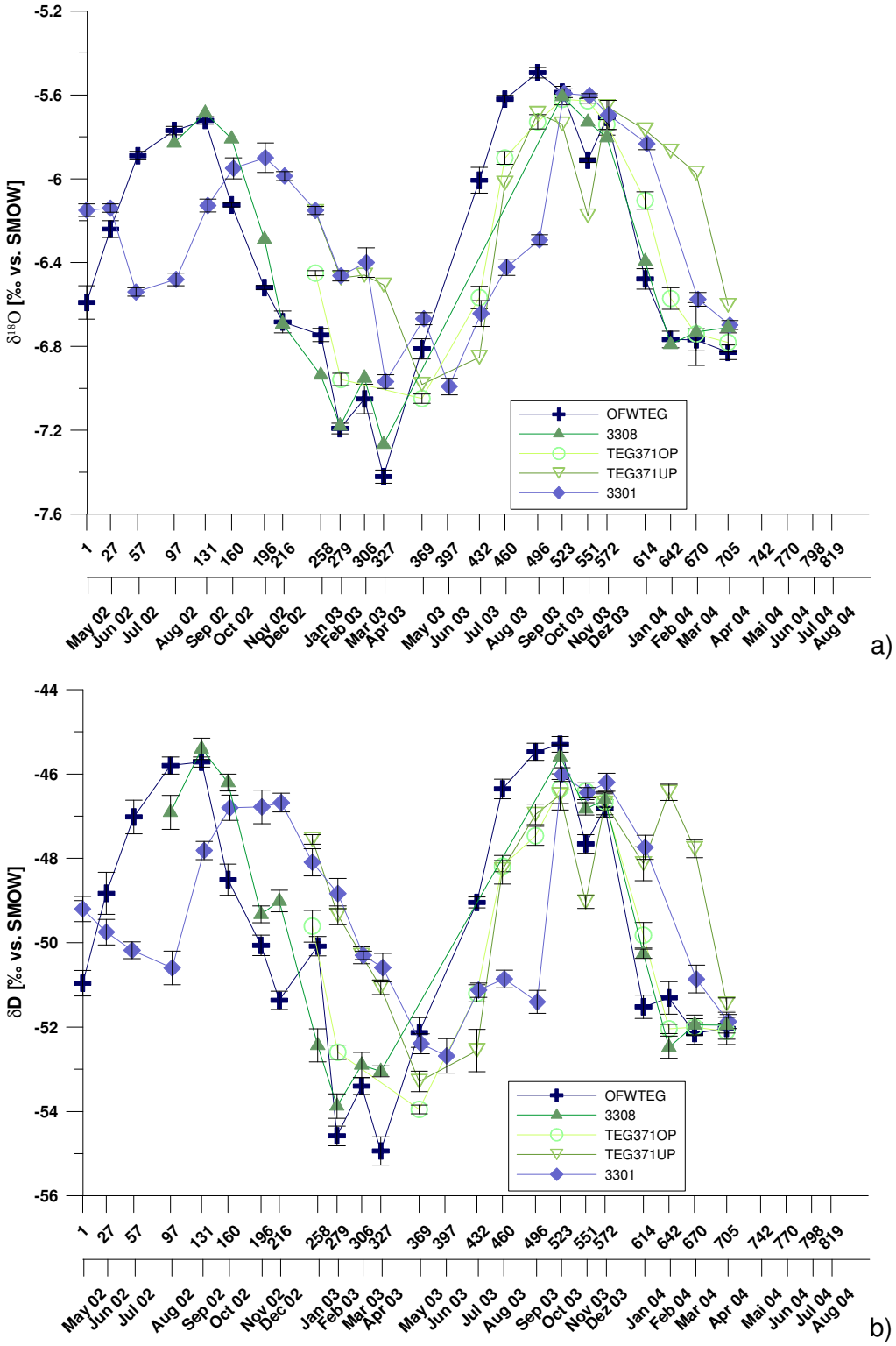

Figure 24: Breakthrough curves of $\delta^{18}O$ (a) and δD (b) from shallow (3308) to deep (3301) observation wells at one location (compare figure 14). Data source (AWI). Month of sampling and days since start of NASRI are given on x-axis.

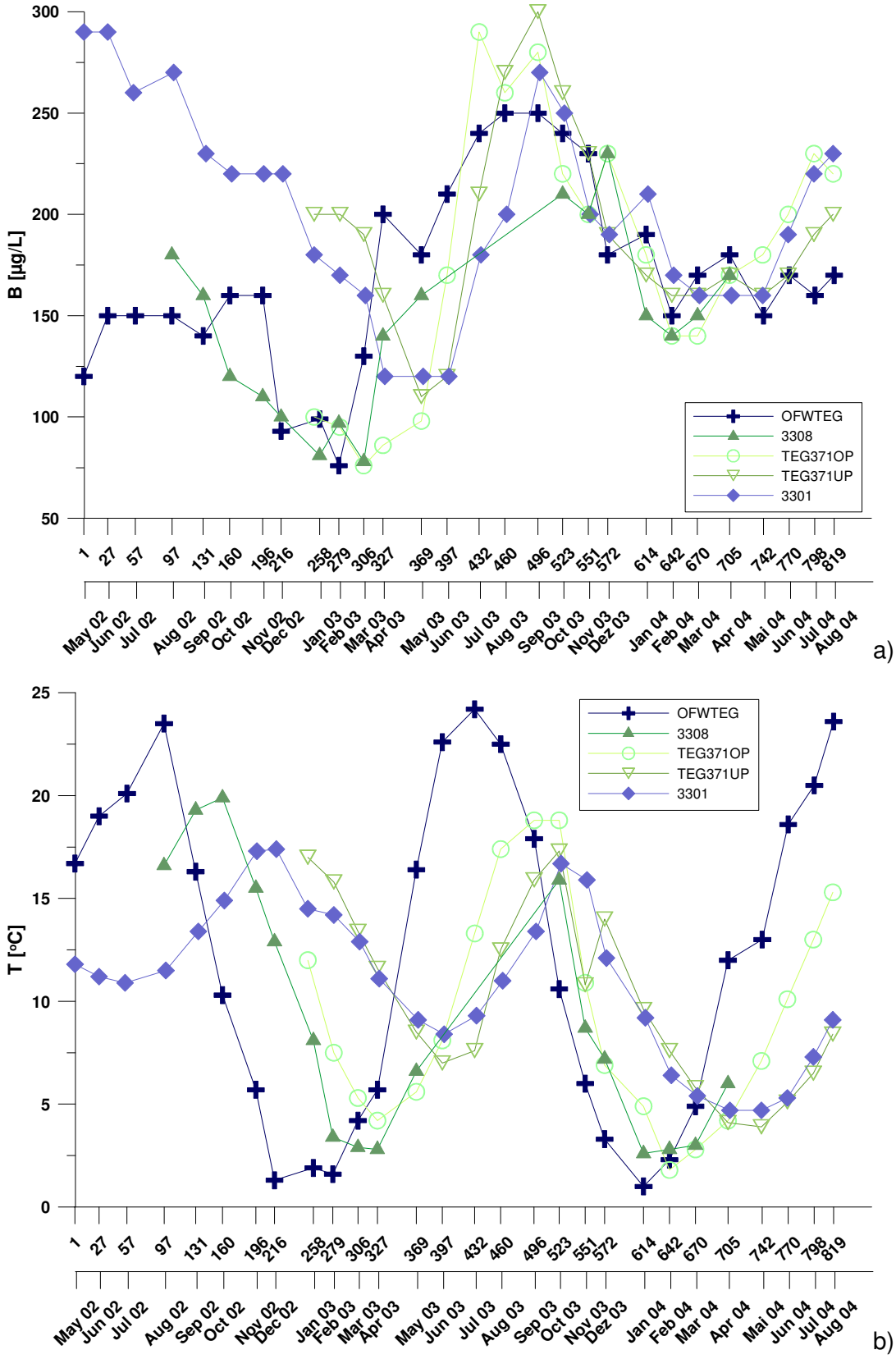

Figure 25: Breakthrough curves of $\delta^{18}O$ (above) and δD (below) from shallow (3308) to deep (3301) observation wells at one location (compare figure 14). Data source: BWB. Month of sampling and days since start of NASRI are given on x-axis.

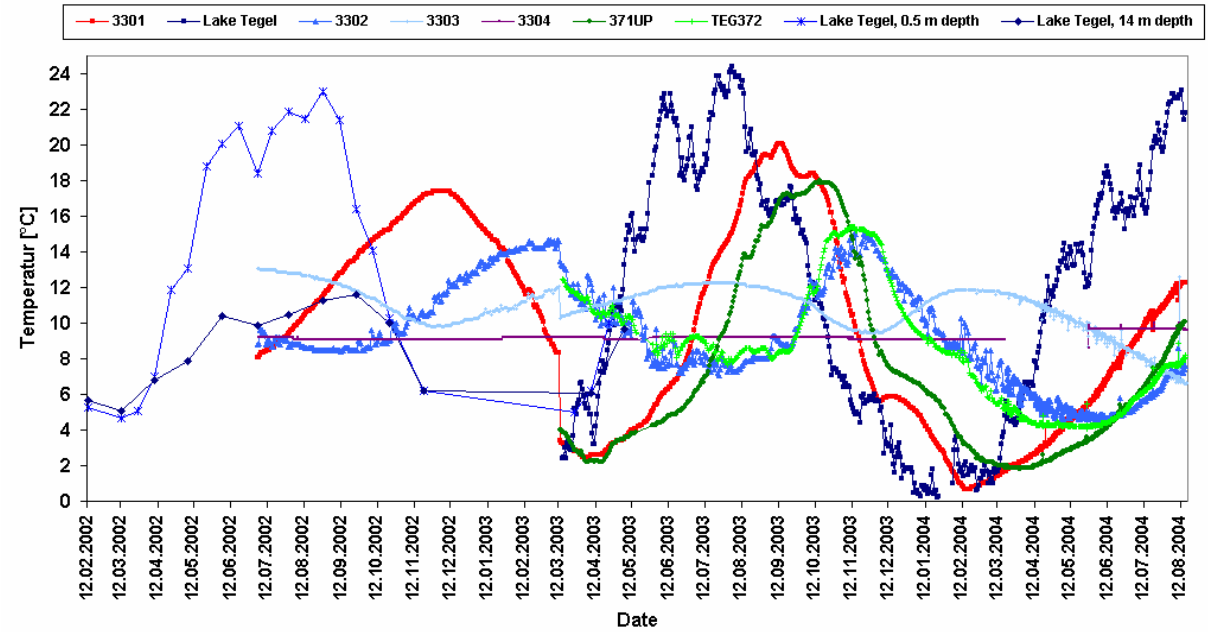

Figure 26: Temperature breakthrough curves registered with data loggers at the transect Tegel.

The temperature breakthrough curves from the data logger are shown in figure 21. With hourly measurements, they have a better resolution than the temperatures from monthly hydrochemical samplings. But, because the temperature sensor is combined with the pressure sensors, the logger are installed more or less at the same depth in all observation wells. Rather than reflecting the groundwater temperature of the filter screen depth, the curves are representative for the depth the loggers are installed in, which is usually shallower. Therefore, the data of the temperature logging cannot be directly compared with the chemical data from the filter of the observation wells. From comparison with the conventional tracers, the retardation factor (R) can be estimated from observation wells with shallow filters, where the logger is installed in the filter level which would result an R of 2 for TEG371OP, given as an example in figure 22.

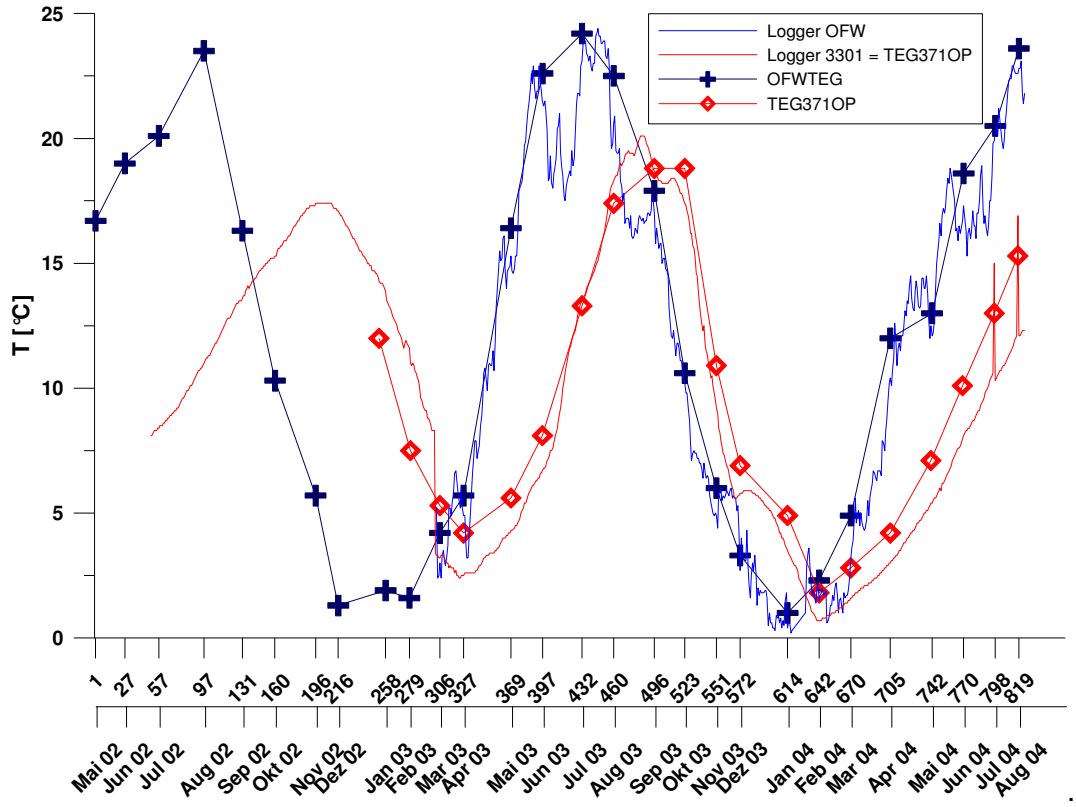

Figure 27: Logger data from Lake Tegel and observation well 3301, as well as temperature data from monthly sampling of Lake Tegel and TEG371OP. Month of sampling and days since start of NASRI are given on x-axis.

To obtain a better overview, the combined findings of the tracer evaluation are summarised in figure 23 (minimum and maximum travel times from May 2002 to August 2004 are given). The effective T/He age is shown in figure 24 (sampling took place in spring 2003).

Because observation wells between the lake and the production well except the very deep TEG374 show hardly any dampening of the amplitude of the input signal of the lake, they must largely consist of bank filtrate from the nearest shore, which should show an effective T/He age of <0.5 years (resolution of the method) as is the case for TEG371OP and 3303.

Although 3301 and 3302 resemble each other largely and have a similar dominating travel time, 3301 sometimes deviates strongly from the lake and 3302 with regard to some of the WW constituents (for example much higher B concentrations in summer 2002, figure 18a) which indicates that 3301 gets at least to a minor extent water from elsewhere and lies on a different flow path. The effective T/He age of 3301 is 1.7 years. If 100 % of the water of 3301 was originating from the direct lake shore, the effective age should be 0-0.5 years (resolution of the method for this site), like it is for TEG371OP and 3303. The effective T/He age is not a "real" age but the result of a mixture of T and ^{2}He of several water bodies. It does therefore not stand as a contradiction to the remaining tracer results. It only indicates that a (probably small) proportion of the water of 3301 is considerably older than 6 months. It is not possible

to say precisely how large this water volume is and what effective ages it is composed of. It does, together with results from some of the minor water constituents (see below), suggest that some water may be infiltrating around the islands within the lake or at the western lake side and is flowing beneath Lake Tegel, which is basically sealed as soon as the laccustrine sappropels become thick.

The background groundwater well 3304 (inland, data not shown) shows no seasonality because it does not contain bank filtrate. Therefore, a calculation of travel times does not make sense. The effective T/He age of observation well 3304 is 11.9 years.

TEG374 was installed in order to clarify remaining uncertainties concerning the vertical age stratification of the entire aquifer, since the former “deep” wells did not reach the lower parts of the aquifer. It was not possible to calculate a travel time for this well from tracer breakthrough curves, because TEG374 was only sampled over 7 months and appeared to show very little seasonality. The effective T/He age for this well is 25 years, which, together with the lack of seasonality, illustrates that there is a water component present in the lower aquifer that is decades, rather than months old. The fact that, for example the temperature, does still show a little seasonality does nevertheless show that TEG374 is probably not the end member of this old water component itself and might contain a lower percentage of water of a younger age. From its chemical composition, the water pumped from TEG374 is, however, clearly former surface water, even though one may argue that the name bank-filtrate might not be appropriate anymore.

The production wells themselves show a strongly dampened tracer signal due to mixing of bank filtrate with background groundwater and due to the fact that the long filter screen abstracts water of variable ages. However, when a signal is visible, it correlates to a dominant (or effective) travel time of 4-5 months. This shows that travel times have decreased compared to 1999-2000, when Fritz (2002) observed travel times of 6-8 months for the same well. The effective T/He age of well 13 was found to be 12.7 years which is even larger than the age of the background groundwater. Again, this clarifies that some of the abstracted water (namely the part flowing at the bottom of the aquifer) is considerably older than both, the “young” bank filtrate and the background groundwater.

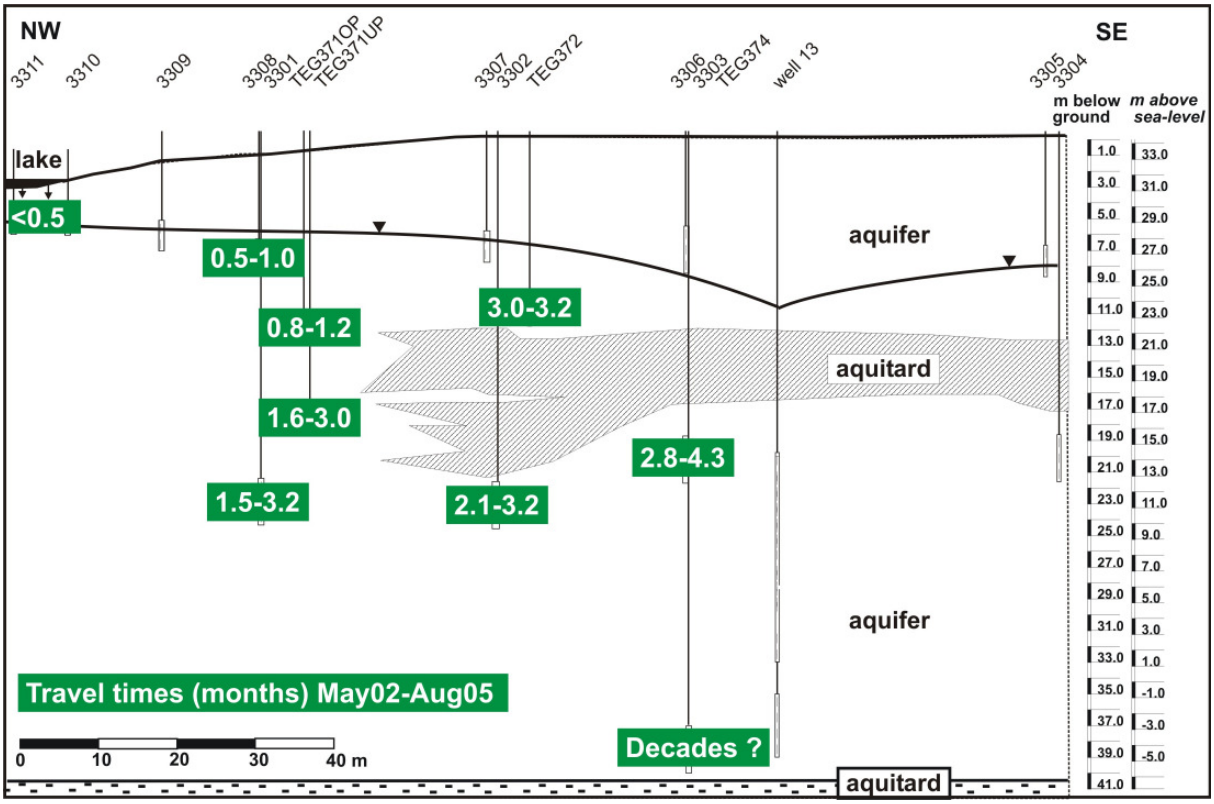

Figure 28: Summary of results from visual travel time estimation using breakthrough curves of $\delta^{18}O$, δD, B and temperature. Range of travel times observed from May 2002 to August 2004.

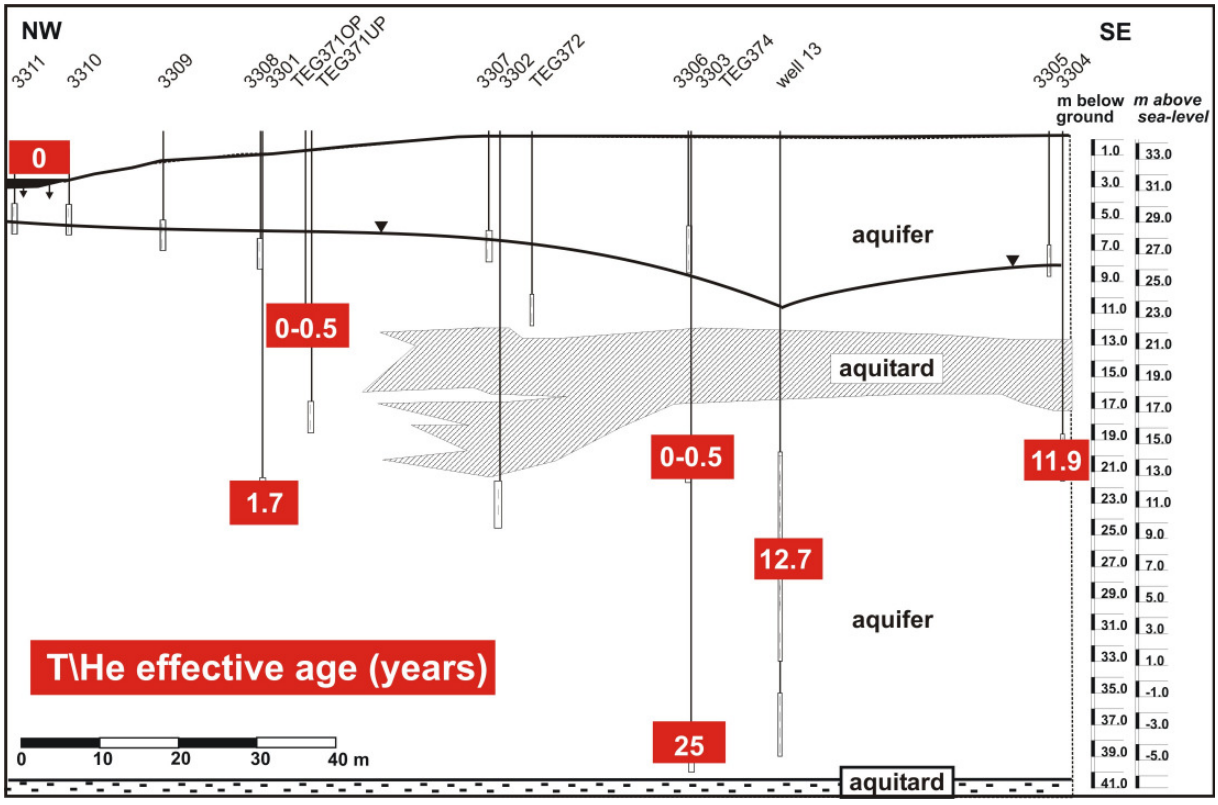

Figure 29: Effective T/He ages. Results do not necessarily represent travel times, since mixing of water alters the age.

1.4.6 Tracer evaluation: Mixing

Figure 25 shows that on a stable isotope scatter plot, the production wells 12, 13 and 14 lie between surface water and background groundwater. To calculate the proportion of bank-filtrate in the production wells, conservative tracer with a clear difference in concentration between groundwater and surface water and fewer seasonal variations are ideal. Average values of the background groundwater (3304), the surface water (or alternatively 3303) and the production wells of stable isotopes, K, EDTA and B which show a sufficient difference between groundwater and surface water (figure 26) were used to calculate the overall BF percentage in the production wells. The differentiation between old and young BF was not undertaken when these tracer were used, since the concentrations in the old BF resemble more or less those of the surface water average (despite lacking seasonality) for these substances (figures 27, 28).

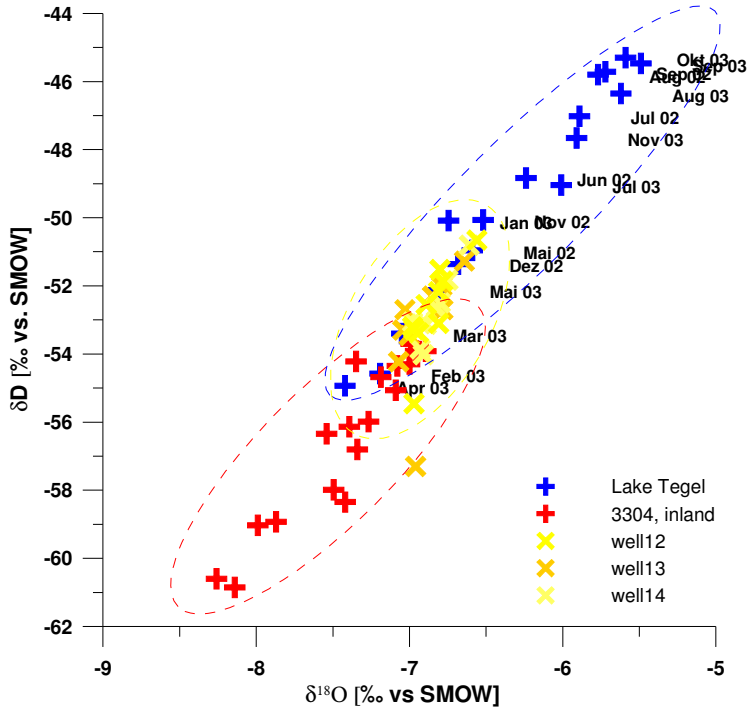

Figure 30: δD versus δ18O in surface water (blue), background groundwater (red) and abstracted water (yellow) in Tegel (May 2002-October 2003, data source: AWI).

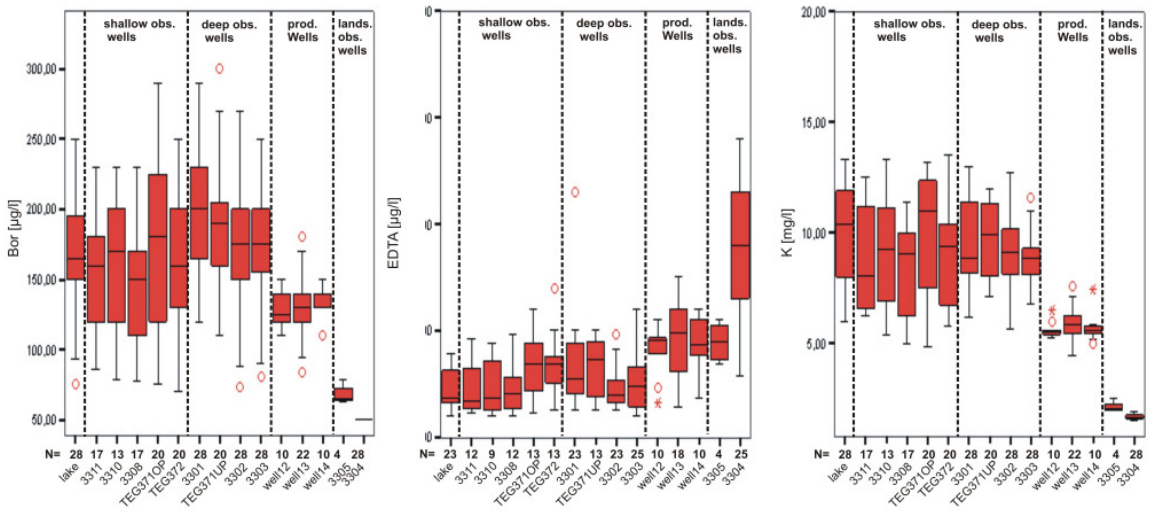

Figure 31: Boxplots for B, EDTA and K, illustrating the difference between the surface water and BF wells and the background groundwater, represented by 3304. Data from May 2002-August 2004, N = number of samples for respective well.

Some difficulties arouse. For example, the time-series show that all parameters strongly varied in the surface water over the period of sampling. Also, EDTA concentrations (figure 28) and isotope values (figure 27) in the background groundwater (3304) strongly changed in 2003 for unknown reasons, after having been more or less stable in the past (FRITZ, 2003). The isotope values increased to an extent that they even resembled surface water values in February 2003. The fact that the deeper, old BF and the production wells showed little seasonal variations suggested that it is more useful to use long-time averages only, rather then trying to calculate monthly percentages (because the time-lag which would have to be taken account for is not equal throughout the water column). The results of the calculations vary, depending on what parameter is used, whether concentrations of the lake water or 3303 are used for the calculations, whether or not the time offset was taken account for when calculating the average over a comparable time-period), what background groundwater concentration was assumed when concentrations were below detection limit (e.g. zero or detection limit of 50 µg/l for B) etc… Considering all these difficulties and choosing the most appropriate assumptions lead to a proportion of bank filtrate in well 13 of 58-69 % (for both young and old bank filtrate together).

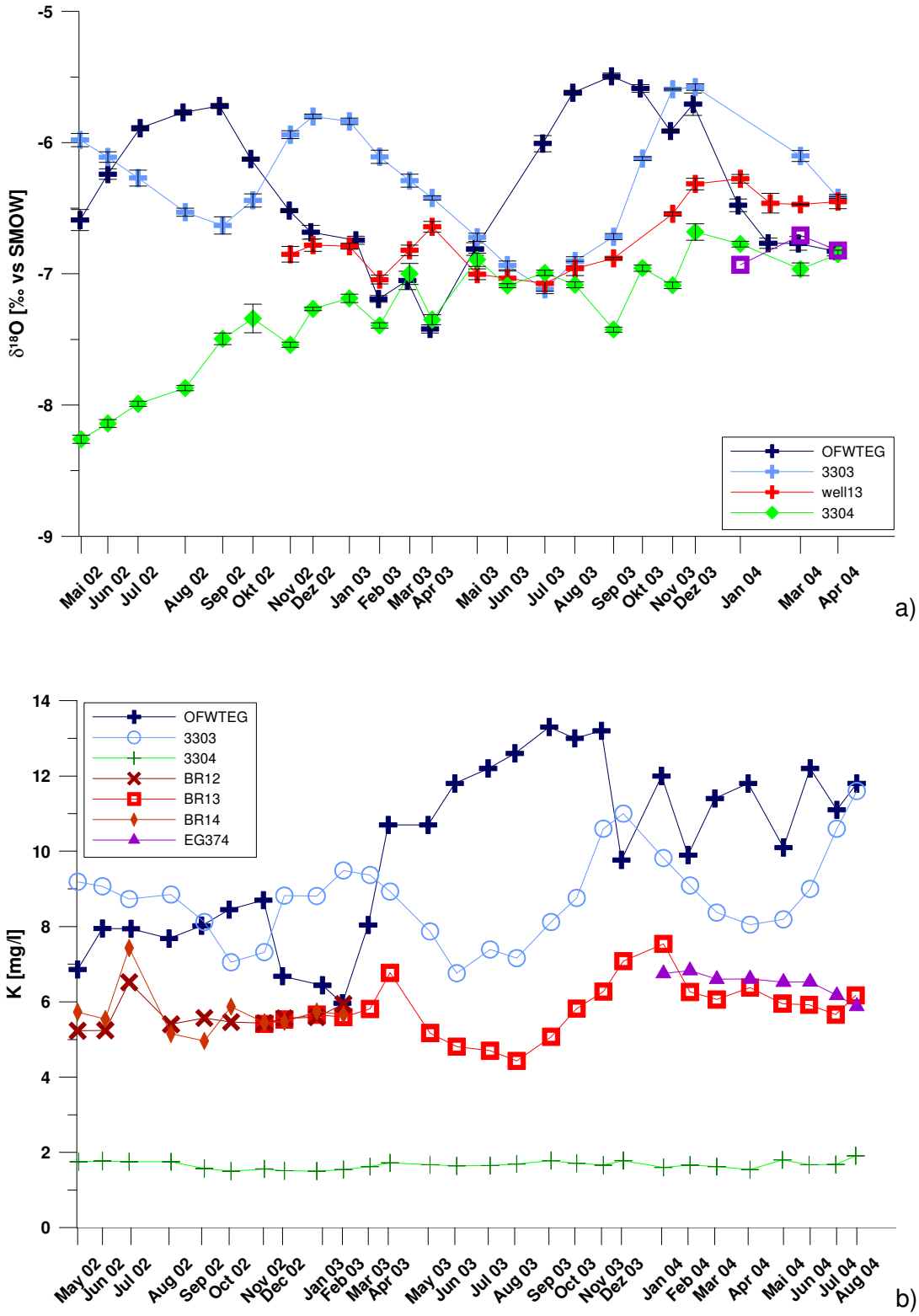

Figure 32: Time-series of δ18O (a) and K (b) in surface water, production wells and shallow observation wells 3303 & 3304 and deep observation well TEG374.

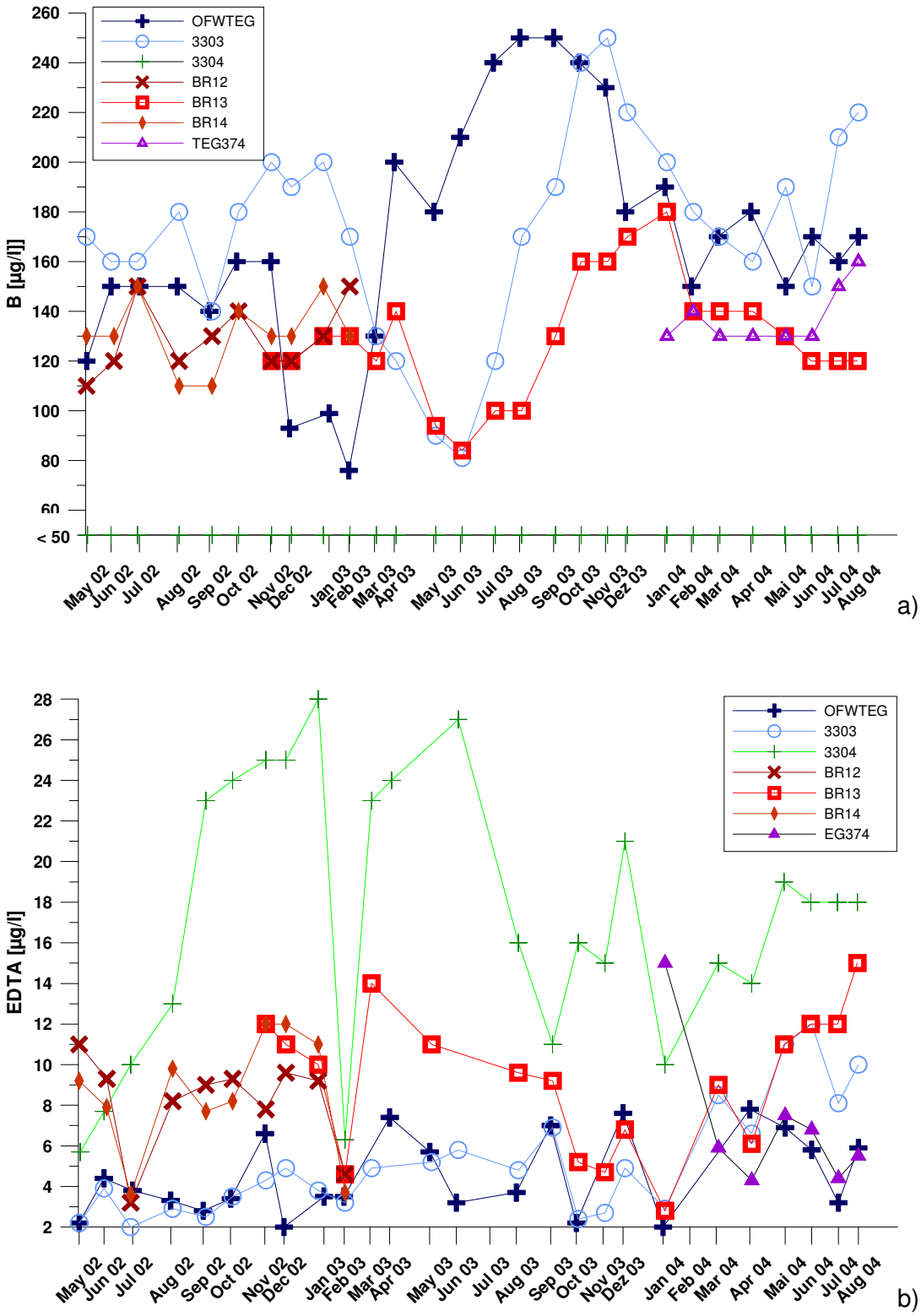

Figure 33: Time-series of δ18O (a) and K (b) in surface water, production wells and shallow observation wells 3303 & 3304 and deep observation well TEG374.

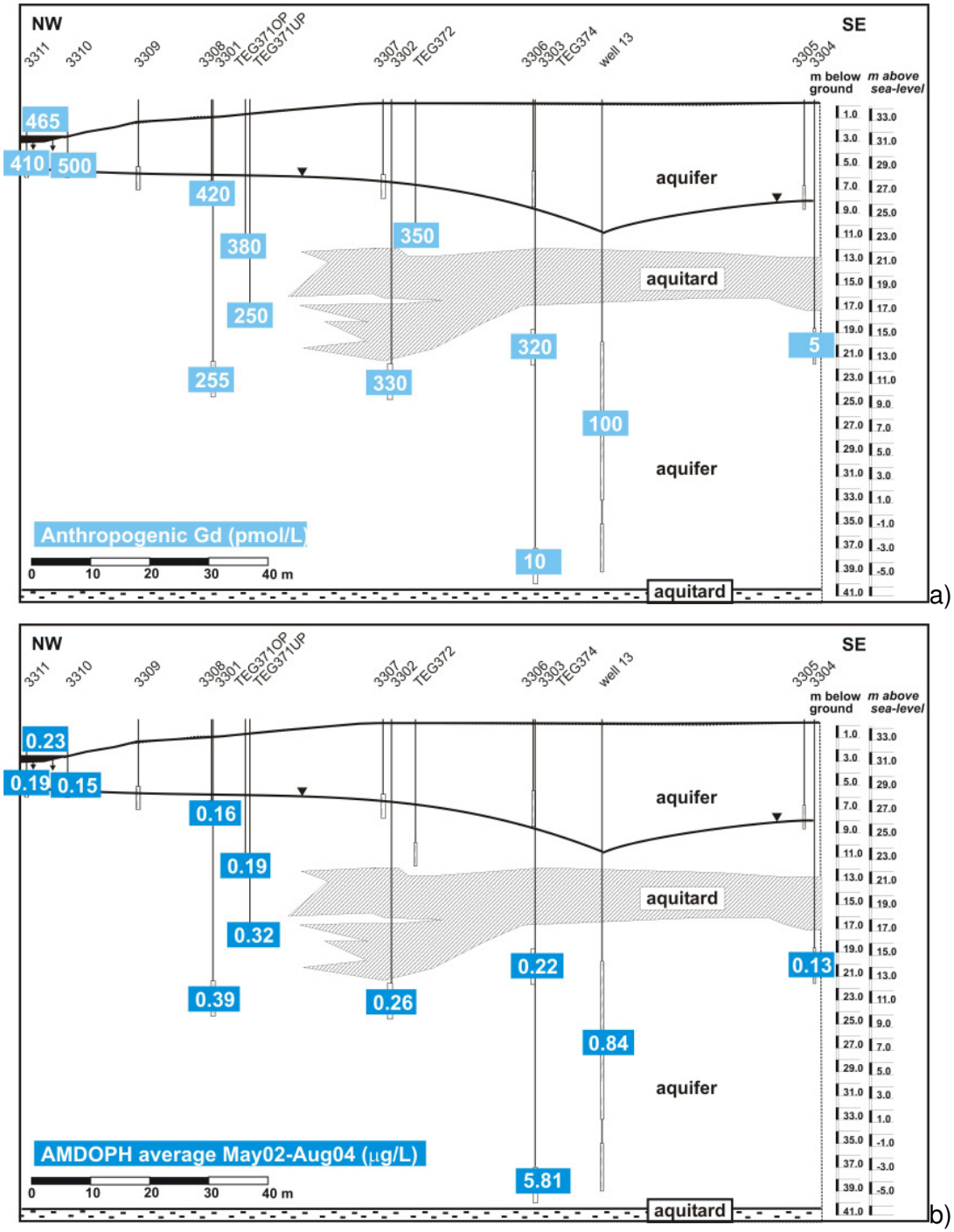

Figure 34: Average concentrations of Gd-DTPA (a) and AMDOPH (b) in wells at the transect Tegel.

Several facts indicated that the samples from the production wells (red colours in figures 27, 28) are not only a mixture of bank-filtrate encountered in the shallower parts of the aquifer (represented by observation wells 3301-3303; blue colours in figures 27, 28) and water from inland of the production wells (represented by observation well 3304; green colours in figures 27, 28).

1. The effective T/He age of 12.7 years of well 13, which is even older than the age of 3304 (11.9 years).

2. The fact that seasonal variations of all tracers in the production wells are rather small.
3. Most importantly: The fact that the production wells strongly differ from the “young” bank filtration wells with regard some of their minor water constituents. For example, some PhAC’s, namely AMDOPH (figure 29a) and Phenazone are present in higher concentrations than in today’s surface water, while others, for example Gd-DTPA (figure 29b) and Carbamazepine are present in much lower concentrations which cannot be explained by mixing of bank filtrate with background groundwater.

With the installation of the deep observation well TEG374 reaching the base of the aquifer it became clear that the deeper BF strongly differs from the shallow BF in some respects. Like the production wells, the seasonal tracer variations in the deeper groundwater are small, while the T/He age was 25 years. The concentrations of the minor water constituents mentioned under point 3 above differ even more strongly from the remaining wells. While the concentrations of AMDOPH (figure 29a) and Phenazone are even higher in TEG374 than in the production wells, the concentrations of Gd-DTPA (figure 29b) and Carbamazepine are very low or below detection. Hence, AMDOPH which appears to behave like a conservative tracer can be used to calculate the percentage of deeper, older BF in well 13 (~11 %). However, the time-series (figure 30) shows that the AMDOPH concentration in TEG374 also varies. In addition, the slight seasonal temperature variations indicate that TEG374 is not perfectly representative as an end-member for the deeper, old BF (assuming that this is decades old, it should not show any seasonal variations).

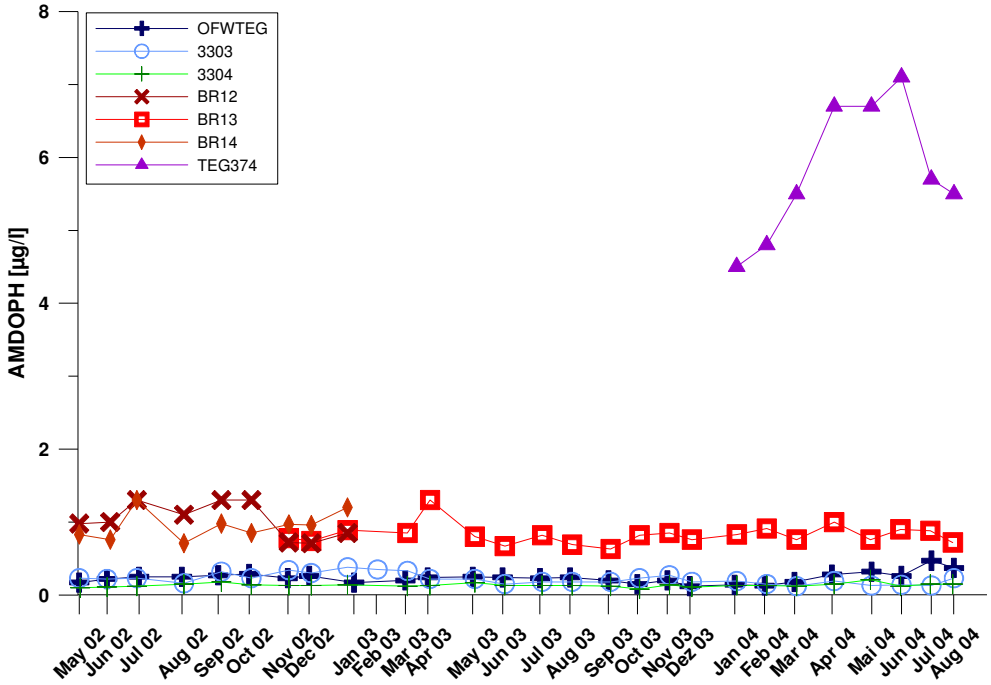

Figure 35: Time-series of AMDOPH in the production wells 12, 13 and 14, and the observation wells TEG374 (violet, deep BF), 3303 (light blue, shallow BF) and 3304 (green, inland) as wells as in Lake Tegel water (dark blue).

Therefore, with an average proportion of total BF of 58-69 % and an average proportion of deep, “old” BF of 11 %, an average of 47-58 % of the water in well 13 would be “young” BF, originating from the nearest shore in front of the transect.

All groundwater observation wells with the exception of the very deep TEG374 contain practically only (> 95%) young bank filtrate which infiltrated at the nearest shore which becomes apparent in the virtually undamped tracer breakthrough amplitudes (except of course for temperature) and the fact that the average concentrations for all non-reactive minor water constituents (e.g. AMDOPH) are similar to those of the lake. As mentioned above, 3301 and TEG371UP differ slightly from the remaining wells with regard to their T/He age which is slighly larger and also with regard to the concentrations of B or other tracer. Using average AMDOPH data to calculate the proportion of deep „old“ bank filtrate (represented by TEG374) in 3301 would result in a value of 3 %, for TEG371 the percentage would be even lower. The calculation is based on the presumption that TEG374 is an end-member with regard to the deep, old BF.

Even though all of these calculations can not be precise due to the given limitations, they nevertheless give an idea on the order of magnitude of mixing proportions that can be expected.

1.4.7 Hydrochemistry at the transect

In terms of the hydrochemical properties at the transect, redox changes during infiltration are of particular importance, since they cause the appearance of the undesired metals Fe^{2+} and Mn^{2+} (BOURG & BERTIN, 1993), influence the behavior of a number of organic pollutants such as pharmaceutically active substances (HOLM et al., 1995), halogenated organic compounds (BOUWER & MCCARTHY, 1993; GRÜNHEID et al., 2004) and effect the pH and calcite solution capacity (RICHTERS et al, 2004).

Generally at Tegel, the deeper the well, the more reducing it is. In addition, wells located underneath the lake tend to be more reducing the further out into the lake they were installed. The observation wells from the upper aquifer above the till contain oxygen throughout most of the year while the deep observation wells are mostly anoxic or more precisely ferrous. Boxplots of the redox indicators are shown in figure 31. They show that the median of oxygen and nitrate is larger in the shallow observation wells than in the deeper observation and production wells, whereas these contain more ammonia, manganese and iron.

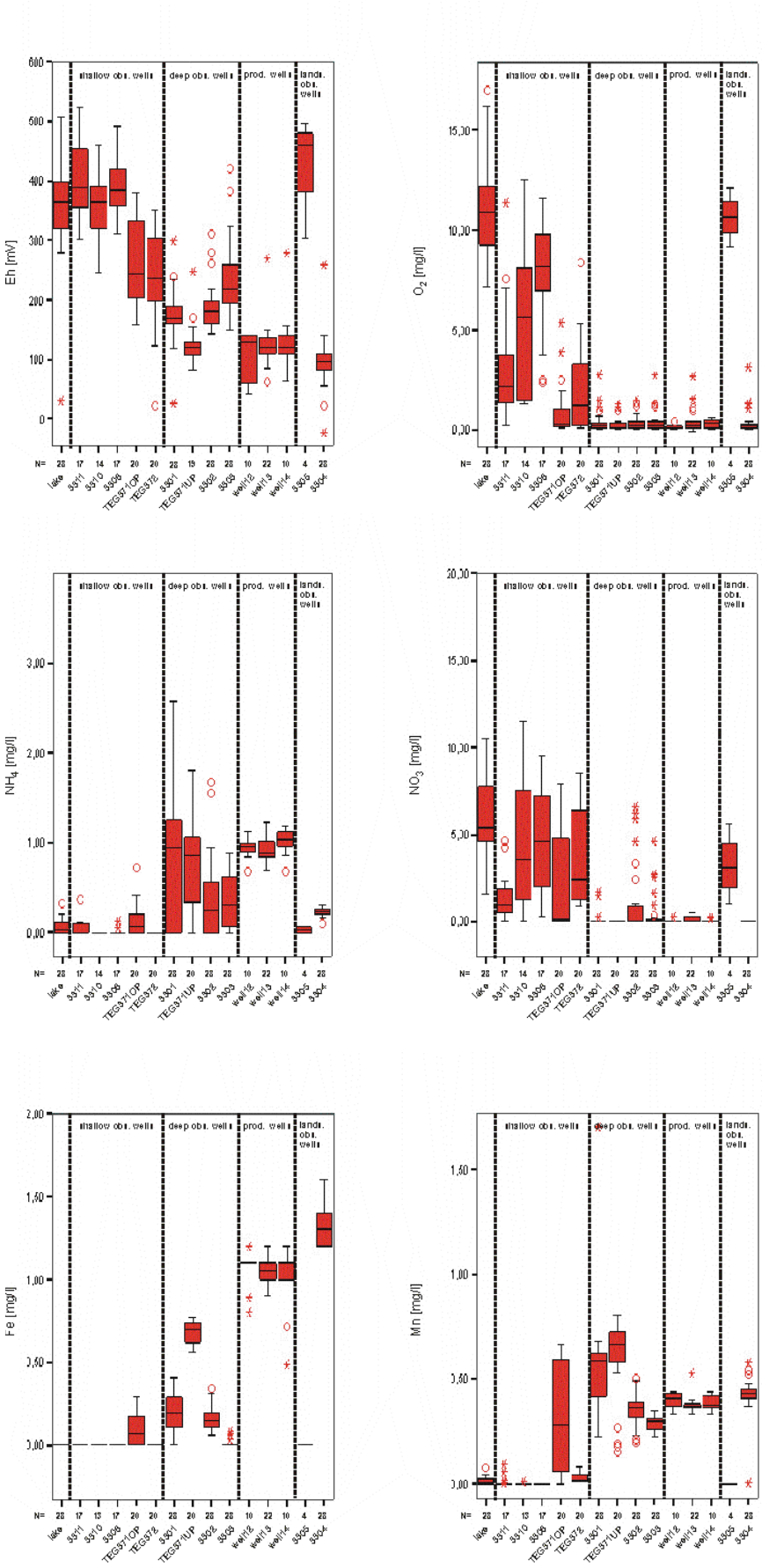

Figure 36: Boxplots of redox indicators Eh, O_2, NO_3^-, NH_4^+, Mn^{2+} & Fe^{2+} at the transect Lake Tegel. Data from May 2002-August 2004, N = number of samples for respective well.

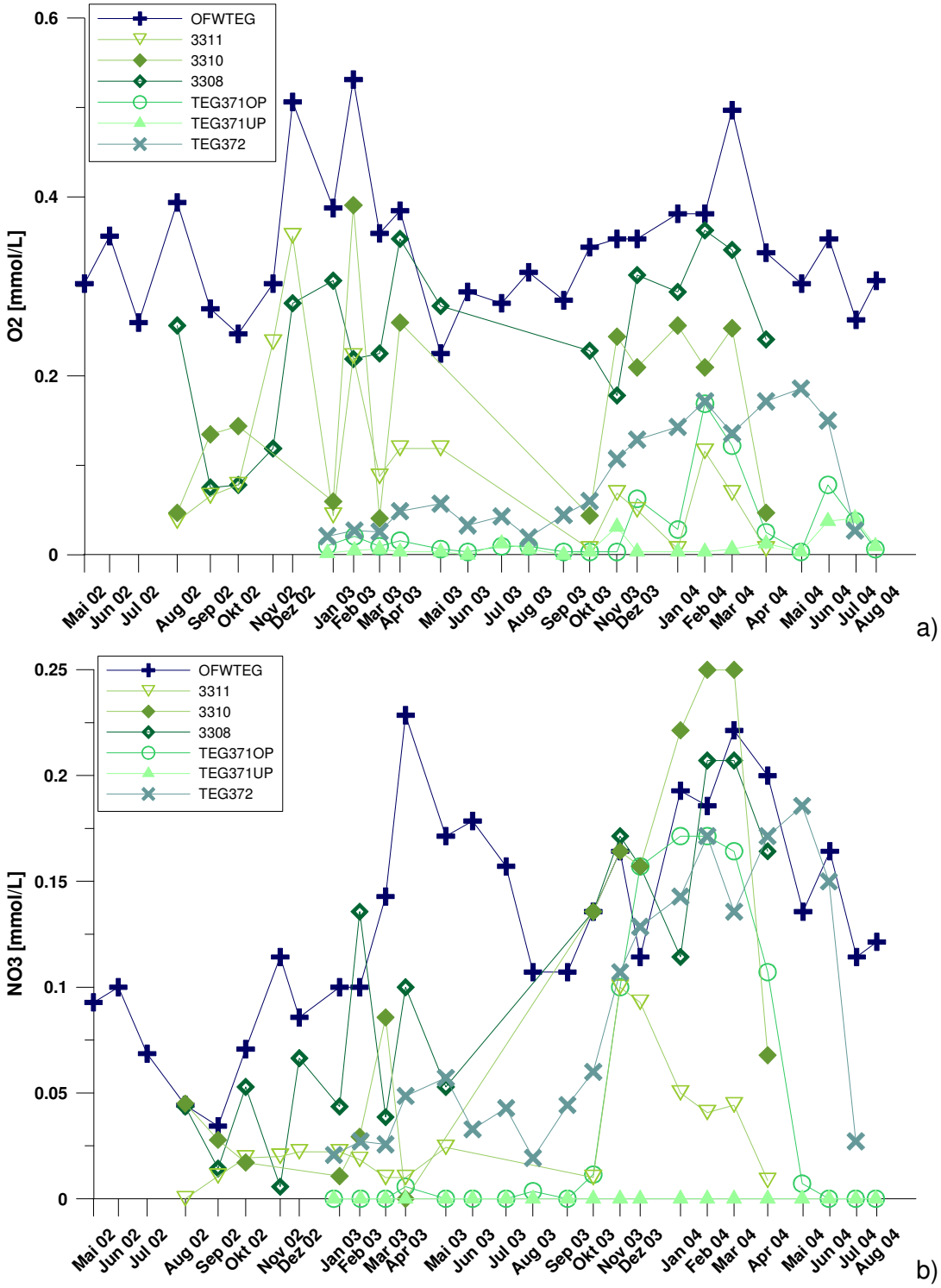

Figure 37: Oxygen and nitrate concentrations in the lake and the shallower observation wells at Transect Tegel. Data source: BWB.

However, the redox zones are not immobile and redox boundaries move seasonally. The younger bank filtrate (age < 5 months) undergoes strong seasonal temperature changes of up to 25 °C, depending on the distance from the lake. Because redox processes are microbially catalysed, these changes lead to differences in microbial activity (e.g. DAVID et al., 1997; PROMMER & STUYFZAND, 2005). As a result, oxygen and nitrate largely disappear in the very

shallow observation wells which do not fall dry at times when temperatures are highest (summer or autumn, depending on the respective time lag to the well). For some reason, nitrate concentrations in winter 2003/2004 were much higher in the shallow observation wells than in the previous year, even exceeding the concentrations in the lake itself (figure 32b).

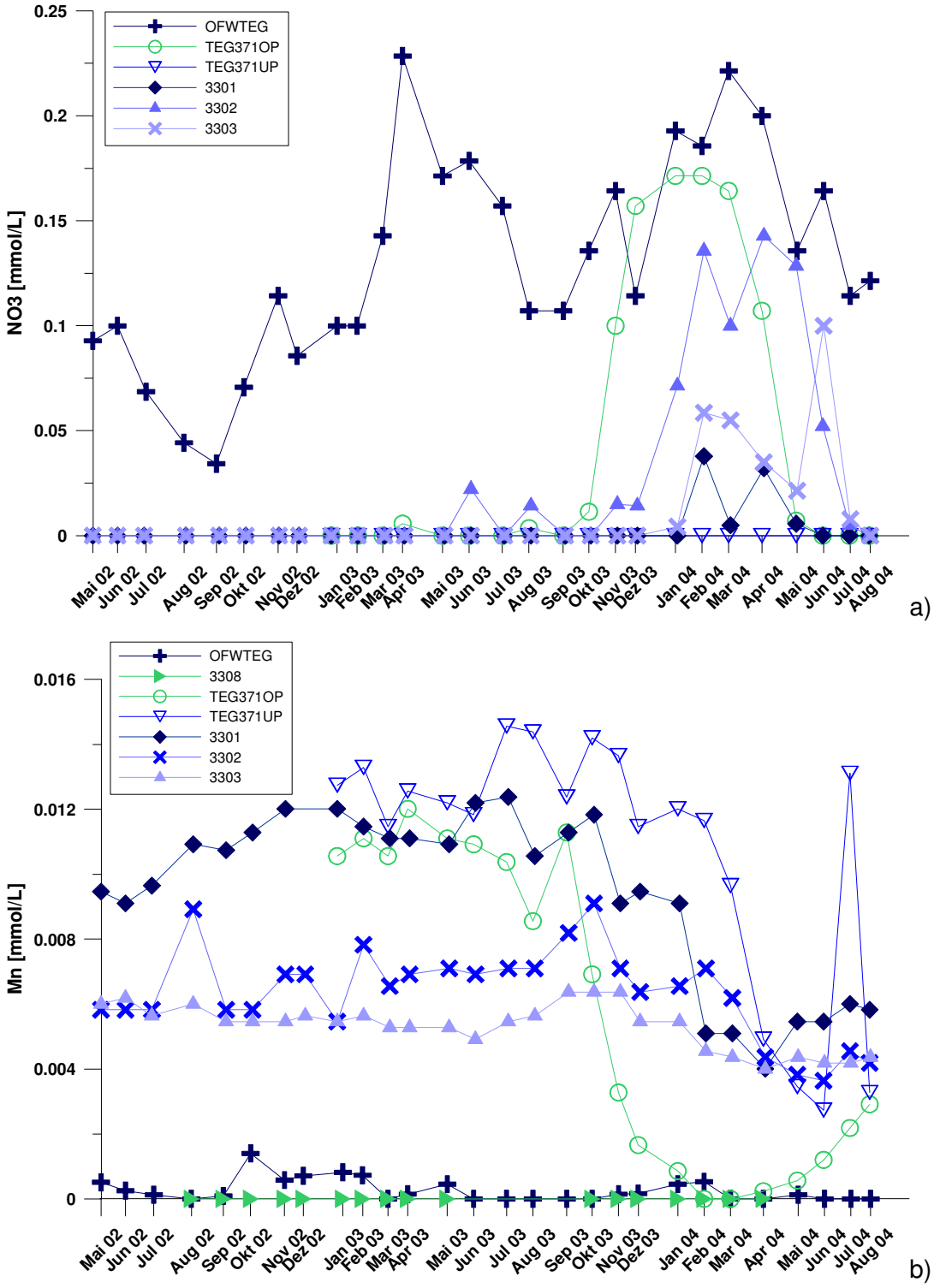

Figure 38: Time-series of nitrate and manganese in the deeper observation wells (and lake and the shallow wells 3308 and TEG371OP for comparison)

In addition, unlike in the previous years (FRITZ, 2002), nitrate was found to break through (with the respective time lag) into the deeper observation wells 3301, 3302 and 3303 (figure 33a), while manganese (figure 33b) and iron concentrations decreased at the same time. This shift of the redox zones towards less reducing conditions is probably related to the extreme drawdown in summer 2003, which exceeded the "normal" drawdown of previous years of about 3 metres. Another factor could be the fact that travel times have generally decreased from summer 2002 to summer 2003. None of these changes had any effect on the DOC concentration. Because of the time-lag, the effects are seen much later in winter 2003/2004. Redox zones as characterised by the disappearance of reactants (oxygen, nitrate, sulphate) or the appearance of reactants (iron, manganese) as suggested by CHAMP et al. (1979) were drawn into figure 34 for summer 2003 and winter 2004. Teg371UP tends to be more reducing than 3301 or 3302, probably due to locally deviating sediment properties (hydraulic conductivities and/or organic carbon content).

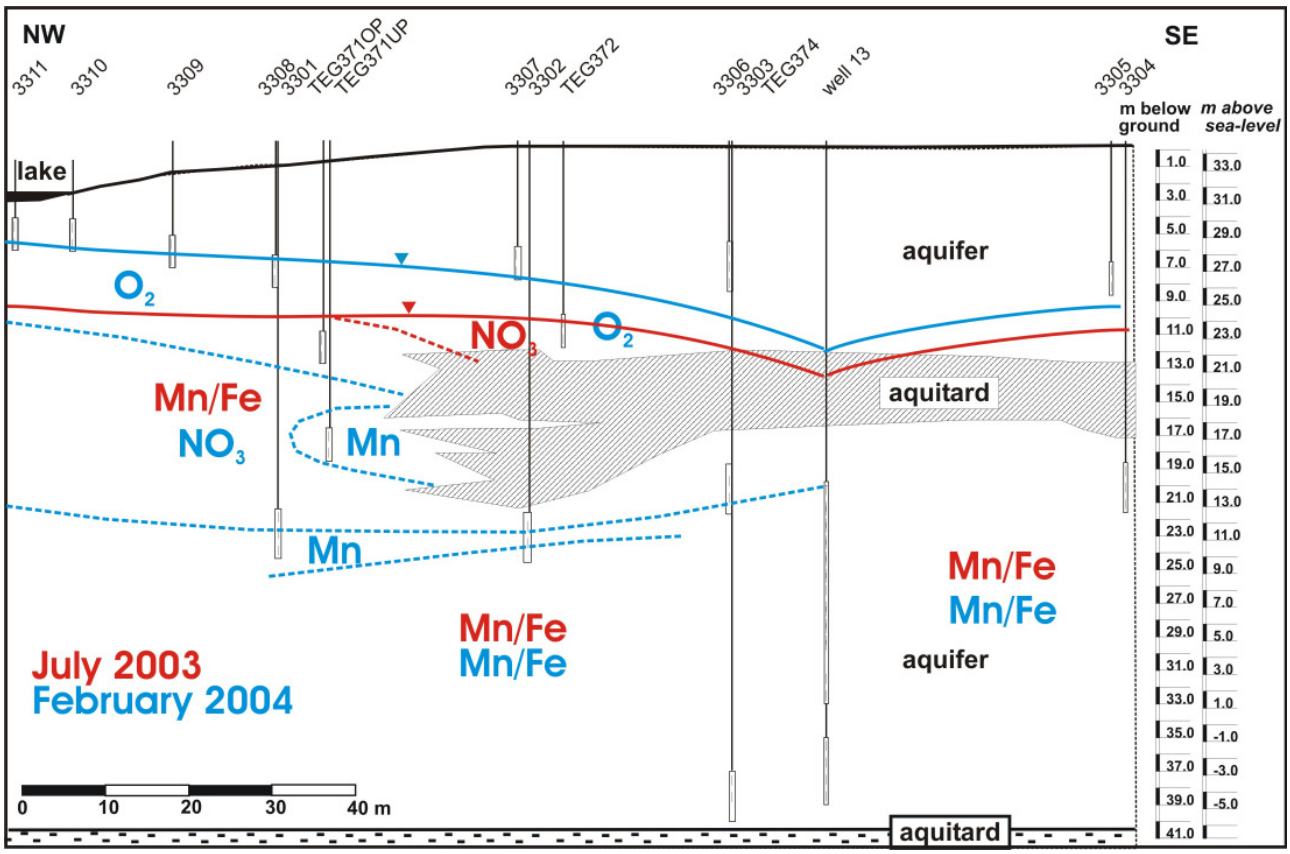

Figure 39: Approximate redox zoning as indicated by presence O_2, NO_3^-, Mn^{2+} and Fe^{2+} in July 2003 and February 2004.

The sulfate concentrations of the lake and the BF observation wells between lake and production well largely resemble each other with respect to sulfate concentrations and isotopic composition of sulfate (figure 35). Hence, a sulfidic redox milieu is never encountered. Only the sulfate concentrations of the deep observation well TEG374 appear to be a little lower at

times. In addition, the isotopic concentration of sulfate of TEG374 is slightly higher (the sulfate is heavier), which is an indicator for commencing sulfate reduction.

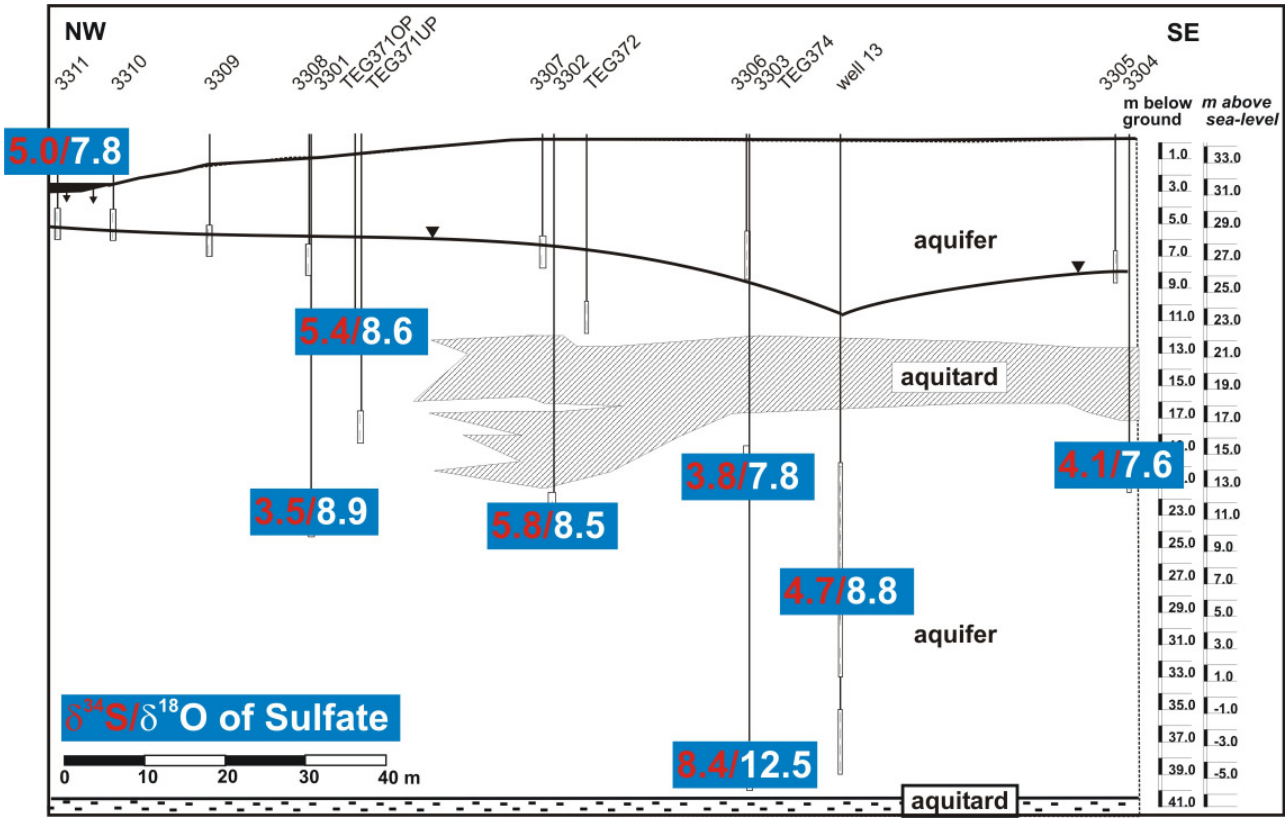

Figure 40: $\delta^{18}O$ [‰ vs. SMOW] and $\delta^{34}S$ [‰ vs. CDT] of sulfate from July 2004.

1.4.8 Major conclusions and summary Lake Tegel site

Surface water

- Lake Tegel is under the influence of Upper Havel water entering the lake from the south and treated WW from the WWTP Schönerlinde, which is discharging its effluent into the Nordgraben ditch.
- Evidence of elevated proportions of WW are elevated concentrations of WW indicators such as Cl^-, Na^+, SO_4^{2-}, B, DOC or Gd-DTPA, high temperatures (in winter) and more negative isotopic signatures and is most evident near the outlet of the surface water treatment plant (OWA).
- The surface water sampling point in front of the transect is sufficiently representative for the local surface water providing the source for the bank filtrate near the transect. The spatial variation of the surface water quality is relatively small.
- In average, the surface water in front of the transect contained approximately 21 % of treated WW between May 2002 and August 2004.

Sediments / clogging layer

- Bank filtration mainly takes place near the lake shores, which is why sulfate concentrations of the bank filtrate resemble those of the surface water, despite the fact that sulfate is quickly reduced in the laccustrine sappropels covering the lake base.
- Modelling of a sulfate profile gave a fitted first-order constant for sulfate reduction in the uppermost 10 cm of the mud sediments profile is 1.49×10^{-7} s^{-1}. This value is 7.5 times higher than the fitted constant of 2.0×10^{-8} s^{-1} for the following section, 10-40 cm below the mud surface, which is expected to be a function of variations in the types of organic matter rather than variations in the total organic carbon content.

Travel times

- The most useful tracer for travel time evaluation are stable isotopes, B and the temperature, for which a retardation factor of 2 is appropriate. Using wastewater indicators does only work if they show clear minima or maxima, which is not always the case. Even though the concentrations within the lake are more stable than for example at Lake Wannsee, some difficulties concerning the input signal remain. Using stable isotopes and temperatures, which are largely (even though not entirely) independent of the WW input and show clearer seasonalities is less problematic.
- The vertical age stratification of the bank filtrate within the quaternary aquifer is large.
- The shallow and semi-deep observation wells between the lake and the production well abstract mainly “young” bank filtrate of an age of a few months.
- The deepest observation well screened at the bottom of the aquifer contains “old “ bank-filtrate that is decades rather than months old, probably originating from infiltration zones further west.
- The travel time of the bank-filtrate to well 13 on the shortest pathway is 4-5 months.
- The travel times have decreased in 2002/2003 compared to 1998/1999 (FRITZ, 2002).

Mixing

- The most useful tracers for mixing calculations are stable isotopes, EDTA, B & K.
- The T/He age dating results, in combination with a lack in seasonality in the production wells, (and some chemical data) suggest that the production wells abstract a mixture of young bank-filtrate (several month old; 47-58 %), older bank-filtrate (decades old; 11 %), background groundwater (from inland of the well gallery; 31-42%) and possibly even a very small proportion of deeper groundwater from the underlying next aquifer.

- The background groundwater characteristics changed in 2003 (rising EDTA, δD and $\delta^{18}O$ values). The changes probably have to do with greater strain on gallery West, but exact origin is not certain.

Hydrochemistry

- All shallow wells contain oxygen throughout most of the year, while the deeper observation wells are generally post-oxic or, more precisely, ferrous as classified by BERNER (1981).
- The very deep parts of the aquifer show first signs of sulfate reduction.
- As it is the case at all other sites, the redox zones are transient. Variations are due to the seasonally varying microbial activity caused by the temperature changes and by hydraulic factors such as decreasing travel-times. In summer, higher temperatures generally lead to more reducing conditions, while winter conditions are less reducing. The differences may print through along the transect with a time-lag of several months in accordance to the travel times.

1.5 Hydrogeological Results Lake Wannsee Bank Filtration Site

The Wannsee bank filtration site consists of 2 transects running between the lake and well 4 and well 3 of the production well gallery Wannsee of the water works Beelitzhof (Figure 41). The second transect perpendicular to the adjacent production well 3 was constructed because previous studies could show that the proportion of bank filtrate in the production well 4 of the older transect 1 is particularly low. Altogether, 11 piezometers with a maximum depth of 25 m have been constructed within NASRI (see Figure 68 and Figure 69 for schematic cross sections).

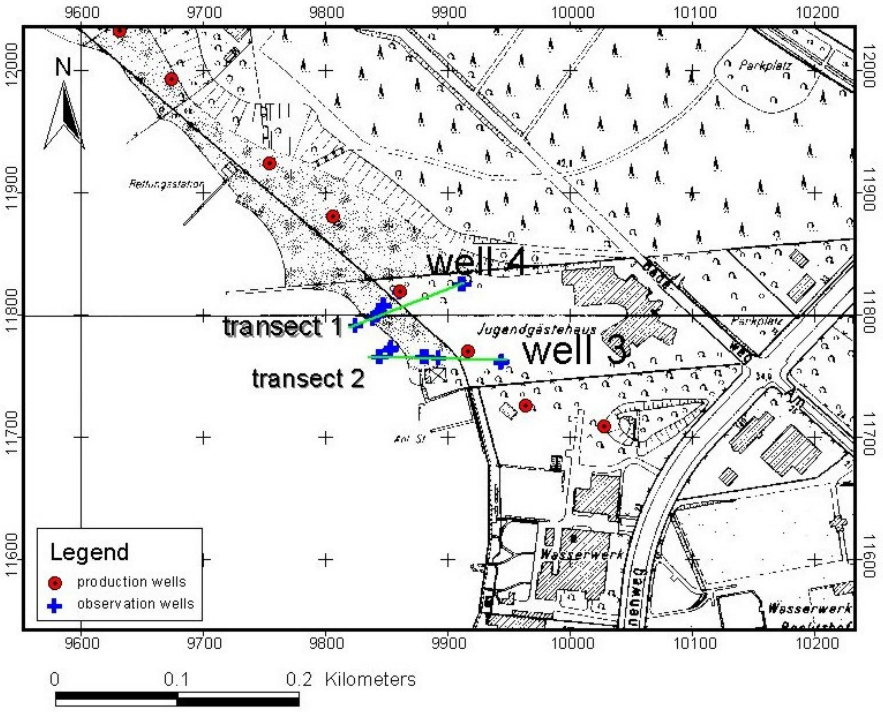

Figure 41: Location of the bank filtration transects 1 and 2 north of the water works Beelitzhof in southwest Berlin.

1.5.1 Surface water investigations

Lake Wannsee is an area where water from the Lower Havel (Unterhavel) with a comparatively low percentage of treated wastewater (WW) and Teltowkanal water with a rather high load of treated WW meet (Figure 42). The Teltowkanal water flows northwards through a chain of lakes ("Kleine Wannsee-Seenkette") into Lake Wannsee. In a surface water sampling campaign in 2001/2002 (Richter, 2003), samples were taken from the Upper and Lower Havel area within Berlin. Chloride (Cl^-) and Boron (B) concentrations of the relevant lower Havel, the Teltowkanal and lake Wannsee itself are shown in Figure 42, illustrating that the lake is a mixture of both sources. The figure also shows that the temporal variations in Cl^- and B concentrations are rather large. The results of Richter (2003) also indicate that the

transects are clearly under the influence of Teltowkanal water (compare figure 3, report part 1/Tegel).

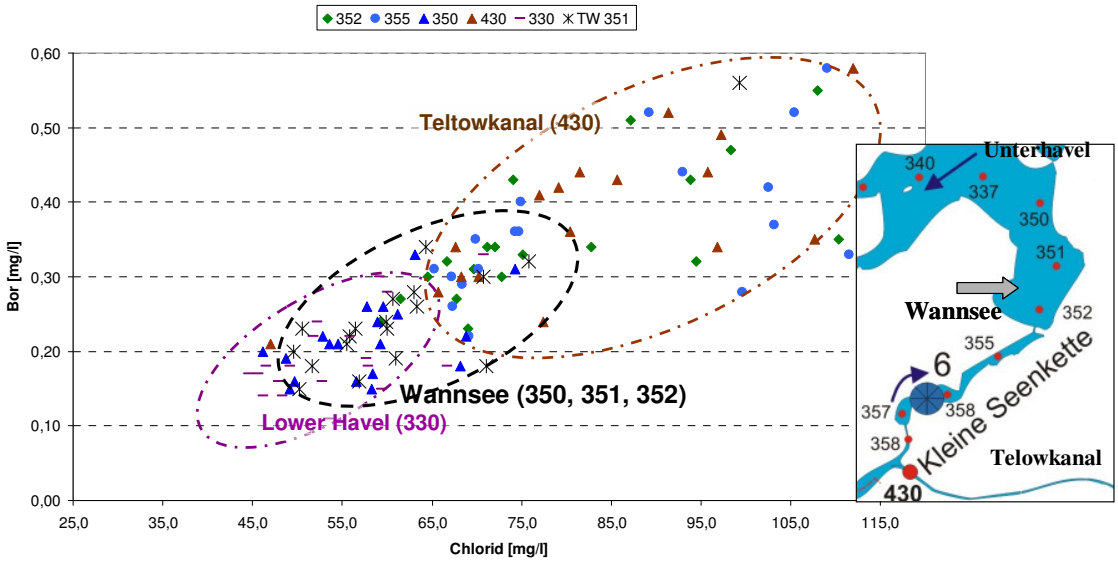

Figure 42: B versus Cl- in the lower Havel, the Teltowkanal and Lake Wannsee (data from 2001-2002; Richter, 2003).

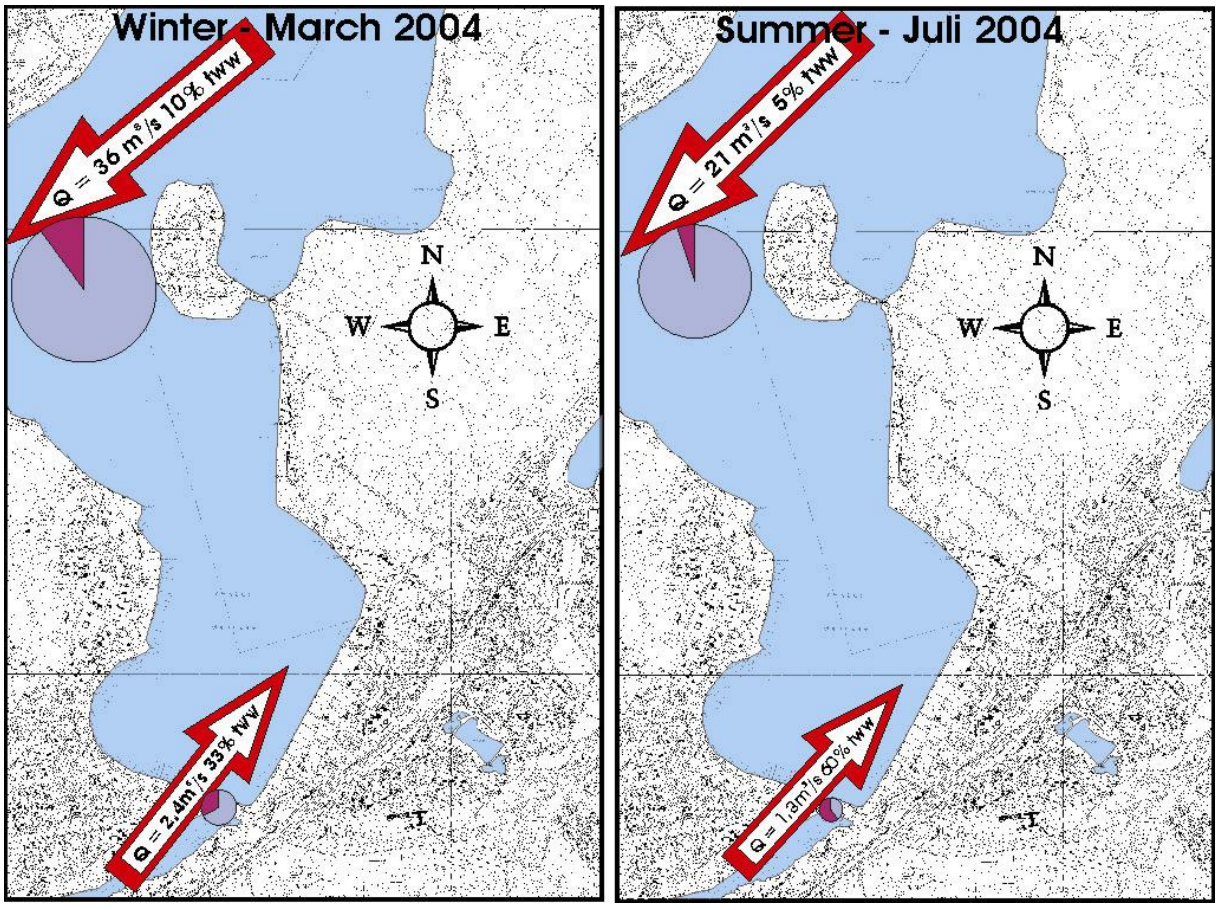

Figure 43: Compared proportions in summer and winter of the surface water runoff of lower Havel and "Kleine Seenkette" and their content of treated wastewater (TWW) (data source: wawimon/SenS & bwb).

Two surface water sampling campaigns were conducted during NASRI at Lake Wannsee in order to get an idea of the spatial variation of the concentration of relevant water constituents within the lake in summer and winter (March and July 2004). Figure 43 shows the monthly discharge of the lower Havel measured at the Frybrücke and Stössenseebrücke and of the "kleine Seenkette" at Alsenbrücke and the calculated proportion of treated wastewater in the corresponding water body during the time of sampling (March and July 2004). Because the WWTP Ruhleben discharges into the Teltowkanal in summer (between April and September), while it discharges into the Spree in winter, the percentage of wastewater in the Teltowkanal is considerably higher in summer. The proportions of treated wastewater were calculated as percentage of WWTP discharge of the total discharge at the respective gauging station (evaporation and abstraction disregarded). More detailed calculations for previous years were done by Schuhmacher & Skripalle (1999).

The distribution of electrical conductivities [µS/cm] and $\delta^{18}O$ [‰ vs. V-SMOW] in the surface water are shown as an example for March 2004 (Figure 44). High electrical conductivities and low $\delta^{18}O$ values are indicators for elevated WW proportions in the surface water (Knappe et al., 2002; Massmann et al., 2004). Figure 44 illustrates that at the time of sampling, the Teltowkanal water flowed north along the eastern lake border, with the largest WW concentrations present at this lake site. The lake is subject to relatively large spatial variations as a function of the mixing between lower Havel and Teltowkanal water. Figure 44 also clarifies that the surface water right in front of the transects shows a particularly large variability of the electrical conductivity and the $\delta^{18}O$ values. This constitutes a problem, because only one surface water sample was taken during NASRI sampling each month (in front of well 4), which is therefore not necessarily representative for the entire bank-filtration source. This may explain why the time-series of several potential tracer in the shallow observation wells within the lake show peaks appearing earlier than in the lake's time-series (e.g. TEG205 and TEG206, Figure 45). Because the transects are located in an area subject to large concentration gradients within the lake, 50 m further south concentrations may already be very different. In addition, transect 2 is not orientated perfectly perpendicular to the flow direction and it may receive water from 100 m further SE of the surface water sampling point.

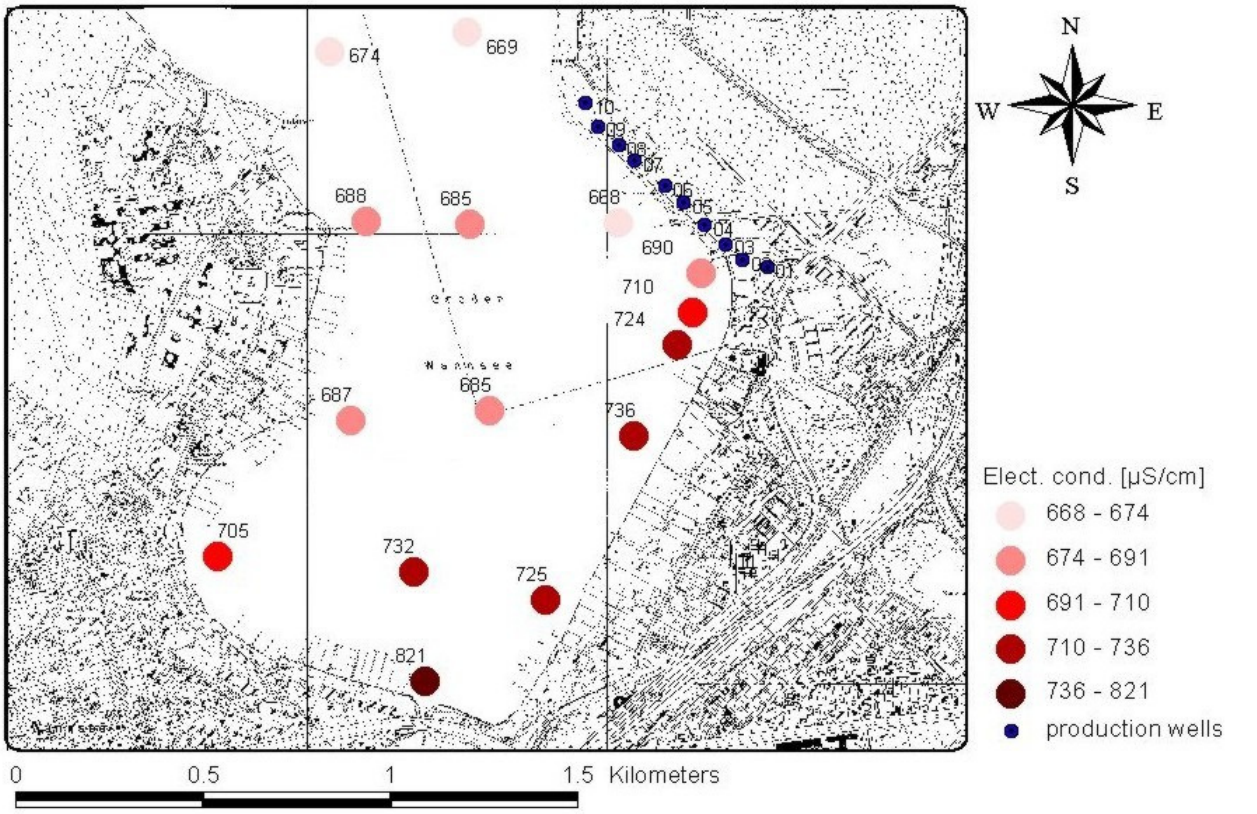

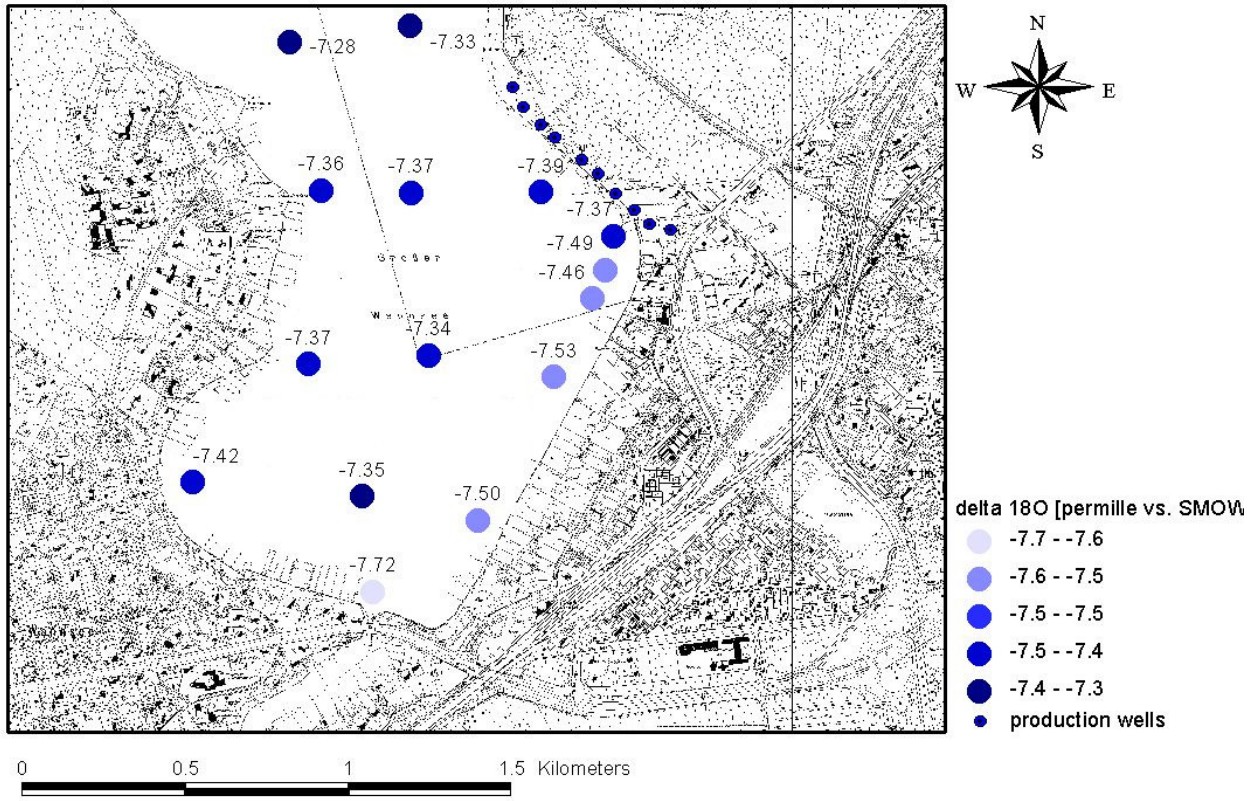

Figure 44: Electrical conductivity [µS/cm] and $\delta^{18}O$ [‰ vs. SMOW] in the surface water (sampling depth 0.2 m) in March 2004.

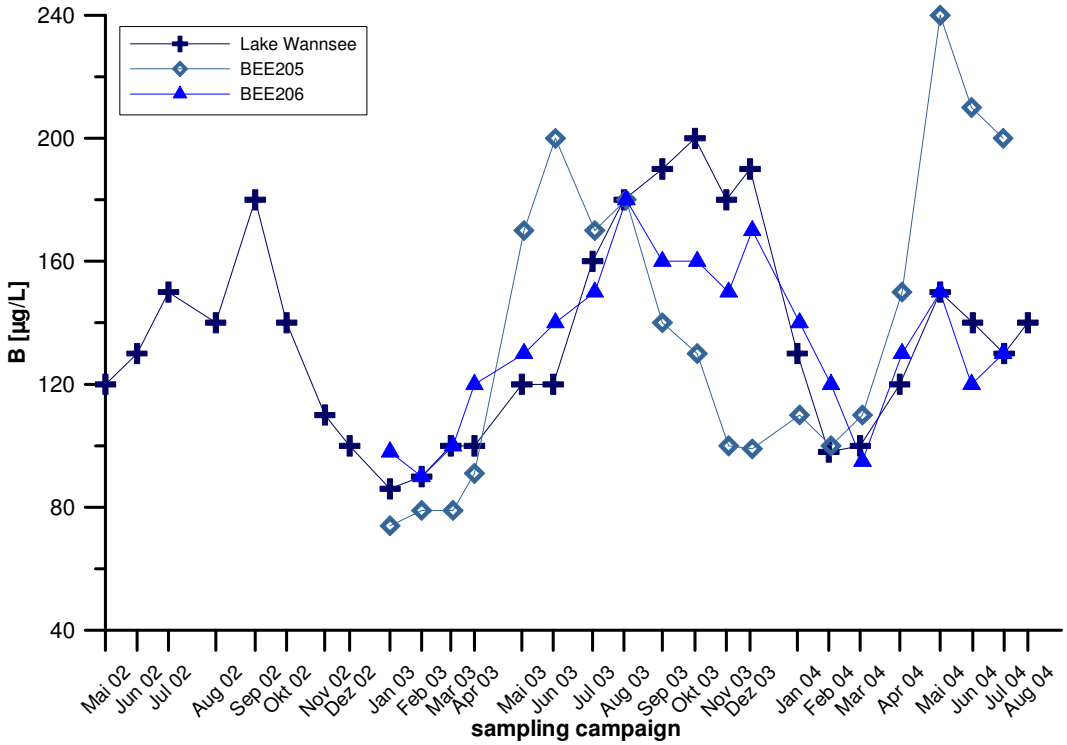

Figure 45: Time-series of boron (B) in shallow observation wells below the lake of transect 2. Dark-blue curve represents surface water sample (data source: BWB).

The northward flow direction of Teltowkanal water along the eastern lake border was not observed in July 2004. Exemplary comparison of temperature, electrical conductivity and MTBE distributions in the lake in March and July shows that in July, the electrical conductivity and the concentration of MTBE (and also: Cl^-, K^+, B, not shown) appear to be even higher along the western lake border. This may be caused by the fact that the various boat harbours at the eastern lake border are diffuse contaminant sources and may increase the concentration of these substances. Another possibility is that the flow patterns are temporarily different. Winter temperature differences of almost 5 °C between the warmer Teltowkanal and the colder Havel water may cause the warmer water to flow on top. The sampling of the uppermost 0.2 m of the water column may thereby also not be representative for the entire water column.

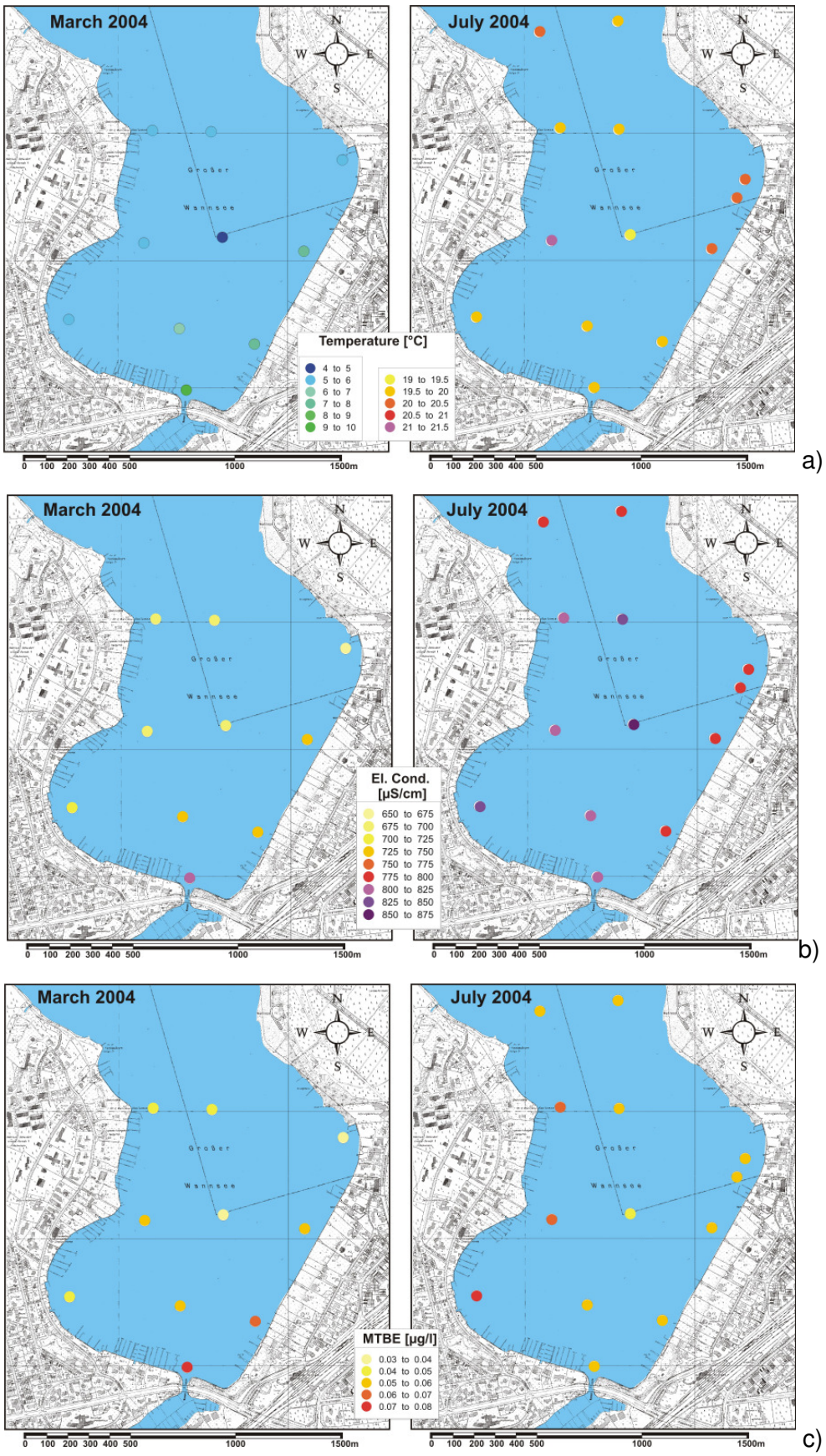

Figure 46: a) Temperature [°C]; b) electrical conductivity [µS/cm] and c) MTBE [µg/L] in the surface water in March (left) and July (right) 2004 at a depth of 0.2 m.

Figure 46 also illustrates that the electrical conductivity is generally higher in July than in March, owing to the seasonal influence (more dilution with natural discharge in summer) leading to the fact that the proportion of WW is higher in summer. The seasonal influence becomes clearest in the time-series of WW indicators (Figure 47). The very wet summer 2002 differs from the dryer summer 2003, which is why Cl^-, Na^+ (not shown), K^+ and electric conductivity do not show the typical summer peak in 2002. Only EDTA (not shown), B and mainly the stable isotopes showed the expected peaks in summer 2002. The isotopic signal is more or less independent on the dilution with treated WW and a function of the temperature during the formation of the precipitation only, which is why the always show a seasonal effect. It is unclear why the time-series of the tracer differ from each other.

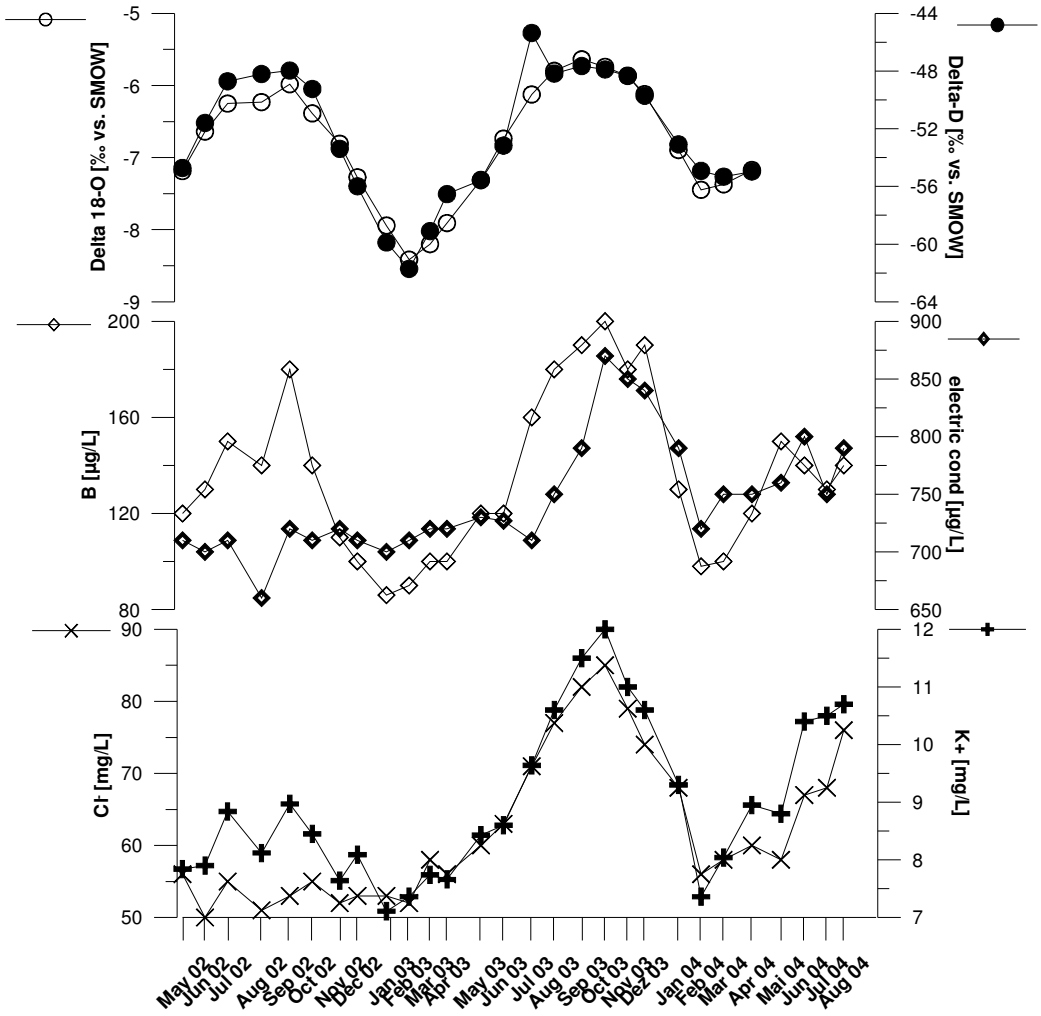

Figure 47: Stable isotope values, electrical conductivity, Cl^-, K^+, B and in the surface water of Lake Wannsee (data source: AWI & BWB).

1.5.2 Clogging layer

Figure 48 displays a geological cross-section at the field site Wannsee (SenS, 2000), reaching a depth of down to 100 meters below the lake surface. The sediments are mainly sands incoherently interbedded with finer grained material, such as silts, clays and glacial tills. The

lake base is mainly made of laccustrine sapropels with a thickness of close to 20 m, which were deposited during the Holocene. These sediments have a low hydraulic conductivity, thereby restricting the infiltration capacity. Only the lake margins, where the water depth is less than a few meters, the lake is underlain by sands.

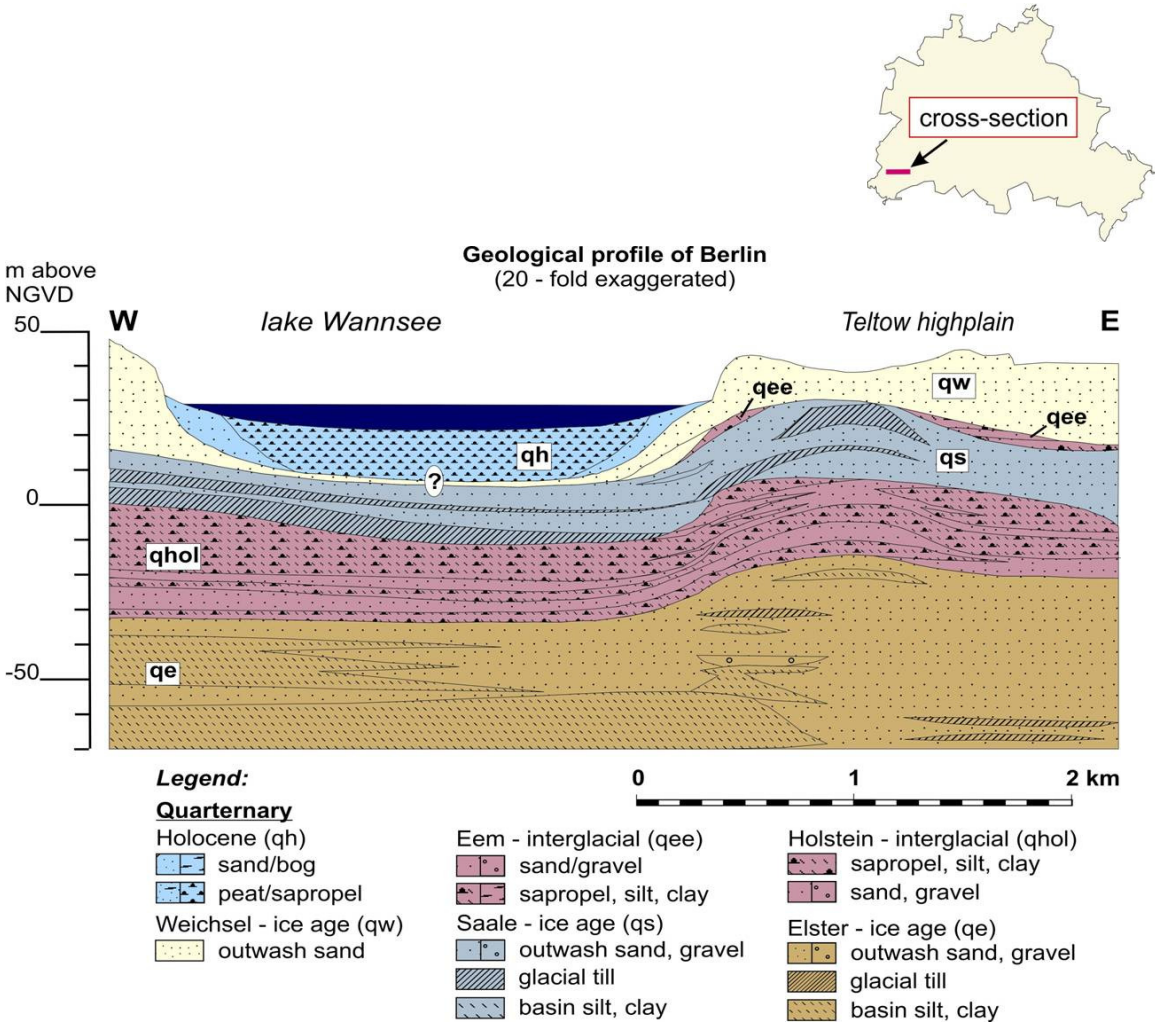

Figure 48: Geological cross-section of the Wannsee area in south-west Berlin (SenS 2000).

The presence, permeability, thickness and characteristics of the sediments covering the lake floor, i.e. the clogging layer, are of major importance for the behaviour of the entire bank filtration system, since they form the direct interface between surface water and groundwater. Several authors could show that the success of bank filtration schemes generally depends on microbial activity and chemical reactions which are mainly taking place in the very reactive clogging layer (Fritz et al., 2002; Hiscock and Grischek, 2002).

Because no previous detailed information existed at Lake Wannsee, the infiltration zone was investigated in greater detail. The investigations can be subdivided in 3 major parts:

1. Mapping of the infiltration zone with regard to the lithology, hydraulic conductivities and organic carbon content (including infiltration tests).
2. Drilling of several cores closer to the shore to determine the lithology as well as hydraulic and geochemical properties of the sediment in greater detail.
3. Column study with an undisturbed core from the lake shore to evaluate the hydrochemical changes directly at the surface water/ground water interface, in particular with regard to the redox chemistry.

Despite decreasing the infiltration capacity, the presence of the clogged sediments has two very positive effects: First, their relatively low permeability slows down the travel times from the lake to the well. Secondly, they are far more effective in removing contaminants than the unclogged sands of the aquifer because their adsorption and reduction capacities are larger owing to higher proportions of organic and/or fine grained material.

1.5.3 Mapping of the Wannsee lake sediments

Methods

The aim of the work was to map the extension of the area offshore of the relevant production wells at Lake Wannsee, in order to determine the extent of the zone where the surface water can infiltrate efficiently into the aquifer.

In August and October 2004, 180 disturbed sediment samples (Figure 49) were taken with a Van Veen-sediment dredge from a swimming platform at the grid points. Orientation on the lake was provided by several landmarks, so that each sampling place could well be fitted to the grid points. At each point, the recovered sediments were examined for the following criteria:

- grain size (finger test, DIN 4022)
- content of organic material (finger test, DIN 4022)
- colour

- shell content
- content of H_2CO_3 and H_2S (test with diluted HCl)

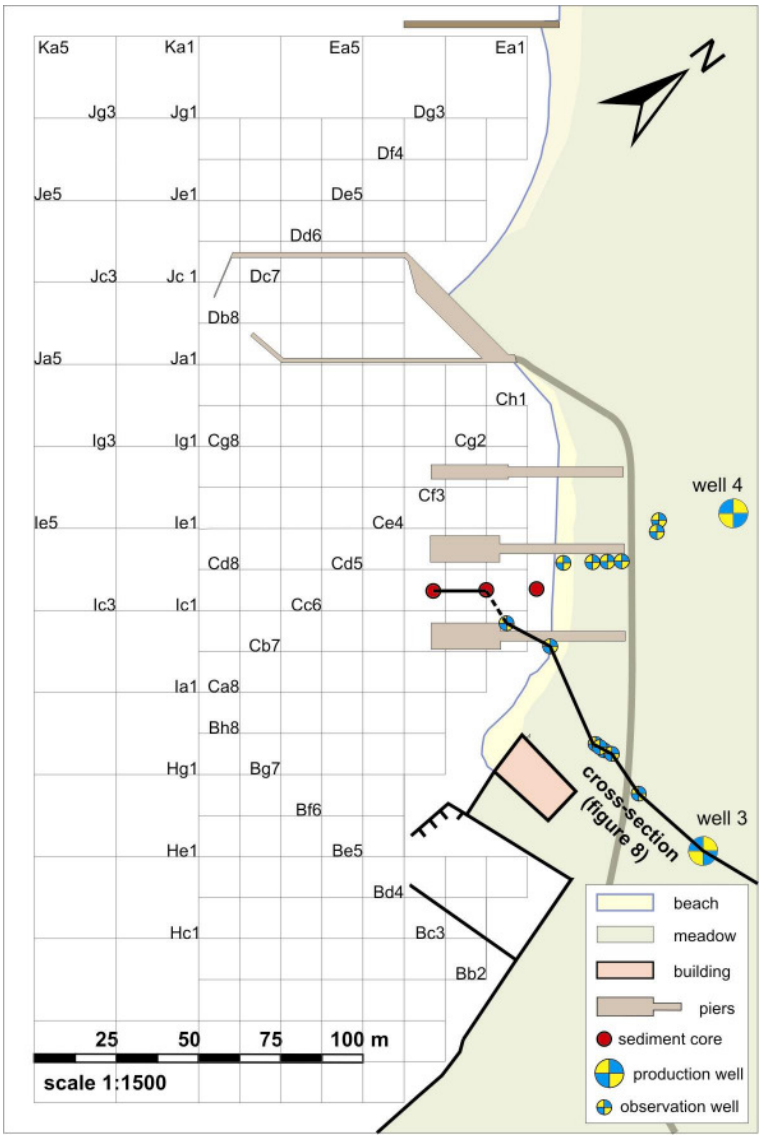

Figure 49: Sketch of the field site at lake Wannsee, showing the mapping grid in a 12.5 m raster (25 m outwards on the lake) with systematic naming of the grid points and the location of the cross-section presented in Figure 48.

In addition, the water depth was noted at each point by measuring the diving length of the dredge rope. The instability of the swimming platform inhibited the drilling of deeper cores by hammering or machine-driven methods. It was therefore not possible to map the thickness of the covering laccustrine sappropel layer.

Based on these findings, the sediments were classified according to the geopedological mapping instruction (AG Boden, 1996). In addition, the water depth was noted at each point by measuring the length of the dredge rope.

Grain-size distribution, which determines the hydraulic conductivity, as well as the organic carbon content, were determined in the laboratory with disturbed samples by sieving analyses, transient permeability experiments (Langguth & Voigt, 1980) and loss of ignition (for more detail see Nogeitzig, 2005).

Open-end tests were carried out in a narrow stripe along the bank of the lake (Figure 50). Tubes of PE material of one metre length were hammered softly 10 to 15 centimetres deep into the sediment. The volume of water (Q) seeping into the underground by gravity was monitored with a gauged flask and a stop watch in several intervals at each point and the hydraulic conductivity is calculated after Langguth & Voigt (1980).

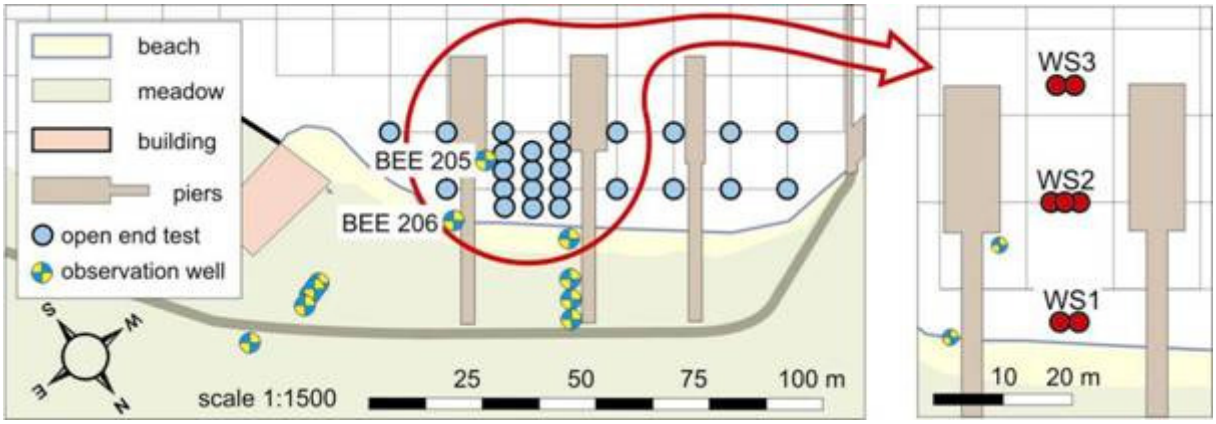

Figure 50: Infiltration experiments (open end tests) near the bankline of the lake (on the left), drilling places of the sediment cores taken for laboratory examinations (in detail on the right).

Results

Figure 51 displays the depth contours of the sediment surface below lake Wannsee. Within one hundred metres distance from the shoreline, the water depth is dropping from very shallow to more than eight metres where the sediment surface flattens out to a wide lacustrine basin, with maximum depths of about nine metres. Further in the northwest and in the southeast, the slope is less steep.

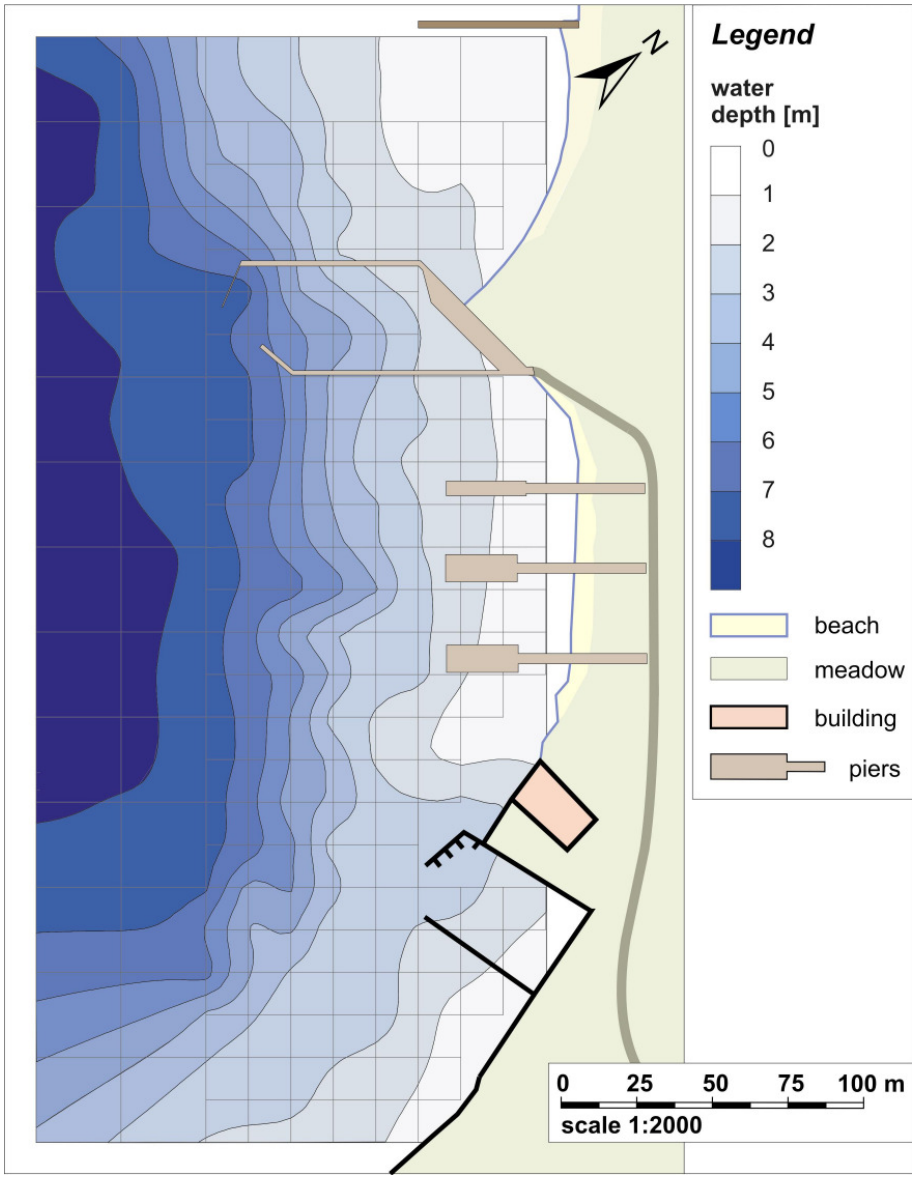

Figure 51: Map of the water depth in the field site at lake Wannsee.

The sediment samples of the mapping campaign are predominantly composed of fine grained sands with variable organic and inorganic carbon contents (Figure 52). In shallow water depths of down to two metres, the sands are coloured in light brown to greyish tones, and they are frequently covered by a film of green organic substances and interspersed with remnants of vegetation. Along with rising water depth from 2 to 6 metres, the colour of the sands is transiently changing from grey to darker olive-brown and dark grey tones. In a depth of more than 6 metres, their colour darkens to olive-black and black colours. The sands are generally getting finer grained with water depth. In a depth of more than 6 metres, fine grained sand sediments contain an increasing amount of silt. In a transitional depth between 6.5 and 7.5 metres, the sediments are composed of fine sand and silt in varying proportions, the latter dominates along with increasing water depth. In a depth of more than 7.2 metres, the packing density of the surface sediments changes from compact deposition to increas-

ingly lower packing densities. The granular structure is replaced by a watery, unconsolidated and non-granular structure of the sediments: At depths above 7 metres, laccustrine sapropels prevail.

With exception to the sand sediments in low water depths of < 2.5 metres, all samples contain minor amounts of sulphides, already noticeable by greyish colours. In depths to about 4.5 metres, the sands are settled by colonies of mussels which are a few centimetres thick. Along with rising depth, a layer of shells and detritus, increasingly crushed to finer fragments, replaces the mussel colonies. In depths exceeding 6 metres shells and shell detritus disappears; carbonate detritus of sand-grain size occurs within the sands on the sediment surface. The laccustrine sapropels contain carbonate in a fine-dispersed form.

The organic matter content (Figure 52) in the sands varies from 0.2 to almost 10 weight-percent with neither the presence of the mussel colonies, nor the water depth determining the amount of organic matter. The reason for the irregular distribution is possibly the depositional history of the sediments and the variable input of vegetation remnants from the land. In greater water depths, corresponding to the sedimentation of finer grained material, the amount of organic matter increases to values of regularly more than 10 weight-percent. The silty sediments mixed with laccustrine sapropels contain more than 10 weight-percent of organic matter (mostly > 15 weight-percent). The maximum content detected at the field site is 25.7 weight-percent in a loose, watery and unconsolidated laccustrine sapropel.

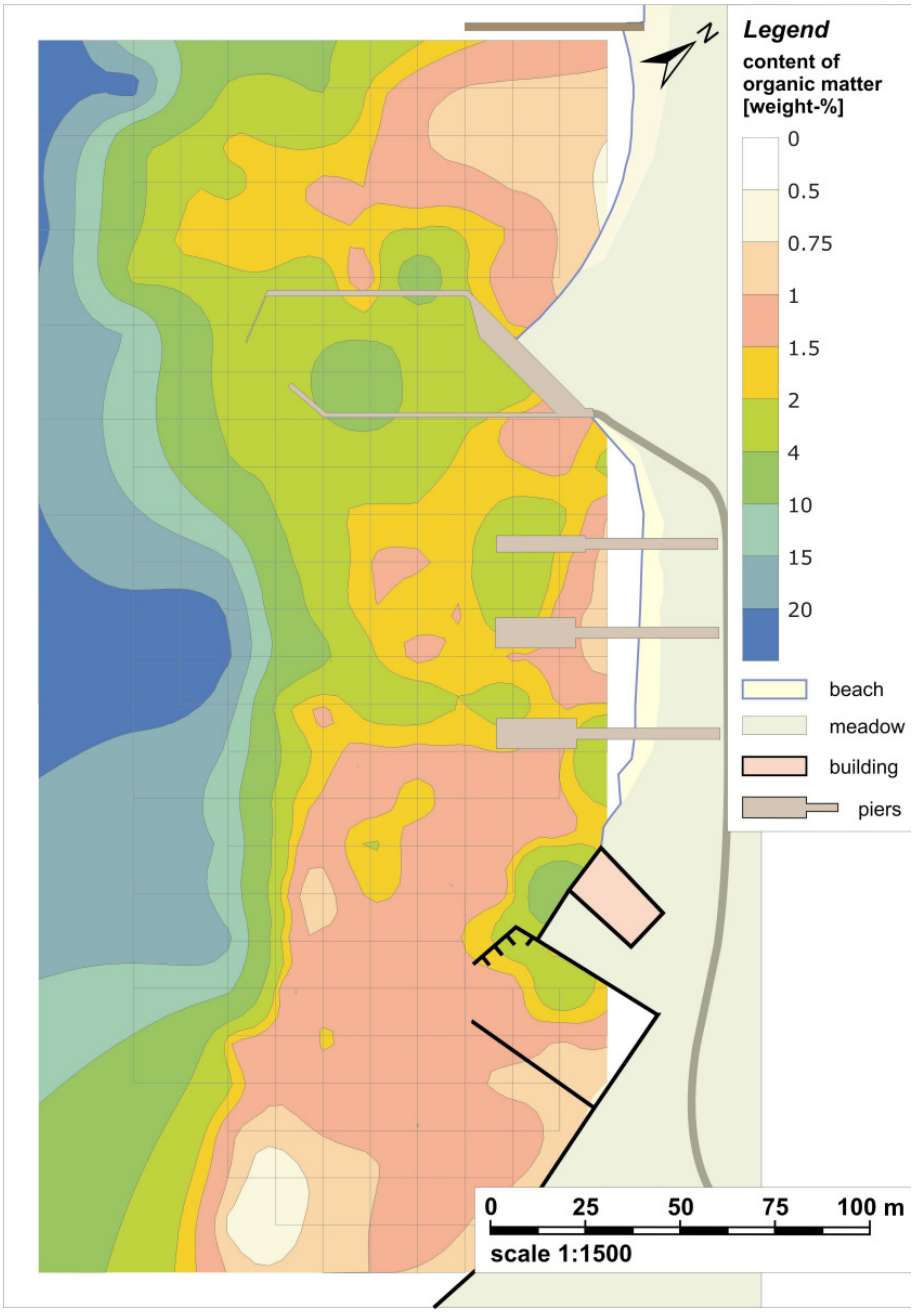

Figure 52: Map of organic carbon content of the lake bottom sediments.

Figure 53 shows the distribution of the hydraulic conductivity of the lake bottom sediments in derived from transient permeability tests of 79 samples. The hydraulic conductivity does not drop to small values in a stringent correspondence with the water depth. However, towards the basin edge, in more than seven metres water depth, the hydraulic conductivity rapidly decreases to values below $1*10^{-6}$ m/s. Figure 53 also displays the shape of an area where 28 additional open-end tests were conducted which is shown enlarged in Figure 54. The hydraulic conductivity of the sediments derived from the transient permeability tests are in the range of $1*10^{-6}$ to $5*10^{-5}$ m/s, whereas the open end tests resulted in distinctly lower values of $1*10^{-7}$ to $5*10^{-6}$ m/s. The differences are likely to be caused by the fact that the permeabil-

ity tests were conducted with disturbed samples, the vertical permeabilites are therefore expected to be lower than those given in Figure 53. The k_f-values derived from sieving are distinctly higher than those of corresponding permeability tests (Nogeitzig, 2005) and are likely to be the least representative. While hydraulic conductivity derived from sieving range from about $5*10^{-5}$ to $5*10^{-4}$ m/s, values from the corresponding tests range from $5*10^{-7}$ to $5*10^{-5}$ m/s. In addition, sediments below the lake bottom are unsaturated in the area where open end tests were conducted which further reduces the hydraulic conductivity.

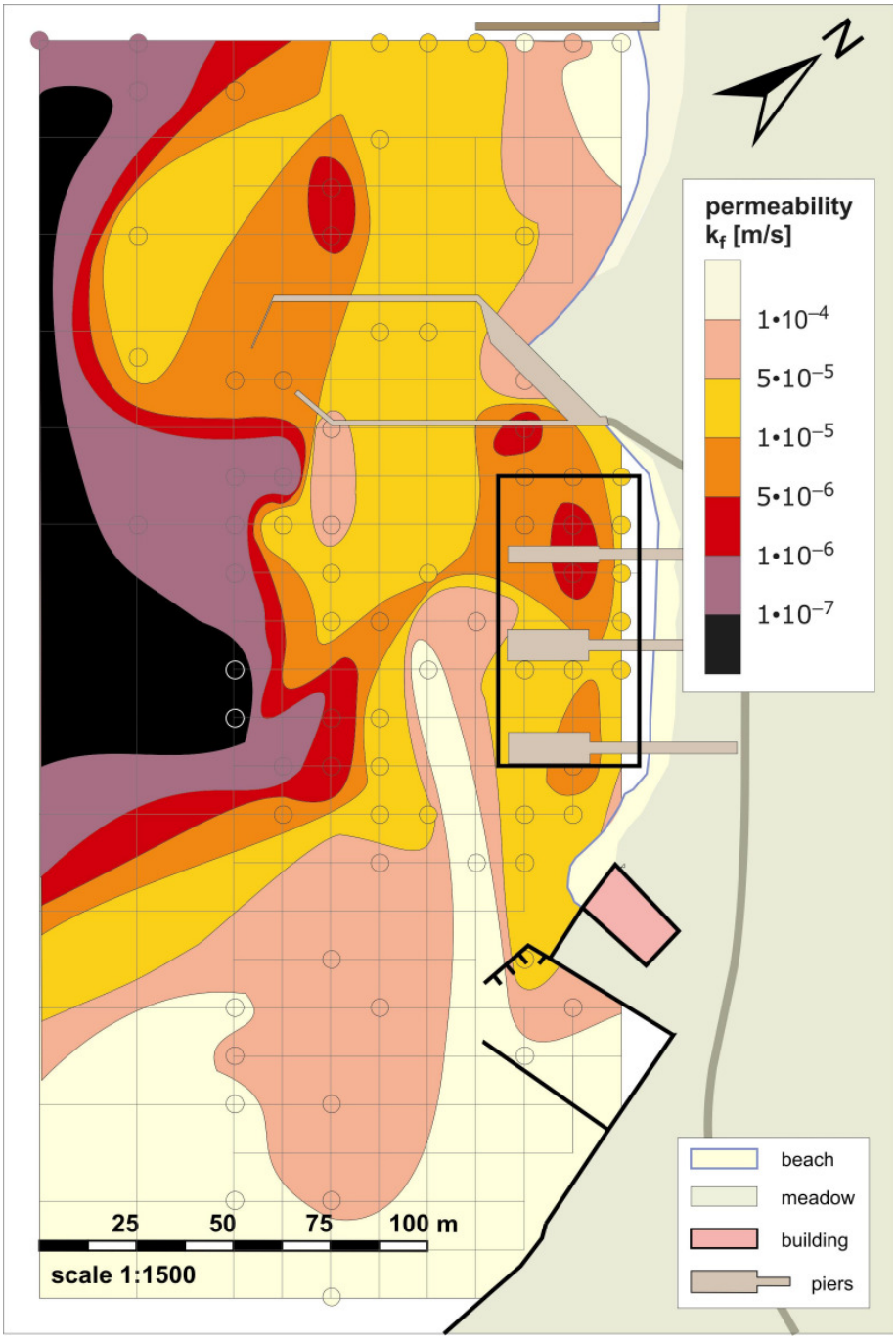

Figure 53: Map of the hydraulic conductivity at the field site, derived from transient permeability tests (small squares). The black rectangle is shown in Figure 54.

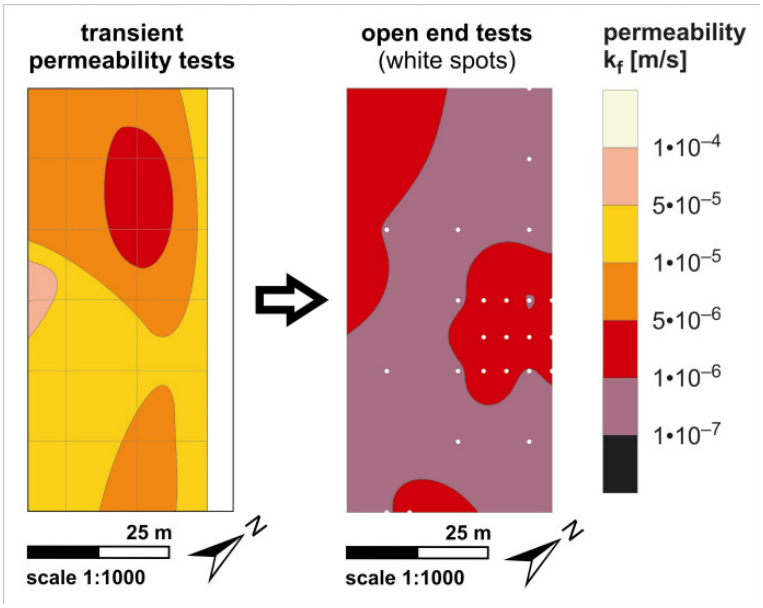

Figure 54: Enlargement given in figure 13 with hydraulic conductivities of the sediments derived from transient permeability tests (on the left) and from open end tests (on the right).

1.5.4 Physical and geochemical characteristics of the Lake Sediments

Methods

In January 2004, seven sediment cores were drilled in between two jetties of the aquatic sports centre of the Free University of Berlin in front of the wells 3 and 4 (Figure 55, location Figure 50). Two undisturbed sediment cores of approximately 1 m length were drilled each at three distances off the bank for sedimentological examinations. At the central place, the seventh sediment core was drilled and captured in a transparent liner of Perspex material for a column experiment. Table 1 provides an overview of the capture and to the destination of each sediment core. The cores from each location were drilled in < 0.5 m distance from each other. One core from each location was cut open for a lithological description (grain size distribution) and geochemical analysis (cation exchange capacity, organic carbon, inorganic carbon, total sulfur, pyrite, Fe- and Mn(hydr)oxide content). The second core at each distance was used to measure hydraulic conductivities by steady-state Darcy experiments (Langguth & Voigt, 1980).

Table 4: Overview of the drilling location and destination of the sediment cores. See also figure 8, figure 9 and figure 11 (on the right).

sediment core	distance from the bank	water depth	core category	destination
WS 1A, 1B	1.5 m	0.15 m	WS 1, 2, 3 A:	sediment chemistry
WS 2A, 2B, 2C	20 m	0.60 m	WS 1, 2, 3 B:	physical properties
WS 3A, 3B	40 m	2.30 m	WS 2 C:	column experiment

Figure 55: Taking cores from the drilling platform at Lake Wannsee.

Results

Figure 56 displays a lithological cross section from the shore to core location 3 (which is adjacent to observation well BEE205). The sediments are fine to medium sized sands containing strongly differing amounts of organic substances, such as remnants of vegetation fibres or pieces of coal. Thin layers of shells, broken shell detritus or gravel were also encountered. The grains-size distribution of core segments is shown in Figure 57. Coarse material is almost absent, while silt and clay occur at the bottom of WS 2B, the top of WS 1B and almost the entire core WS 3B in considerable proportions.

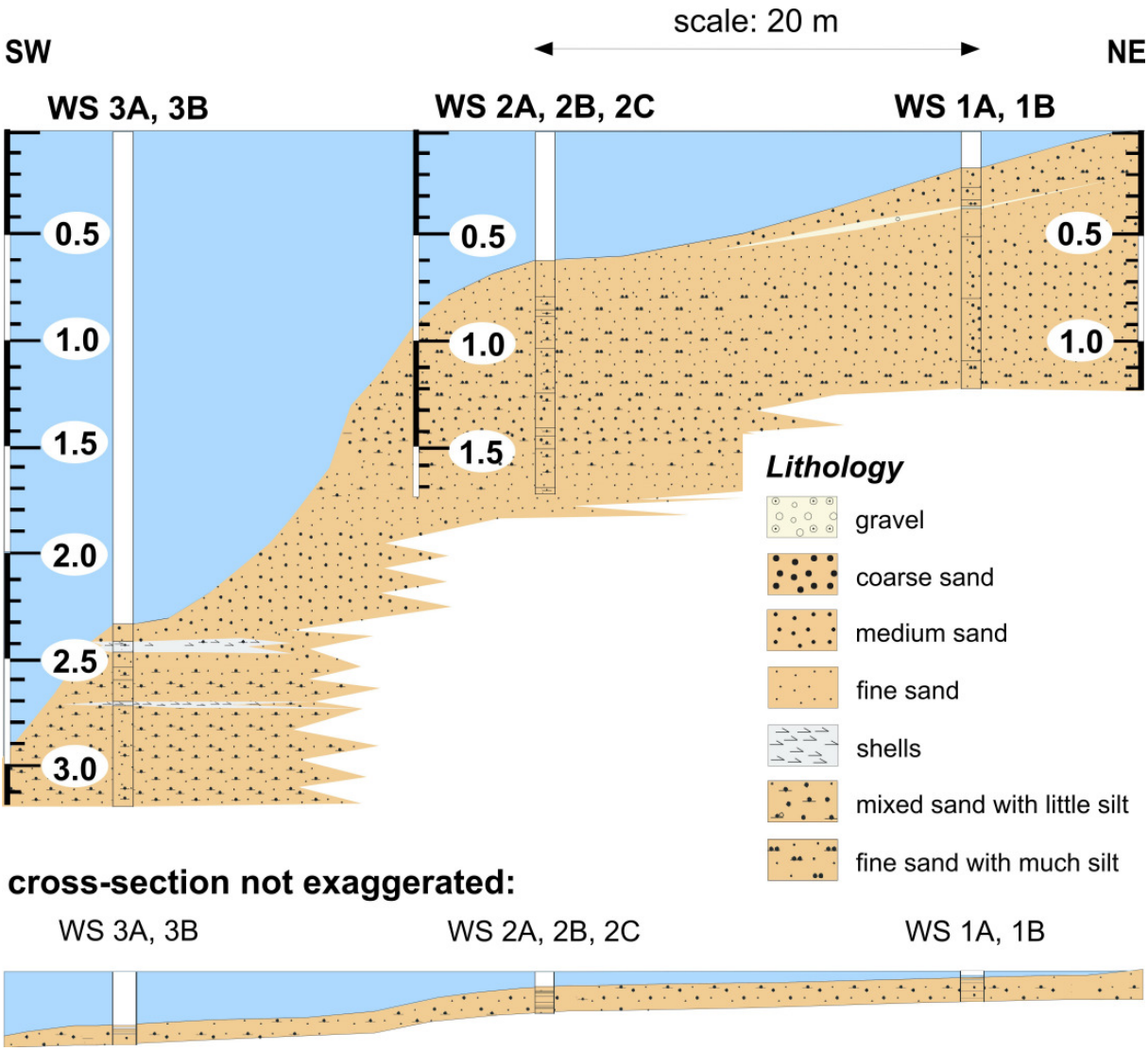

Figure 56: Cross-section of the drilling cores WS 1, WS 2 and WS 3, captured in 1.5, 20 and 40 m distance from the shoreline of the lake Wannsee.

The hydraulic conductivities from steady-state permeability tests (Figure 58) show variabilities between 1*10-4 and1*10-6 m/s and appear to be greater than those obtained in the open-end tests (Figure 54). They seem to decrease from the shore (location W1) to the 40 m distant W3. They also appear to be lowest in the uppermost decimeters with an increasing trend with depth. Local finer grained layers (e.g. WS 2B, 80-100 cm depth) form an exception to this rule. Again, k_f-values derived from the grain size analyses are distinctly higher than those from steady-state permeability tests with undisturbed material and are less representative, since the disregard the clogging effect. It is not surprising that the open end tests deliver the lowest values for hydraulic conductivities. They are performed in the field under undisturbed condition, accounting for both grain-size distribution and packing effects. In addition, local layers such as in WS 2B with elevated silt and clay proportions are determining the vertical hydraulic conductivity, even though the remaining core may have a larger hydraulic conductivity.

However, even though the mapping and the core results revealed large heterogeneities in hydraulic conductivities and differences between the methods applied, the general trends became clear: The k_f-values decrease from values in the order of $10^{-4}/10^{-5}$ m/s close to the shore to $>10^{-7}$ m/s (and probably much less) within the basin, where water depths exceed 8 m and the organic carbon content is >20 weight-%.

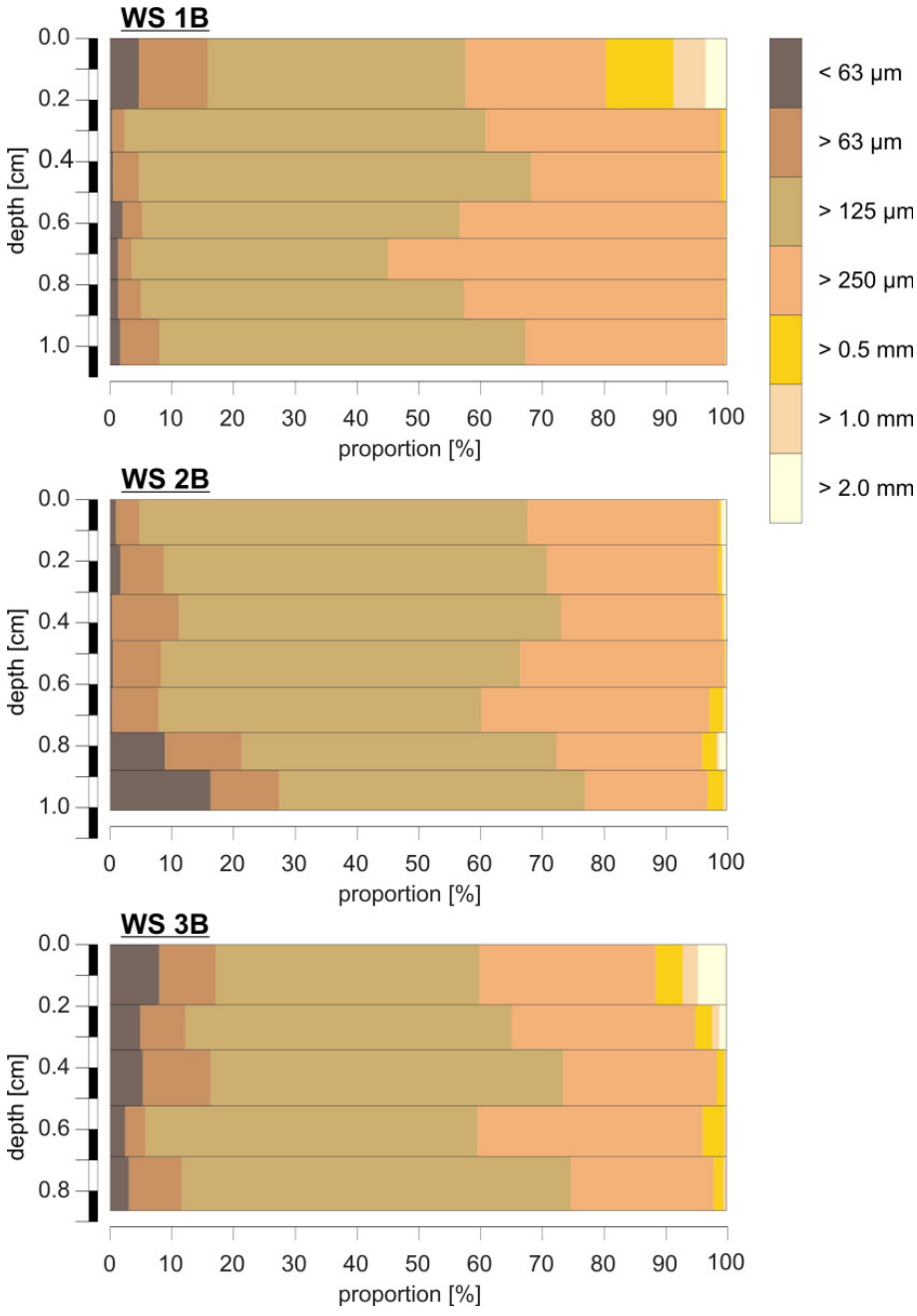

Figure 57: Grain size distribution of the drilling cores WS 1B, WS 2B and WS 3B in segments.

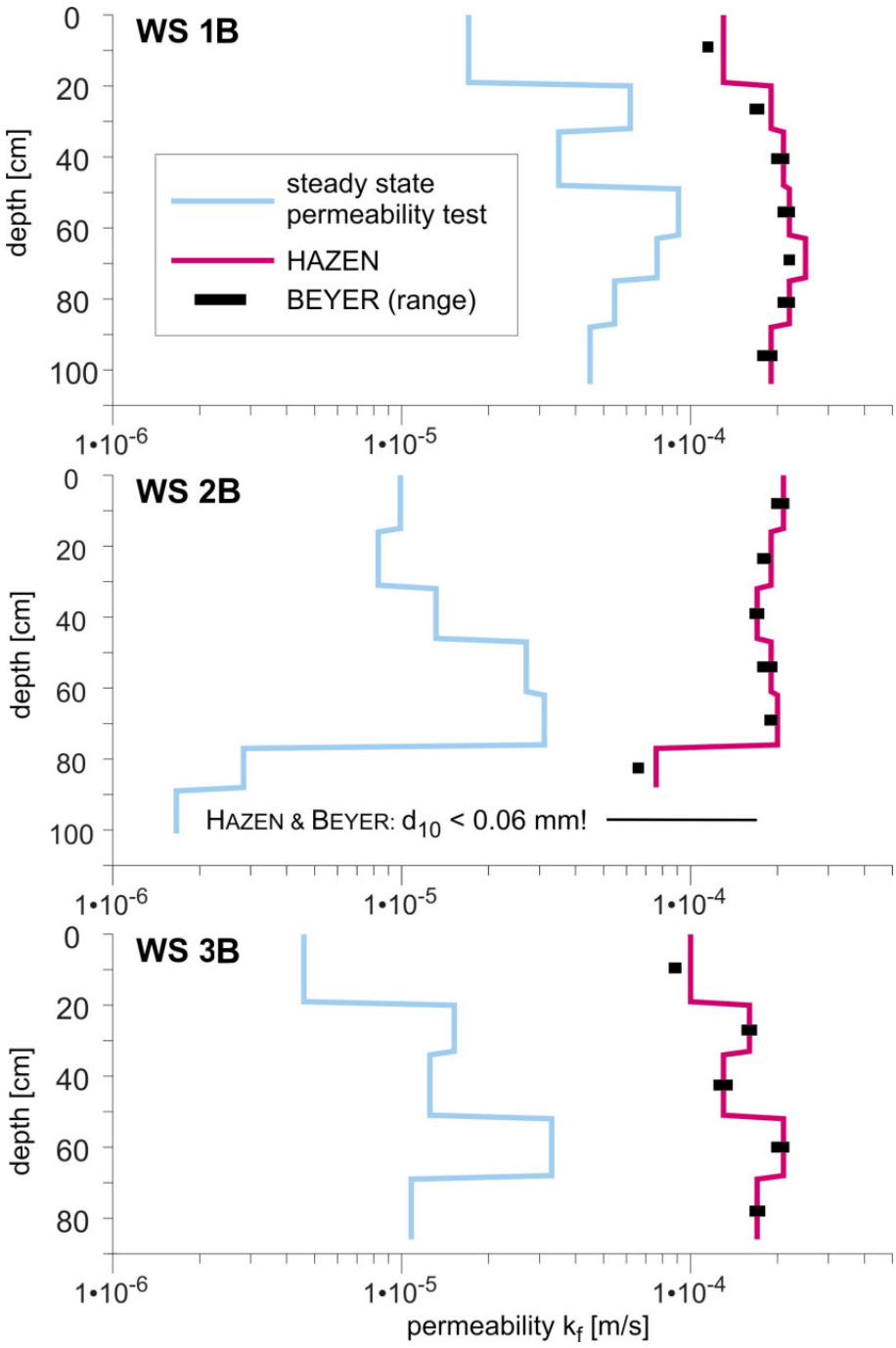

Figure 58: Results of the steady-state permeability tests show that the k_f-values range about one order of magnitude lower than the ones, derived from corresponding sieving analyses of the core segments WS 1, 2 and 3B.

The cores contain between 0.1 to 2 weight % organic carbon (Figure 59), with the exception of the uppermost decimeters of core WS 3A, containing up to 8 % of organic carbon. The sediments contain inorganic carbon as carbonate at an amount of up to 1 weight % C, with exception to the top layers of WS 1A and WS 3A and the bottom of WS 2A (Figure 59) with higher contents.

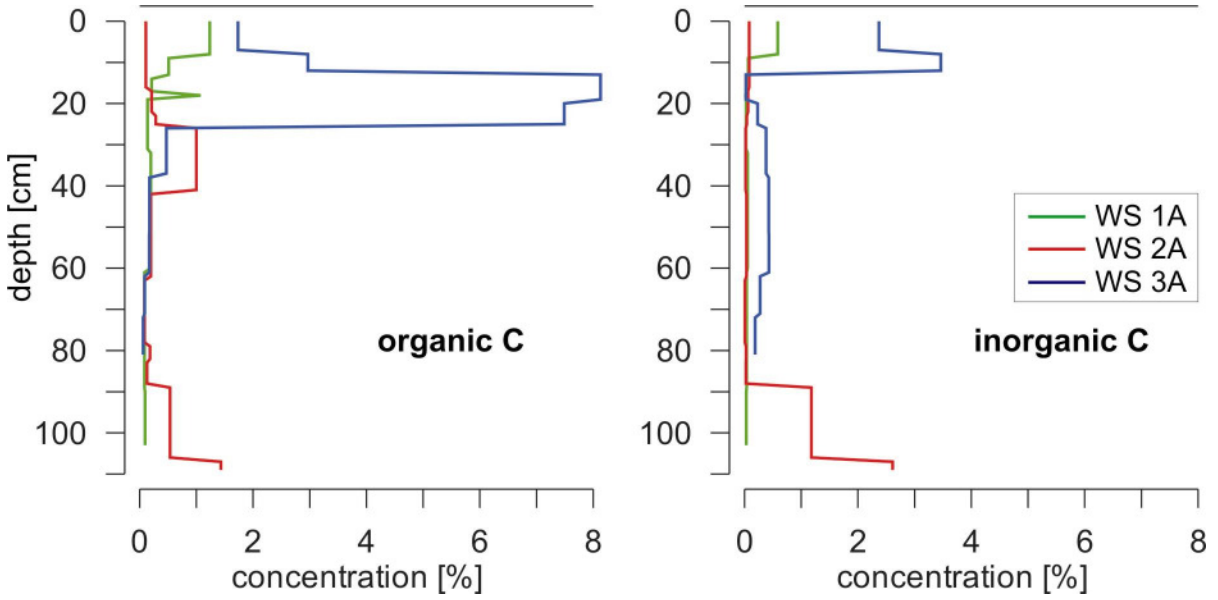

Figure 59: Distribution of organic C (left) and inorganic C (right) in the core segments WS 1,2 and 3A;

The concentrations of total sulphur and pyrite-S were measured in segments of the core WS 2A only; the proportion of pyrite-S varies in the range of about 10 to 35% of the total S in average (Figure 60).

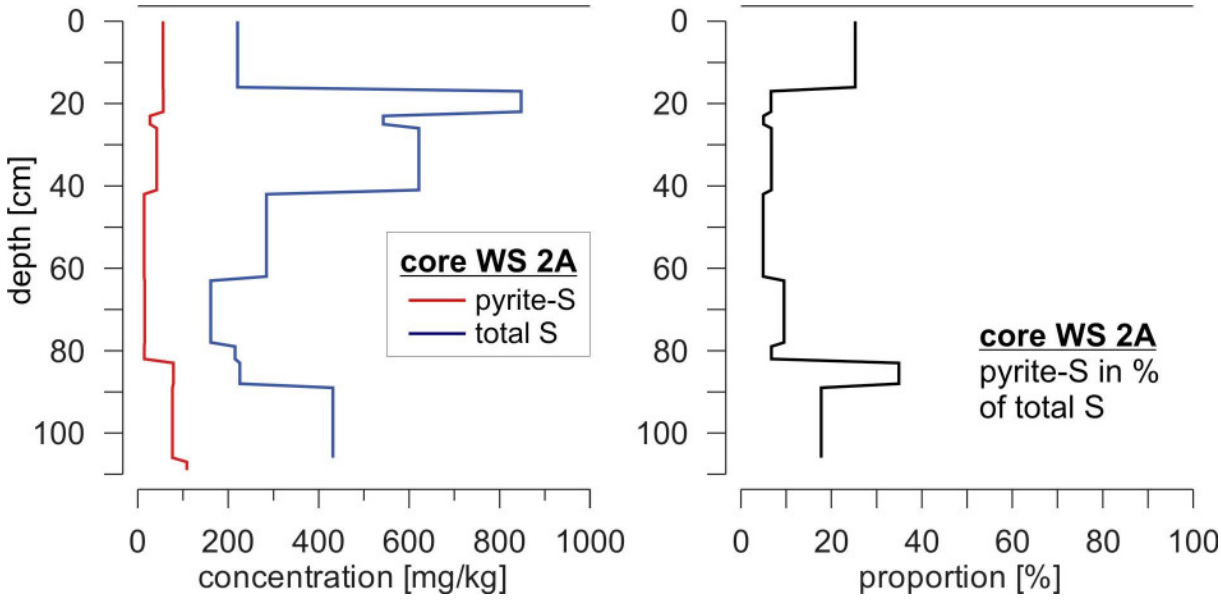

Figure 60: Distribution of pyrite-sulphur and total sulphur in the core WS 2A (left) and of the pyrite proportion of the total sulphur content (right).

The figures 29 displays the dithionite-reducible iron(III) and manganese(IV) contents and total iron and manganese contents within the three sediment cores. Dithionite-reducible iron(III) and manganese(IV) are present in sediments at considerable amounts. The ones of dithionite-reducible iron are varying in between of 200 to 1000 mg per kg, only the top of WS

3A and of WS 1A are containing values of up to 8800 mg/kg. The dithionite-reducible manganese contents are about one order of magnitude lower (Figure 61).

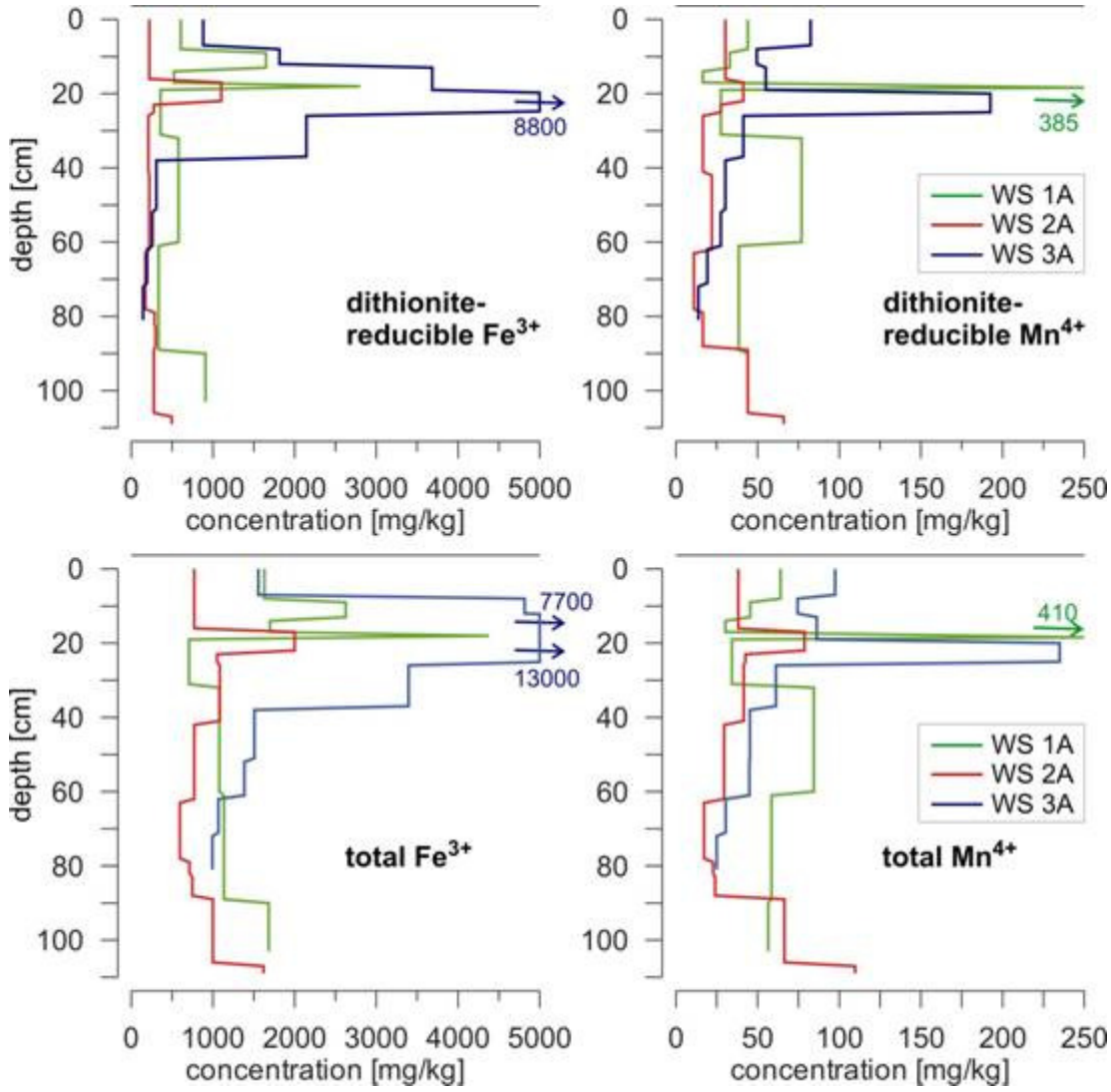

Figure 61: Distribution of the total (below) and of the dithionite-reducible (above) Fe(III) and Mn(IV) content in the cores WS 1, 2 and 3A.

The cation exchange capacity lies in the range of about 0.4 to 0.6 mmol-eq/100 g sediment (not shown).

1.5.5 Column study

Experimental set-up

The undisturbed core WS 2C of 0.99 m length was set up vertically in the laboratory at room temperatures of 20° to 22° C. The column was operated in downwards mode, using a pulsating pump. To simulate natural flow conditions, fresh surface water from Lake Wannsee was used which was stored in a container of 25 L volume and was bubbled with air by an aquarium air pump to retain constant saturation of oxygen. The aerated inlet water was led to the

column at super sufficient rate in order to avoid any drainage. The surplus of inlet water was branched off by an overflow outlet, which was fixed 20 cm above the sediment surface. Nine sampling ports to inlet water and outlet water were connected as water taps to the flexible pipes and as waterproof connections screwed into the Perspex tube of the column, which is shown in Figure 62. In addition, seven waterproof connections were screwed into the Perspex tube for the installation of O_2-probes directly in the sediment material. The outlet of the column was connected by flexible pipes of airtight Viton and glass material and fastened 40 cm above the bottom to set up a constant hydraulic gradient, forcing the inlet water to infiltrate at conditions similar to those at the drilling place at lake Wannsee (0.6 m water depth). In order to build up constant flow rates of the filtration water in the column, an additional pulsating pump was installed on 12th of August 2004 due to an irregularly and persisting rise of the flow rate.

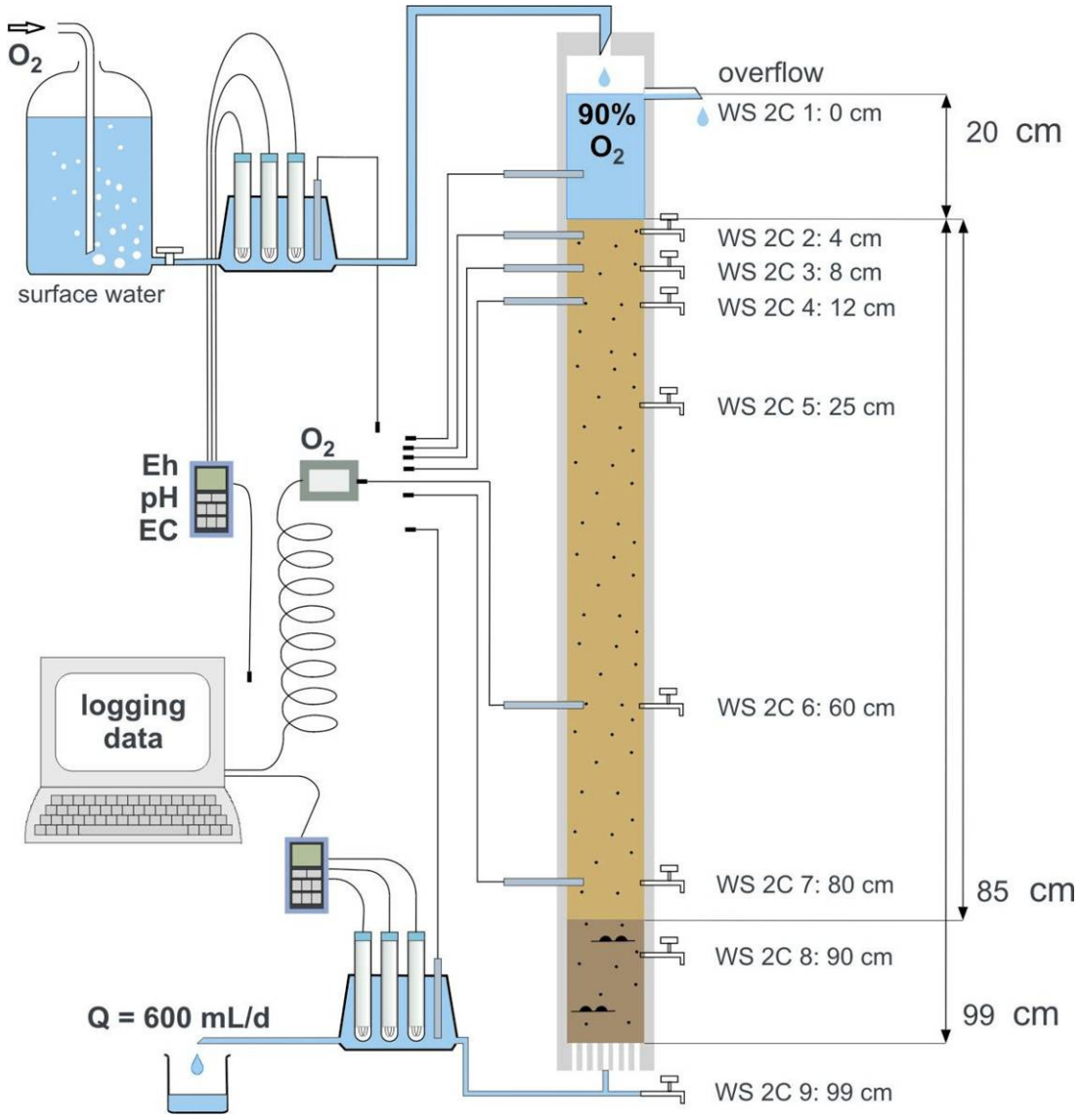

Figure 62: Column set up in the laboratory. Nine sampling ports and seven O_2-probes were installed.

The physicochemical parameters (pH-value, Eh-value and electric conductivity) of the filtrate water were measured in the inlet water and outlet water. Probes were installed into the flexible pipes of inlet and outlet. Sampling for cations (Na^+, K^+, Ca^{2+}, Mg^{2+},Mn^{2+}, Fe^{2+}, NH_4^+,) and anions (Cl^-, HCO_3^-, SO_4^{2-}, NO_3^-, PO_4^{3-}, HS^-) and for dissolved organic carbon (DOC), took place monthly. O_2 was measured with seven luminescence probes (Presens 2003), placed directly into the sediment body inside the column.

Hydraulic properties

A tracer test was conducted from the 16th to the 26th of July 2004 by increasing the electrical conductivity with NaCl. The breakthrough curve was fitted using the analytical solution by (Ogata, 1970), which resulted in a flow velocity (v_a) of $6*10^{-6}$ m/s (or 0.52 m/d) and a dispersion coefficient (D_l) of $7.8*10^{-8}$ m²/s (0.0067 m²/d). The test was conducted at average flow rates of 600 ml/d, which, at an area of 0.035 m² would be equivalent to a Darcy velocity (v_f) of $1.8 \cdot 10^{-6}$ m/s. The effective porosity (n_e), equal to v_f/v_a would therefore be ≅ 30 %.

However, these values (v_a and D_l) are only valid for the time period at which the tracer test was conducted, since the amount of water (Q) flowing through the column was not constant (Figure 63). Sampling extractions at the installed sampling ports contributed to the irregularities of the flow volumes. Temporally, entrapped gas was extracted with the water samples and new pathways were created. In order to stabilize the flow an additional pulsating pump was installed at the outlet on the 12th of August 2004 (day of operation 128). However, irregularities still persisted and Q varied between 200 and 1600 ml/d. The flow velocity therefore varied between 0.17 and 1.40 m/d within the experimental period. Even though this was not intended, it is not entirely unrealistic, since the flow velocity variations in the field will be comparatively high, due to variations in the pumping rates, the lake water level and the temperatures.

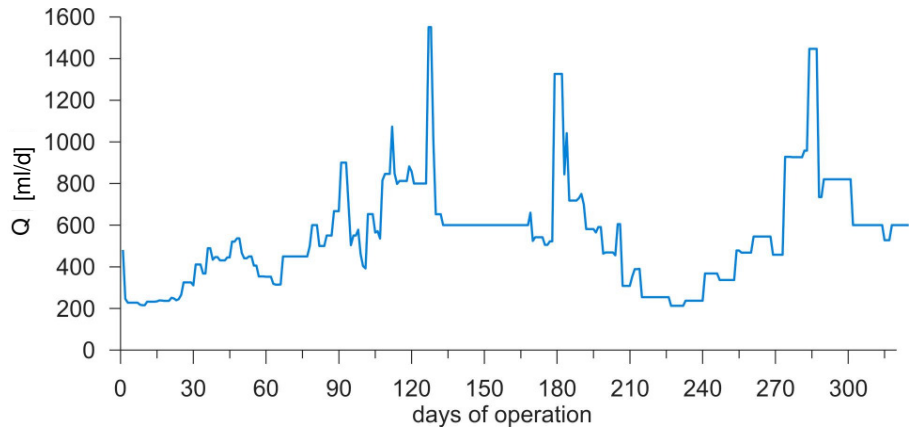

Figure 63: Temporal variations of the flow (Q) through the column.

Hydrochemistry

The electric conductivity (EC), pH and Eh (mV) measured regularly in the inflow and outflow are shown in Figure 64. Variabilities in the inflow are due to the tracer test performances, biological activity and evaporation in the fresh water container. Additionally, the surface water quality from the lake Wannsee, refilled at roughly monthly intervals, changes naturally.

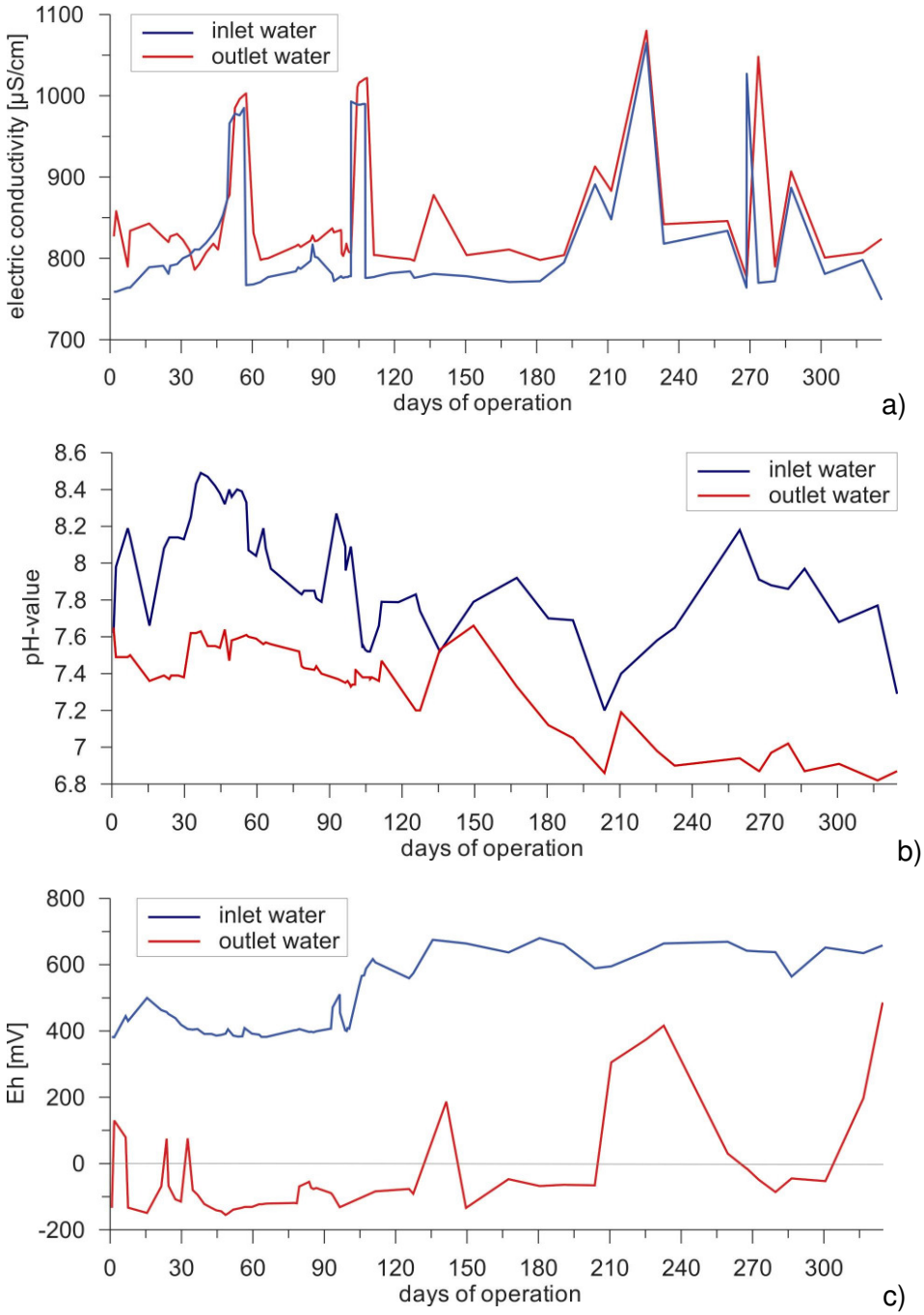

Figure 64: a) EC (µS/cm), b) pH and c) Eh (mV) values measured in inflow and outflow over the entire experimental period.

The ECs of the outflow were continuously slightly higher than those of the inflow, probably mainly caused by the dissolution of carbonates. The pH-value of the filtrate water persistently

decreased by 0.5 to 1.5 units from inflow to outflow which is due to biological activity of microorganisms producing CO_2. The redox potential strongly decreases within the column. The inflow is saturated with regard to oxygen, the Eh-value of the inlet water varies between +400 and +650 mV. Microbiological activity leads to a decrease of the Eh-value in the column to distinctly reducing conditions in the range of –100 to –150 mV. Elevated redox potentials in the outflow are likely to be the results of leakages in the outlet water pipe connections or measurement errors of the Eh-probes.

Figure 65 illustrates the development of the oxygen concentration at several depths within the column over the experimental period. It seems that quasi-steady state conditions were reached only towards the end of the experimental period. During the first 33 days of operation, oxygen was completely consumed in the uppermost four centimetres of the column. After one month, a change of color from darker grayish-black to light grey and brownish tones became visible in the sediments of the column, descending downwards from the top. After 3 months, oxygen was observed in 8 cm depth. More than 230 days were needed to detect oxygen in the depth of 12 cm. Over the entire experimental period, the oxidation of the sediments visibly advanced to a depth of more than 25 centimeters. However, oxygen did not reach the 60 and 80 cm probes. Because the column was stored stagnant for several months before it was set up, the sediments had become more reducing than under natural conditions and it took roughly 9 months before steady-state conditions were re-established.

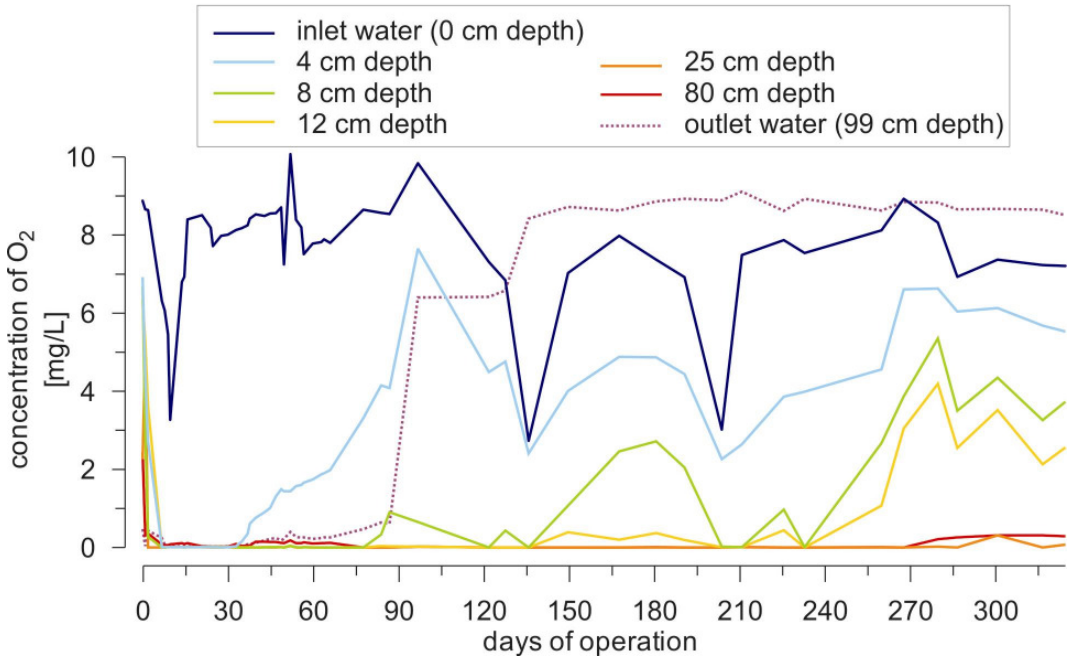

Figure 65: Oxygen concentrations at various depths in the column with time.

In Figure 66, the overall changes in the water chemistry from the inflow to the outflow of the column are shown as a mass balance (in mmol/L) over the entire experimental period. The median concentrations of the major ions and of the redox indicators are shown. The calcium,

magnesium and, most distinctly, the hydrogen carbonate concentrations are increasing during the sediment passage, most likely due to the dissolution of carbonate minerals caused by the slight pH drop. The gain of hydrogen carbonate is also a result of the microbial redox processes. The amounts of sodium, potassium, chloride and sulphate are decreasing insignificantly, considering their absolute concentration.

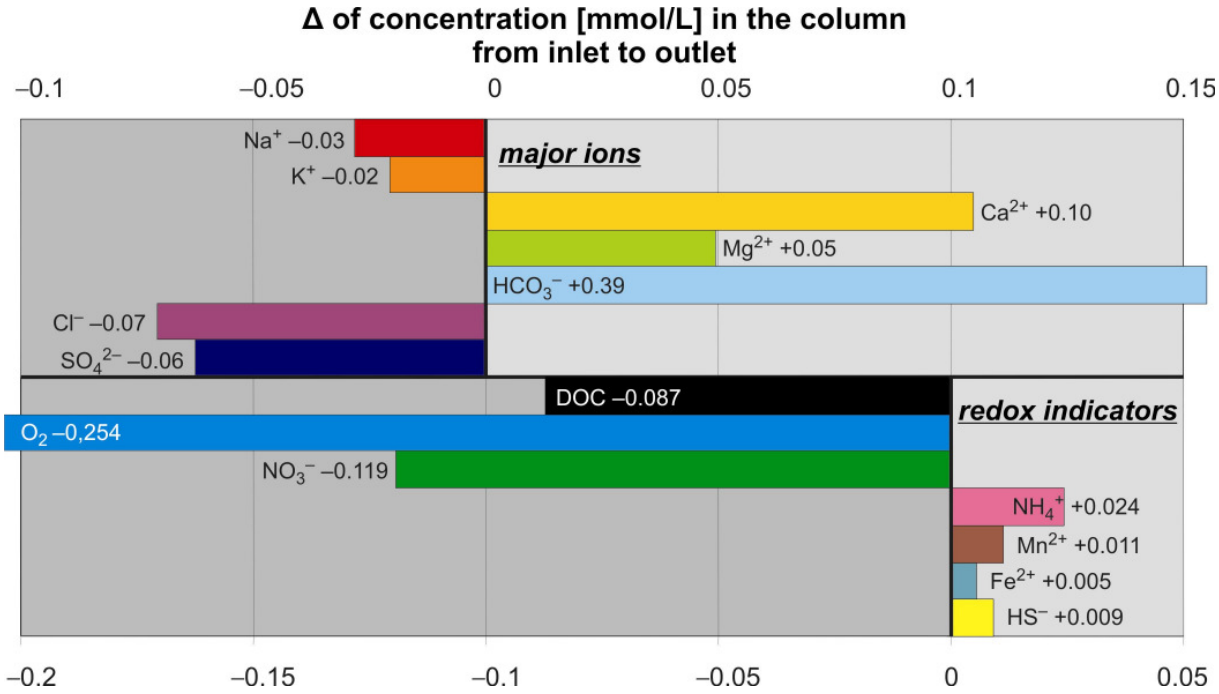

Figure 66: Concentration gains and losses of the water constituents from inflow to outlow.

Figure 66 additionally displays the gains and losses of the redox indicators (oxygen, nitrate, ammonia, manganese, iron and hydrogen sulfide) within the column. Roughly 15 % of the total dissolved organic carbon is oxidized in the column. Oxygen and nitrate are completely consumed while ammonium, manganese(II) and very low concentrations of iron(II) and hydrogensulfide are generated during the flow. Figure 67 shows the depth profiles of the redox indicators (median concentrations of the entire experimental period). Oxygen penetrates 25 cm into the sediment while nitrate reaches a depth of 90 cm. Manganese appears in 25 cm depth. An overlapping of the redox zones was observed. Hydrogen sulfide was only observed in the first few months and is therefore probably a relict of the stagnant storing period rather than a true indicator of sulfate reduction.

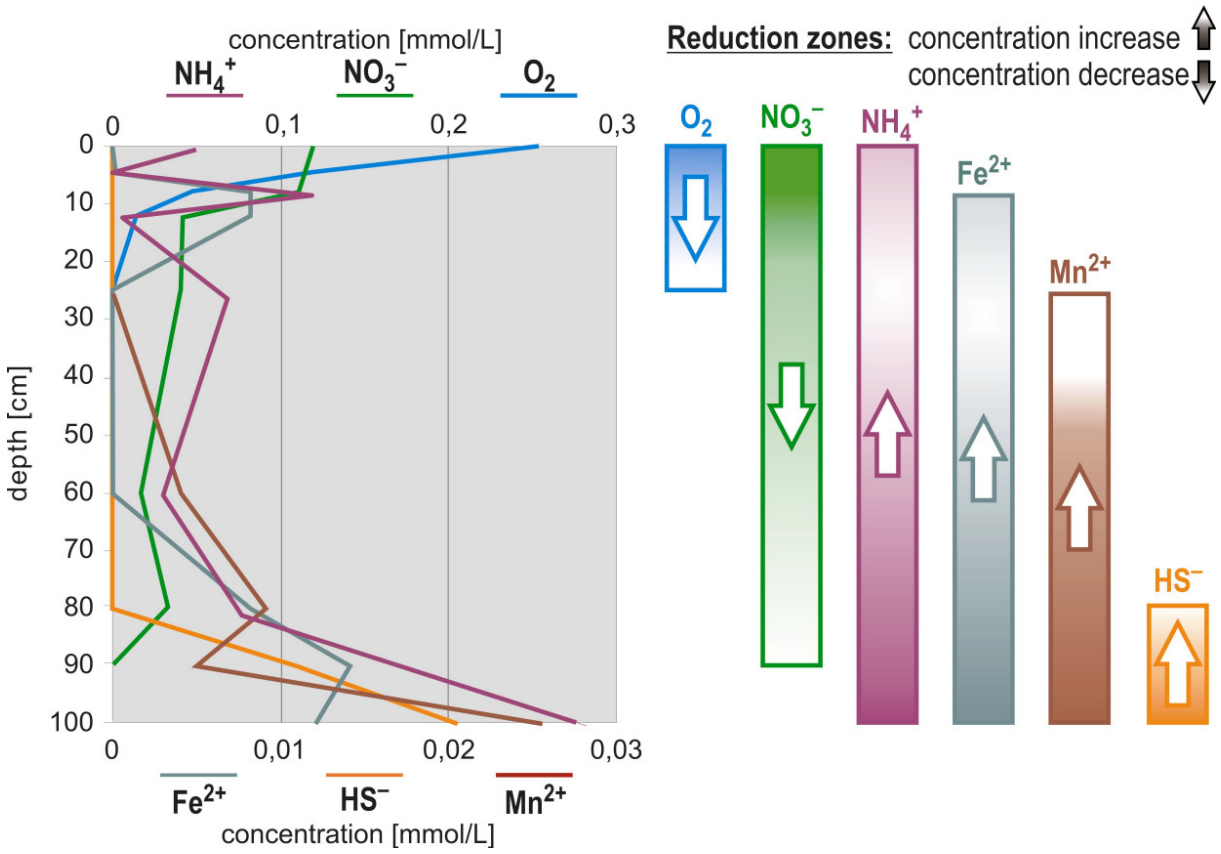

Figure 67: Depth profiles of the redox indicators (median concentration) and extent of the respective redox zone.

Hydrogeochemical Modeling

In order to get more detailed information about saturation indices of mineral phases and species distribution of the dissolved components hydrogeochemical calculations of analysed samples of the column study were carried out with Phreeqc-2. (version 1.5.09). The simulations were performed for samples with a complete number of analysed components and an electro balance error of less than 4 %. This reduced the data-set to a suit of 25. Since the samples taken from the in- or outflow of the column provided a more complete amount of analysed components, these samples were mainly used for the simulations. But nevertheless, analyses from all depths of the columns have been considered at least once.

If possible, the redox potential was defined in the Phreeqc-2 input file according to direct measurements. This was possible only for a number of samples of inflowing and outflowing water taken outside of the column. For water samples taken from the sample ports in the column, no redox measurements existed. In this case the redox potential was calculated by Phreeqc-2 using the measured redox couple N(-3)/N(5). Due to the fact that the redox couple is rarely in equilibrium, this may affect the accuracy of the results. In most cases the redox values calculated by Phreeqc were high in comparison with measured values of the outflowing water. This may be owing to the high concentrations of nitrate analysed in the column

The results of our calculations are compiled in Table 5. The simulations yielded slight oversaturation of calcite and aragonite in most samples. The rising alkalinities along the flow path are mainly the result of biodegradation of organic carbon and only to a lesser extent caused by calcite dissolution.

The calculated oversaturation of trivalent iron phases seems reasonable for in- and outflowing water with temporarily elevated measured redox values. With regard to the water in the column the authors suppose that calculated oversaturation of trivalent iron phases is a consequence of overestimated redox values and not reliable here. Furthermore the analytical results of the column study indicate mobilisation of iron and manganese which is in contrast to the results obtained with Phreeqc.

Gypsum and anhydrite never reach saturated conditions as a result of comparatively small concentrations which are always below 300 mg/l. Hence no reduction of sulphate occurs in our experiment, Pyrite keeps also permanently undersaturated.

Table 5: Calculated saturation indices (SI) for different mineral phases with Phreeqc.

depth	port name	date of analyses	pH	Eh (mV)	Electro neutrality (%)	SI Calcite	SI Aragonite	SI Dolomite	SI Siderite	SI Gypsum	SI Anhydrite	SI Goethite	SI Fe(OH)3	SI Pyrite
0	C1	11.01.2005	7.9	658	-3.5	0.42	0.27	0.11	-8.18	-1.36	-1.6	8.52	2.63	-211.83
0	C1	16.07.2004	8.2	426	-2.2	0.74	0.59	0.86	-5.17	-1.40	-1.64	8.35	2.46	-160.59
0	C1	28.07.2004	8.3	626	-2.2	0.83	0.68	1.02	-8.51	-1.36	-1.6	8.52	2.63	-211.96
0	C1	12.08.2004	8.1	592	-2.0	0.65	0.50	0.67	-8.16	-1.39	-1.62	8.05	2.16	-201.29
0	C1	03.09.2004	7.7	685	-1.7	0.29	0.14	-0.10	-8.48	-1.38	-1.62	8.33	2.44	-215.88
0	C1	22.07.2004	8.0	586	-1.1	0.58	0.44	0.54	-7.79	-1.40	-1.64	8.05	2.16	-197.68
0	C1	20.08.2004	7.9	696	0.8	0.46	0.31	0.24	-9.02	-1.39	-1.62	8.52	2.63	-223.09
0	C1	08.07.2004	8.4	657	4.0	1.01	0.86	1.37	-9.19	-1.36	-1.6	8.63	2.74	-222.3
4	C2	02.08.2004	8.0	0	-2.7	0.51	0.37	0.41	-3.27	-1.38	-1.62	8.05	2.16	-130.57
8	C3	30.07.2004	7.8	0	-2.5	0.36	0.22	0.11	-2.26	-1.40	-1.63	8.94	3.05	-129.76
12	C4	29.07.2004	7.5	0	-2.2	0.03	-0.12	-0.56	-2.93	-1.40	-1.64	7.98	2.09	-130.29
90	C8	09.05.2004	7.4	0	3.6	-0.03	-0.17	-0.72	-1.67	-1.30	-1.54	9.12	3.23	-128.15
100	C9	29.07.2004	7.7	0	-2.8	0.27	0.12	-0.09	-0.95	-1.33	-1.57	8.45	2.56	-104.34
100	C9	29.06.2004	7.6	-45	-2.3	0.16	0.02	-0.32	-0.12	-1.40	-1.63	4.24	-1.65	-34.85
100	C9	22.07.2004	7.5	-101	-2.1	0.07	-0.07	-0.48	-0.21	-1.42	-1.66	3.04	-2.85	-20.46
100	C9	12.07.2004	7.7	-97	-1.9	0.25	0.10	-0.11	-0.04	-1.38	-1.61	3.64	-2.25	-24.22
100	C9	22.12.2004	7.3	31	-1.0	-0.03	-0.18	-0.67	-0.52	-1.30	-1.53	4.64	-1.25	-49.04
100	C9	08.07.2004	7.5	-92	-1.0	0.13	-0.01	-0.34	-0.04	-1.34	-1.57	3.5	-2.39	-23.32
100	C9	11.01.2005	7.6	-88	-0.6	0.12	-0.03	-0.48	0.34	-1.33	-1.57	3.99	-1.9	-23.8
100	C9	09.05.2004	7.6	-138	-0.3	0.21	0.07	-0.25	0.22	-1.38	-1.62	3.14	-2.75	-13.67
100	C9	18.02.2005	7.4	203	0.5	-0.06	-0.21	-0.78	-0.94	-1.32	-1.55	7.35	1.46	-90.93
100	C9	20.08.2004	7.8	286	1.3	0.36	0.22	0.07	-1.47	-1.39	-1.62	8.94	3.05	-117.53
100	C9	03.09.2004	7.6	78	2.0	0.22	0.08	-0.18	0.54	-1.34	-1.58	7.08	1.19	-63.88
100	C9	17.11.2004	7.8	386	2.5	0.29	0.15	-0.06	-4.11	-1.28	-1.52	8.04	2.15	-143.34
100	C9	23.05.2004	7.6	-148	3.1	0.23	0.08	-0.17	0.12	-1.29	-1.53	2.95	-2.94	-11.56

1.5.6 Aquifer Sediments

The sediments encountered during the drilling campaign for the new observation wells at the Lake Wannsee transect 3 are fairly homogenous (depth < 26 m below ground). They mainly consist of fine- to medium sized sands of light greyish to brown colours. They are of glacial-fluvial origin (*Saale* to *Weichsel* glacial period). They are underlain by a finer grained, clayey organic rich aquitard of the *Holstein* interglacial period, which was not encountered during the new drilling. From previous drilling campaigns it is known that they can be expected around sea-level, which is equivalent to 35 m below ground at the site. Underlaying the Holstein are *Elster* sands, which are separated by an *Elster* silt aquitard. The production wells of the water works are screened above and below the *Holstein* aquitard as well as below the *Elster* silt. Lithological cross-sections of the transects Wannsee 1 and Wannsee 2 with available k_f data (from sieving) are shown in Figure 68 and Figure 69. Figures of the geochemical analysis of the core BEE202UP obtained during the drilling campaign are given in Figure 70 and Figure 71.

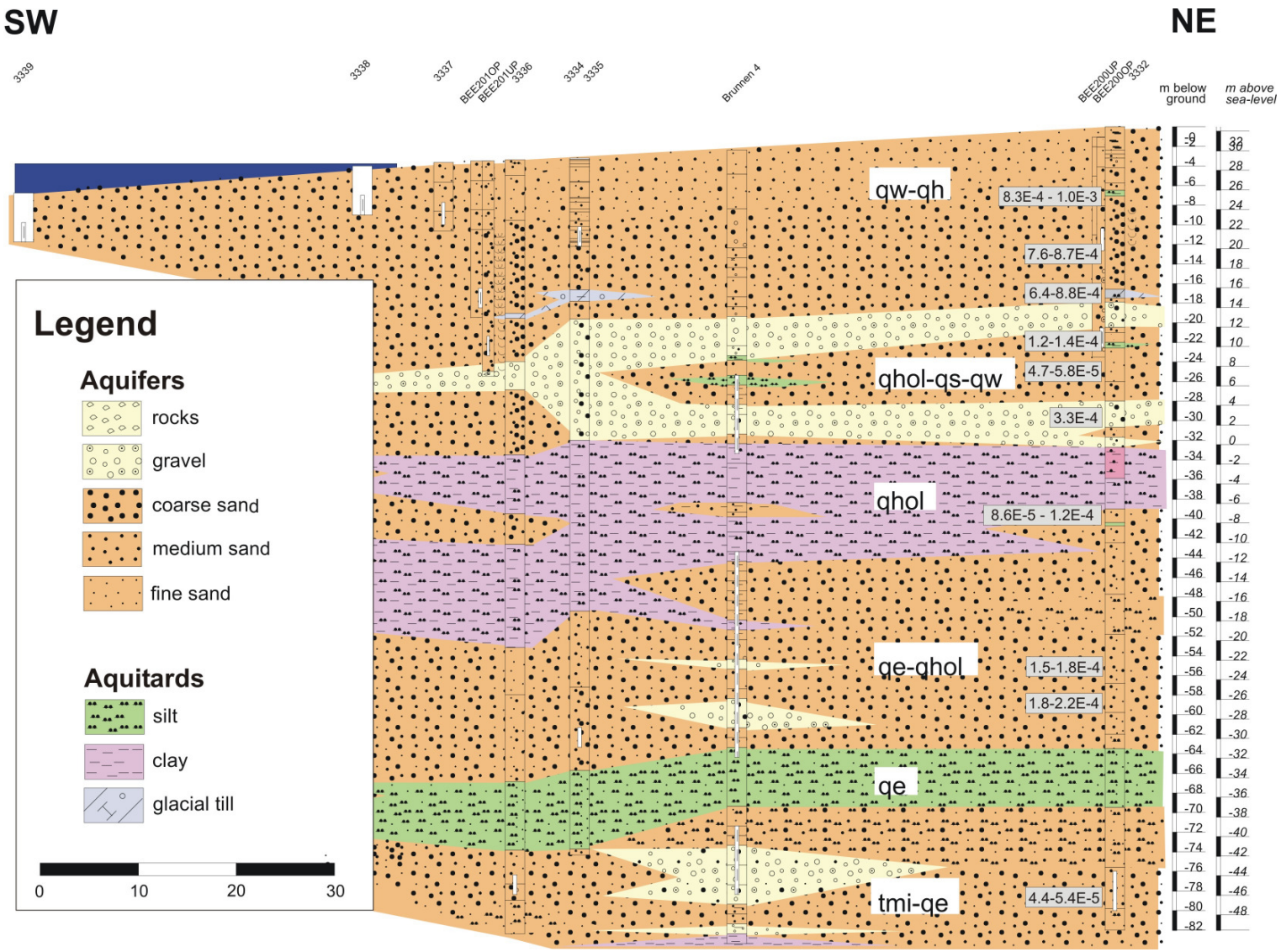

Figure 68: Lithological cross section of Wannsee 1 with k_f data of core 3332 (modified after Hinspeter, 2002).

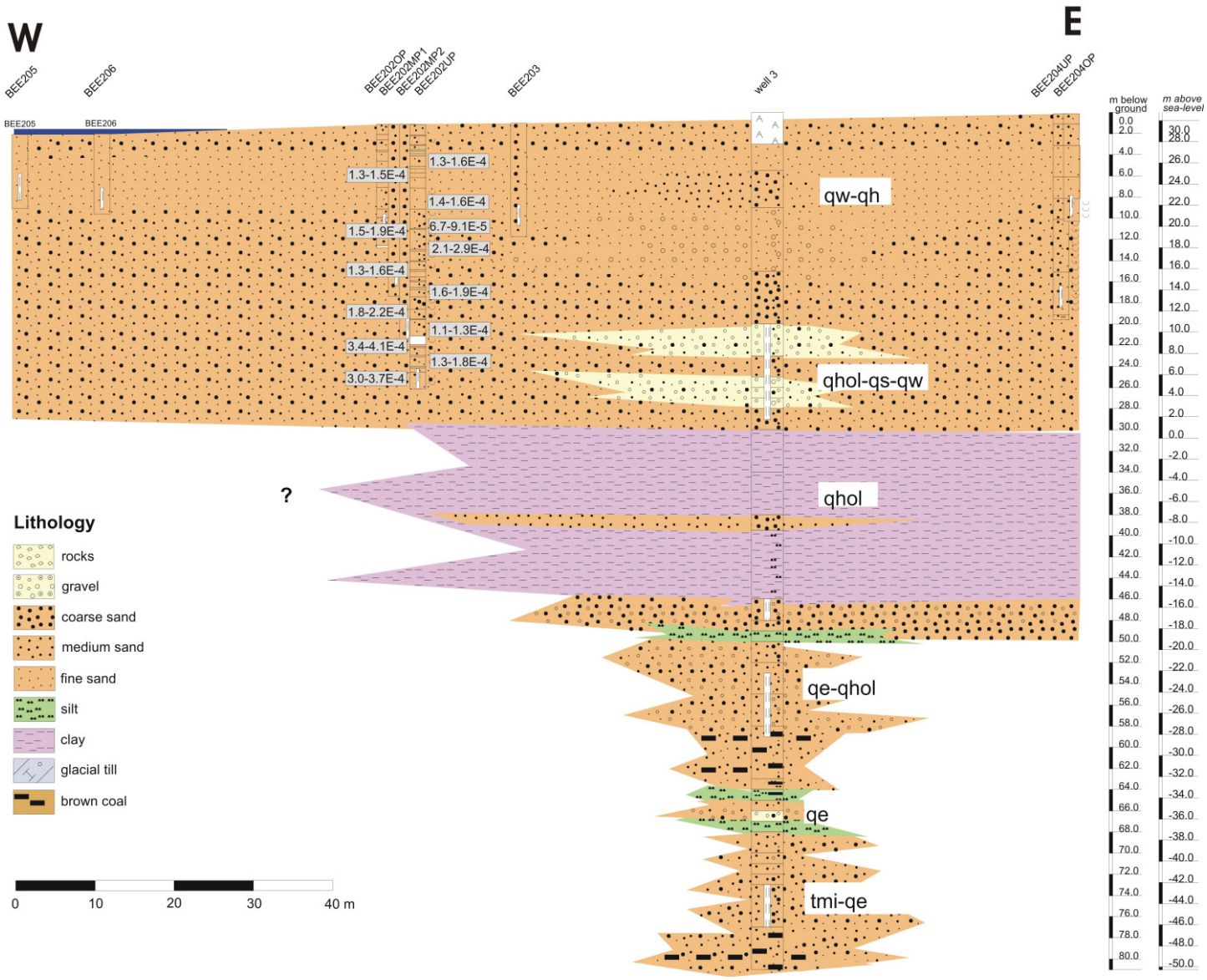

Figure 69: Lithological cross section of Wannsee 2 with k_f data of BEE202UP.

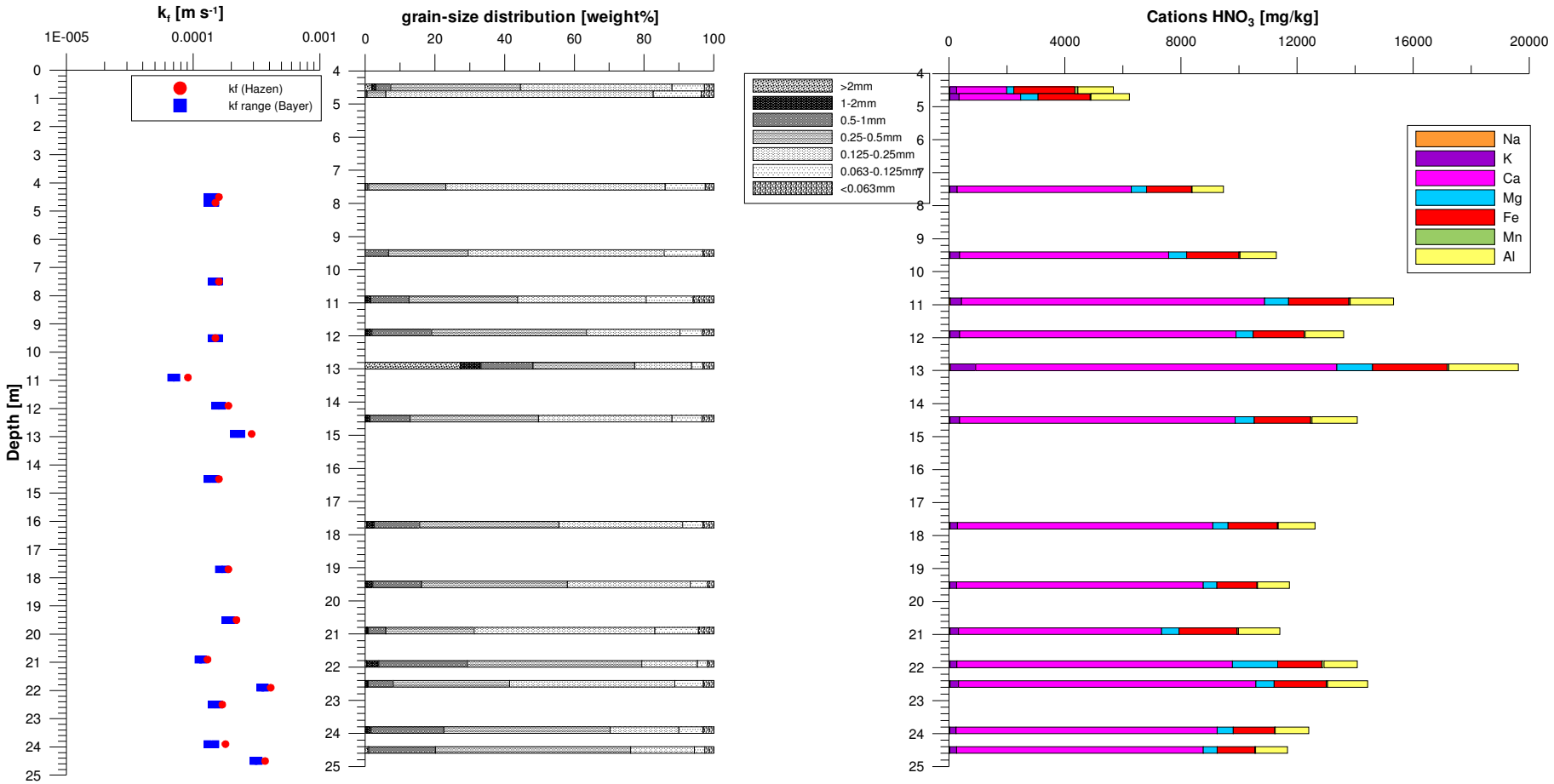

Figure 70: Hydraulic conductivities (k_f), grain-size distribution and cations from HNO_3 extraction in core BEE202UP.

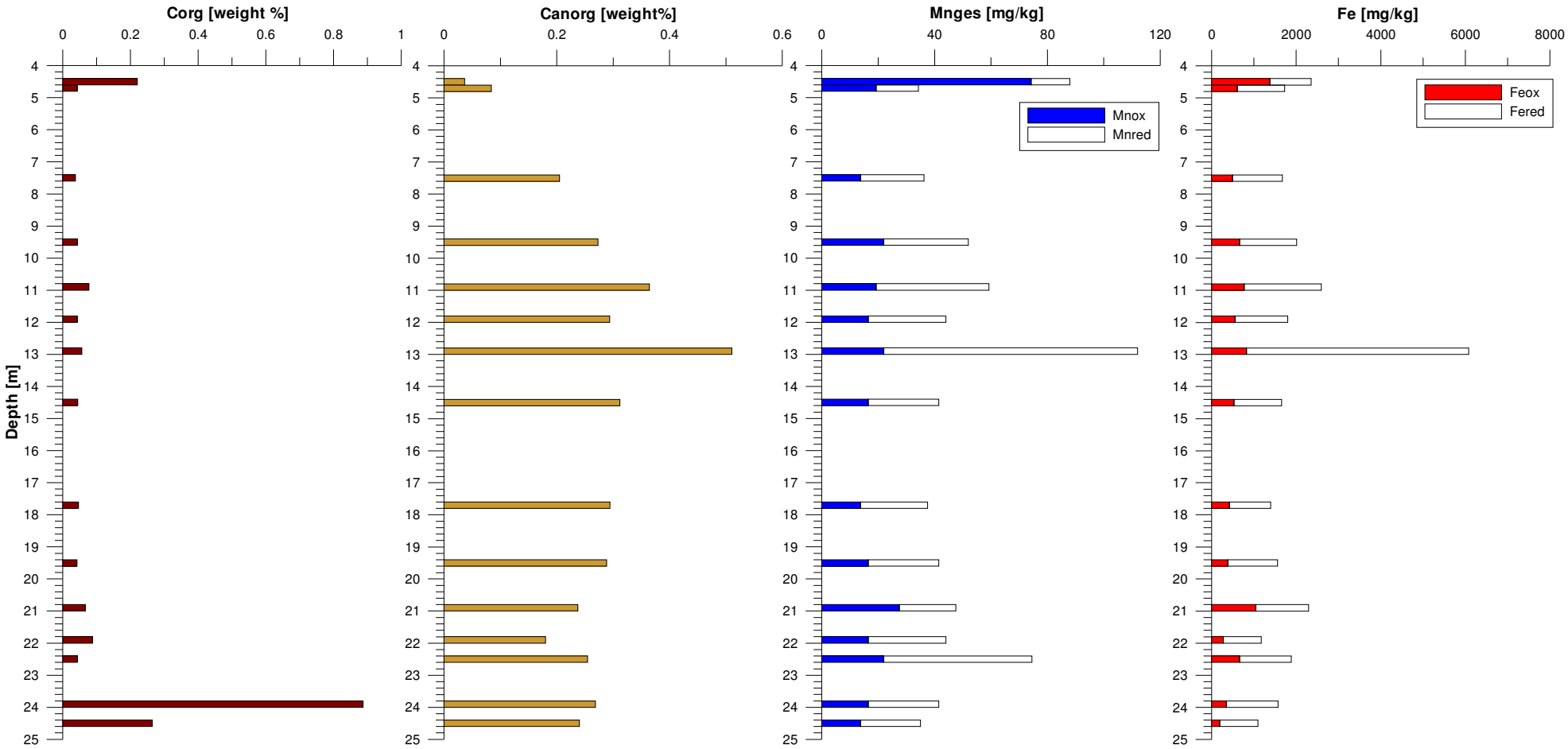

Figure 71: Organic and inorganic carbon content, Fe(III) and Fe(II), Mn(III) and Mn(II) content in core BEE202UP.

The sands of BEE202UP are fairly homogenous in terms of their hydraulic conductivity, which varied from $6.7*10^{-5}$ to $4.1*10^{-4}$ m/s (Figure 70). The hydraulic conductivities of the clogging layer are considerably lower (Figure 53, Figure 58), even though those values obtained from sieving are actually remarkably similar. The organic carbon content in the aquifer sands (Figure 71) is 0.04 to 0.26 weight %, with the exception of a sample containing 0.9 weight % organic C, because of small coal pieces. Compared to the uppermost decimetres of the lake sediments (Figure 52), the organic carbon content of the aquifer is low. All samples analysed contain inorganic carbon (carbonate) at amounts of 0.04-0.51 weight % C.

1.5.7 Tracer evaluation: Travel times/groundwater age

The Tritium/Helium (T/He) age dating results can give a first idea on the groundwater age, i.e. the average travel time from the surface to the sampling location; in the case of bank filtrate, from the lake to the relevant well. T/He dating was used to calculate the travel times of bank filtrate by Stute et al. (1997), Beyerle et al. (1999) and Sültenfuß & Massmann (2004). The combined T/He results of all sites are given in the Appendix.

Transect 1, which contains observation wells in the uppermost, but also in the lower aquifers, was dated with the T/He method in summer 2001. Instead of the calculated ages, Figure 72 shows Tritium (T) concentrations (TU) originating from atmospheric hydrogen bomb testing in the 1960s and radiogenic Helium-4 ($^4He_{rad}$) concentrations (Nml/kg) from the Uranium (U) and Thorium (Th) decay within the aquifer. If there is hardly any T left, because it has all decayed (pre-bombing age) or if there is no tritiogenic Helium present (Helium from the Tritium decay, He_{tri}) because the sample is very young and the T concentration is similar to that of the surface water, a reliable age cannot be given. Because the dated observation wells are either He_{tri}-free (i.e. very young as in the case for the shallower wells 3335, 3337, 3339) or T-free because they are very old (3332, 3334, 3336, wells screened below the Hostein aquitard), are precise age cannot be given.

If the Uranium and Thorium contents of the sediment were known, ^{4}He could be used to date the deeper groundwater (Beyerle et al., 1999). Because the U and Th contents are unknown, elevated concentrations of radiogenic ^{4}He can only be used as an indicator for a relatively "old" groundwater. The concentration of $2.8*10^{-4}$ Nml/kg the deepest observation well 3336 suggests that the water is not 99 years old (as calculated), but at least centuries old (pers. communication Sültenfuß, 2003). In both deeper aquifers, the groundwater is clearly considerably older than 50 years since T has already decayed and the ^{4}He values are high. Consequently, any "younger" substances (for example pharmaceutical residues or contrast agents) which were applied in the past decades only, should not be present in the 2 deeper aquifers. The deeper aquifers have not been sampled regularly within NASRI because they do not belong to the bank-filtration system, which becomes clear when looking at the T/He data. A

single sampling campaign conducted in March 2004 confirmed that the aquifers below the Holstein aquitard (wells 3332, 3334, 3336) do not contain any pharmaceutical residues or other substances (compare chapter 1.5.8).

In contrast to the deeper T/He results, the shallow wells reflect the atmospheric concentrations of T at the time of sampling, while radiogenic ^{4}He and tritiogenic ^{3}He could not be detected. The resulting calculated effective T/He age is 0 years, which is equivalent to less than 6 months, which is the resolution of the method at the site.

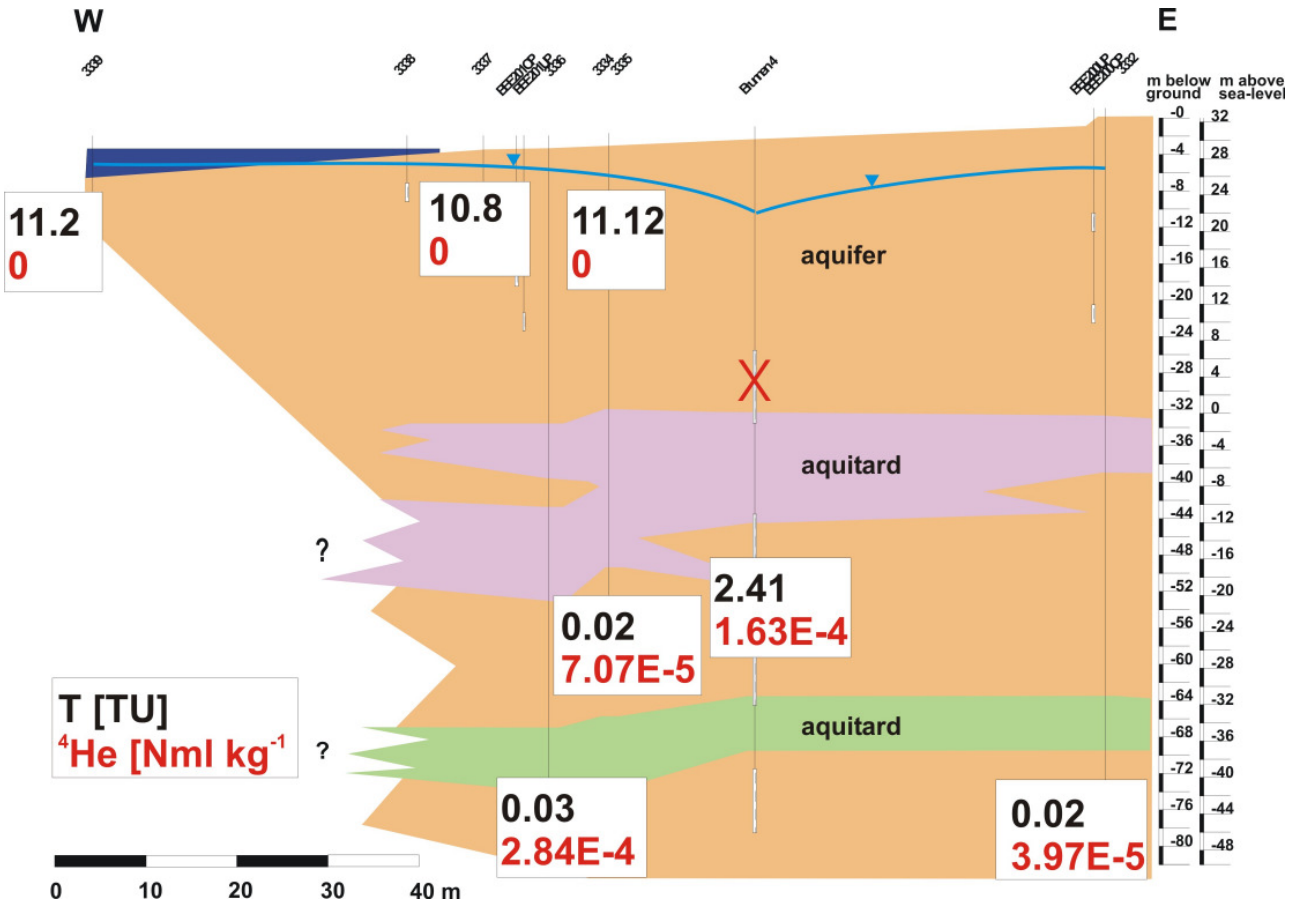

Figure 72: Tritium and radiogenic ^{4}He at Wannsee 2, sampling campaign summer 2001.

The production well is a mixture of all aquifers. The effective T/He age of well 4 is 25 years. This is not a “real” age in terms of an actual travel time but the results of mixing of water with distinctly different ages. A clear indicator of this (rather expectable) fact is the offset of well 4 from the precipitation input versus year curve. When plotting the “stable” tritium concentration (remaining T plus decayed tritiogenic He) of an unmixed sample against its calculated infiltration year, the sample should lie directly on the input curve given by the actual T concentration in the precipitation at the time. As shown in Figure 73, well 4 plots below the input curve as expected from its mixed nature. The T concentration of well 4 (2.4 TU) can be used for a mixing calculation. According to the T value, the production well 4 abstracts ~ 22 % of water from the uppermost aquifer; a distinction between bank-filtrate and background groundwater

from inland cannot be made. Therefore, results show that well 4 is not completely sealed. For simplicity, the deeper wells 3332, 3334 and 3336 were given an age of 1950 in Figure 73, even though they might be considerably older.

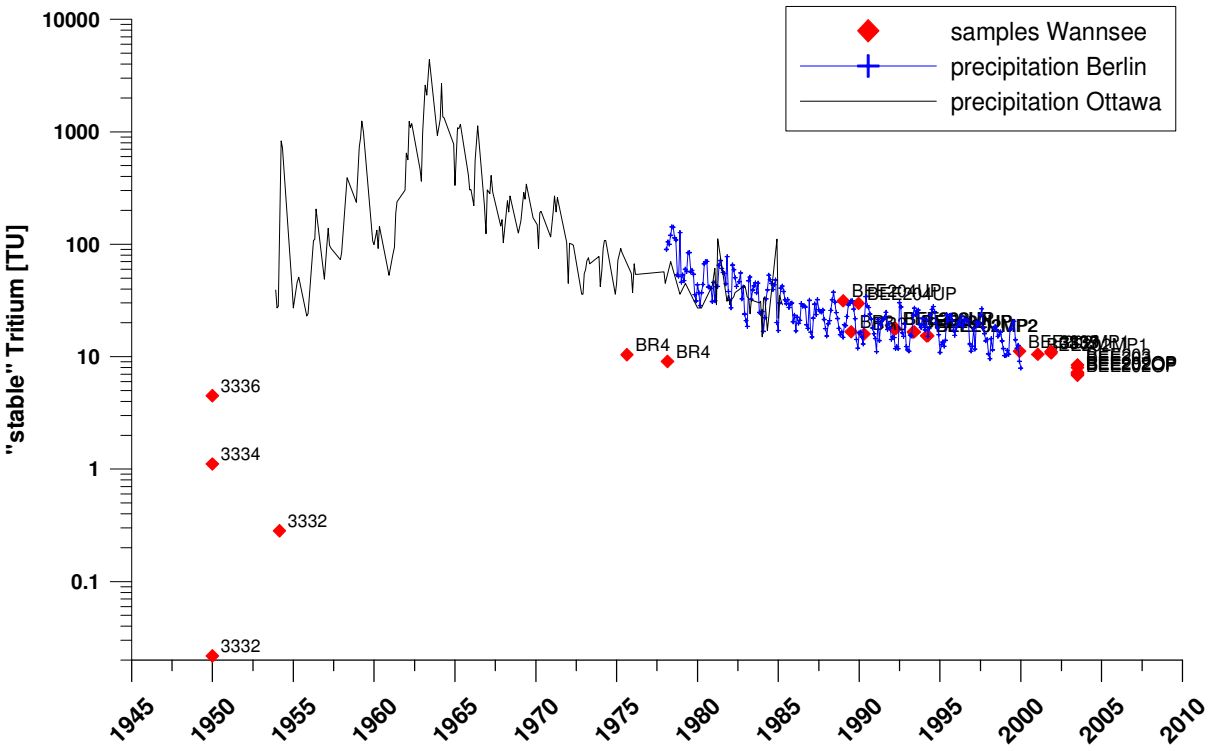

Figure 73: "Stable" T concentration (T+$^3He_{tri}$) versus calculated infiltration year for the Wannsee samples and time-series of T in the precipitation of Berlin and Ottawa (due to lack of data at the respective time in Berlin). Data source: IAEA, BfG.

Figure 74 presents the effective T/He ages of samples collected at transect Wannsee 2 in July 2003. The dating results showed that only the observation wells with the uppermost, shallowest filter screens contain "young" bank-filtrate (which is less than 6 months old). These are also the wells which show an almost undampened breakthrough of tracer curves. The T/He ages of the well group BEE202 with filter screens in 4 different depths of the uppermost aquifer (above the *Holstein* aquitard) increase from 0 to 10.7 years with depth. This clearly indicates that the groundwater in the uppermost aquifer shows a very strong vertical age differentiation, which had not been expected at first. The T/He-dating illustrates that water abstracted from the deeper observation wells (in the upper aquifer) is years to decades rather than months old. The same phenomenon was observed at the Lake Tegel bank filtration transect. As in Tegel, this also explains the different composition of the bank filtrate regarding a number of minor water constituents in the respective "layers" (compare chapter 1.5.8). It also indicates that bank filtrate must be flowing underneath the lakes, which are therefore not water divides. Rather than flowing in 4 layers with different "real" travel times as indicated by the coincidental number of filter-screens, it is likely that the bank filtrate is either

"young" (< 6 months, originating from the nearest shore) or "old" (years to decades, originating from an opposing shore). Intermediate ages would be the result of mixing to variable degrees between these two sources. However, the use of particle tracking within the hydraulic model also suggested that the travel times of the two deeper wells (BEE202MP2 and BEE202UP) vary strongly between summer (8 and 13.5 years) and winter (0.24 and 3.75 years). The catchment areas of well 3 and 4 simulated in the hydraulic model varied seasonally but basically reached to the opposing south-western lake shore.

Production well 3 has a mean T/He age of 13.6 years, which is the result of mixing of water from 3 different aquifers (the two deeper aquifers are not shown in Figure 74) from 2 sides. The groundwater from the inland side displays a similar age.

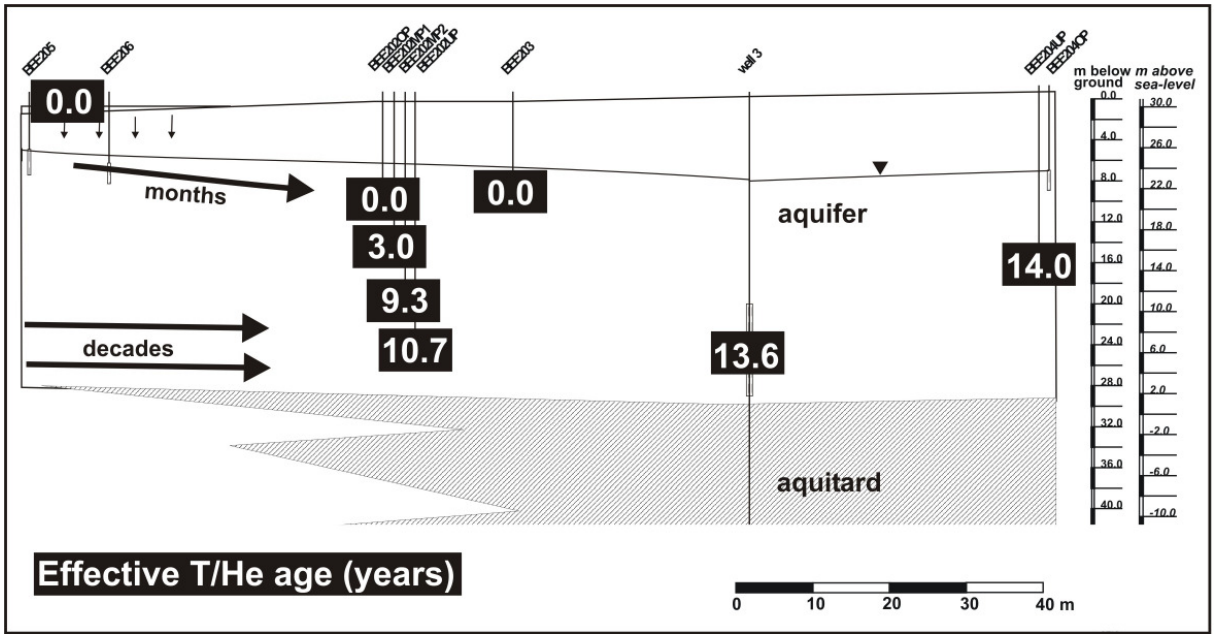

Figure 74: Effective T/He ages plotted at the position of the filter screen depth. Samples taken in July 2003.

The tracer evaluation with breakthrough curves turned out to be more complicated than expected. Isotope data of 2000/2001 and 2002/2003 shows that breakthrough curves of the shallow observation wells of transect 1 (3339, 3338, 3337 and 3335) and transect 2 (BEE205, BEE206, BEE202OP, BEE203) reflect the surface water signal, a clear indication that these wells contain young bank-filtrate. Because sampling of 3339, 3338 and 3335 was stopped in February 2003, data of 2000/2001 was added for reference. Figure 75 illustrates that residence times for the shallowest wells are rather low at this particular site. Travel times are around 20 days from the Lake to 3337, ~ 30 days to 3338, < 30 days to 3335 and 65 days to 3339. The travel times are shorter to the wells at the shore than to those below the lake which probably a consequence of the decreasing permeability of the sediments away from the shore. Observation well 3335 is at approximately 2/3 of the way to the production

well. Therefore, on the very shortest (shallowest) pathway, the travel time of the bank filtrate to well 4 is roughly 1.5 months.

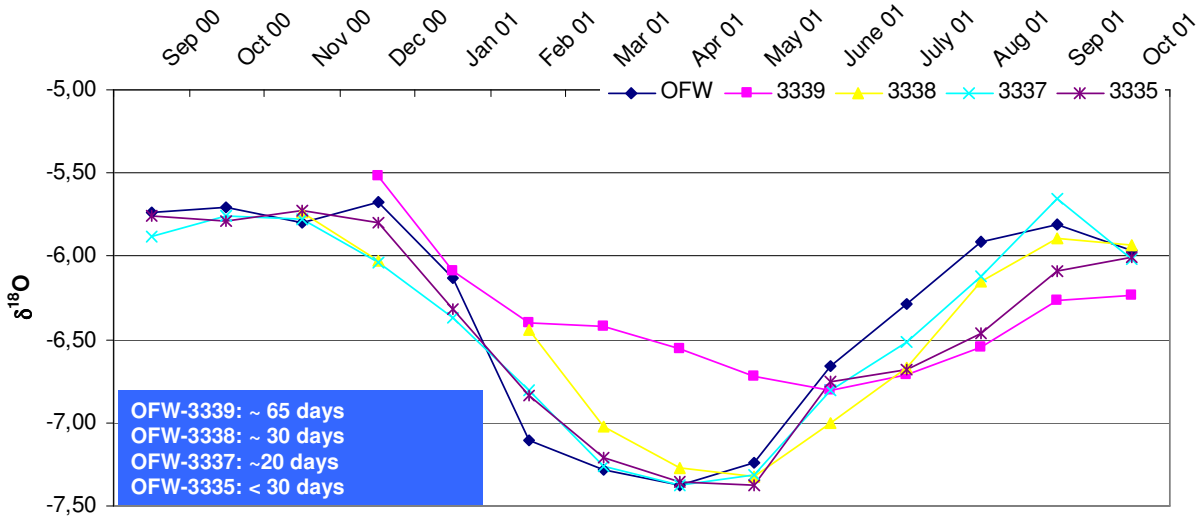

Figure 75: Isotope data from September 2000 to October 2001 (Hinspeter, 2002).

None of the remaining tracer (boron, chloride, potassium or EDTA) are of much use at the transect Wannsee 1. Potassium does not behave conservatively as it almost does in Tegel, EDTA fluctuates too in the input. The interpretation of Cl^- and B is difficult because of the lack of a clear peak in summer 2002 (sampling was stopped in winter 2003). The uncertainty of the input signal of the surface water of Lake Wannsee, caused by strong temporal and spatial variations was discussed earlier (chapter 1.5) and causes problems, for example in 3338 (transect 1) or BEE205 and BEE203 (transect 2). In the following, tracer breakthrough curves are shown for transect 2 only, which was sampled for much longer.

The breakthrough curves of the stable isotopes δD and $\delta^{18}O$ (Figure 76) and of Cl^- (Figure 76) show almost no delay from the lake to BEE206, while the temperature (Figure 77) is slightly off set. In contrast, the tracer break through about one month after peaking in the lake in BEE205, which is further out in the lake (Figure 74). The best estimates for travel times of the shallowest wells at Wannsee 2 are therefore ~1 month to BEE205 and less to BEE206 closer to the shore (maybe even less than 14 days) because of a better hydraulic conductivity of the clogging layer. BEE205 is located close to core 3B, while BEE206 is close to 1B (Figure 58), where hydraulic conductivities are about an order of magnitude higher. A better resolution can not be achieved with monthly sampling. The hydraulic model estimated travel times of a few days for both observation wells.

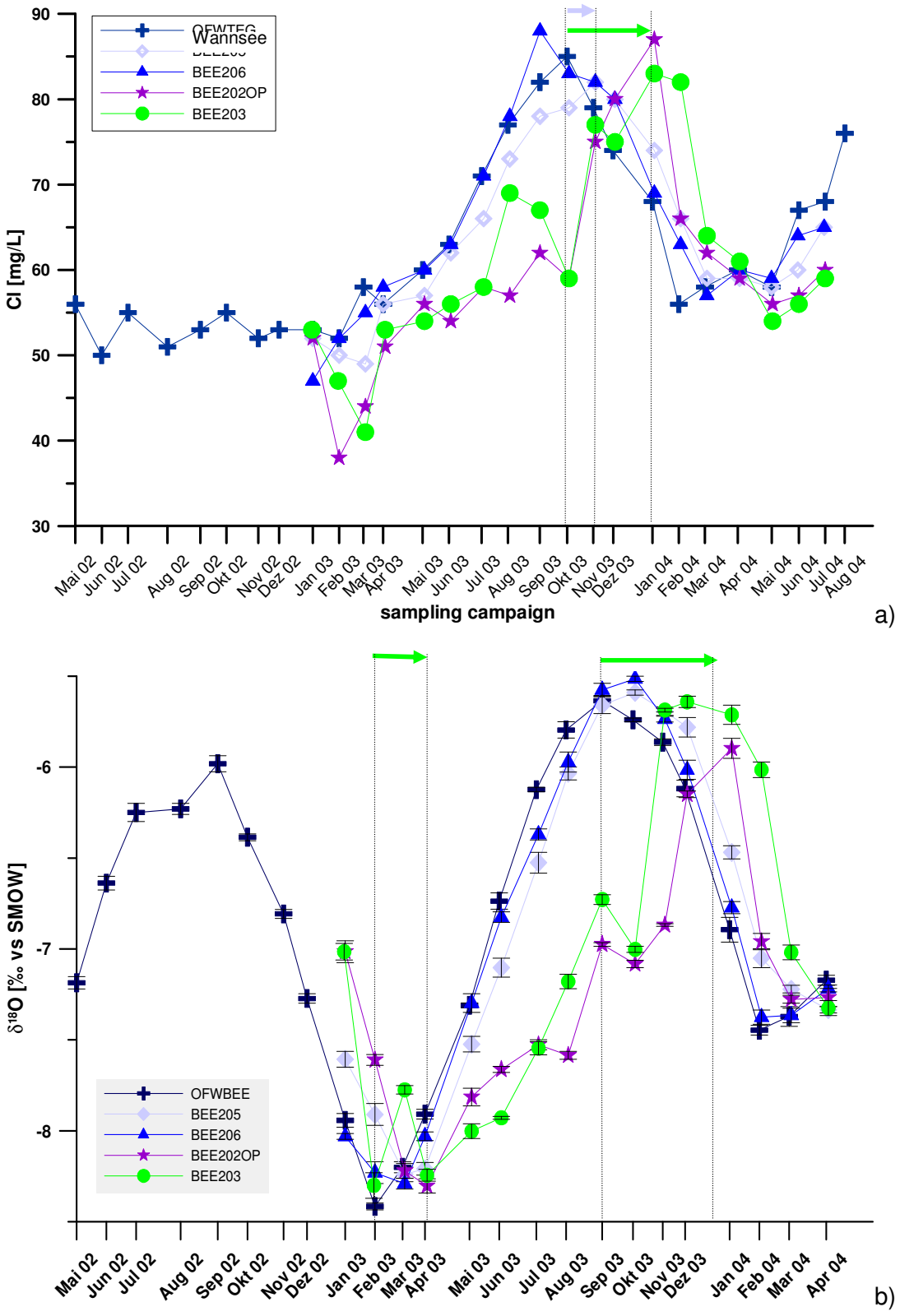

Figure 76: Time-series of Cl^- (a) and $\delta^{18}O$ (b) in the shallow wells of transect 2 in Wannsee (Data source: BWB & AWI).

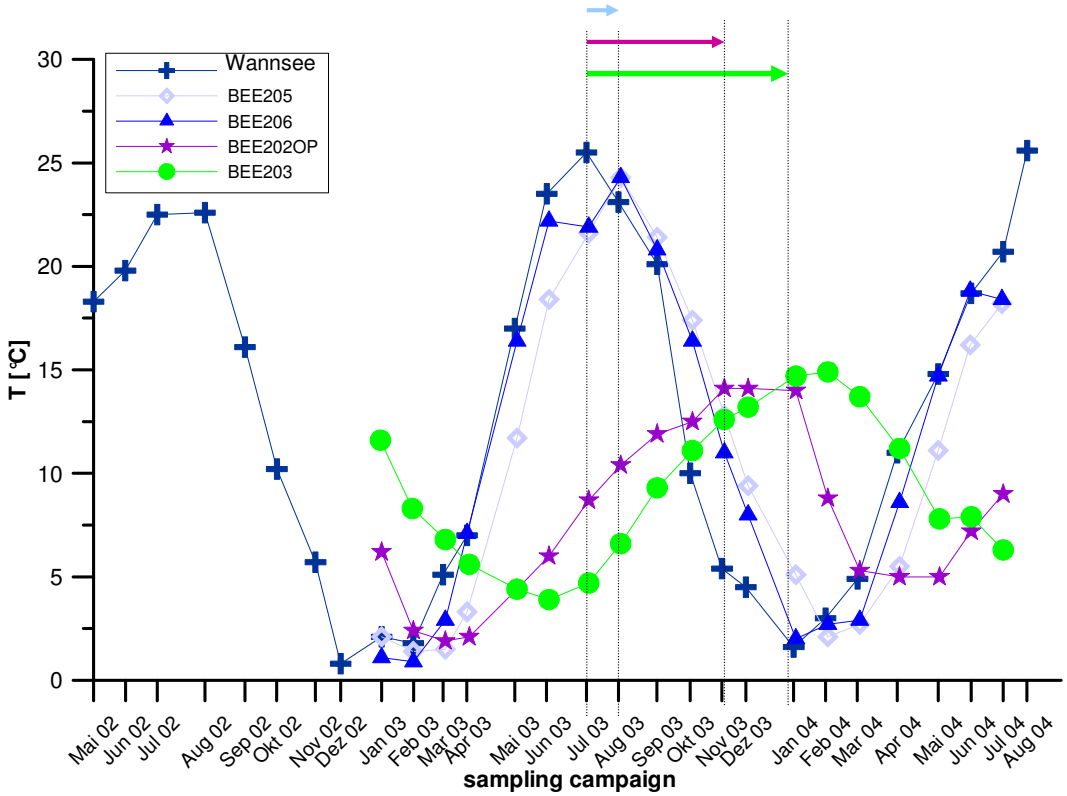

Figure 77: Time-series of temperature in the shallow wells of transect 2 in Wannsee. Note that temperature is retarding in comparison with a tracer, R ~ 2.1.

Breakthrough curves of BEE202OP and BEE203 are relatively similar to another, only the temperature shows a clear delay of BEE203 compared to BEE202OP. They both show an average time-lag of 2 and 4 months, depending on the time. Judging from Figure 76, it seems that the travel times are much longer in summer 2003 than in winter 2002/2003 and 2003/2004. The hydraulic model resulted in travel times of similar magnitudes, but with a tendency of longer travel times in winter (BEE202OP summer: 2 months, winter: 2.5 months; BEE203 summer: 2 months; winter 2.4 months). However, since BEE203 is about two thirds the way to the production well, the travel time on the fastest pathway is likely to be in the order of 3-6 months, depending on the hydraulic regime.

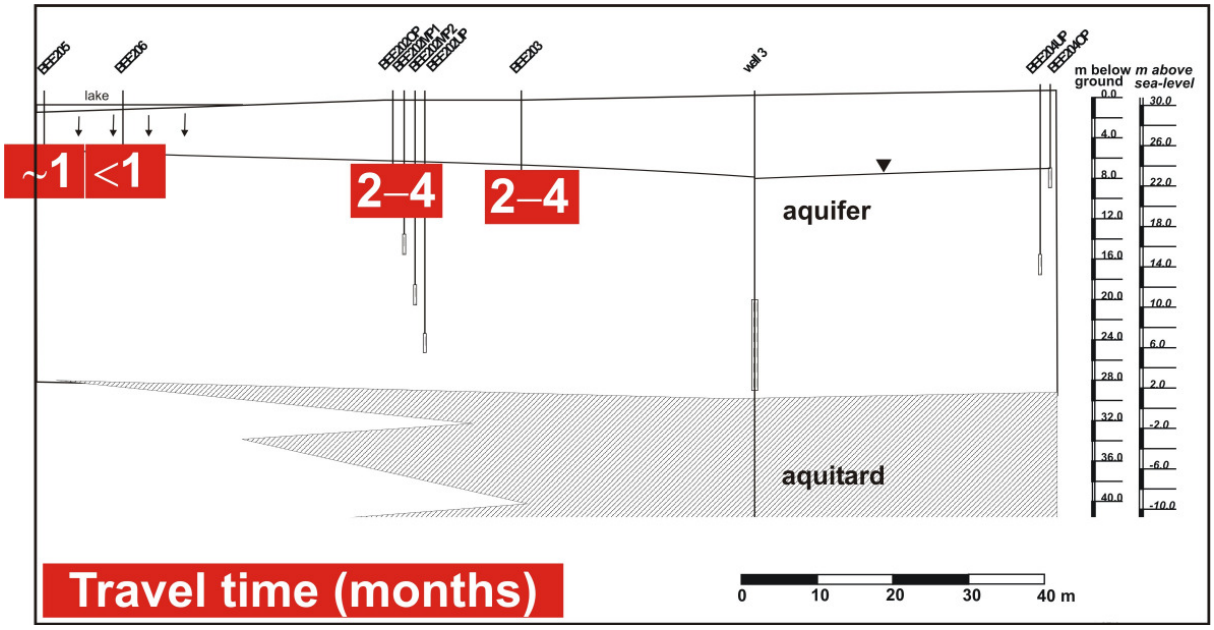

Figure 78: Summary of best estimates for average travel times from tracer breakthrough curves of the lake Wannsee transect 2.

The new deeper observation wells BEE201OP (filter screen 13-15 m below ground) & BEE201UP (18-20 m below ground) at Wannsee 1 and BEE202MP2 (18.3-20.3 m below ground) and BEE202UP (23.1-25.1 m below ground) do not show a seasonal isotopic variation and resemble average surface water values with regard to the isotopes (Figure 79b). The also show no variability in the concentration of any other potential tracer (e.g. B, Cl^-, EDTA). The same is true to some extent for the shallower well BEE202MP1 (13.3-15.3 below ground) which already has a strongly damped signal. The succession of the 4 observation wells at BEE202 therefore does not reflect a chronological sequence (with increasing travel times with depth) but a decrease of the proportion of “young” BF (in terms of BF directly from the adjacent shore) and an increase of “old” BF with depth. Even though this does reflect an age/travel time succession, these wells do definitely not lie on a single flow-path. The maximum depth of Lake Wannsee is ~ 9 m. The groundwater flow direction is from SW towards the well gallery. The elevated concentrations of wastewater indicators B (Figure 79) or EDTA in greater depth within the first aquifer and in particular elevated concentrations of substances such as phenazone and AMDOPH (compare chapter 1.5.8) which presumably have been present in the surface water in higher concentrations in the past, suggests that these wells contain bank filtrate which is at least partly originating from the past decades rather than from the past months, which had already been suspected by the T/He age dating results (Figure 74). The elevated concentrations could also be (at least partly) caused by the location of the catchment area of well 3 in the south of Lake Wannsee, where due to the closer location to the Teltowkanal, concentrations are presently (and have probably been for a long time) higher than in front of the transect (Figure 44, Figure 46).

The water abstracted in production well 3 does not show any seasonalities either. Therefore, the proportion of very young BF in the well itself can also not be very high (compare chapter 1.5.8).

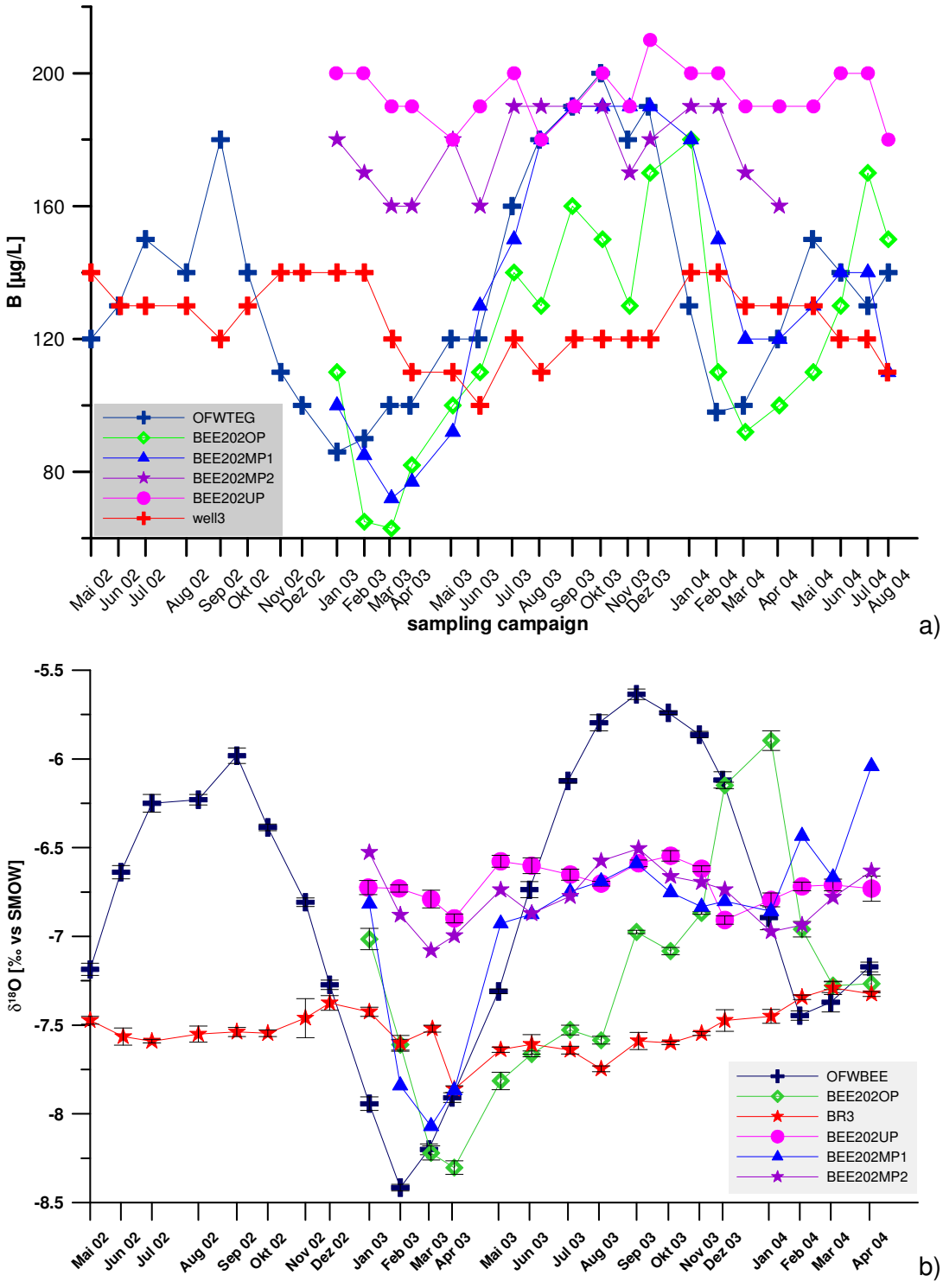

Figure 79: B (a) and $\delta^{18}O$ (b) in the lake, observation wells BEE202OP-UP and production well 4 (Data source: BWB & AWI).

1.5.8 Tracer evaluation: Mixing

The water abstracted at Lake Wannsee is a mixture of water from at least 6 distinctable sources, which makes the calculation of individual proportions in the production wells rather complicated, in particular since they are likely to differ with time too. Figure 80 displays the exemplary concentration of Cl^-, SO_4^{2-} and AMDOPH in the single sampling campaign in March 2004 in order to illustrate the differences between the water types. The ages have already been given in chapter 1.5.7.

The different water components are:

1. Bank filtrate with an age of a few months, originated from a close shore. The BF is characterised by a T/He age of 0 (i.e. < 6 months), a reflection of the variable (seasonal) input curve of all tracers and therefore a tracer concentration of similar magnitude as presently observed in the lake (encountered in 3335, 3337, 3338, 3339, BEE205, BEE206, BEE202OP, (BEE202MP1), BEE203).

2. Deeper, older bank filtrate with an age of years to decades, originating from a distant shore. The T/He age of this BF is at least a few years; tracer curves display no seasonality and the concentration of a number of minor water constituents differs largely from the present concentration in the lake (i.e. higher EDTA, B, AMDOPH, Phenazone; lower Carbamazepine, Gd-DTPA). Major water components and the stable isotopes tend to be present in the same order of magnitude as today, only with a lack of the seasonal variability (encountered in BEE201OP, BEE201UP, BEE202MP2, BEE202UP).

3. Background groundwater characterised by slightly elevated Cl^- concentrations, very high SO_4^{2-} (above the drinking water limit) and higher Ca^{2+}, a T/He age of 14 years and a general absence of waste-water indicators such as PhAC`s, B or EDTA. However, the occasional presence of some waste-water indicators suggests that the groundwater inland may at least sometimes and in parts be under surface water influence (observation wells inland: BEE200OP, BEE200UP, BEE204OP, BEE202UP).

4. Deeper groundwater from the *Elster* aquifer below the *Holstein* aquitard. The groundwater is of “pre-bombing” age (pre-1950) and shows no anthropogenic influence at all. Substances denoting bank filtration influence are not present. The hydrochemical conditions are sulfate-reducing; the water is almost SO_4^{2-} -free. The isotopic signature is more negative than at present because the formation temperature was much lower (3334).

5. Very deep, slightly more saline groundwater from the *Elster* aquifer below the second (*Elster)* aquitard represented by 3336. Again, the water is (at least) of pre-bombing

age but probably much older, the groundwater displays no anthropogenic influence, the hydrochemical conditions are sulfate-reducing, the water is almost SO_4^{2-} -free and the isotopic signature is also more negative than at present. The main difference to 3332 ad 3334 is that 3336 contains more Cl^-, Na^+ and B and appears to be influenced by saline deeper groundwater (Na-Cl-HCO_3 water type). When the well was sampled monthly in 2001 (Hinspeter, 2002), the Cl- concentration varied between 268 and 495 mg/L.

6. Very pristine groundwater is encountered in 3332, in the same aquifer as 5 but inland. The concentration of Cl^- is very low (typical for pre-industrial freshwaters). As 4 and 5, the water is very old, sulfate reducing and isotopically more negative than at present.

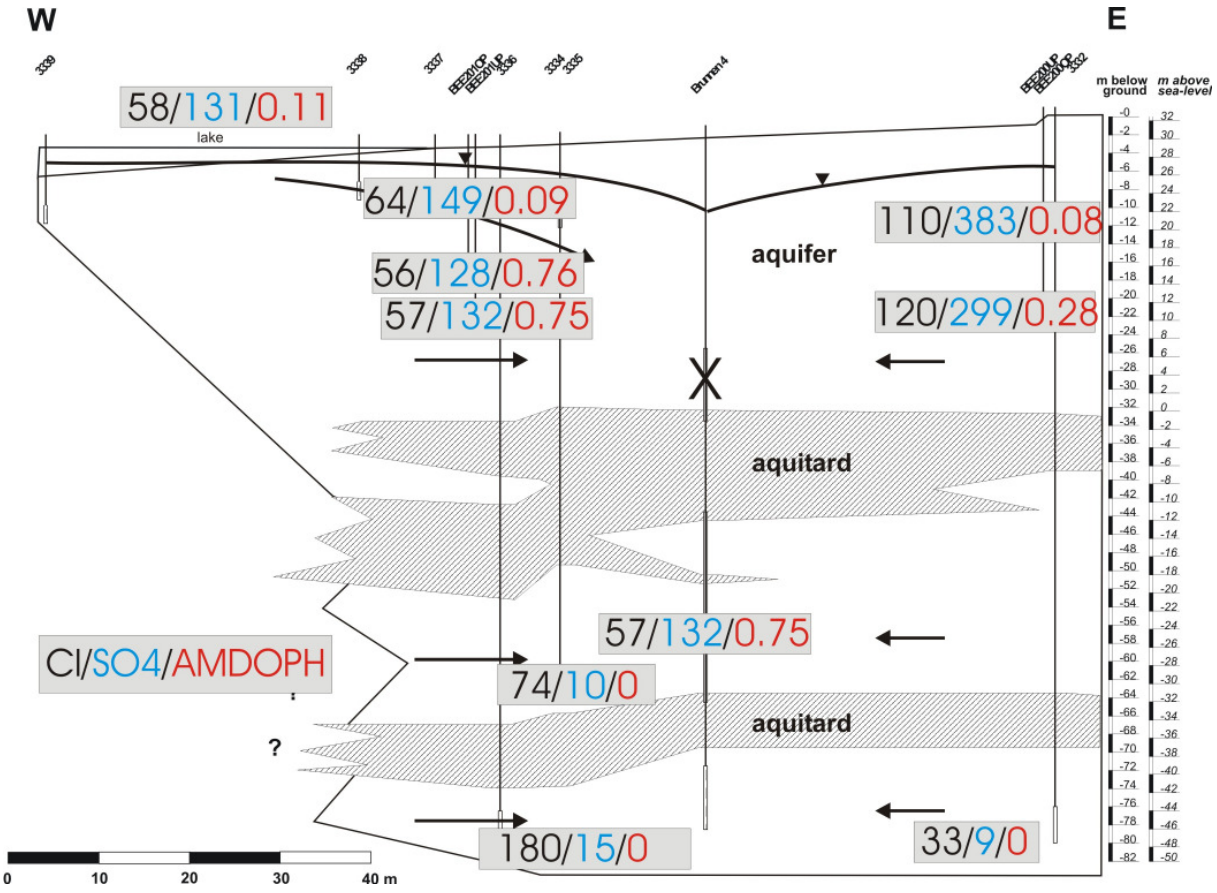

Figure 80: Concentration of Cl^- (mg/L), SO_4^{2-} (mg/L) and AMDOPH (µg/L) at transect Wannsee 1 in March 2004 (values plotted at loction of the relevant filter screen (data source: BWB). Values inland are those of BEE204OP & UP at Wannsee 2.

The two deeper aquifers at the site are free of Gd-DTPA (< 5 pmol/L), Carbamazepine, AMDOPH or any other persistent (and likewise less persistent) wastewater indicator, the same is (mostly) true for the groundwater inland of the production wells. Therefore, in order to estimate the proportion of “old/deep” bank filtrate (2) and “young/shallow” bank filtrate (1) in the production well, 3 parameters with clearly differentiable concentrations in 1 and 2 and similar

concentrations in the remaining groundwater (3, 4, 5 and 6) were chosen, namely AMDOPH (Figure 82a), Carbamazepine (Figure 82b) and the value of $\delta^{18}O$ (the slight differences between 3, 4, 5 and 6 were neglected and a value of -8.8 was assumed, Figure 83). The individual proportions can then be calculated by solving a system of equations with the average concentrations of AMDOPH, Carbamazepine and $\delta^{18}O$ in the different water components:

$$c_{br} = c_1 * x + c_2 * y + c_r * z$$

with: c_1 = concentration in young BF (value of BEE203 used)
c_2 = concentration in old BF (value of BEE202MP2 used)
c_r = concentration in groundwater (3, 4, 5 and 6)
c_{br} = concentration in production well 3 or 4

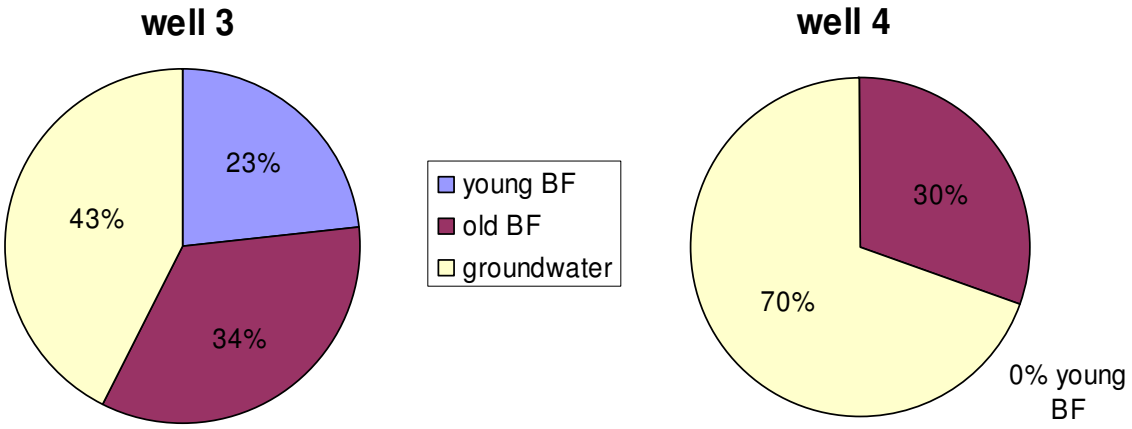

Figure 81: Percentage of young and old bank filtrate and remaining groundwater in well 3 and 4, calculated with average concentrations of AMDOPH, Carbamazepine and $\delta^{18}O$.

The results, shown in Figure 81, are clearly only a very rough estimation, since the proportions are likely to vary, depending on the pumping regime and the data/time-period used. Also, the calculation assumes that both Carbamazepine and AMDOPH are perfectly conservative tracer, which is, even though they are largely persistent, not correct. In order to reduce the effect of degradation, the concentrations of BEE203, close to the production wells, rather than the surface water concentrations were used. EDTA could also be use for calculations but its detection limit of 2 µg/l leads to even bigger uncertainties in the numbers.

According to the calculations, well 3 abstracts a total of 57 % BF, while well 4 only abstracts 30 %. Because Carbamazepine was always below the detection limit in well 4, the calculated percentage of young BF in well 4 is 0, compared to 23 % in well 3. However, this may be a slight underestimation due to the confining detection limit. Using anthropogenic Gd (Figure 82c, data from 2003) instead of Carbamazepine for the calculation of the proportion of young bank filtrate yields a proportion of young BF of 15 % in well 3 (Gd_{anth}= 10 ng/l) and 4.5 % in well 4 (Gd_{anth}= 10 ng/l). Again, this assumes that anthropogenic Gd is a conservative tracer which is not the case. Knappe (in prep.) could show that it is subject to very slow biological

degradation. However, using BEE203 instead of the surface water concentration for the mixing calculation diminishes the error associated to the degradation. Since the exact travel time from BEE203 to the well is unknown, degradation cannot be included in the caclulation. Therefore, the mixing proportion may be underestimated and the real proportion of young BF slightly higher.

Hinspeter (2002) used EDTA and anthropogenic Gd to calculate the monthly proportion of BF in well 4, which resulted in 10.3 ± 6.6 % and 3.6 ± 1.1 % respectively. With the new knowledge of the vertical stratification of Gd (Figure 82c), the first value (EDTA) is representative for the proportion of total BF, while the latter (Gd) for the proportion of young BF only, which explains the difference between the values.

The lack of any seasonality in the production wells at Wannsee can therefore be explained with the low proportion of young bank filtrate. However uncertain and approximate, the calculations give an idea on the mixing proportions in the production wells themselves. Using minor water components such as anthropogenic Gd and AMDOPH has the advantage that young (i.e. < 1 year) and old (i.e. <<1 year) proportions of bank filtrate can be differentiated. While well 4 abstracts only a few percent of young BF, it does abstract a considerable proportion of older BF. In general, well 3 has a rather high (> 50%) proportion of BF in total, while well 4 has a rather low percentage of total BF, caused by the (incomplete) sealing of the uppermost filter screen.

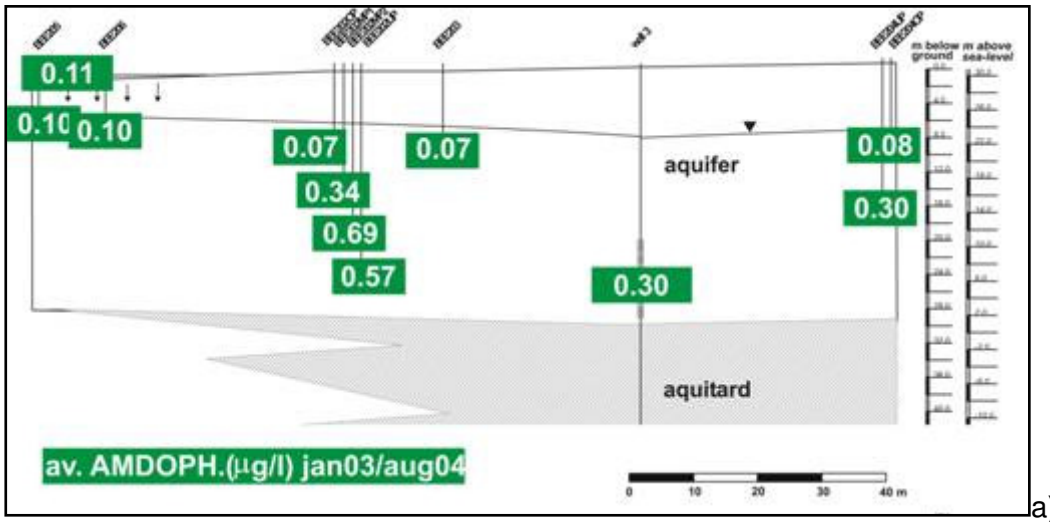

a)

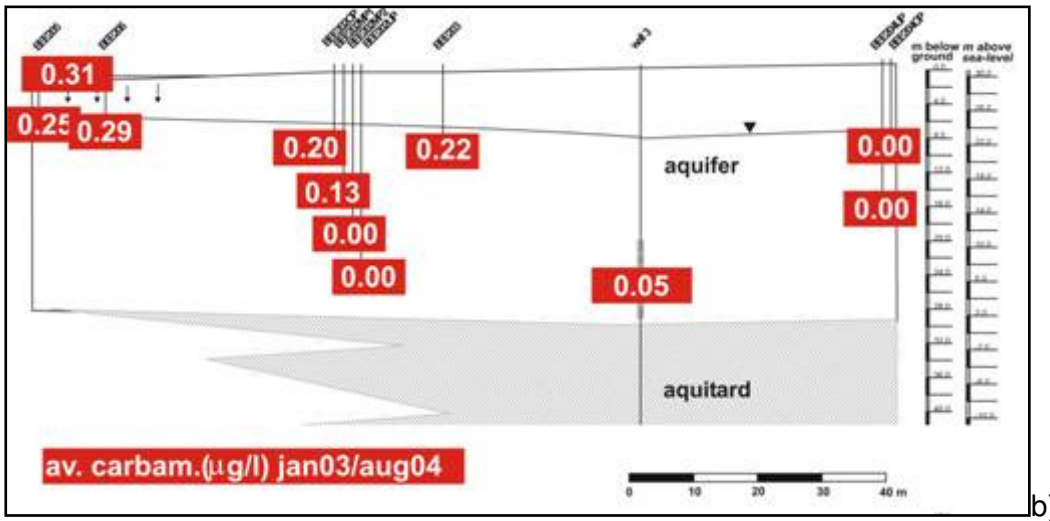

b)

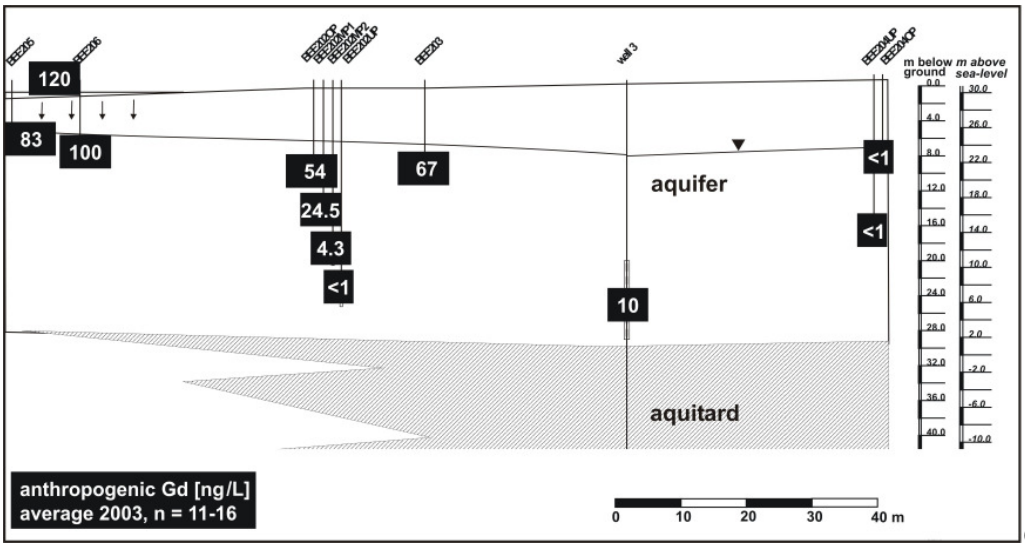

c)

Figure 82: Average AMDOPH (µg/L), Carbamazepine (µg/L) and Gd (pmol/L) concentrations in observation wells of transect Wannsee 2. Production well 3 has filter screens in the deeper aquifers too. AMDOPH and Carbamazepine concentrations from January 2003-August 2004 (Data source: BWB) Anthropogenic Gd concentration from January 2003-December3003 (Knappe, in prep).

The scatter plot of δD versus $\delta^{18}O$ in surface water, production wells, deeper groundwater and background groundwater inland of the wells illustrates that well 4 has the lowest and well 3 the highest proportion of bank filtrate. It also shows that the isotopic signature is comparatively similar in the observation wells inland and those in deeper aquifers.

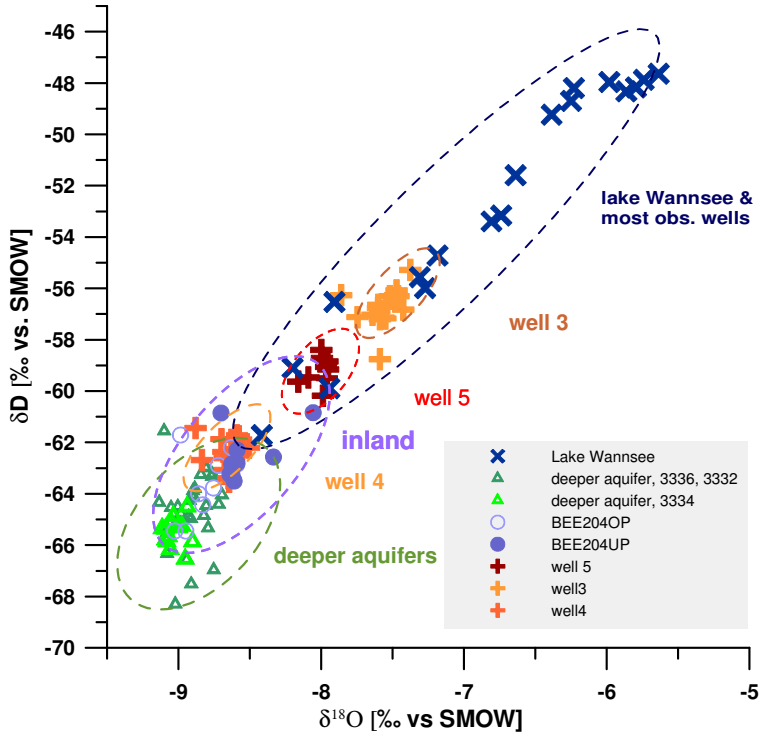

Figure 83: δD versus $\delta^{18}O$ in surface water, background and deeper groundwater and abstracted water in Wannsee. Deeper aquifers: Data 10/2000 –11/2001 (Hinspeter, 2002); remaining samples from May 2002-October 2003, data source: AWI.

The elevated concentrations of wastewater indicators and more positive isotopic signatures give evidence that since autumn 2003, the groundwater observation wells inland of the production wells have been under surface water influence (Figure 84). This could be due to the catchment area of well 3 seasonally reaching Lake Schlachtensee as illustrated in the hydraulic model. The model also suggested that due to the low abstraction of well 4 in the upper aquifer and local bulges in the Holstein aquitard, bank filtrate from Lake Wannsee can reach well 3 from inland.

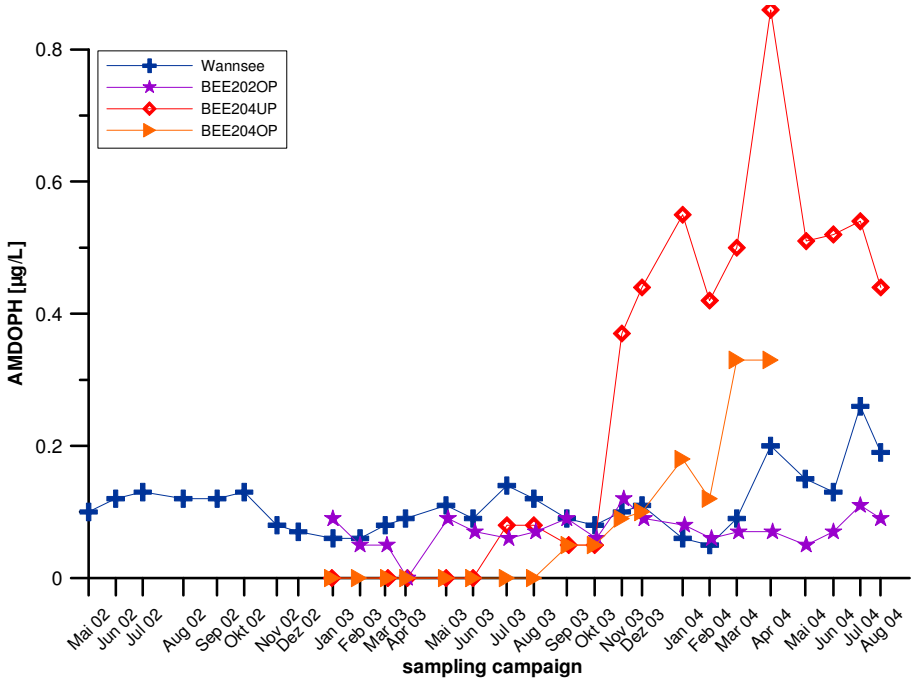

Figure 84: Time-series of AMDOPH in surface water, bank filtrate and groundwater inland (BEE202UP & OP) in Wannsee (Data source: BWB).

1.5.9 Hydrochemistry at the transect

Redox processes during bank filtration

As at transect Tegel, redox changes during infiltration are of particular importance, since they cause the appearance of the undesired metals Fe^{2+} and Mn^{2+} (Bourg and Bertin, 1993), influence the behavior of a number of organic pollutants such as pharmaceutically active substances (Holm et al., 1995), halogenated organic compounds (Bouwer and McCarthy, 1993; Grünheid et al., 2004) and effect the pH and calcite solution capacity (Richters et al, 2004).

Rather than concentrating on the Eh, redox zones may be characterised by the disappearance of reactants (oxygen, nitrate, sulphate) or the appearance of reactants (iron, manganese) as suggested by Champ et al. (1979). Boxplots of redox indicators in Figure 85 give a first idea on the redox conditions. While the shallower (younger) wells contain oxygen and nitrate throughout most of the year, the deeper observation wells are free of these but contain manganese (Mn^{2+}), iron (Fe^{2+}) and often ammonia (NH_4^+).

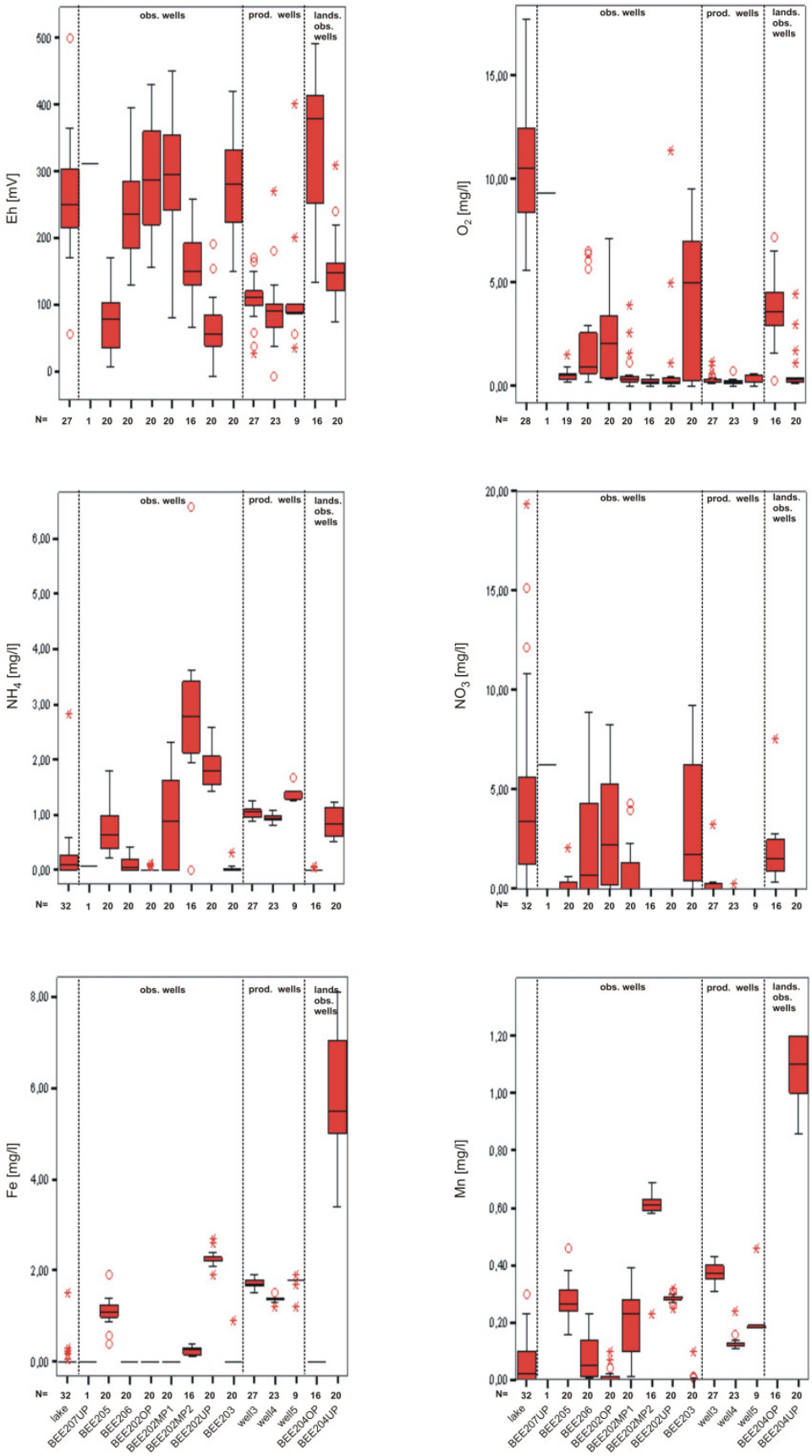

Figure 85: Boxplots of redox indicators at the transect Lake Wannsee 2 (May 2002-August 2004).

The two observation wells below the lake are quite different from each other with respect to their hydrochemistry. While BEE206 closer to the shore is still aerobic, BEE205 is mostly oxygen and nitrate-free which is likely to be due to the higher amount of organic carbon and lower hydraulic conductivities (chapter 1.5.2) which results in longer travel times and more reducing conditions at BEE205 in comparison to BEE206.

Figure 86 indicates the approximate redox zoning as indicated by the presence (or absence) of redox indicators given in Figure 85. The vertical redox zoning may be a result of the different groundwater ages. However, it may also be caused by re-oxidation of more reducing bank filtrate by oxygen penetrating though the permeable unsaturated zone, possibly enhanced by the water-level fluctuations caused by the irregular pumping regime (compare chapter 1.5.10). Bourg and Bertin (1993) investigated biogeochemical changes during bank filtration at the Lot River. They observed a similar reduced anaerobic zone close to the river followed by aerobic conditions further along flow direction. They concluded that the observed redox processes were reversible and oxidation caused by aeration through the permeable unsaturated zone close to the river. Similar to our findings, Richters et al. (2004) describe a vertical redox zonation at a bank filtration site near the River Rhein.

The deeper aquifers (not shown in Figure 86) are sulfidic (Figure 80) and do not contain oxygen, nitrate and only little sulfate.

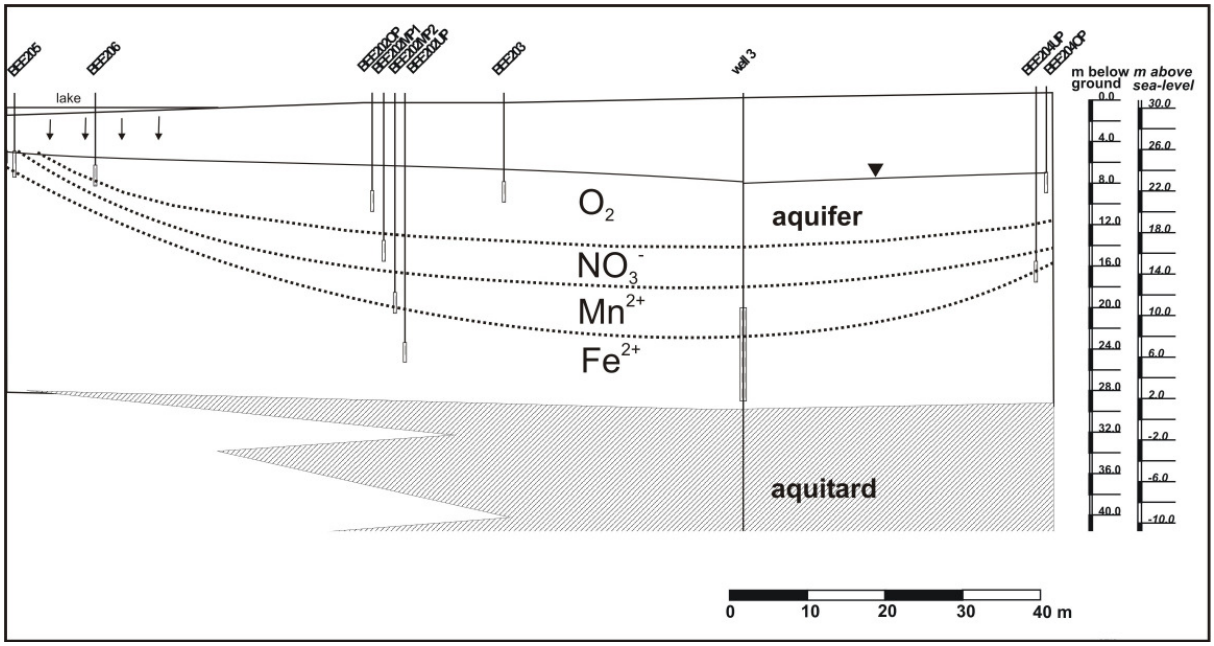

Figure 86: Approximate redox zoning as indicated by O_2, NO_3, Mn and Fe presence.

However, these zones (Figure 86) are not immobile and redox boundaries move seasonally (Figure 87). The younger bank filtrate undergoes strong seasonal temperature changes of up to 25 °C, depending on the distance from the lake. Because redox processes are microbially catalysed, these changes lead to differences in microbial activity (e.g. David et al., 1997;

Prommer and Stuyfzand, 2005). As a result, oxygen and nitrate disappear at times when temperatures are highest which is in summer or autumn, depending on the respective time lag to the well. It is interesting to note that nitrate concentrations in the lake itself decrease to zero in summer, probably due to consumption by algae. The disappearance of nitrate in the observation wells therefore appears to reflect the input signal rather than a reduction in the aquifer itself (figure 3).

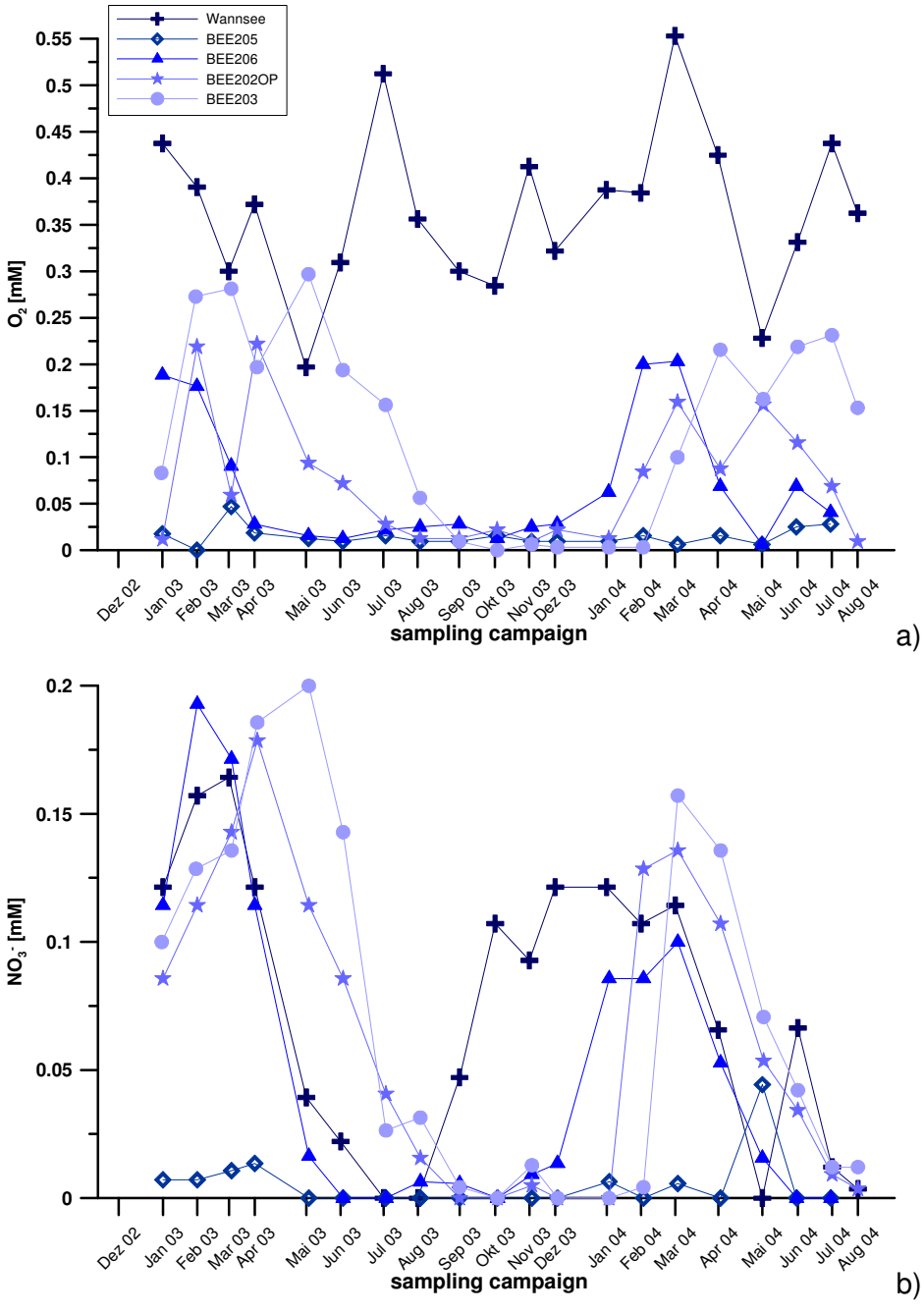

Figure 87: Seasonal variation of oxygen (a) and nitrate (b) in Lake Wannsee the shallow observation wells (data source: BWB).

Hydrochemical conditions of inland groundwater/origin of sulfate

As mentioned in chapter 1.5.8, the groundwater inland of the production wells strongly differs from the bank filtrate between observation wells and lake. In particular sulfate (SO_4^{2-}) but also Calcium (Ca^{2+}), Magnesium (Mg^{2+}), hydrogen carbonate (HCO_3^-) and carbon dioxide (CO_2) concentrations are higher than in the BF while the pH is lower (around 6.9 instead of 7.5). Boxplots of sulfate and calcium are shown in Figure 88.

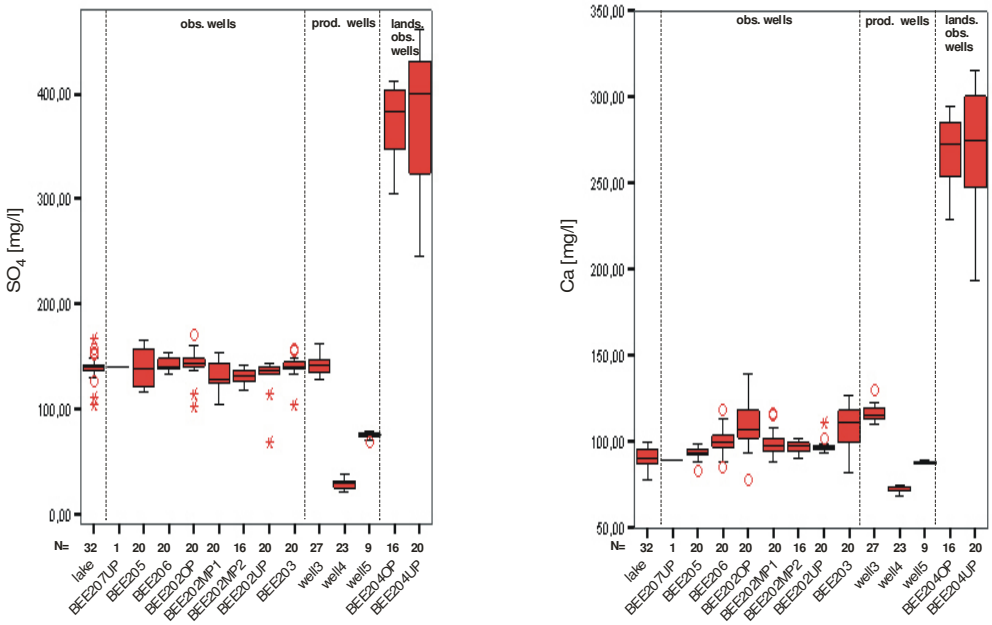

Figure 88: Boxplots for sulfate and calcium in transect 2 at Wannsee (Data source: BWB).

In particular the sulfate concentrations of almost 400 mg/l in average could potentially be problematic, since they exceed the drinking water limits. At present, they are unproblematic, because the groundwater is diluted by bank filtrate with a much lower sulfate concentration (chapter 1.5.8). The sulfate concentrations (and also Ca and Mg content) are explainable with:

1. gypsum resolution from war debris as often described for the shallow Berlin groundwater (Sommer von Jarmerstedt et al., 1998).
2. oxidation of finely distributed sulphides in the sediment due to the permanent fluctuations and lowering of the groundwater table induced by the pumping regime. Since the oxidation also releases acidity, this may also explain the lowered pH and the elevated calcium and alkalinity in the groundwater, which would be the result of dissolution of the calcite present in low contents in the sediment (Figure 71).

3. the influence of sewage farms formally present upstream of the catchment area of the well gallery.

Isotope analysis of ^{34}S and ^{18}O of sulfate was performed at the Institute of Mineralogy of the Technical University Bergakademie Freiberg. The results for transect 2 are shown in Figure 89 and Figure 90.

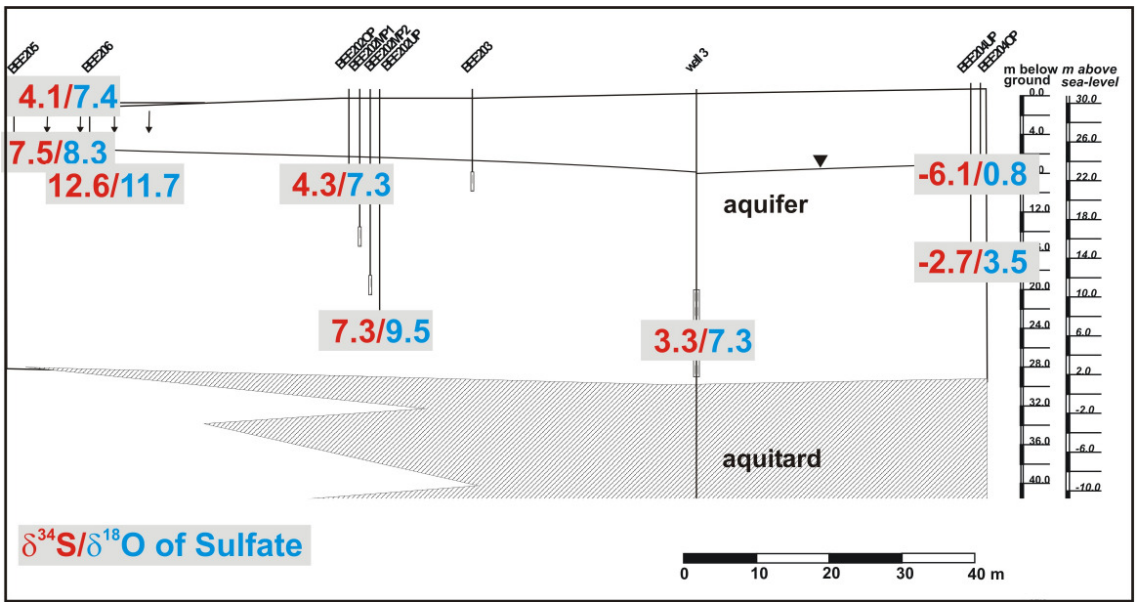

Figure 89: $\delta^{34}S$ (‰ vs. CDT) and $\delta^{18}O$ (‰ vs. V-SMOW) of sulfate at Wannsee 2 in March 2004, analysed at the Institute of Mineralogy of the Technical University Bergakademie Freiberg.

Because the isotopic signature of the observation wells inland is very low (negative values for $\delta^{34}S$), an origin from gypsum dissolution can be excluded for the Wannsee site. Marine sulfate (which is where gypsum is most likely to originate from), has positive values around +10 - +35 ‰ CDT for $\delta^{34}S$, depending on the geological time of formation (Clark and Fritz, 1997). Negative values like the ones observed are typical for biogenic pyrite or shales (Krouse, 1980). Hence, possibility 1, gypsum dissolution can be excluded. Possibility 2, pyrite oxidation triggered by the regular water-level fluctuations, is a possible explanation. Possibility 3, an influence of the sewage farms south-west of Berlin, can also not be exluded, in particular since the groundwater of the same shallow aquifer in Lankwitz (3756, Figure 90), in south-west Berlin revealed a similar sulfate concentration and isotopic signature, which cannot be explained by water-level fluctuations at the site. It is not possible to solve the question of the sulfate origin with the limited amount of data within this project. If water table oscillations were the cause for the elevated sulfate concentrations, optimisation of the pumping regime could, at least, reduce the sulfate input.

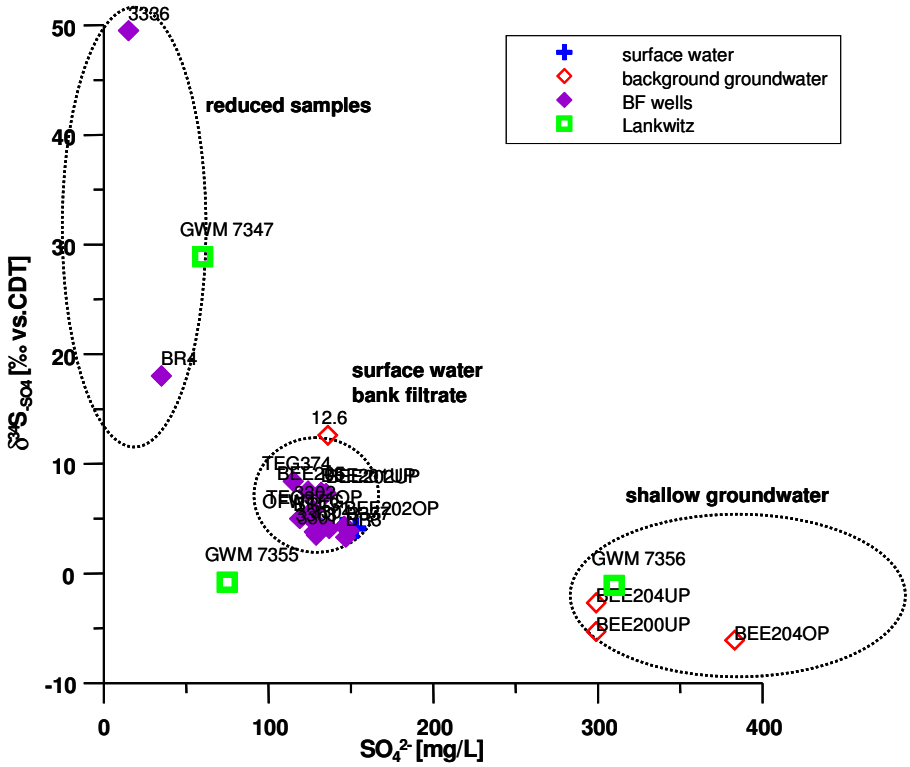

Figure 90: $\delta^{34}S$ (‰ vs. CDT) versus sulfate concentrations (mg/l) at Wannsee and Lankwitz in March 2004, analysed at the Institute of Mineralogy of the Technical University Bergakademie Freiberg.

1.5.10 Input of oxygen into groundwater during bank filtration

Introduction

As discussed in chapter 0, the redox conditions, in particular the amount of oxygen in the groundwater used for the drinking water supply is a crucial factor for the drinking water quality as well as for the operating production wells. Microbial degradation of pharmaceuticals may depend strongly on redox conditions. Furthermore the durability of the production wells is decreasing considerably at the presence of oxygen, which leads to precipitation of trivalent iron- oxides and subsequent clogging. And thirdly, the elevated sulfate concentrations may be caused by the continuous input of oxygen (chapter 0). The different potential pathways of oxygen input into the aquifer are illustrated in Figure 91.

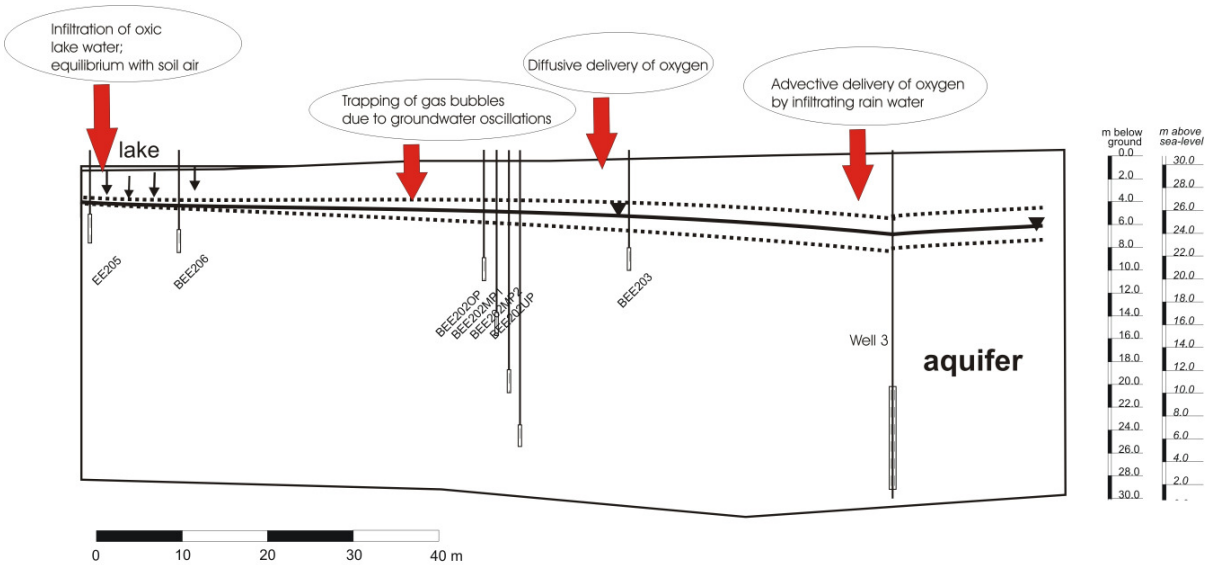

Figure 91: Sketch describing different sources of oxygen input into the groundwater during bank filtration exemplified for the Wannsee Transect 1.

Figure 91 shows four different mechanisms of oxygen input represented by the red arrows which are described in the following from the left to the right:

The first oxygen source is related to the infiltration of oxic lake water and the subsequent equilibration of seepage water with soil air of the unsaturated zone below the lake. According to the measured time series of oxygen at the observation wells (Figure 87) this mechanism works only during the cold period when microbial degradation is inhibited due to the low temperatures. This can be observed for example at BEE206, BEE204 OP and BEE203 (Figure 87). At BEE205, the colmation layer is thicker and shows a higher content of organics (Figure 59) which leads to oxygen consumption all over the year (Figure 86, Figure 87).

The second mechanism of oxygen input is related to the oscillations of the groundwater level due to the pumping regime of the production wells. Rising groundwater tables always lead to entrapped gas bubbles within the newly saturated zone of the sediment. Laboratory experiments with columns have shown that upward saturation of sediments may lead to volumetric entrapped air content up to 10% or more of the sediment bulk volume (Faybishenko, 1986). It was found that entrapped air can be divided in mobile bubbles of air and immobile entrapped air that is captured in pores and can be removed from the sediment only by dissolution leading to rising oxygen contents of the groundwater. Faybishenko (1995) found that with upward saturation the remaining volume of entrapped air was less than 5%, which corresponds to a sixth part of the pore space assuming a porosity of 30%.

The third way of oxygen input is caused by diffusive delivery of oxygen from soil air into the groundwater and the fourth mechanism considers the oxygen delivery by infiltrating rain water.

The seasonal character of the oxygen time series in the study area with low concentrations in summer and high concentrations in winter indicates that the oxygen input due to oxic bankfiltrate seems to be a major component in our system. But nevertheless more oxic conditions and vertical broadening of the oxic zone along the pathline of bankfiltrate towards the wells Figure 86) lead to the conclusion that other mechanisms also have to be taken into account. To get a deeper understanding of the processes which lead to elevated amounts of oxygen in the groundwater during bank filtration, rough estimates about the quantitative importance of the different mechanisms are described in the following. The calculations can be adapted easily to hydraulic and hydrogeochemical conditions at other locations.

Methods

Oxygen input by bankfiltrate:

The oxygen input below the lake into the groundwater was derived by measured oxygen concentrations in groundwater at offshore observation wells close to the shoreline. The redox conditions are related to the infiltration of oxic lake water, microbial mediated consumption of oxygen and the subsequent equilibration of seepage water with soil air of the unsaturated zone below the lake. The total mass input of oxygen was calculated by multiplying observed concentrations with the oxic volume according to

$$nO_2 = cO_2 \times L \times A$$

where nO_2 is the total amount of moles of oxygen, cO_2 is the measured oxygen concentration of groundwater below the lake, L is the vertical thickness of the oxic zone below the lake and A is the unit area of 1 m^2.

In the case of the Wannsee 1 the observation well BEE206 shows an oxic zone with an approximate vertical thickness of 2 m. Between 2002 and 2004, oxygen concentrations around 0.8 mg/l were measured in summer and 5 mg/l in winter, which is owing to reduced microbial activity in winter because of the low average temperature of about 4° C.

Diffusive oxygen delivery:

The diffusive delivery of oxygen was calculated using the analytical solution of the advection-diffusion equation from Ogata and Banks (1961) simplified for pure diffusion without advection:

$$c(x,t) = c_0 + \frac{c_{in} - c_0}{2} erfc\left(\frac{x}{2\sqrt{Dt}}\right)$$

where *c(x,t)* is concentration as a function of space and time, c_0 stands for the initial concentration, D represents the effective diffusion coefficient corrected for porosity and tortuosity ($L^2\ t^{-1}$). The equation is valid for the boundary condition

$$c(x = 0, t) = c_0$$

The molecular diffusion coefficient D_0 was corrected according to (Troeh et al., 1982) as follows:

$$D = \frac{D_0 \times \theta}{\tau^2}$$

with D_0 =molecular diffusion coefficient of oxygen in water ($L^2\ t^{-1}$), θ =porosity (-)and τ = tortuosity (-) which means the ratio of the actual path length over the direct path length.

The total amount of diffusive oxygen input into the groundwater during the entire travel time was calculated for a volume with cross-sectional unit area according to:

$$nO_2 = \sum_{i=1}^{m} (c_i \times dz)$$

where nO_2 is the total amount of moles, *i* and m are index variables which refer to different depths, *dz* is the vertical distance, c_i is the calculated oxygen concentration of groundwater at depth *I*.

Infiltrating rain water:

The calculation of the oxygen delivery by infiltrating rainwater is based on the assumption that 1 litre water contains 10 mg of oxygen considering an average annual groundwater recharge of the corresponding location.

$$nO_2 = cO_2 \times GWR \times t$$

where nO_2 is the total amount of moles entering during travel time in a unit area of 1 m^2, cO_2 is the oxygen concentration of rainwater, *GWR* is the annual water flux of recharge in litre per m^2 per year and *t* is the travel time.

Entrapped soil air:

The amount of oxygen in the groundwater related to trapped gas bubbles is calculated according to the ideal gas law:

$$nO_2 = \frac{\theta_{air} \times pO_2}{RT} \times \omega$$

where nO_2 is the number of moles oxygen, θ_{air} is the entrapped air volume within one oscillation, pO_2 means partial pressure of oxygen in soil air, R is the gas constant, T is the temperature in Kelvin and ω is the number of oscillations during travel time. The calculations are based on an average value of the oscillation amplitude which is applied for the entire transsect at the location.

Input data:

The defined input data for all scenarios is given in Table 6.

Table 6: Input data for the simulations and calculations. Unless stated otherwise, the data are based on compilations given in the CRC Handbook of Chemistry and Physics, adjusted as necessary to bank filtrate conditions of Berlin.

Parameter	Units	Value	Comments
D_0:	cm^2s^{-1}	1E-05	Based on the diffusion of oxygen at infinite dilution.
□	(-)	1.57	ratio of the half periphery of an ideal shaped circular particle over its diameter,
c_0:	mg/l	summer: 0.2: winter: 5:	averaged value derived by measured oxygen concentrations at observation wells showing oxic conditions below the lake
c_{in}:	mg/l	10	We assumed oxic concentrations of 10 mg/l at the groundwater surface which is in contact with soil air
θ_{air}	(-)	0.025	entrapped air volume with relation to the bulk sediment volume estimated according to Faybishenko (1995)
θ	(-)	0.2	Porosity estimated based on representative sediment analysis in study area
R:	$J\ K^{-1}$	8.31	gas constant
T	K	285	average annual temperature
pO_2	(-)	0.1	Estimated value for partial pressure of oxygen representative for soil air
GWR	mm/a	100	groundwater recharge

Scenarios:

Calculations have been performed for the conditions documented in Table 7:

Table 7: Scenarios for the calculation of oxygen input into the groundwater from different sources

	scanario A1	**scanario A2**	**scanario A3**
oscillation amplitude (m)	0.5	2	5
oscillation frequency	daily	daily	daily
traveltime (month)	3	3	3
	secanario B1	**secanario B2**	**secanario B3**
oscillation amplitude (m)	2	2	2
oscillation frequency	daily	weekly	monthly
traveltime (month)	3	3	3
	secanario C1	**secanario C2**	**secanario C3**
oscillation amplitude (m)	2	2	2
oscillation frequency	daily	daily	daily
traveltime (month)	1	3	6

Limitations and simplifications of the calculations:

The above described methods for the calculations were carried out based on the following simplifications:

- These calculations represent a one dimensional flow path for the upper oxic zone of the aquifer.
- The oscillation amplitude is constant over the entire pathway of the bank filtrate towards the well.
- The observed concentrations of oxygen below the lake are representative for the entire oxic profile below the lake
- The partial pressure of oxygen in soil air is constant in time and does not show seasonal variations.
- Constant temperature of 285 K is used in gas law.
- The different mechanisms are not correlated, i.e. an increasing oscillation frequency does not change the travel time etc.

Results

The contributions of oxygen calculated for the different sources are illustrated in Figure 92.

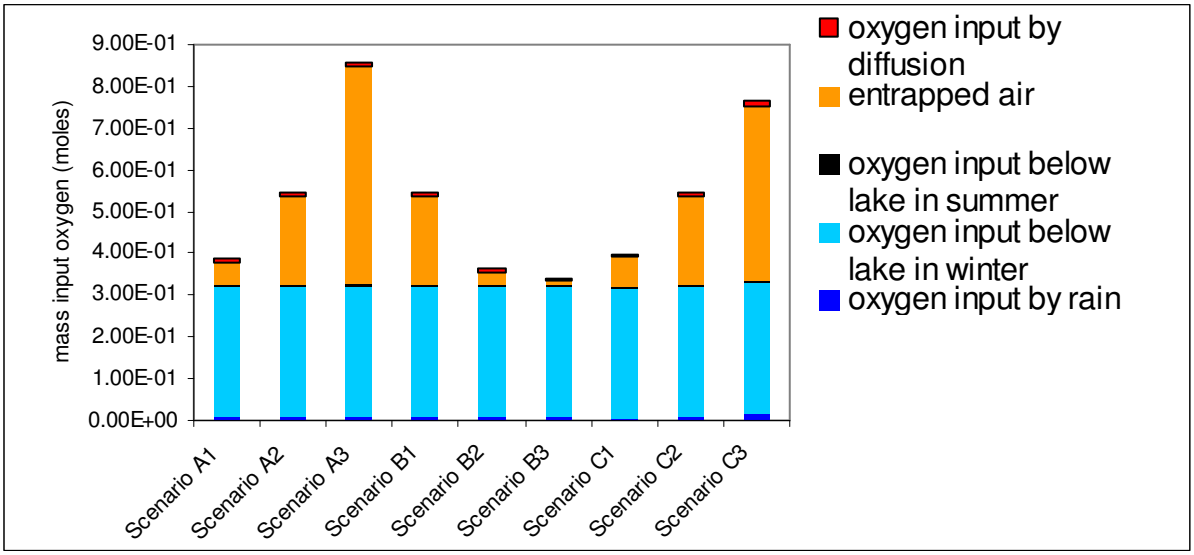

Figure 92: Estimated input of oxygen into the groundwater originated by different mechanisms

Due to the simplifications which have been specified for these rough estimates, the quantitative results obtained from this study can be interpreted in a relative and qualitative sense only. The calculations are representative for a one dimensional flow path only and can not be applied directly to a three-dimensional flow field of a production well. Therefore the results are not feasible for predicting and interpreting concentrations observed at the production wells itself, which shows only a certain amount of water originating from young bank filtrate. However, some important results have emerged from this study, which are enumerated in the following points:

1. Bank filtrate during winter and entrapped soil air due to oscillations constitute the major sources of oxygen in the hydrogeochemical system of the study area. Sources of oxygen input by percolating rain water and by diffusive delivery of oxygen in the gas phase are negligible.
2. Conditions of daily oscillations of 5 m and travel times about 6 month may lead to oxygen input by entrapped soil air comparable with the oxygen source due to bank filtrate in winter.
3. Due to the importance of water oscillations for the oxic conditions in our system the operational mode of the production wells can be used to control oxic conditions in the aquifer in order to optimize drinking water quality and durability of production wells.

1.5.11 Major conclusions and summary Lake Wannsee site

Surface water

- The surface water quality and conditions varies strongly within Lake Wannsee and also with time, in particular close to the transects. The sample taken each month in

front of transect 1 is not sufficient to cover temporal and spatial variations in front of the transect.

Clogging layer / Infiltration zone

- The mapping showed that the geochemical and hydraulic conditions are highly variable over small distances.
- The sediments deposited in 0 to 7 meters water depth consist of fine grained sand with increasing proportions of silt and clay and decreasing proportions of fine grained sand along with the water depth.
- The organic carbon content generally increases with distance from the shore and water depth, reaching levels of > 20 weight-% in the laccustrine sappropel.
- Impermeable laccustrine sappropel dominates in water depths below 7 meters.
- Oxygen is completely consumed in the uppermost few cm of the sediment recovered as an undisturbed column taken in 20 m distance from the shore (at the location of BEE205). The redox conditions reach Mn(IV)/Fe(III) reducing conditions within only a meter of flow, equivalent to the conditions observed in the groundwater well BEE205.
- Oxic bank filtration can therefore only take place at a narrow stripe of less than 20 m width.

Travel times/age

- A realistic travel time evaluation is only possible with the combination of T/He age dating with breakthrough curves of stable isotopes, boron, chloride and temperature.
- Like at Lake Tegel, the bank filtrate is strongly stratified with regard to the age distribution. The shallow young bank filtrate is only a few months old while the deeper bank filtrate (in the upper aquifer) is several years old.
- The travel times of the bank filtrate to the production wells vary between < 3 months in the fastest case to > 10 years in the deeper layers of the uppermost aquifer.
- For observation wells deeper than ~10 m, i.e. those deeper than the lake, the share of young BF (directly from the shore) decreases with depth.
- The travel times of the young BF, determinable by the travel breakthrough curves appear to show large differences between summer and winter.

Mixing

- At least 6 distinguishable types of water from 3 different aquifers mix in the production wells including young and old bank filtrate, high sulfate groundwater from inland,

deeper groundwater from the *Elster* aquifer below the *Holstein* aquitard and very deep, slightly more saline groundwater from the *Elster* aquifer below the second (*Elster)* aquitard and very pristine groundwater is in the same aquifer but from inland.

- Young and old bank filtrate contain different concentrations of a number of minor water constituents, reflecting the surface water quality changes of the past few years.
- Well 3 abstracts at least 57 % of BF, out of which less than half are young BF, while well 4 abstracts much less BF (~30%), containing hardly any young BF.

Hydrochemistry

- The redox zones are vertically stratified and zones are broadening towards the production well.
- With increasing distance from the shore, the redox zones become narrower, due to higher organic carbon contents in the lake sediments and longer retention times. In 20 m shore distance, the redox conditions are already anoxic.
- In the shallow groundwater, the redox zones are seasonally variable and more reducing in summer, when the microbial activity is higher due to higher temperatures.
- Entrapped soil air due to water-level oscillations and, in winter, bank filtration are the main sources for oxygen input into the shallow aquifer.
- Gypsum dissolution as the cause of elevated sulfate concentrations in the shallow groundwater inland of the production wells can be excluded.

1.6 Hydrogeological Results Artificial Recharge Pond Tegel

The field site lies within the catchment area of Tegel water works, which belong to the Berlin Water Company (Berliner Wasserbetriebe, BWB). Near Lake Tegel, three ponds surrounded by over 40 production wells are used for groundwater replenishment (Figure 93); pond 3 is the subject of these investigations. The pond bottom is located approximately 3 m below ground (31 masl). A transect of groundwater observation wells screened in various depths was installed between pond 3 and production well 20 of the Saatwinkel production well gallery to study processes occurring during infiltration and passage to the production well (Figure 94). The filter screen of the production well 20 extends from 20-34 m below ground; the length of the observation well screens is restricted to 2 m, allowing a vertical differentiation of the groundwater.

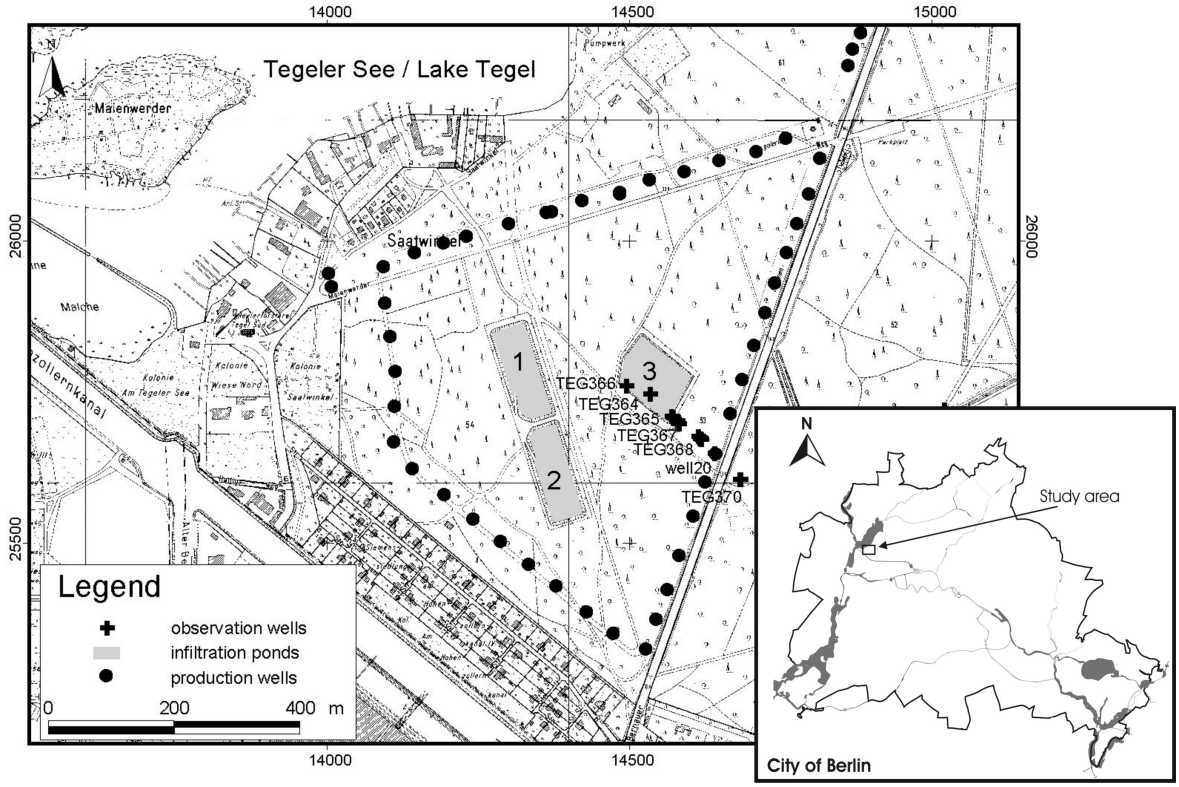

Figure 93: Recharge ponds 1, 2 and 3, production well triangle and transect at the artificial recharge site Tegel (Massmann et al., subm.)).

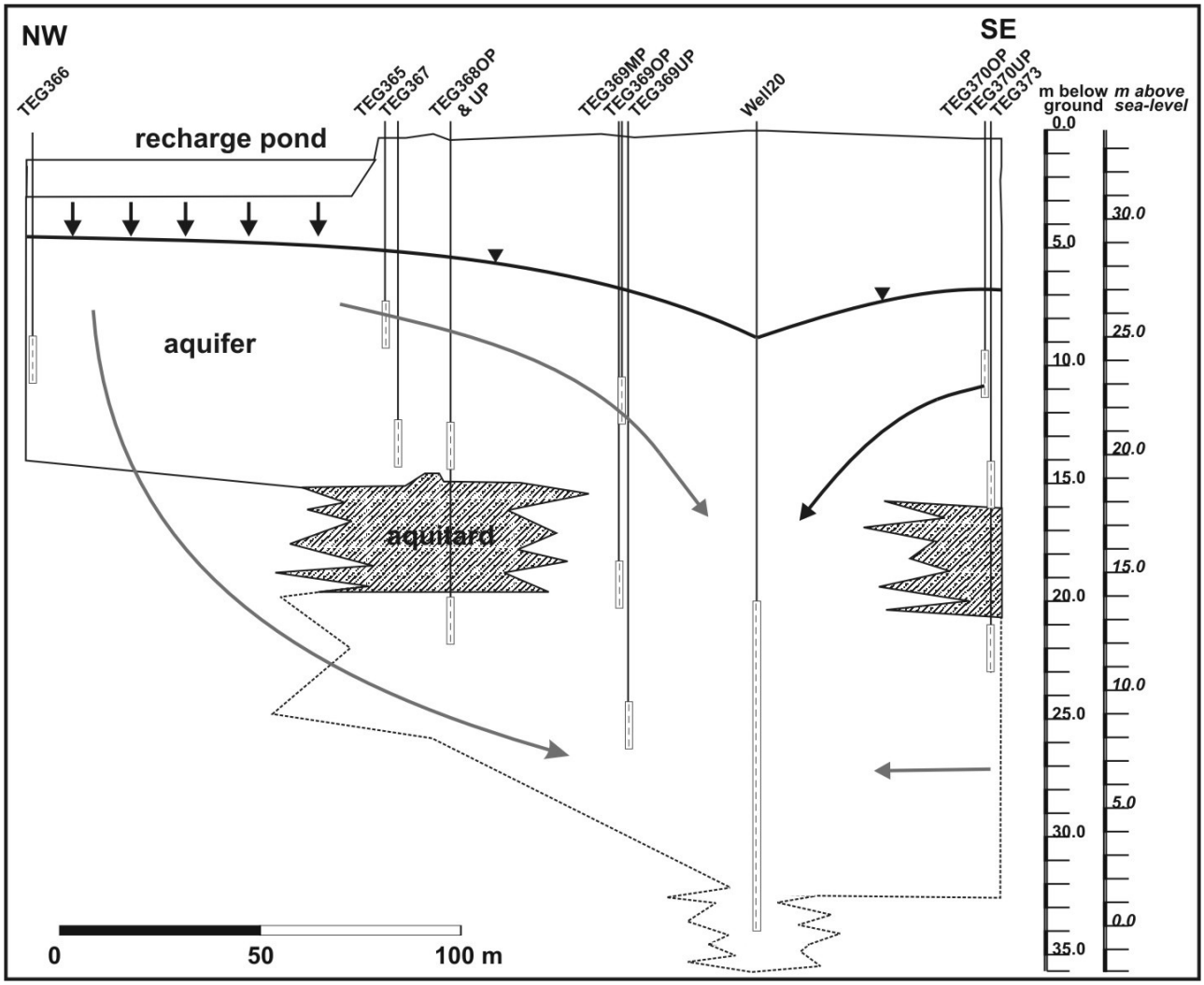

Figure 94: Schematic cross section of the transect between recharge pond 3 and production well 20 (Saatwinkel well gallery). Filter screens shown as dashed bars. The flow direction is indicated. The aquitard (glacial till) is not consistent and was not encountered below (parts of) the pond and at the location of the production well (Massmann et al., subm.)).

1.6.1 Pond operation/Hydraulic situation

Surface water of the adjacent Lake Tegel is pumped into the pond (pond area: 8700 m²) after passing through a microstrainer for pre-filtration. In 2002 (and 2003), 3.39 (4.79) million m³ of surface water were recharged via pond 3.

Figure 95: illustrates the principal operational cycle at the site, starting after the pond has been emptied and the pond bottom sands (the upper ~0.1 m) have been washed and cleaned of finer grained material and algae. The pond is refilled and the groundwater level below the pond rises owing to the infiltration of water, causing hydraulic conditions below the pond to change from unsaturated to fully saturated (reached when the groundwater-table is ~1 m or less below the pond, Figure 95, No. 1). The infiltration capacity is largest when saturated conditions prevail. With time, the pond bottom becomes increasingly more clogged un-

til, at some stage, the infiltration capacity decreases to such an extent that conditions below the pond become unsaturated again owing to decreasing groundwater levels (Figure 95, No. 2). As soon as this happens, the infiltration capacity decreases even more. The pond has to be redeveloped. During redevelopment, the pond bottom is exposed to the atmosphere (Figure 95, No. 3).

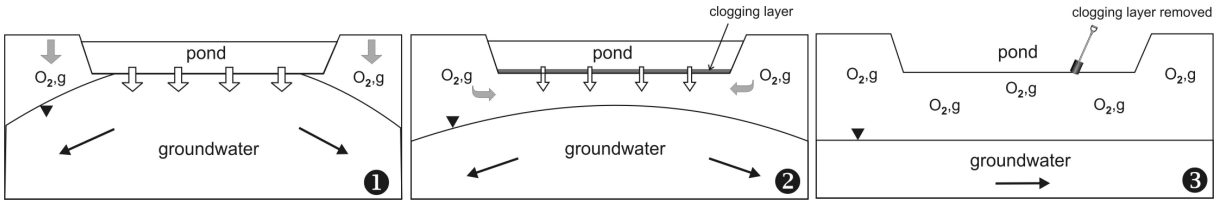

Figure 95: Schematic illustration of the operational cycles of the recharge pond. 1: The pond has been refilled and the conditions below the pond are fully saturated. 2: The infiltration rate decreases due to clogging of the pond base, leading to a drop of the groundwater mount and the development of an unsaturated zone below the pond. Oxygen can penetrate below the pond from the pond margins. 3: The pond is emptied for redevelopment (Massmann et al., subm.)).

Figure 96 shows the water-level of the pond (a) and groundwater well TEG364 below the pond (filter screen depth 5-7 m below pond base, b), the infiltration rate (c, equivalent to amount of water recharged divided by pond area) and oxygen concentration in the groundwater below the pond (d). During operation of the pond, the water level in the pond was kept more or less constant around 32.5 metres above sea-level (masl). The pond bottom level lies around 31 mNN (m above sea-level), but may vary slightly both spatially and temporarily due to the sediment cleaning procedures. The hydraulic conditions below the pond were highly transient; the groundwater-level fluctuated by almost 6 metres (Figure 96, b). The decline of the infiltration capacity with time due to clogging is clearly visible Figure 96, c). Clogging and the associated drop of the water-level and the infiltration capacity occurred more rapidly in summer, probably due to sudden algae growth. The decrease of the hydraulic conductivity of the pond bottom due to clogging has often been described in artificial recharge via ponded infiltration (Okubo and Matsumoto, 1983; Schuh, 1990; Bouwer, 2002).

Altogether, 9 cycles can be defined for the monitoring period (Figure 96). The intervals between redevelopments varied strongly. For example, in October 2002, the pond was in operation for only about a month. By contrast, from November 2002 till the end of March 2003, the pond was in operation for almost 4 months without being redeveloped. In addition, redevelopments were not always similarly efficient. In winter 2001/2002, for example, the infiltration capacities after two redevelopments did not come near those reached later (groundwater-level data does not exist for winter 2001/2002).

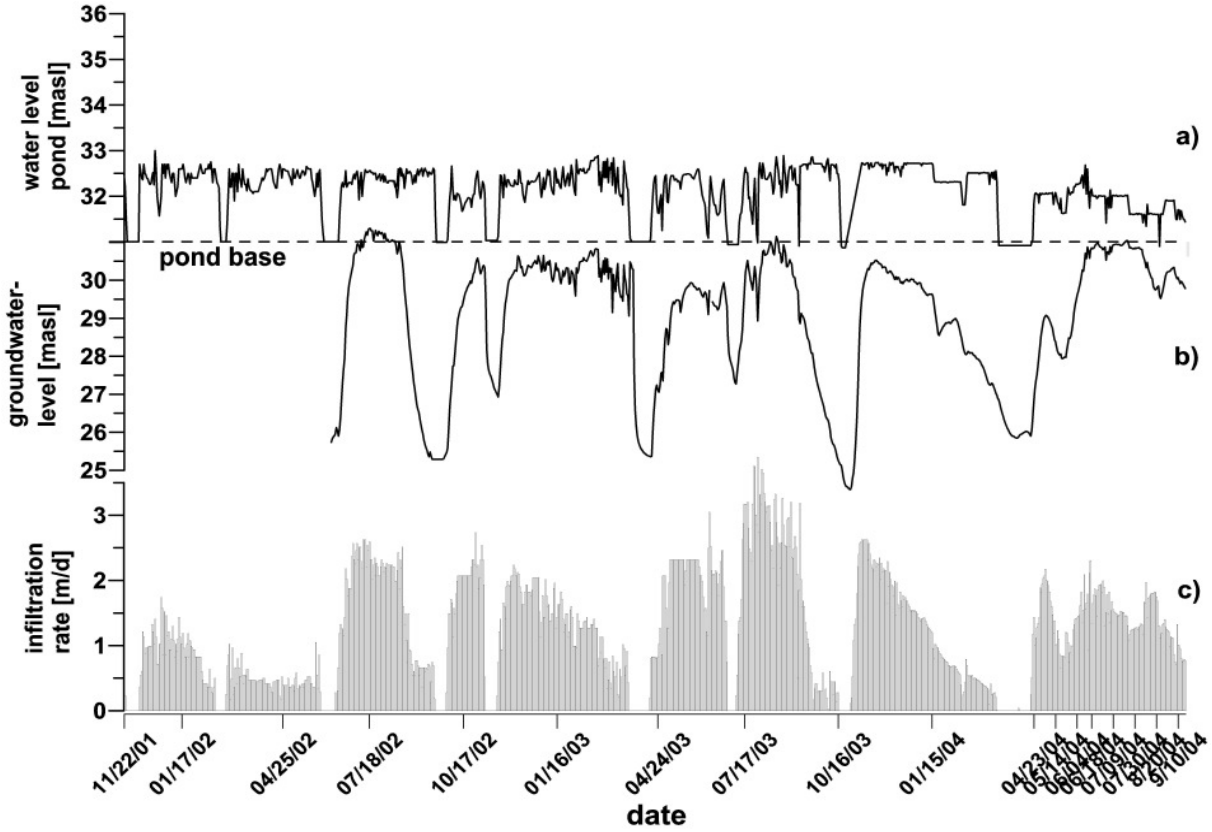

Figure 96: a) Water-level of the pond [masl] and b) groundwater below the pond (TEG364) [masl] and c) recharge rate [m/d]. The infiltration rate was provided by BWB.

Because of the groundwater elevation below the pond and the abstraction of water from production wells in the well triangle around the ponds (Figure 93), the groundwater flows concentrically away from the ponds to the production wells. The monitoring transect (Figure 93) is oriented in flow direction. But because the pumping performance of the wells is irregular, wells are not operating constantly and the 3 ponds are emptied at different times, individual flow paths may deviate slightly from the transect. Average travel times to individual wells of the transect can be estimated with the help of breakthrough curves of conservative tracers and a number of wastewater residues such as B or EDTA (Table 3, part 1 Tegel).

Figure 97 shows the water level of pond 3 and the groundwater in selected observation wells between pond and well 20 as well as of the production well and an inland observation well. The pond water-level was mostly around 32.5 masl, times where the pond was empty display a value of 31.0 masl. Towards the end of the project, around May 2004, the pond water-level was lowered to 32.0 masl. The data shows that like the groundwater-level below the pond (Figure 96b) as discussed above, the groundwater-level of the entire transect is governed by the pond operation and the infiltration and clogging dynamics. Lowest groundwater elevations are encountered when the pond is empty. Close to the pond, the water-level fluctuates up to 6 m. Even at TEG369UP, closest to the production well, the groundwater-level still varies up to 5 m, depending on the infiltration dynamics. Towards the production well, the

groundwater-level declines gradually. When the pump is turned of, the groundwater level of the production well is similar to the level of TEG369UP. When turned on, it decreases about 3 m. Whenever the pump is turned of, the surrounding groundwater level responds and increases slightly, but relatively little compared to the changes caused by the pond cycling.

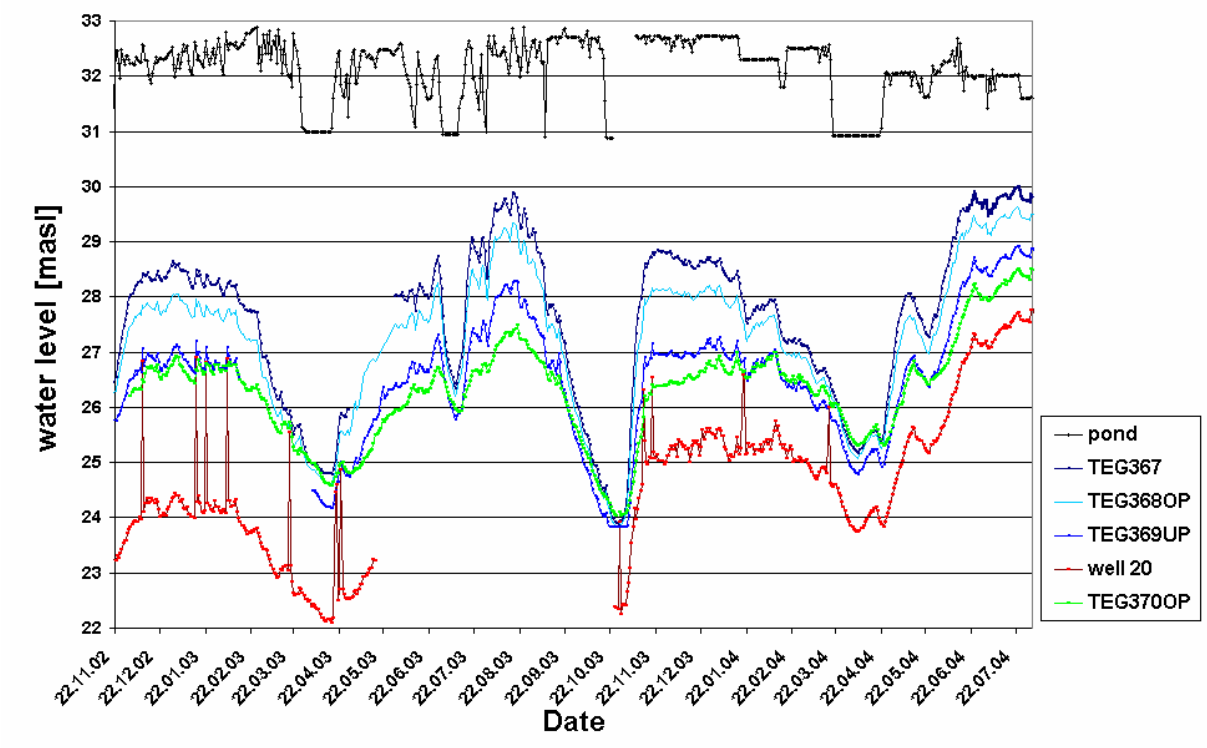

Figure 97: Daily measurements of the pond level and the groundwater-level from data logger in observation wells TEG367, TEG368OP, TEG369UP, production well 20 and TEG370OP (inland).

1.6.2 Surface water investigations

The surface water in pond 3 is essentially Lake Tegel water which passes through a microstrainer before it enters the pond. The intake of the pond water is in the southern part of Lake Tegel, which itself receives treated WW via the Nordgraben ditch from the WWTP Schönerlinde, in the north of Berlin (*compare chapter 3.1, part 1*). Like Lake Tegel, the pond contains a variable amount of treated WW.

The pH of the pond water varied from 7.5 to 9.1 but was usually around 8. The pond water was always saturated with oxygen, which is why the Eh was high (∅ 365 ± 85 mV). The NO_3^- concentrations in the lake showed a strong seasonality with the highest concentration in winter and lower concentrations in summer, probably due to algae consumption in the pond. Similar changes of total inorganic N have been observed in a recharge pond by Haeffner et al., (1998). A summary of the average surface water composition is given in Table 8. Because the pond water contains a proportion of treated effluent from the WWTP Schönerlinde, a number of WW residues were detectable, such as AOX (Grünheid et al., 2005), B and EDTA a number of PhACs (Massmann et al., 2004). The sulfate concentration was also ele-

vated, because $FeSO_4$ is added in the surface water treatment plant of Lake Tegel. The concentration of dissolved organic carbon (DOC) was relatively low. The pond water is oversaturated with regard to calcite (Greskowiak et al., 2005).

Table 8: Average pond water composition and standard deviation from November 2001 to September 2005.

Parameter	Average concentration and standard deviation
pH	8.0
Redox potential, Eh	365 ± 85 mV
O_2	0.34 ± 0.09 mmol/L
Electrical conductivity, EC	686 ± 57 µS/cm
Ca^{2+}	2.09 ± 0.19 mmol/L
Na^{+}	1.71 ± 0.39 mmol/L
Mg^{2+}	0.40 ± 0.06 mmol/L
K^{+}	0.24 ± 0.06 mmol/L
HCO_3^{-}	2.85 ± 0.22 mmol/L
Cl^{-}	1.43 ± 0.28 mmol/L
SO_4^{2-}	1.22 ± 0.20 mmol/L
NO_3^{-}	0.16 ± 0.05 mmol/L
DOC	0.61 ± 0.06 mmol/L

In general, the concentration of most tracer, including some WW residues in Berlin tends to show some seasonality, with higher concentrations in summer and lower concentrations in winter due to higher natural discharge (and consequent dilution of the treated WW) in winter (Massmann et al. 2004). In Lake Tegel, the situation is somewhat more complicated because a pipeline pumps river Havel water into the northern end of the lake (mainly in summer) to improve the water quality (*compare chapter 3.1, part 1)*. In addition, the total discharge of the WWTP Schönerlinde increased strongly at the end of 2002 (it approximately doubled). Therefore, similar to Lake Tegel itself, a seasonal influence is not visible for any WW residues (Figure 98) and the increase of WW residues including several PhACs in the second sampling half may have been associated to the increase in the proportion of treated WW in the samples due to the increased discharge of treated WW into Lake Tegel. This did, however, not influence the behaviour of the stable isotopes, which display the classic pattern of more negative values in winter and less negative values in summer (Figure 98).

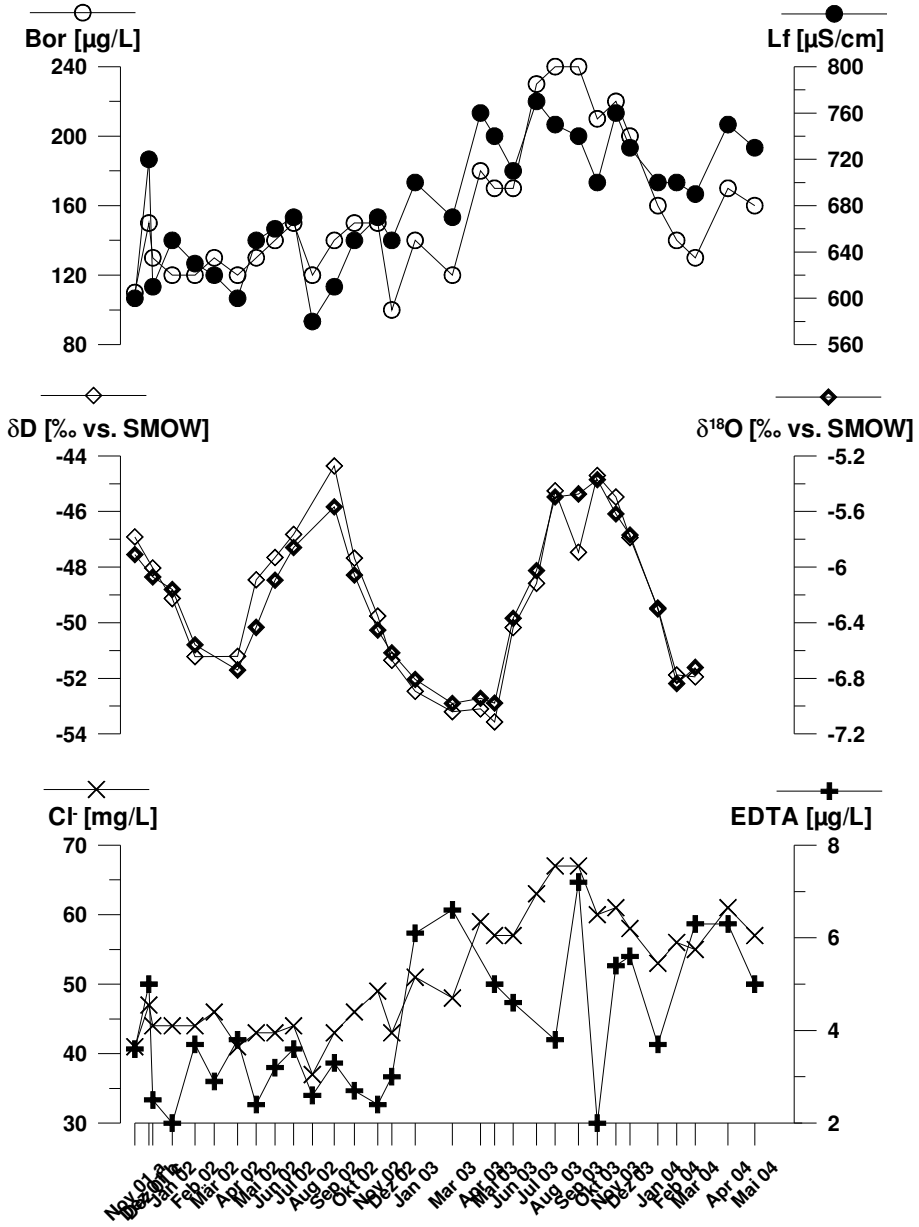

Figure 98: Boron, electric conductivity, $\delta^{18}O$, δD, chloride and EDTA concentration in the pond water (data source: BWB & AWI).

1.6.3 Clogging layer

Generally, the water infiltrating into the aquifer below the recharge pond has to pass through a sediment zone where, over long periods of time, unsaturated conditions prevail. Because the pond level is kept constant at all times, the amount of water infiltrating into the aquifer is mainly a function of the hydraulic conductivity of the clogging layer at the bottom of the pond. During redevelopments, the pond is emptied and the upper sediment layers are scraped of and cleaned to restore the infiltration capacity. Samples from the upper 0.48 m were taken and sieved before and after washing treatment (3 depths with 2 samples each). The hydraulic conductivities increase considerably (by a factor of ~ 2-10, depending on the individual

sample) after washing.

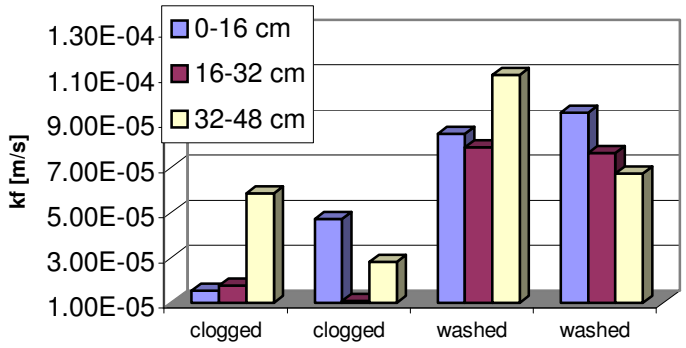

Figure 99: Hydraulic conductivities (k_f) of 6 samples (3 depths, 2 parallel samples each) of the clogged sands and of the same sands after cleaning treatment (data source: FU Berlin).

1.6.4 Aquifer sediments

The porous sediments in the area are of Quaternary age. The lithological cross-section along the transect is shown in Figure 100. The sediments encountered are mainly glacio-fluvial sands with varying proportions of fine, medium and coarse sand. The local aquitard, a glacial till of Saale age (local denotation qsWA), was not always encountered and contains interior holes. While it is present north-west and south-east of well 20 and in the adjacent production wells, it is absent near well 20. According to (Hannappel and Asbrand, 2002), the glacioflu-vial sediments above the till were deposited during the Saale (Warthe, qsWA) glacial period, while those below belong to the Saale (qs) only. The aquifer is underlain by an aquitard of the Holstein interglacial at less than 5 m below sea-level (Hannappel and Asbrand, 2002).

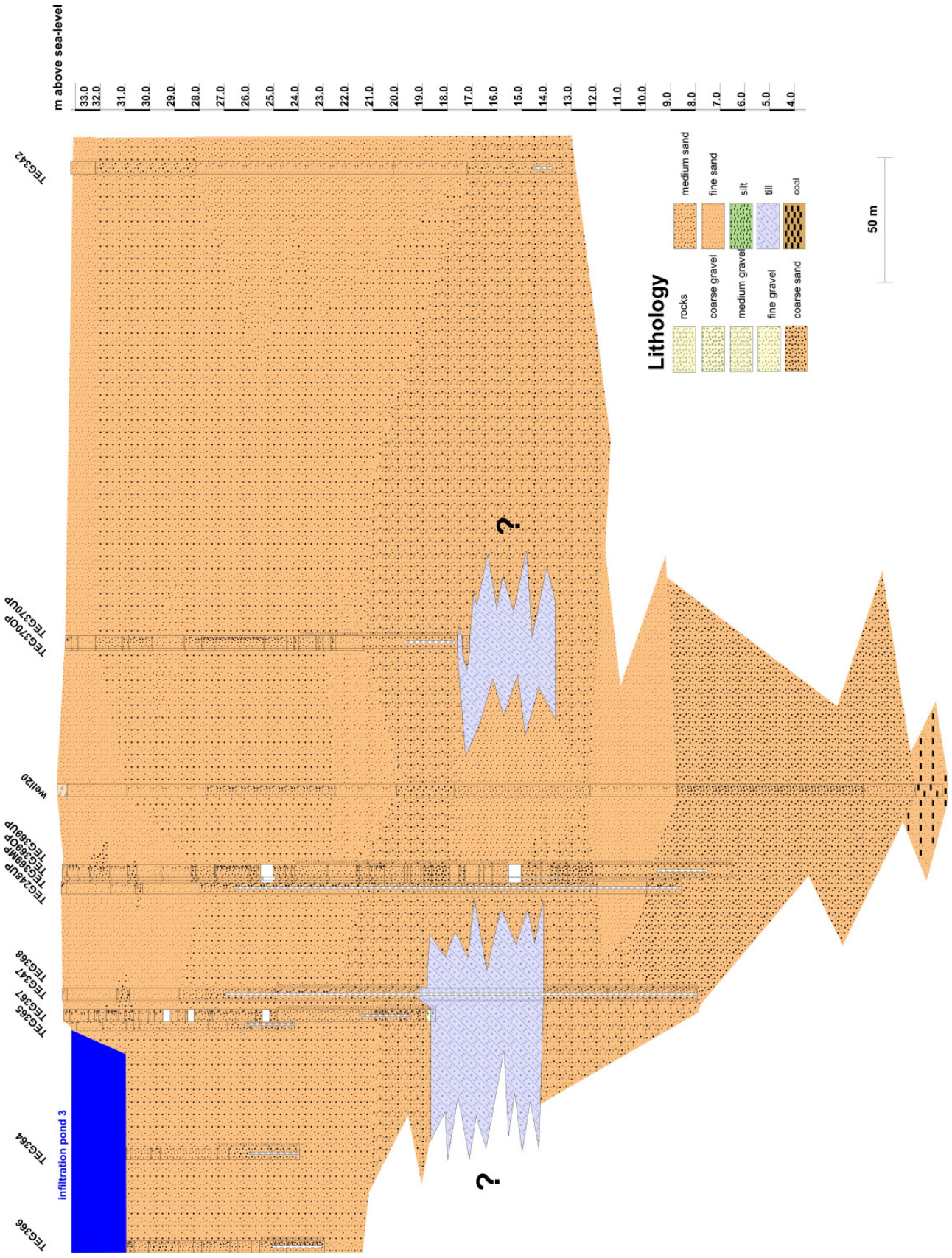

Figure 100: Lithological cross section of the transect at the AR site Tegel.

The extent and distribution of the Saale glacial till (qsWA//gm) was evaluated with statistical methods, because cross-sections only existed for the production well galleries and few was known about the presence of the till below the recharge ponds. Additional drilling data was made available by BWB. The till is rarely thinning out, it tends to be either present or not, usually with a thickness of a few meter. Because for the hydraulic and hydrochemical properties of the area, the presence, rather than the extent of the till, is of importance. The data was interpolated with the inverse distance method (5 m grid) using Surfer 7.02 (Golden Software, 2000) with the criteria present (1, green) or not present (0, red) only. The result is shown in Figure 101 and illustrates that the till, which was encountered in most cores in the north-east, is only present in a few patches in the south-west. The till is missing partly below the recharge ponds. Hence, the recharged water can infiltrate into the deeper aquifer parts and reach all production wells of the galleries Hohenzollernkanal and Saatwinkel, which have filter screens below the till.

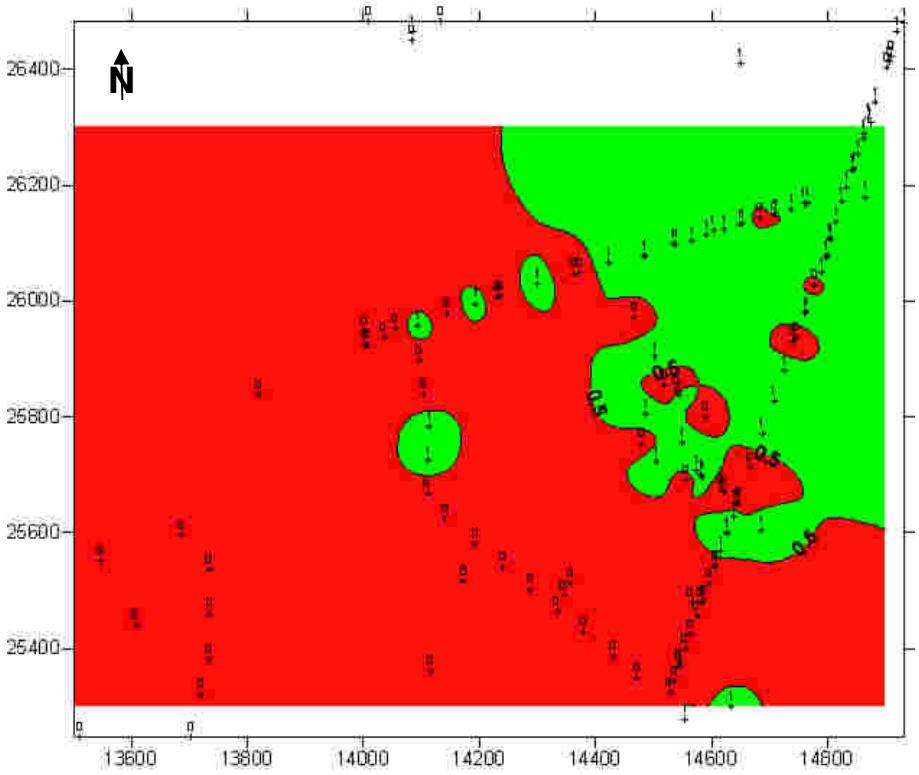

Figure 101: Glacial till distribution, inverse distance method (5 m Grid). 1= till present, 0 = no till. Areas where till is more likely to be present (>0.5) are shown green.

Two cores were taken at the site to get an idea on the major hydraulic and geochemical sediment properties. Results are illustrated for one core only (TEG369UP, Figure 94). The sands are fine to coarse grained with very little silt or clay. The k_f values derived from sieving are fairly similar in both cores and vary over one order of magnitude from 1.5E-04 to 1.1E-03

m/s (Figure 102). In both cores, the most striking differences in terms of the geochemical characteristics of the sediment are found between the unsaturated and saturated sediment zone (water-table depth: 6-9 m, depending on pond level). Carbonate (inorganic carbon) appears from a depth of around 6.4 m onwards (Figure 103). The organic carbon content is low with 0.02-0.16 weight % (Figure 103). With a few exceptions, the total iron content is 1-2 g/kg Fe (Figure 103). The share of reducible iron and manganese (Fe & Mn(hydr)oxides) seems to be getting slightly less with depth. In terms of total ion concentrations (Figure 102), aluminum and iron are the main cations in the unsaturated sands, while calcium dominates within the saturated zone.

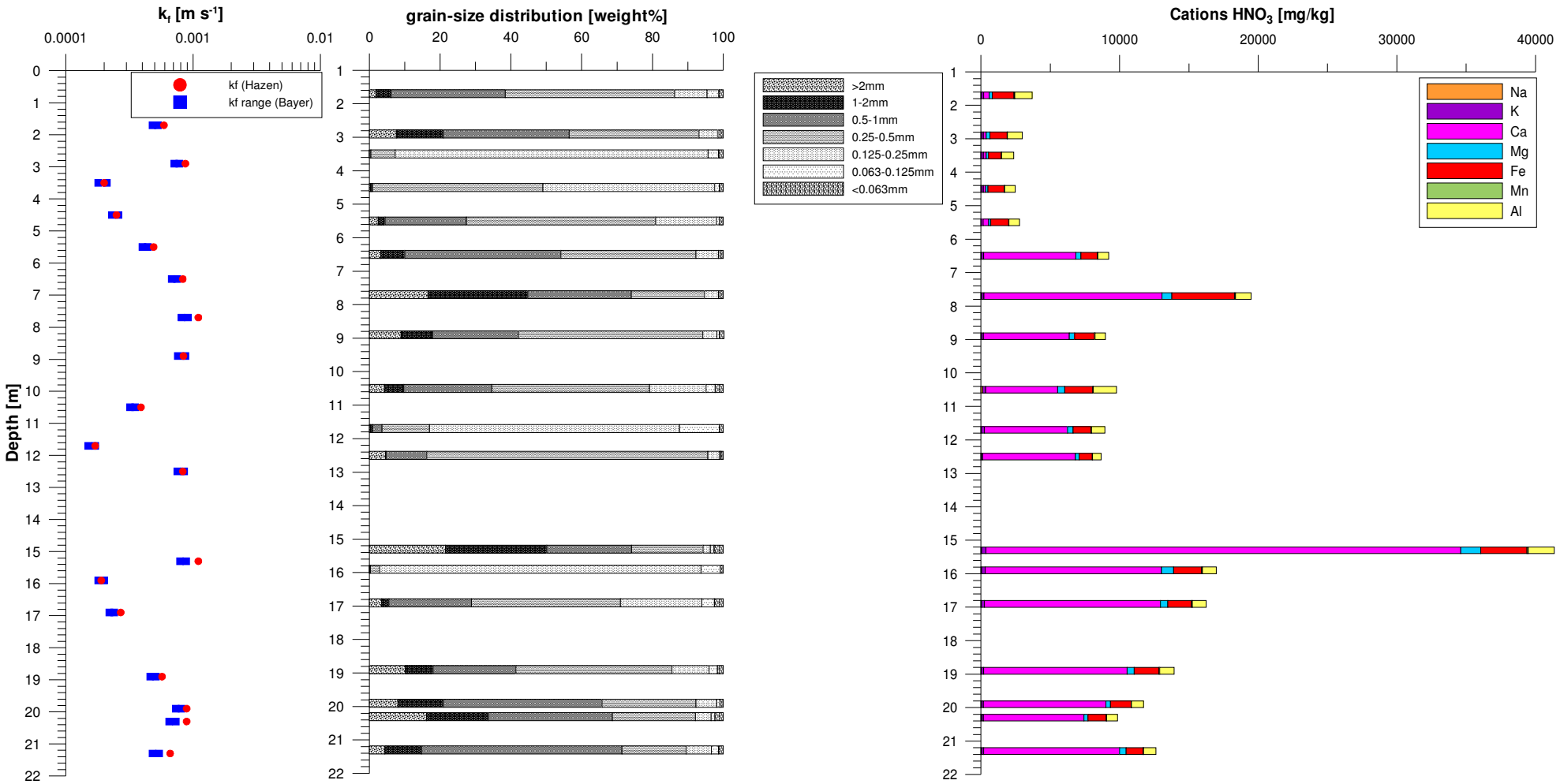

Figure 102: Hydraulic conductivities (k_f), grain-size distribution and cations from HNO3 extraction in core TEG369UP (data source: FU Berlin).

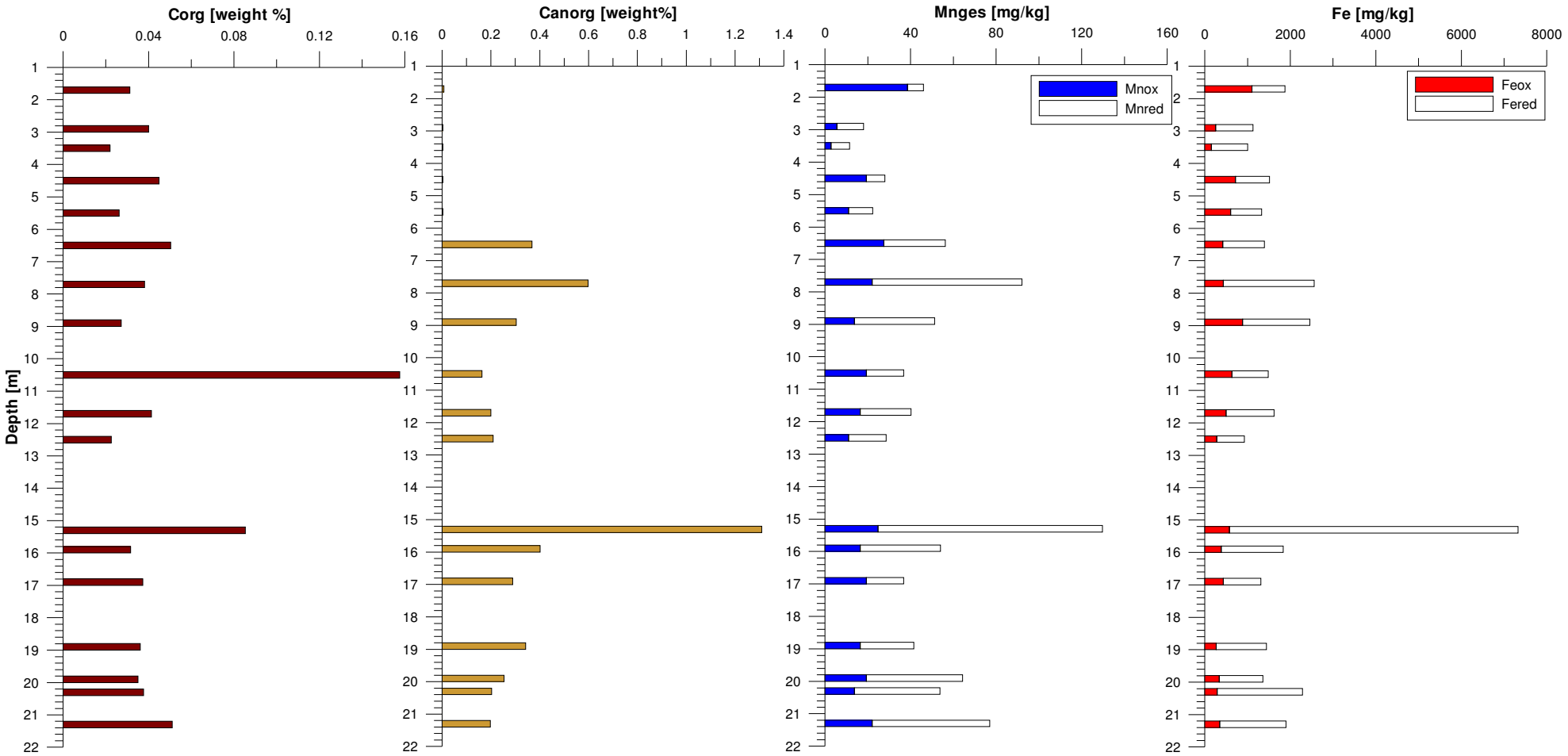

Figure 103: Organic and inorganic carbon content, reducible (Feox) and non-reducible (Fered) iron, reducible (Mnox) and non-reducible Mn(red) manganese content in core TEG369 (data source: FU Berlin).

1.6.5 Tracer evaluation: Travel times/groundwater age

The travel times at the GWA transect are clearly faster than at the bank filtration sites (at least at the transect at well 20, which is one of the closest to a pond of all wells in the triangle (Figure 93). Other than at the bank filtration sites, the resolution of the time-series with a monthly sampling was therefore too low to gain precise travel times from the tracer data. The tracer chloride, boron and, with little retardation, potassium would principally work, since they showed a clear increase in spring 2003 (at least for this time period). However, the fluctuations are too large and the curves are too close to each other to give nice shifts. The following tracer time-series were divided into curves for the shallow observation wells TEG365, TEG366, TEG368OP and TEG369OP as well as the deeper ones TEG368UP and TEG369UP plus production well 20 for a better overview (compare Figure 94).

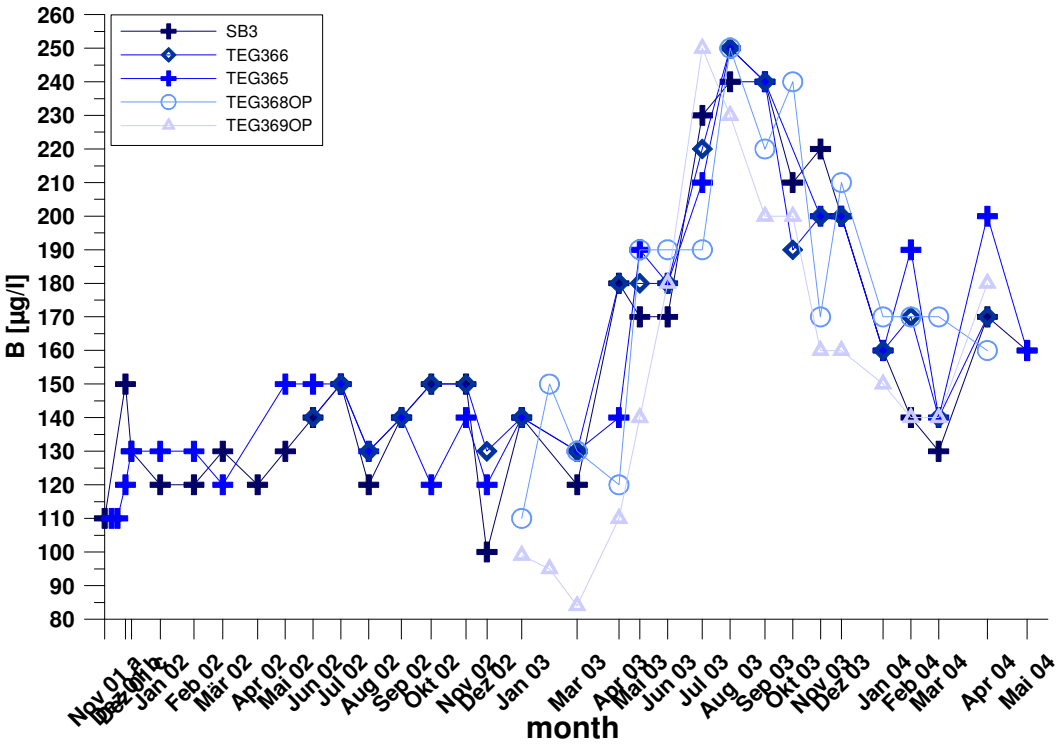

Figure 104: Boron concentrations over time for the shallow observation wells (data source: BWB).

Figure 104 and Figure 105 shows exemplary time-series for B and Cl^- for the shallow observation wells. Clearly, the data does not allow a travel time evaluation or only in the sense that it shows that the travel times are below one month to each observation well. Slightly better curves were gained from the stable isotope analysis. The isotopes showed seasonal peaks in both 2002 and 2003. At least for the shallow observation well TEG369OP, furthest away from the pond, an offset of slightly less than a month (~ 25 days) can be seen. Increasing the sampling frequency for TEG366 below the pond did not result in more precise estimates (Figure 107). The curves lie on top of each other, suggesting a very short travel time.

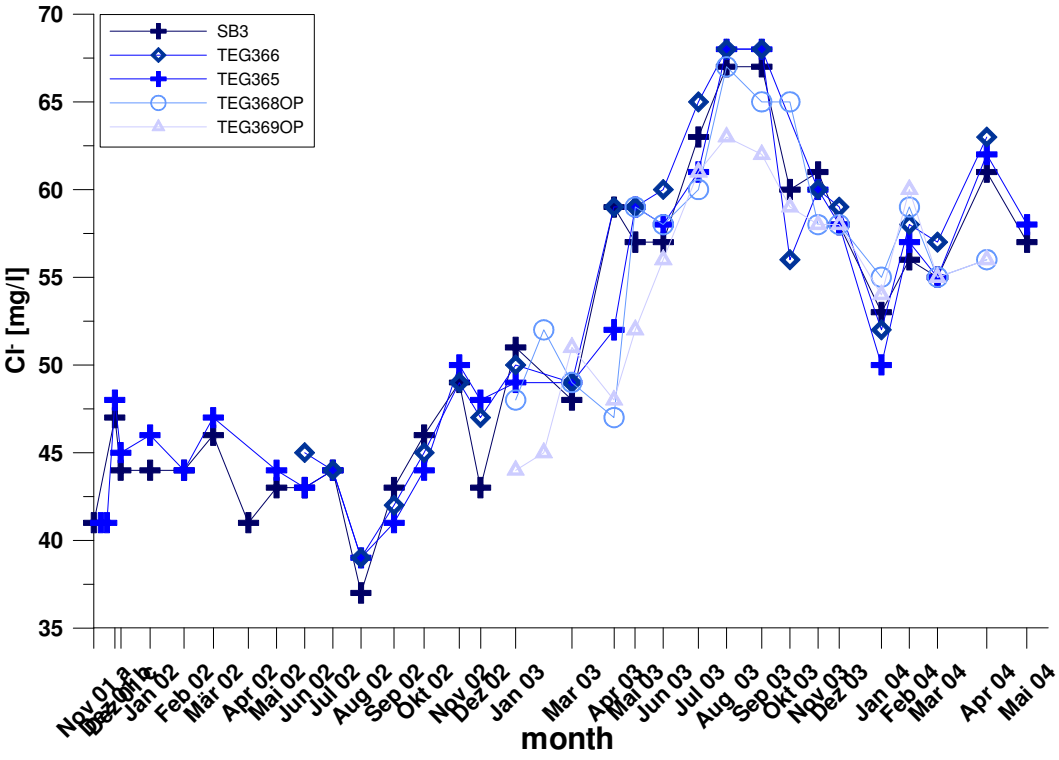

Figure 105: Chloride concentrations over time for the shallow observation wells (data source: BWB).

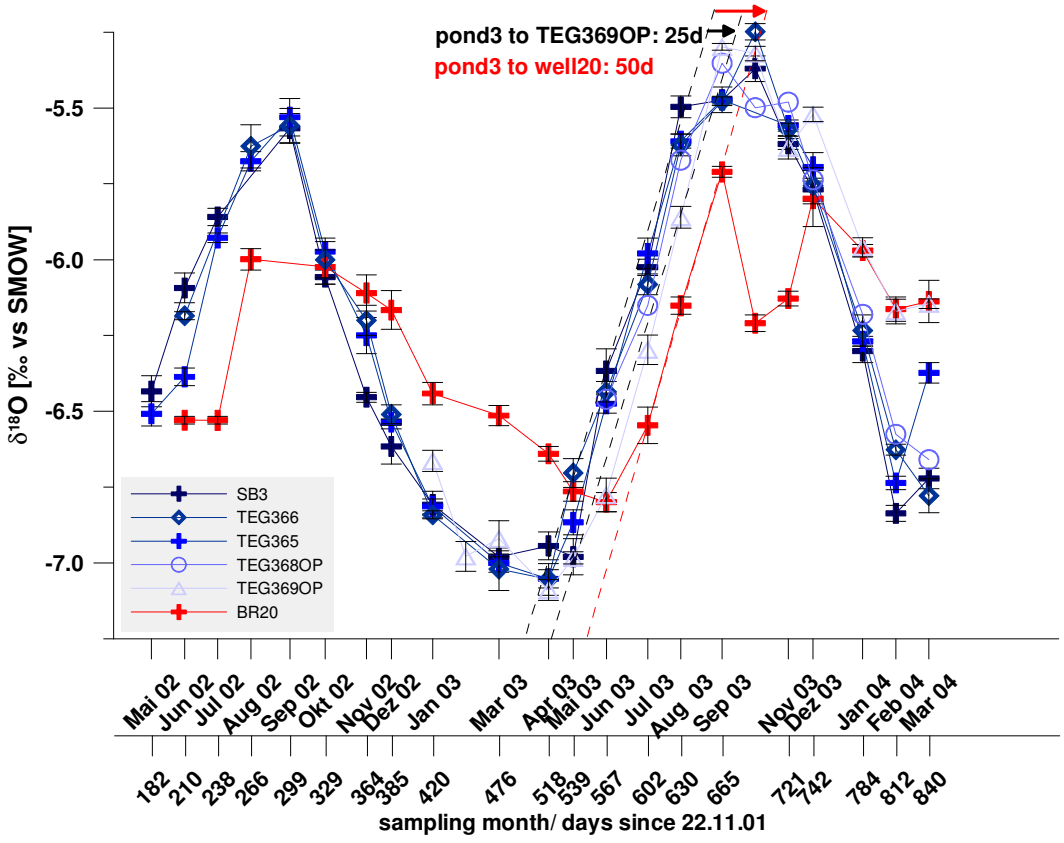

Figure 106: $\delta^{18}O$ values over time for the shallow observation wells and the production well (data source: AWI).

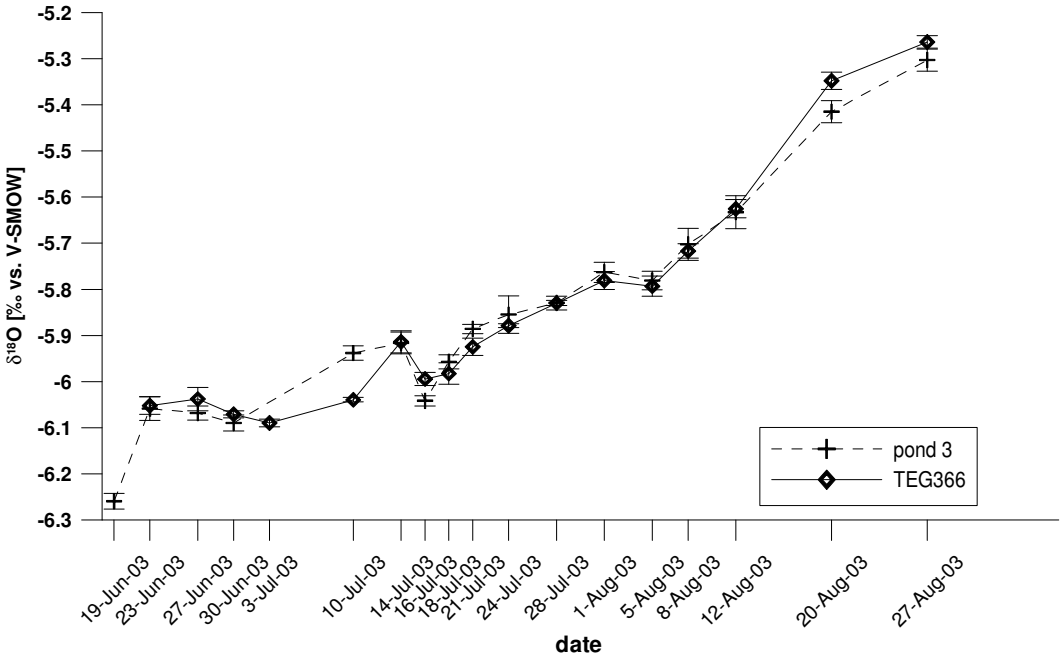

Figure 107: $\delta^{18}O$ values over time for TEG366 (data source: AWI).

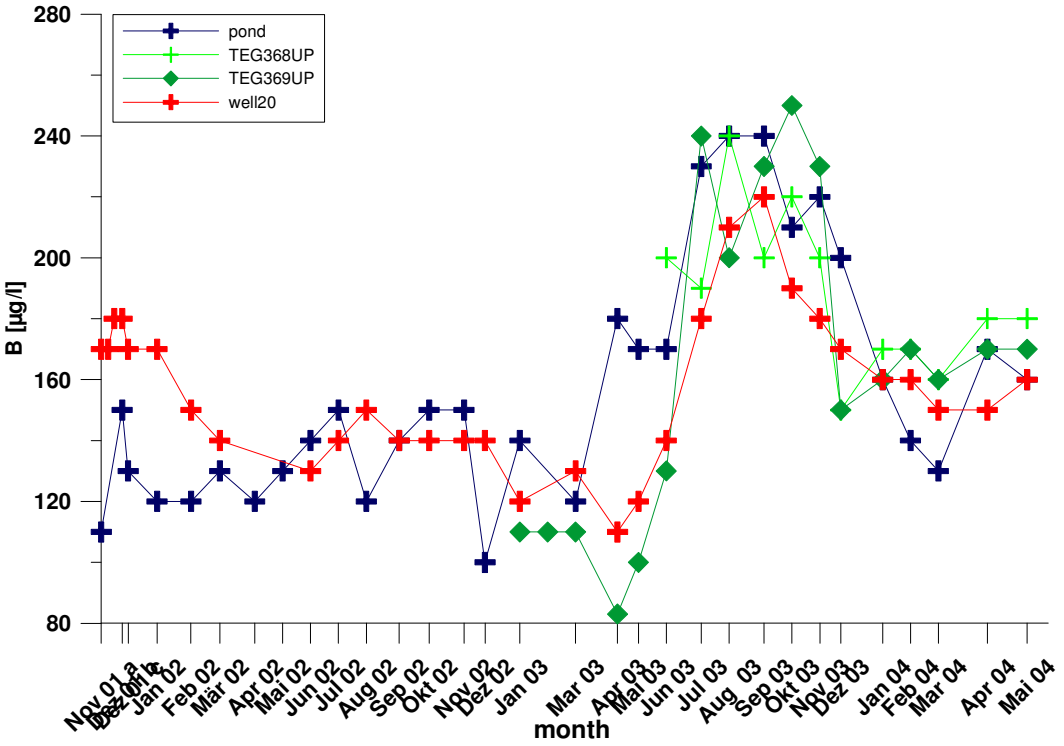

Figure 108: Boron concentrations over time for the deep observation wells (data source: BWB).

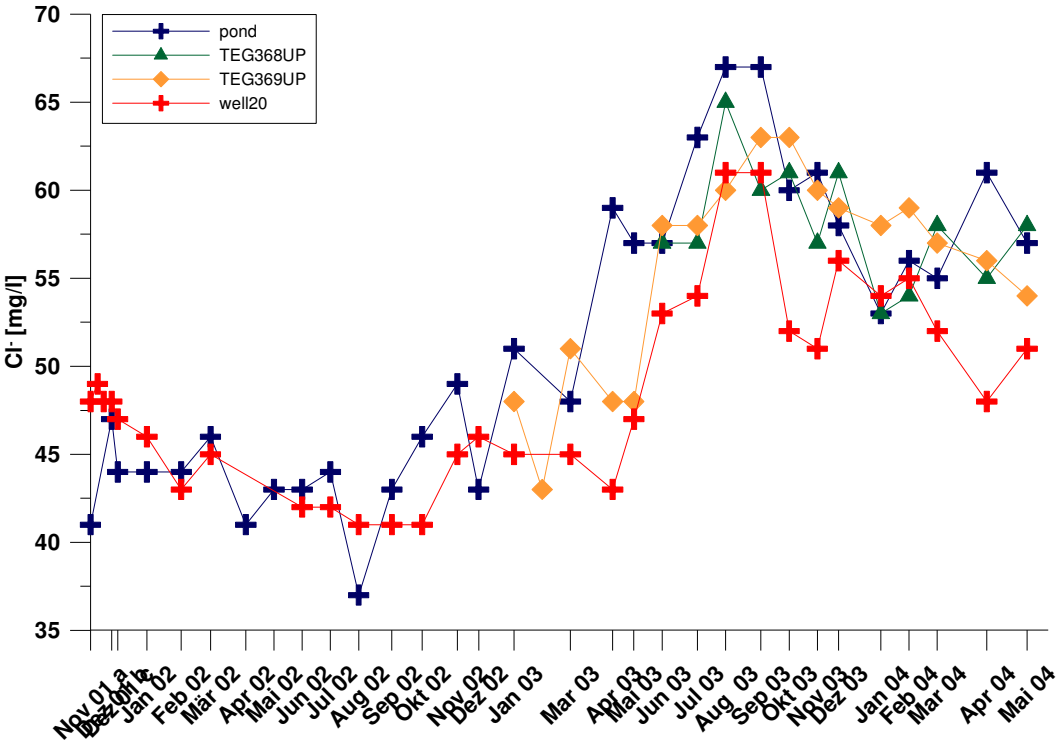

Figure 109: Chloride concentrations over time for the deep observation wells (data source: BWB).

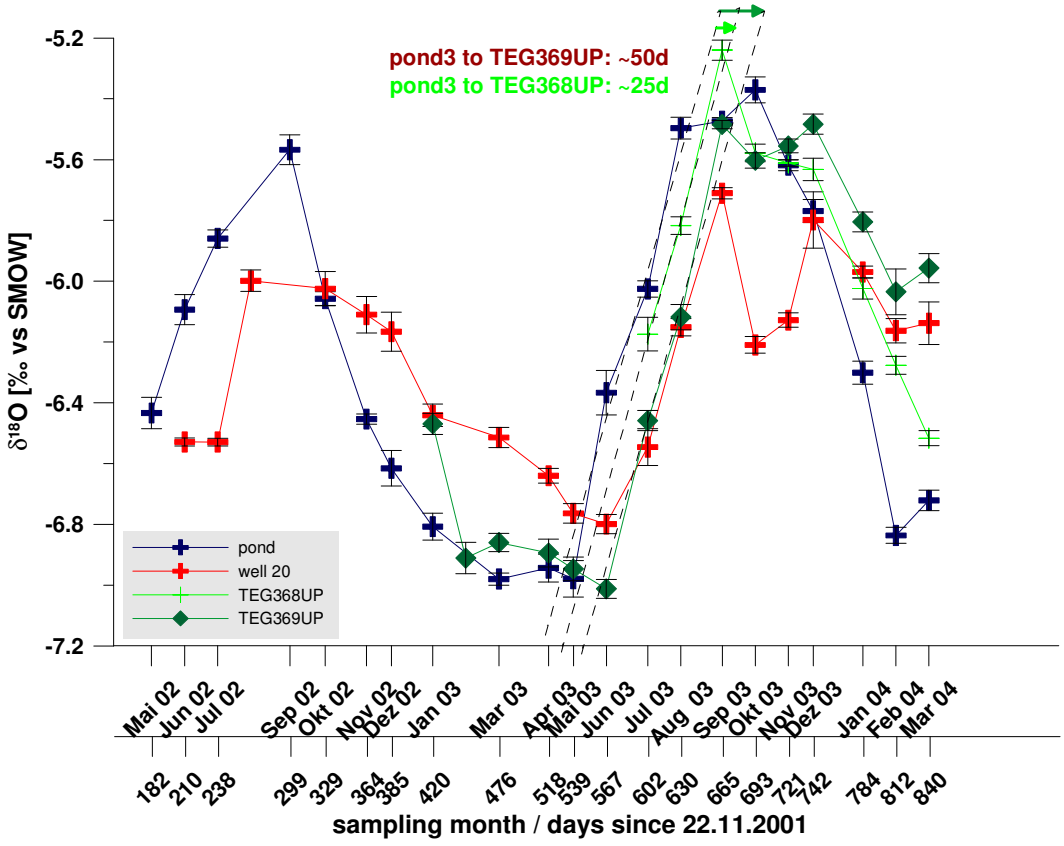

Figure 110: $\delta^{18}O$ values over time for the deep observation wells and the production well (data source: AWI).

The travel times to the deeper observation well (below the glacial till) are likewise short. Using Cl^- and B data, there appears to be a slight offset (Figure 108, Figure 109), however, the fluctuations do not allow a precise determination of the shift. Again, the stable isotopes give clearer signals. Figure 110 indicates that the travel time to TEG368UP is slightly less than a month, whereas the travel time to TEG369UP, closest to the production well, is similar to the travel time to the production well itself (1-2 months or roughly 50 days in spring/summer 2003).

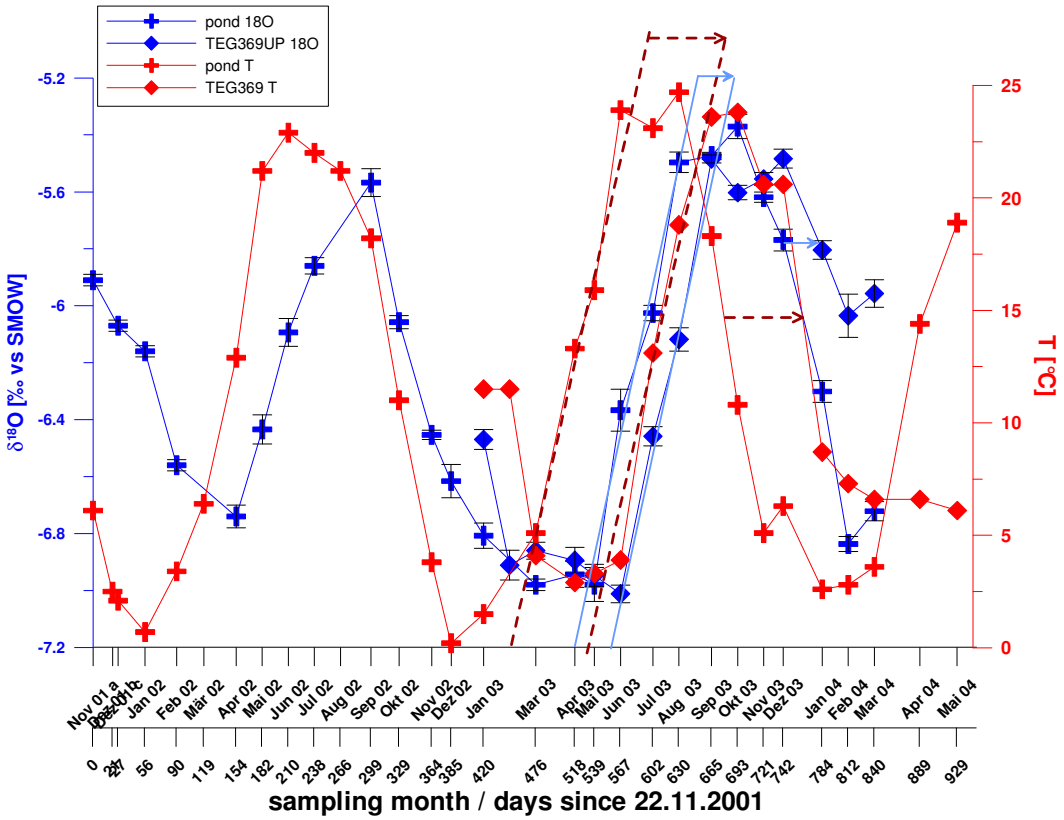

Figure 111: $\delta^{18}O$ values (blue) and temperatures (red) over time

The temperature data has a much better time resolution, because daily values exist. The temperature data can be used to estimate travel times below 1 month. However, temperature is not a conservative tracer and the retardation factor has to be estimated from a conservative tracer. Judging from the difference between the temperature and the $\delta^{18}O$ shift to TEG369UP (Figure 111), the temperature retardation factor is ~ 2.1.

Figure 112 shows the temperature data of the pond, TEG366, TEG365 and TEG368OP with peak shifts indicated by arrows and dotted lines. The grey rectangle indicated the times when the pond was empty. It becomes clear, as obvious from the variable recharge rate (Figure 97), that the travel times vary, depending on the permeability of the pond bottom. In the most extreme cases, the shifts in Figure 112 fluctuate between 4-8 days (TEG366), 5-15 days (TEG365) and 15-44 days (TEG368OP). Hence, using a retardation factor of 2.1, the effective travel time to the wells are 1.9-3.8 days (TEG366), 2.4-7.1 days (TEG365) and 7.1-21.0

days respectively. However, the slower travel times (and larger residence times) appear around times when the pond was empty, while the faster end of the spectrum is representative for larger time periods during operation. Note that the temperature varies between 0 and 25°C, which may have an effect on the behaviour of water constituents subject to microbial degradation, which may be temperature sensitive.

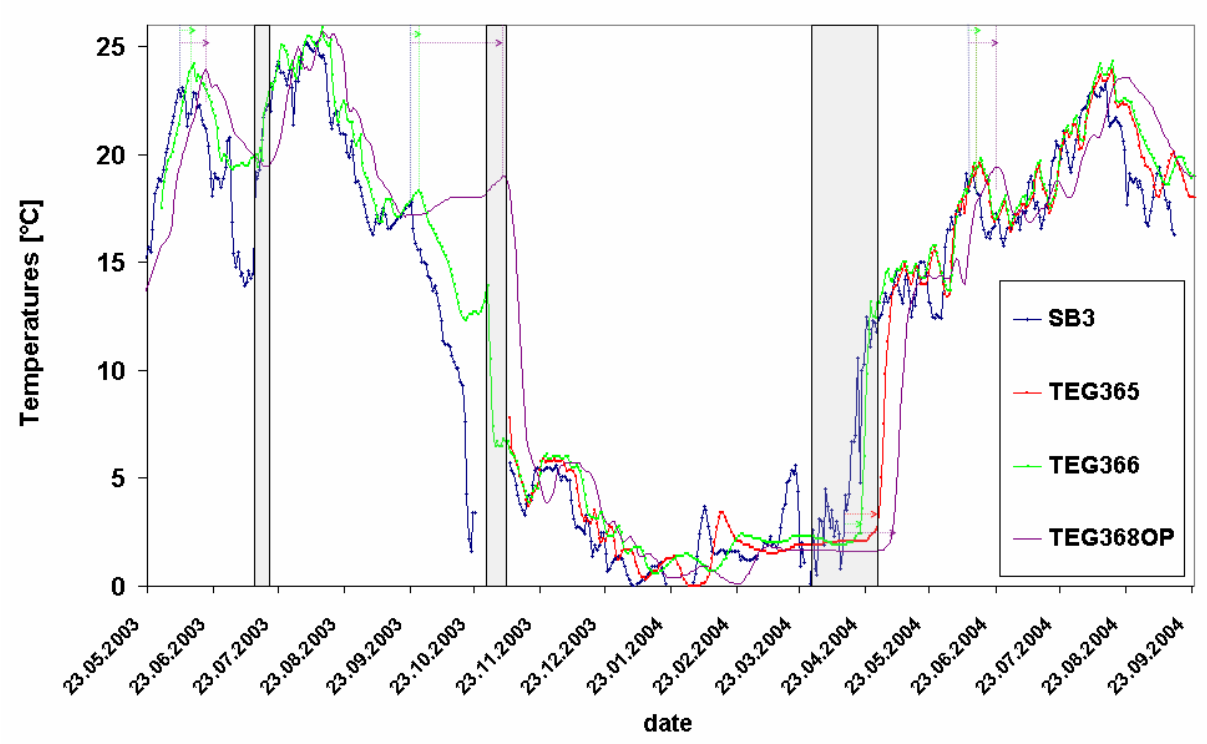

Figure 112: Daily temperature data for the pond (SB3) and 3 observation wells with short travel times. The grey shading indicates times when the pond was empty, the dotted lines and arrows point out the temperature peak shifts.

Figure 113 summarises the results of the travel time investigations and shows effective T/He ages, which are consistent with the travel times. The travel times are only rough estimates for times of pond operation, as discussed above, they vary largely in time. The observation wells TEG369OP and TEG369UP had an effective T/He age of 0. With a resolution of the method of half a year at the side, this could be expected and it proves, that 100% of the sampled water north-west of well 20 are, in fact, originating from the pond only. A vertical age stratification as discovered at the BF sites, with decade old water in greater depth, was not encountered. However, it may still exist at the very bottom of the aquifer. The background water had an effective T/He age of 1.3 (shallow) and 4.3 (deep) and 10.3 (very deep below till) years. The groundwater observation well TEG342 in greater distance from the pond (next to the airport) is screened at 18.4-19.4 m below ground. The T/He age was 27.4 years. It is free of surface water influence and probably recharged by infiltration of seepage water

through the soil. The production well, as a mixture of bank filtrate and native background water, lies in between with 2.3 years.

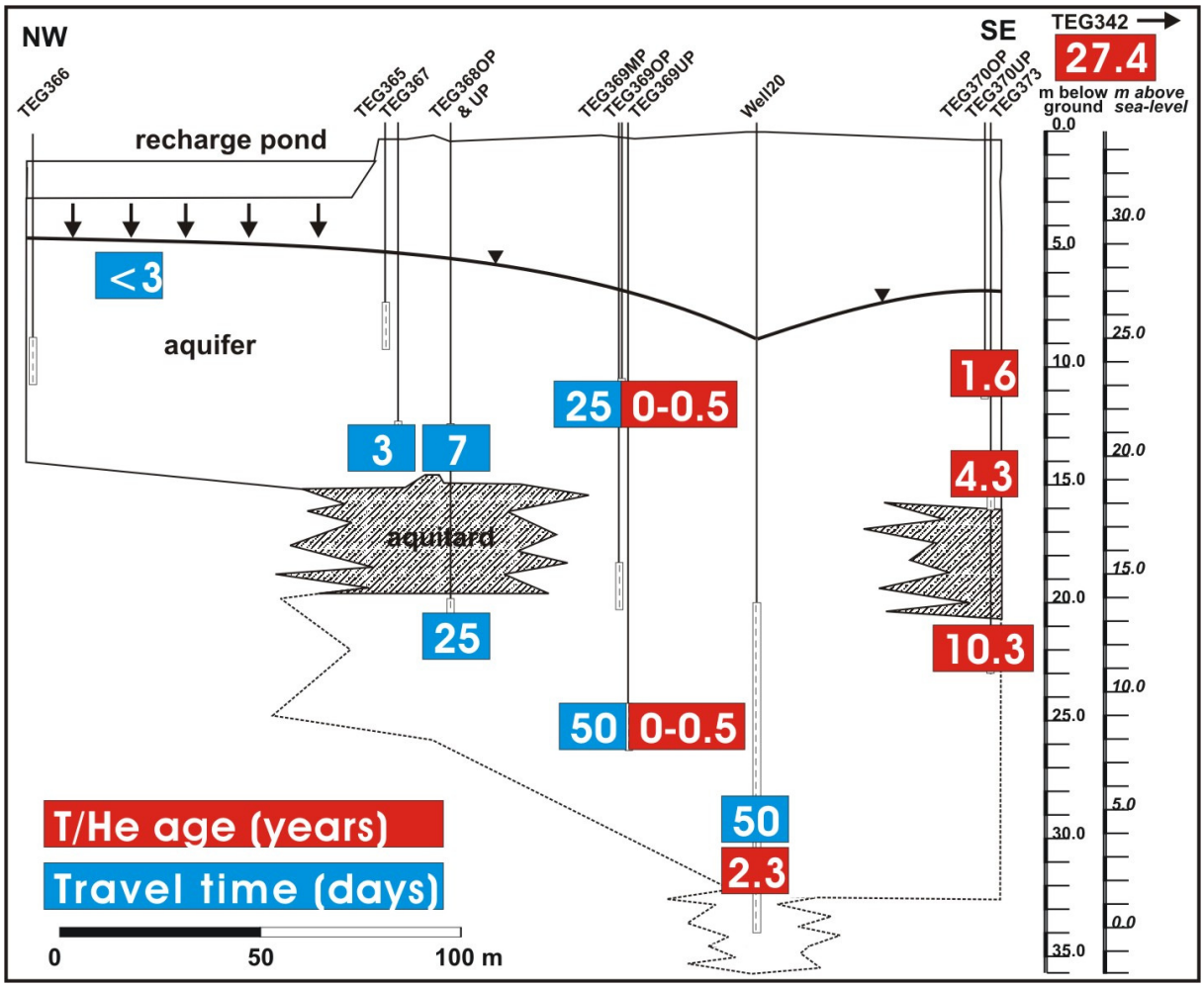

Figure 113: Estimates for approximate travel time for times of pond operation and effective T/He age in observation and production well.

1.6.6 Tracer evaluation: Mixing

The scatter plot of $\delta^{18}O$ data versus δD of the pond and the deep and shallow wells TEG368 and TEG369 (Figure 114) illustrates that the groundwater flowing between the pond and well 20, both below and above the glacial till, is purely made of “young” recharged water. Unlike at the bank filtration site, there is no “older” bank filtrate (or artificially recharged water) with a different chemical composition mixing with the pond water.

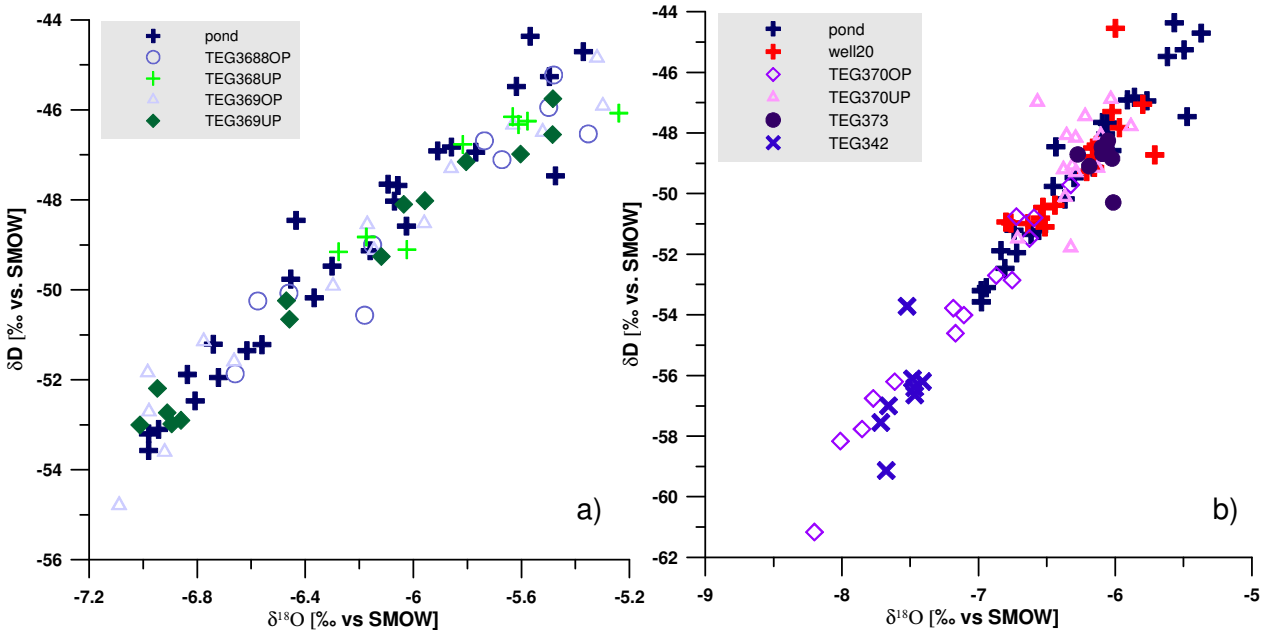

Figure 114: $\delta^{18}O$ versus δD [‰ vs. SMOW] of pond water (SB3), production well and background groundwater (Data source: AWI Potsdam).

The amplitude of the fluctuations of the tracer concentrations in the production well, as it can be seen in the time-series in chapter 1.6.5, is still quite distinct. This is not the case in any of the other production wells at Wannsee or Tegel, where seasonal variations have been largely eliminated by mixing and dispersion processes. The difference is a combination of several facts:

1. The average travel time to well 20 is relatively short (50 days).
2. There is no mixing of recharged water of distinctly different residence times.
3. The proportion of recharge water in the production well is lager than at the BF sites.

Figure 114b shows the isotope scatter plot for pond, production well and the observation wells TEG370OP, TEG370UP and TEG373 directly inland of well 20 (Figure 94) as well as TEG342 in greater distance (Figure 124). It shows that, with regard to the isotopes, the background water does not deviate distinctly from the surface water, as it does at the BF Tegel site. The well plots within the field of the surface water (only with less variability) and so do the two lower inland observation wells. The shallowest (TEG370OP) has a distinctly more negative signal, similar to that of TEG342. Overall, the vertical background groundwater variation is very large as is the spatial variation of the background water (chapter 0).

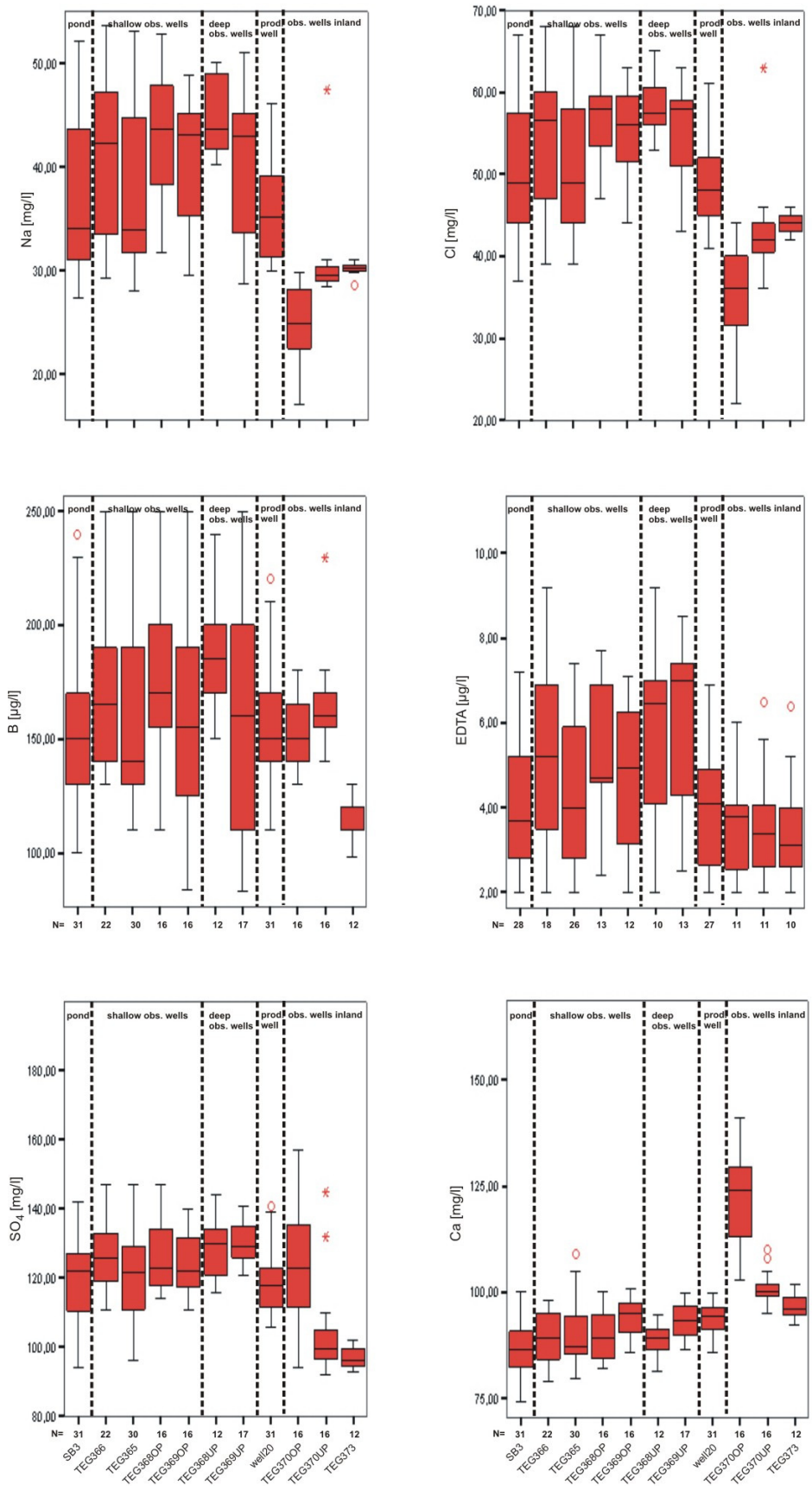

Figure 115: Boxplots for Na^+, Cl^-, B, EDTA, K^+ & SO_4^{2-} at the GWA Tegel (data source: BWB); November 2001-May 2004, N = number of samples (31 at maximum).

Selected box plots of Na, Cl, B, EDTA, K and SO_4 are given in Figure 115. They likewise illustrate, that the pond is the only source of the sampled water north-west of well 20. Differences in the are thought to be due to the difference in samples (some observation wells were constructed later and sampled less often. They also show that it is not possible to calculate proportions of BF in the well with a simple 2 component mixing formula. In most cases, there is no clear difference between the water on both sides of the production well (EDTA or B). If there are clear differences, they are only found in one or two of the inland wells. For example, TEG370OP resembles the surface water in its B, EDTA, and SO_4 content, but contains less Cl and Na and has a more negative isotope signal. TEG370UP differs mainly in the SO_4 content, but resembles the surface water in the remaining water constituents shown. TEG373 contains less B than the transect wells. The vertical differences are even more extreme in some of the pharmaceutical residues, examples for phenazone (analgesic) and AMDOPH (persistent oxidation product of dimethylaminophenazone) are given in Figure 116 , where concentrations increase with sampling depth. These phenomena are currently not fully understood and probably the result of a complicated and transient flow regime. However, it can be concluded that the variations in the background groundwater composition are much larger and far more complicated than expected, both in their vertical and horizontal extent.

From the large scale investigations around the GWA and the existing flow model (compare chapter IGB) it becomes clear that, depending on the pumping regime of the production well gallery, the background groundwater can flow towards the transect from further north or south, which would each result in a very different water quality (chapter 0). However, judging from the strong seasonal variations, the proportion of BF in well 20 is likely to be rather large (> 80 %).

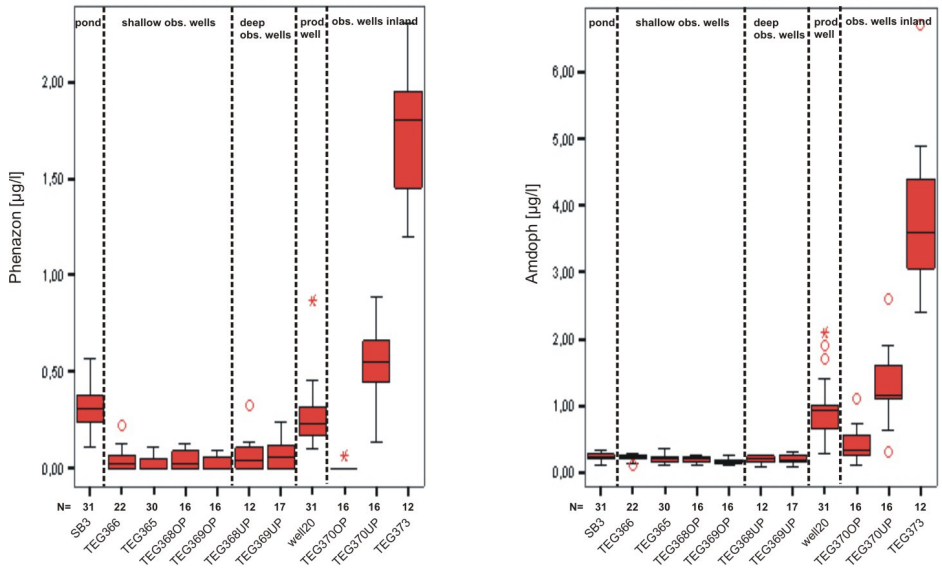

Figure 116: Boxplots for phenazone and AMDOPH at the GWA Tegel (data source: BWB); November 2001-May 2004, N = number of samples (31 at maximum).

1.6.7 Hydrochemistry at the transect

Hydrochemical conditions of the infiltrate

TEG366 and TEG365 are two shallow observation wells below and very close to the pond with a depth of 6-8 m below the pond (23.0-25.0 masl) and 7-9 m below ground surface (24.7-26.7 masl) respectively (Figure 117). They were used for the description of redox conditions of the infiltrate on the first metres of flow (Massmann et al., subm.). According to the isotope and temperature data, both are generally reached within a travel time of hours to less than 3 days, depending on the recharge rate (Figure 96c). The groundwater wells were fully saturated at all times.

Throughout the year, the DOC concentration (Figure 117b) decreased about 0.15-0.20 mmol/L from the pond to the shallowest wells, which is equivalent to a reduction of ~33-48 % of the total DOC present. The DOC input and the degree of removal fluctuated slightly but did not show any seasonality, nor did it show a clear relation to the hydraulic conditions.

The pond water was saturated with O_2 at all times. Because of the temperature dependency of the O_2 saturation, the actual O_2 concentration was ~0.35-0.55 mmol/L in winter and ~0.20-0.35 mmol/L in summer. The O_2 concentration in the shallow groundwater (Figure 117c) showed a strong seasonality. In mid-summer (at water temperatures above 14°C as indicated by the grey shading in Figure 117), all O_2 (~0.20-0.35 mmol/L) was removed before reaching the first groundwater observation well. In winter, O_2 was not reduced completely, only ~0.05-0.25 mmol/L (at maximum) of O_2 was consumed on the way to the shallowest

wells. The temperatures of the infiltrate are given in Figure 117a for comparison. It seems that on top of the seasonal variations, the O_2 concentrations occasionally peaked towards the end of the unsaturated phases, for example in July 2003 (Figure 117c). At all times, but particularly in summer, the decrease in O_2 exceeded the decrease in DOC. If O_2 was the only terminal electron acceptor (TEA), the O_2 decrease should be equivalent to the decrease in DOC (Eq. 1). This indicates that besides dissolved organic carbon, particulate organic matter (POC) present in the aquifer or, more likely, fresh organic matter of the clogging layer may act as an additional electron donator.

$$CH_2O + O_2 \rightarrow CO_2 + H_2O \qquad \text{Eq. 1}$$

A clear difference between the redox potential of the surface water and the infiltrate could only be seen in summer. When conditions turned anaerobic, the Eh of the infiltrate was about 100 mV less than in the surface water (data not shown).

The seasonally variable input of nitrate is largely reflected in the infiltrate (Figure 117d). When O_2 was the only TEA (mainly in winter), NO_3^- concentrations in the surface water tended to be even lower than in the shallow groundwater, because NO_3^- is a reaction product of the aerobic degradation of particulate organic matter which contains nitrogen (van Cappellen and Wang, 1996). Nitrate reduction was rarely observed. If denitrification did take place, it happened mainly in summer and then towards the end of a saturated phase, for example in July/August 2004, when temperatures were high and conditions had been saturated for a while (Figure 117). Nitrate reduction is bacterially catalysed and leads primarily to the production of nitrogen via several complicated pathways with intermediates such as NO_2^-, NO and N_2O. The process can be described by the overall reaction (Appelo and Postma, 1996):

$$5CH_2O + 4NO_3^- \rightarrow 2N_2 + 4HCO_3^- + CO_2 + 3H_2O \qquad \text{Eq. 2}$$

Manganese (Mn^{2+}) appeared only in summer when temperatures exceed 14°C (Figure 117e), at times when O_2 had been fully depleted. During the unsaturated phase in July 2003, when Mn^{2+} had previously been detected, the concentrations dropped to zero again despite the fact that temperatures were high. If observed, Mn(IV) reduction commenced before NO_3^- was fully removed. Iron (Fe^{2+}) was never detected in TEG365 or TEG366 and, likewise, SO_4^{2-} reduction did not occur.

Many authors have described the importance of seasonal temperature variations on redox processes in the groundwater (e.g., Olivie-Lauquet et al., 2001; Carrera et al., 2003; Prommer and Stuyfzand, 2005). Because redox processes are generally microbially catalyzed, the temperature variation influences the microbial activity, reflected in changes in the concentration of redox-sensitive parameters. A temperature dependency of denitrification was reported in various studies and environments (e.g., David et al. 1997; Carrera et al., 2003). A correlation between increased dissolved iron, manganese and trace element con-

centrations with increasing temperatures was observed in a wetland in France by (Olivie-Lauquet et al., 2001). The particular importance of the role of large temperature variation in artificial recharge systems on redox-related hydrochemical changes has recently been acknowledged. (Prommer and Stuyfzand, 2005) discovered during deep well injection of aerobic surface water into an anaerobic aquifer in the Netherlands that reaction rates of pyrite oxidation by oxygen depended significantly in spatially and temporally varying groundwater temperatures. They found that oxygen breakthrough from the injection well to the first observation well 8 m away occurred in winter only, while no breakthrough was observed when the injectant temperatures rose above approximately 14 °C, which is very similar to our findings.

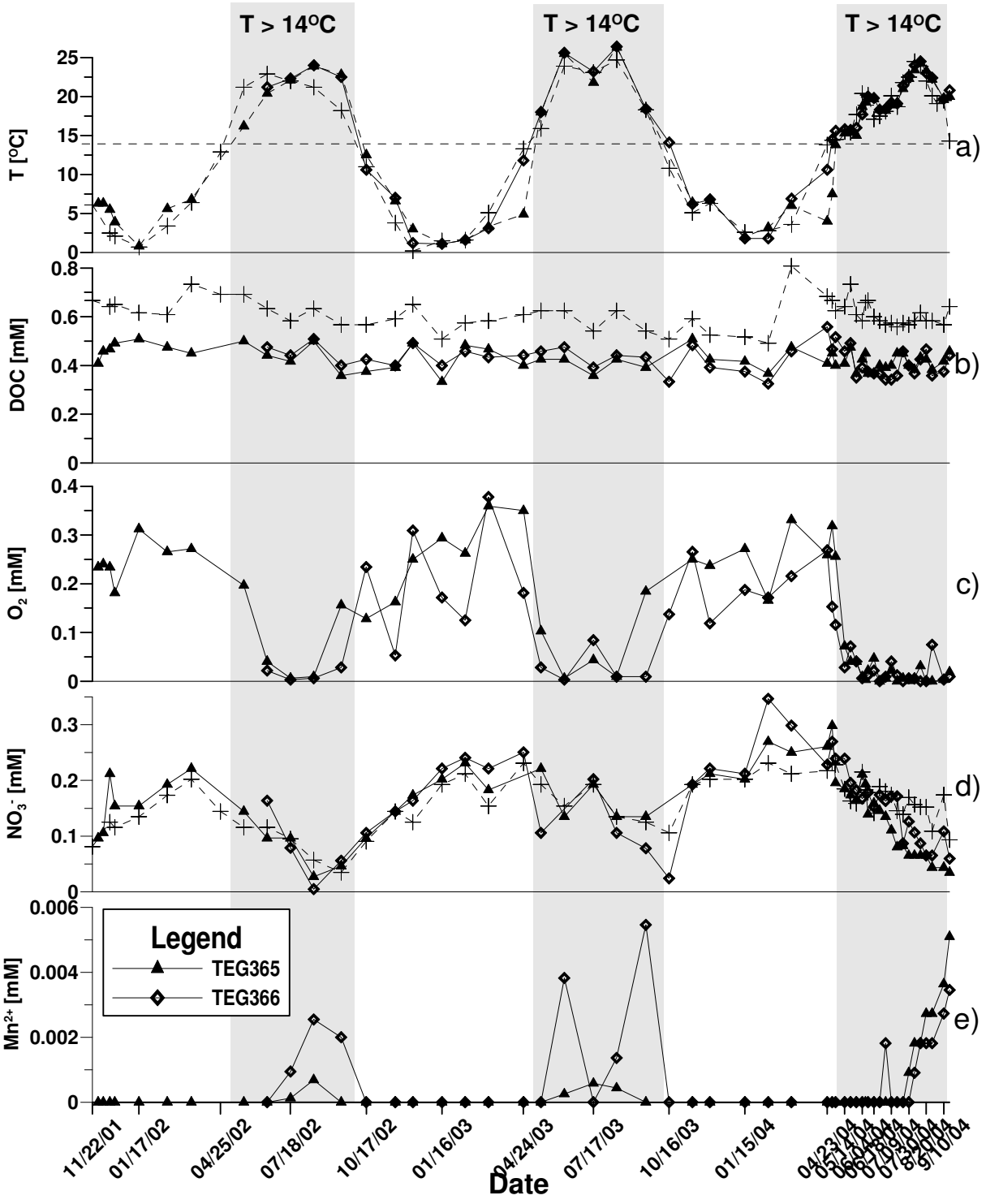

Figure 117: a) Temperatures [ºC] and b) concentration of dissolved organic carbon (DOC, mM) and redox indicators O_2 (c, mM), NO_3^- (d, mM) and Mn^{2+} (e, mM) in pond 3 and groundwater observation wells TEG365 and TEG366 below the pond (compare Figure 94). The times when the temperatures in the surface water and infiltrate were above 14 ºC are marked with grey bars. The pond itself was saturated with oxygen at all times (pond concentration, average 0.36 ± 0.1 mmol/L not shown) and largely free of Mn^{2+} (data not shown). The dominating influence of the temperatures on the redox conditions is visible (Massmann et al., subm.).

Figure 118 illustrates the bicarbonate (HCO_3^-, a) calcium (Ca^{2+}, b) concentrations in the infiltrate in relation to the saturated/unsaturated phases (white/grey shading). In general, the pond concentrations were reflected in the groundwater. However, distinct peaks in the groundwater exceeding the input concentration could sometimes be seen towards the end of the unsaturated phases (u, grey bars). Within these peaks HCO_3^- concentrations increased roughly twice as much as the Ca^{2+} concentrations, indicating that calcite dissolution took place. Calcite dissolution is an important process often induced by redox reactions at the presence of calcite (von Gunten and Zobrist, 1993).

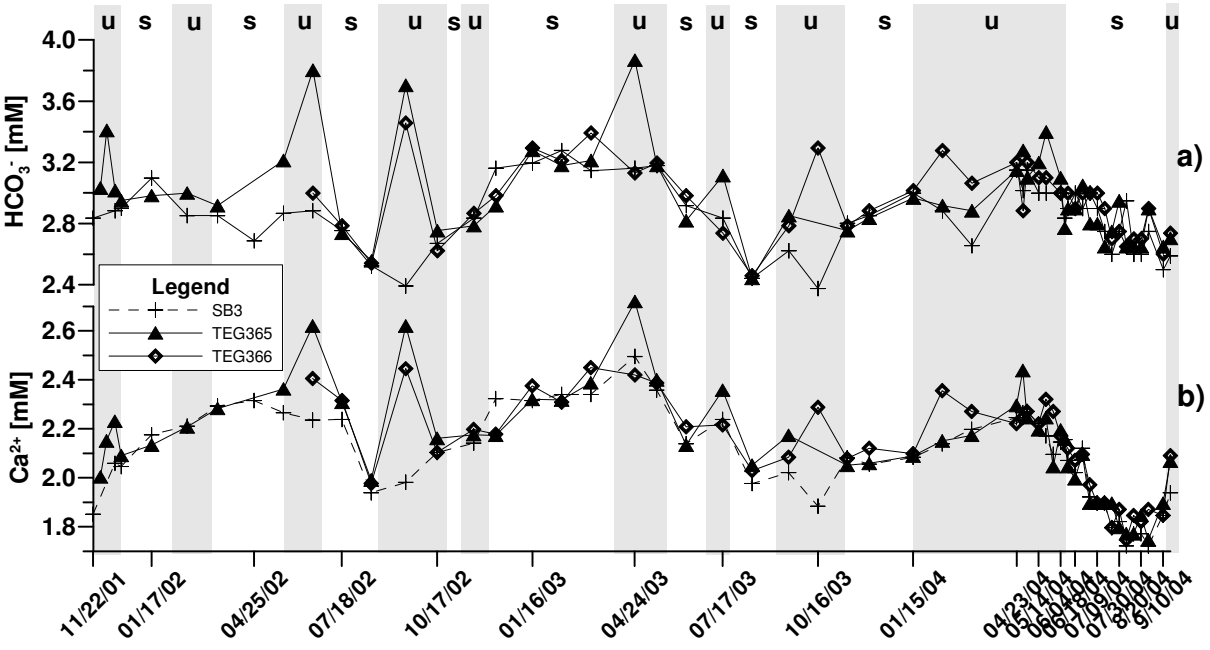

Figure 118: a) Bicarbonate and b) calcium concentrations in the pond and groundwater wells TEG365 and TEG366. Grey shading represents the changes between saturated (annotation s, white bars) and unsaturated (annotation u, grey bars) phases. The groundwater concentrations often clearly exceeded the input concentrations towards the end of the unsaturated phases (Massmann et al., subm.).

Compared to the seasonal temperature variations, the hydraulic changes had only a minor effect on the redox chemistry of the groundwater. An effect was only clearly visible when, as a result of unsaturated conditions, gaseous oxygen intruded into the anoxic environment during summer, leading to a temporary shift from Mn-reducing to aerobic conditions (Figure 117). However, an indirect influence of the cyclic changes in the water saturation was visible in the increased Ca^{2+} and HCO_3^- concentrations in the unsaturated phases (Figure 118). This process could have been enabled by the additional rapid oxidation of filtrated labile organic matter by gaseous O_2 entering the unsaturated zone (Eq. 3). The fact that DOC concentrations did not show an additional decrease when conditions were unsaturated suggests that DOC degradation was outcompeted by the degradation of sedimentary bound organic matter.

$$CH_2O + CaCO_3 + O_2 \rightarrow Ca^{2+} + 2HCO_3^- \qquad \text{Eq. 3}$$

It was found that the redox conditions, which are temperature dependant, appear to affect the behaviour of a number of phenazone type PhACs (Massmann et al., subm.). The removal of phenazone, and possibly also FAA and AAA is not complete at the absence of oxygen. Microbial degradation by aerobic bacteria rather than adsorption was suggested to be the removal process. Results indicate that marginal removal of AMDOPH, a very persistent metabolite of dimethylaminophenazone, might also be coupled to the presence of oxygen (Massmann et al., subm.).

Redox conditions along the groundwater transect

In terms of the redox conditions (Figure 119), the evaluation of the box-plots shows that the shallow observation wells towards the pond still contain oxygen and nitrate. The deeper observation wells TEG368UP (below the till) and TEG369UP contain much less O_2. Nitrate is still present, but in lower concentration than in the shallow wells and in the pond. Most observation wells between pond and production well contain some Mn^{2+}, in particular the deeper wells, but Fe^{2+} was never detected.

The observation wells inland are O_2 free. In the shallowest observation well TEG370OP, NO_3^- could still be detected, but Mn^{2+} is also present. TEG370UP above the till is NO_3^- free and Mn^{2+} and even Fe^{2+} could already be analysed. The highest Fe^{2+} concentrations were encountered in TEG373. TEG373 and also TEG370UP may even be slightly sulfate reducing, since SO_4 concentrations are comparatively low (Figure 115) but sulfide was not analysed and the original background SO_4^{2-} concentration is unknown.

The boxplots (Figure 120) demonstrate that the largest drop in DOC (and TOC) concentration occurs between pond and the first observation well, i.e. in the clogging layer, even though it is removed regularly. A slight decrease along the remaining transect is also visible. The DOC concentration drop is smaller than the O_2 reduction, which is why sedimentary bound organic carbon is likely to be an additional electron donator.

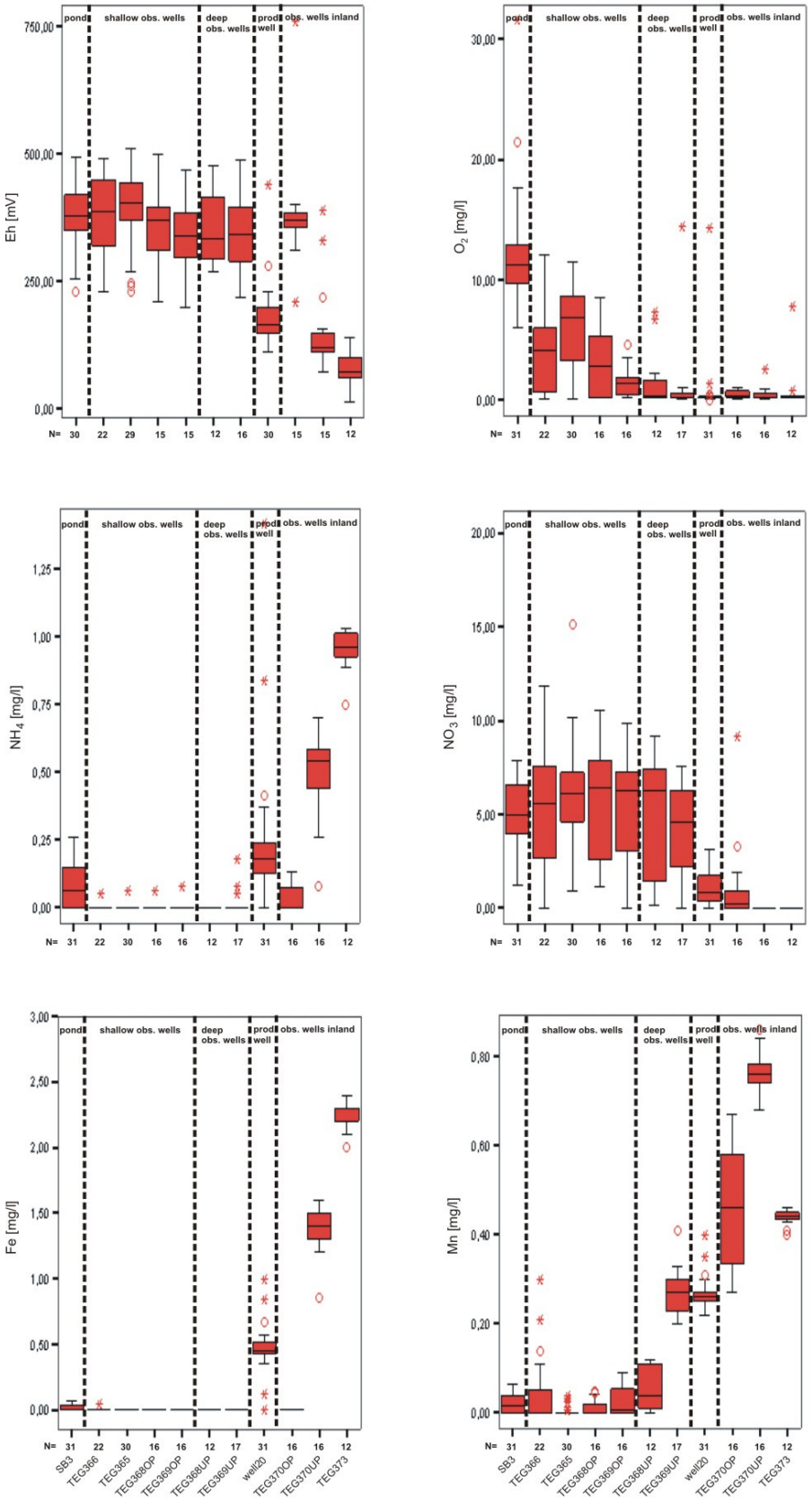

Figure 119: Boxplots for redox indicators Eh, O_2, NH_4^+, NO_3^-, Mn^{2+} and Fe^{2+} at the GWA Tegel transect (data source: BWB); November 2001-May 2004, N = number of samples (31 at maximum).

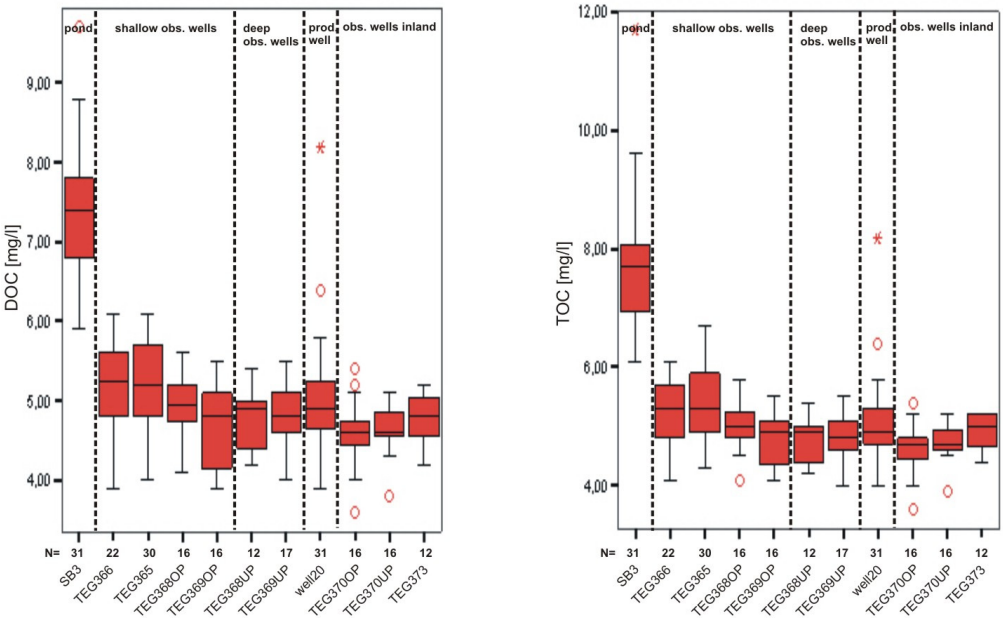

Figure 120: Boxplots for dissolved organic carbon (DOC) and total organic carbon (TOC) at the GWA Tegel transect (data source: BWB); November 2001-May 2004, N = number of samples (31 at maximum).

The seasonal redox changes as described above for the area close to the pond (chapter 0) print through along the entire transect (Figure 121). The NO_3^- concentration of all observation wells decreases largely in the summer months, while at the same time, Mn^{2+} appears. While TEG368OP still contains traces of NO_3^- even in the summer months, Mn^{2+} was analysed in samples from TEG369UP at all times.

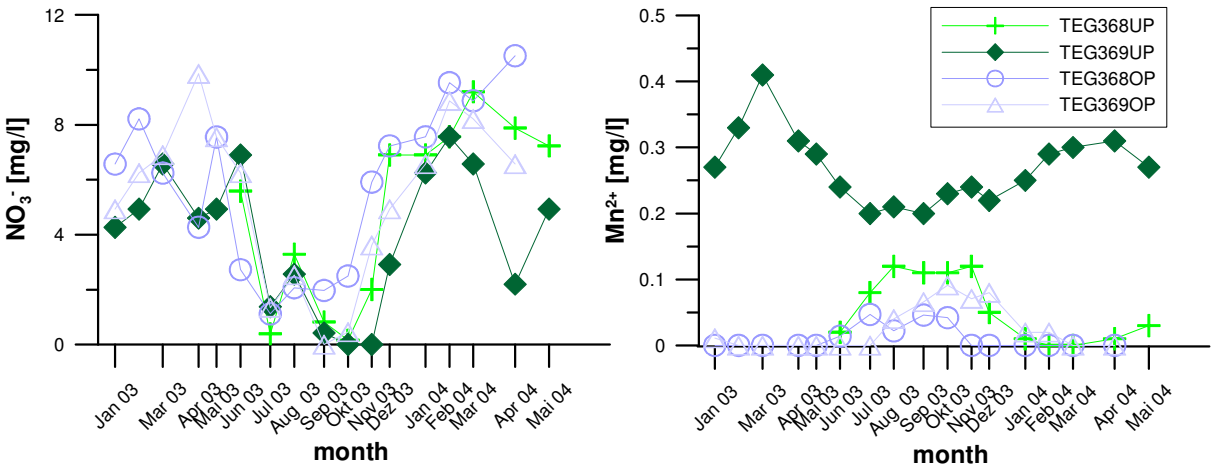

Figure 121: Time series of NO_3^- and Mn^{2+} in deep and shallow screened observation wells TEG368 and TEG369 (data source: BWB).

Figure 122 shows O_2 and NO_3^- concentrations plotted versus travel times along the transect for three summer and winter months in 2003. In summer, O_2 was consumed within the first metres of infiltration as explained above Figure 117c) and oxygen remained absent along the transect. Nitrate reduction, which was rarely observed close to the pond (Figure 117d) continued along the transect, while at the same time Mn^{2+} concentrations increased due to commencing reduction of Mn(IV)hydroxides present in the sediment (not shown). The fit through the plot of NO_3^- versus travel time is shown in Figure 122 (left). Rate constant estimates vary strongly (between 0.01 and 0.043 d^{-1}), probably partly due to the highly variable input concentration and the fact that the time-lag to the observation wells was not considered. The corresponding half-lives of NO_3^- were 16 days to 2 ½ months; hence towards the production well, NO_3^- was largely diminished and Mn^{2+} concentrations were elevated (Figure 119).

In winter, at low temperatures, oxygen was present throughout the entire area between the pond and the production well (Figure 122, right). The O_2 reduction proceeded much more slowly and O_2 was the major TEA along the entire transect (little change in the NO_3^- concentration, Figure 122 right). The fit through the O_2 concentration versus travel time is now exponential with rate constants of 0.049 - 0.061 d^{-1} (Figure 122, right) and corresponding half-lives of 11 to 14 days. Mn^{2+} could only be detected in the observation well TEG369UP, closest to the production well that receives water from above and below the glacial till and also has the longest travel time (Figure 113).

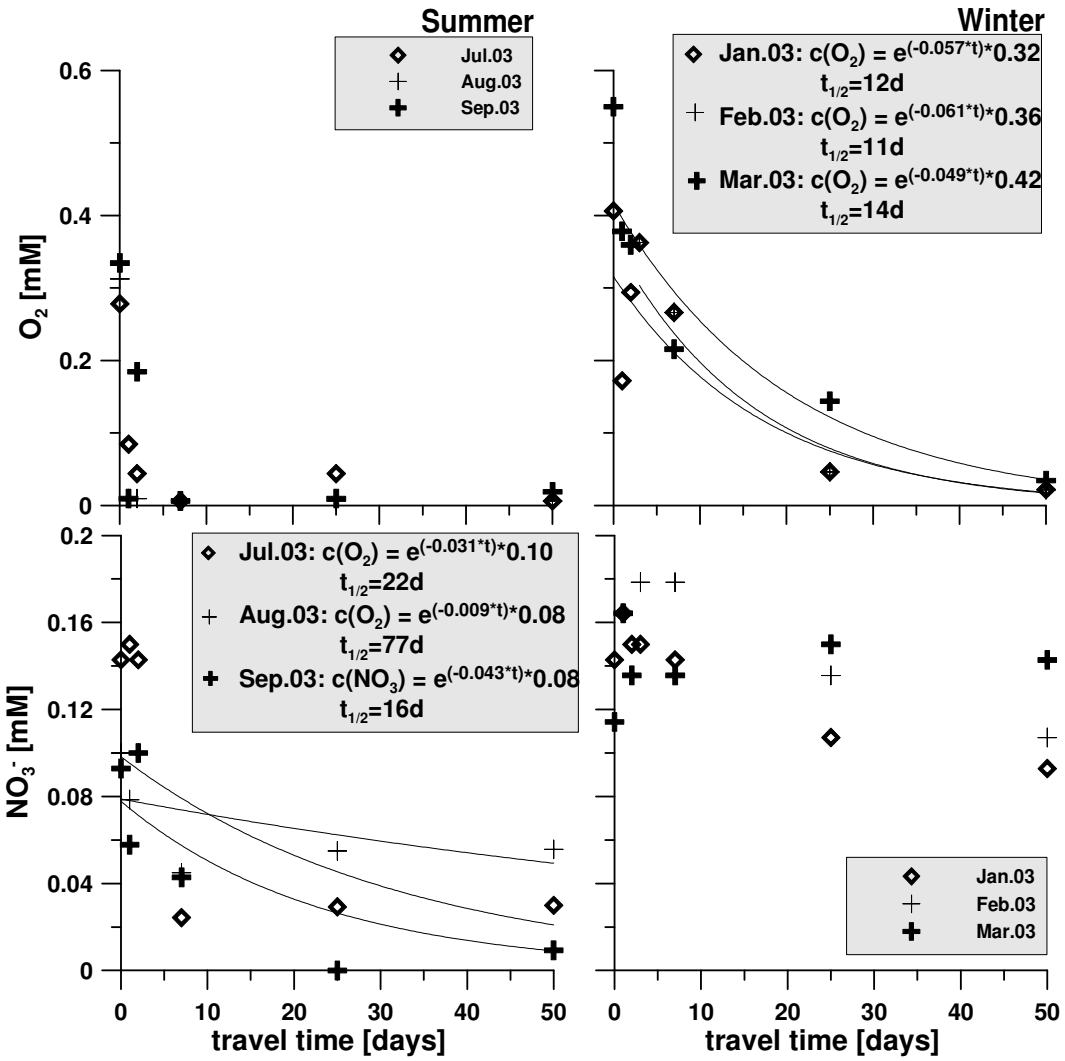

Figure 122: O_2 and NO_3^- concentrations [mM] plotted versus travel times estimated from tracer results for three summer and winter months. The travel times to TEG366 and TEG365, both < 3 days, were assumed to be 1 and 2 days respectively. In summer, O_2 was rapidly consumed in the infiltration zone and NO_3^- reduction observed along the transect, while in winter O_2 reduction continued along the entire transect and little NO_3^- reduction occurred (Massmann et al., subm.).

Figure 123 shows the approximate redox zoning in the groundwater in summer and winter. It exemplifies where O_2 and NO_3^- are still present and where Mn^{2+} and Fe^{2+} appear seasonally. The zoning is different NW and SE of the production wells. Rather than abrupt changes, the transition from one zone to the next is fluent and also moving with time. The redox regime is highly transient and changes seasonally. Hence, the zoning does not primarily depend on the removal of the clogging layer but mainly on the largely variable temperatures (Figure 112).

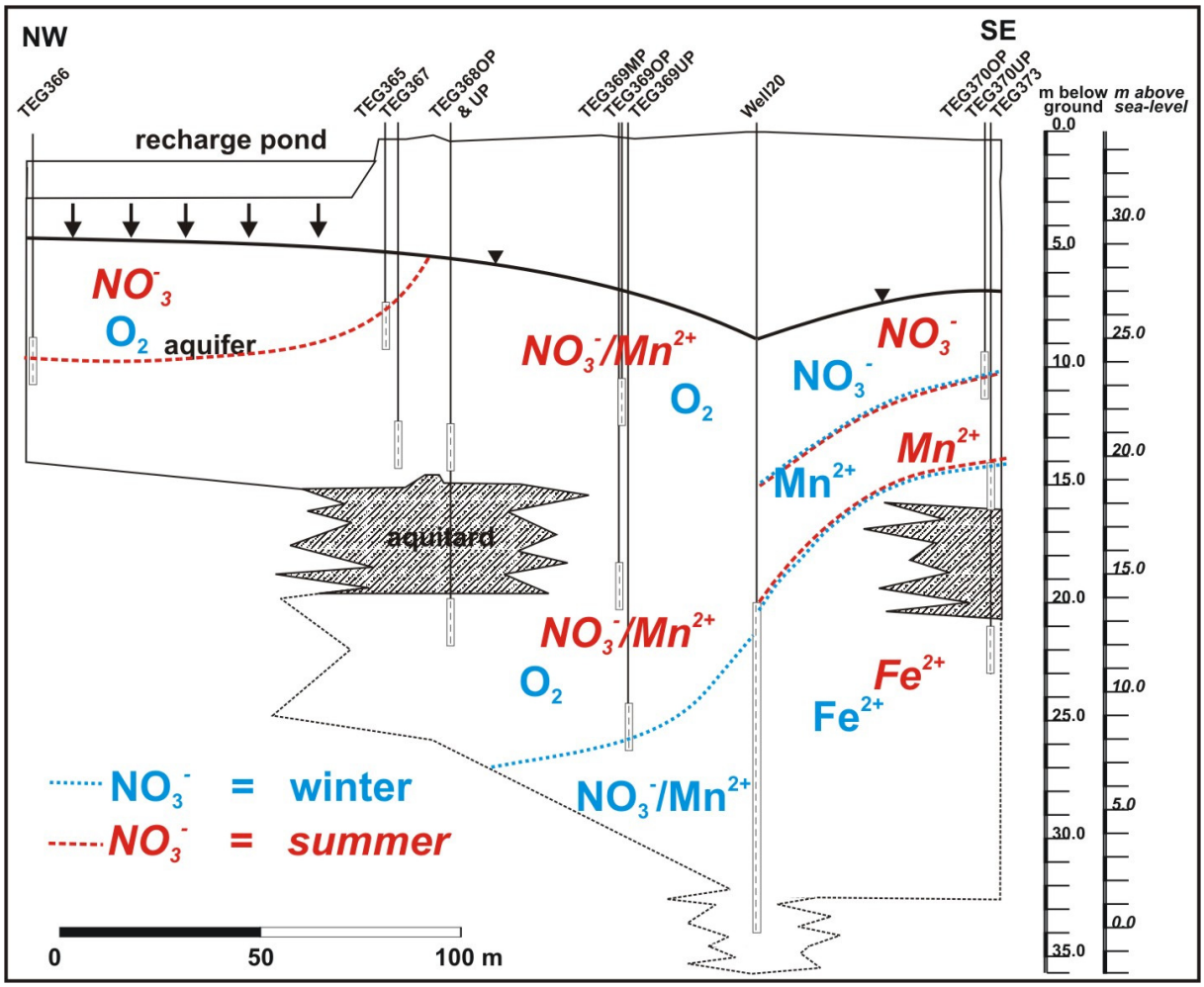

Figure 123: Approximate redox zoning at the GWA transect in summer (red) and winter (blue), defined by the presence of redox indicators.

Large Scale Hydrochemical Investigations

In order to get an idea of the variations in the groundwater and production well chemistry on a larger scale, a joint sampling campaign of the Free University of Berlin and BWB was conducted together in spring 2003. All production wells operating at the time of the well galleries Hohenzollernkanal and Saatwinkel as well as surface water and available groundwater observation wells in the area were sampled (Figure 124).

The sampling was done in order to evaluate the following questions:

What are the hydrochemical properties and the variability of the background groundwater in the surrounding of the well triangle?

What are the effects of variations on single production wells of the two galleries?

What is the share of artificially recharged groundwater in the individual wells?

Did condition change since the last production well sampling campaign in the area in 1999?

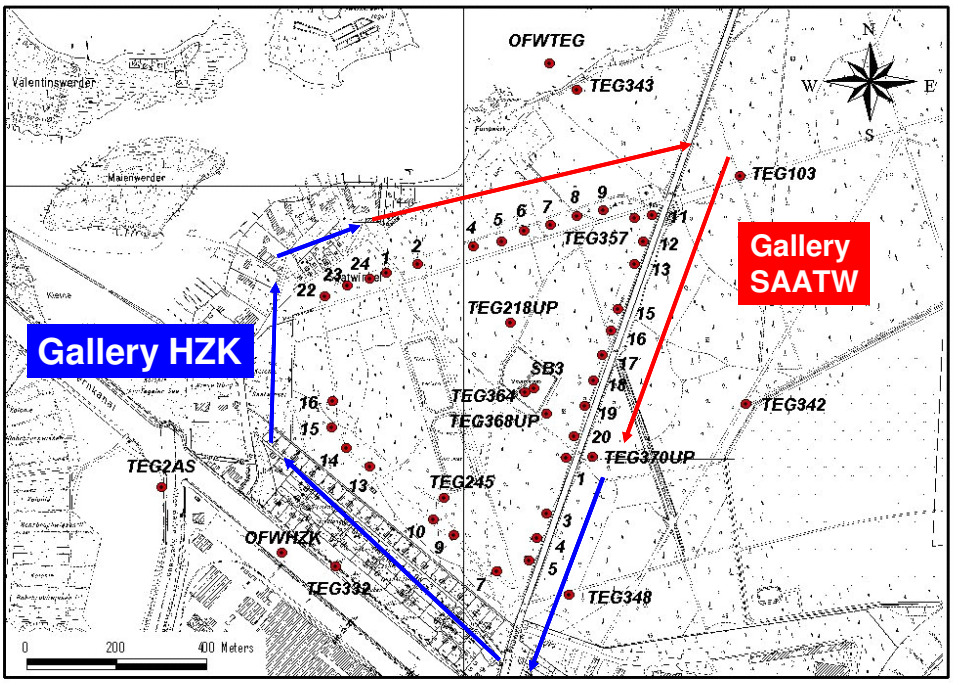

Figure 124: Production wells of the Hohenzollernkanal-Saatwinkel well triangle and surrounding observation wells sampled in spring 2003.

The production wells near the airport (SAAT 11-20; HZK 1-5) are likely to be influenced by background groundwater and artificially recharged groundwater, while the production wells oriented towards lake Tegel (HZK 22-24; SAAT 1-9) should be a mixture of Lake Tegel and pond water, i.e. they should contain approximately 100 % of bank filtrate. The triangle side to the south-east may contain proportions of groundwater flowing below the Hohenzollernkanal which originates from the river Havel located > 1 km west.

Figure 125 shows that the hydrochemistry of the “background” groundwater towards the airport, represented by TEG103, TEG342, TEG370UP & TEG348 is highly variable. While TEG103 and, to an extent, TEG342 represent the “typical” landside groundwater (e.g. low $\delta^{18}O$ & δD, high SO_4 & Ca, low Cl, Na, B), the $\delta^{18}O$ & δD and SO_4 values of TEG348 and TEG370UP lie within the range of those of the surface water (temporal variation of the surface water see previous chapters), indicating that there is a hydraulic connection between surface water (Hohenzollernkanal or even the Spree further south. Because there is hardly a difference between surface water and groundwater in the southern triangle, the proportion of BF can only be calculated for production wells SAAT 11-20 (Figure 125 calculated with TEG103 only) and values are probably only accurate for well 11-13, which receive water from the TEG103 direction and differ strongly from the remaining wells (lower $\delta^{18}O$ & δD, higher SO_4 & Ca, lower Cl, Na, B).

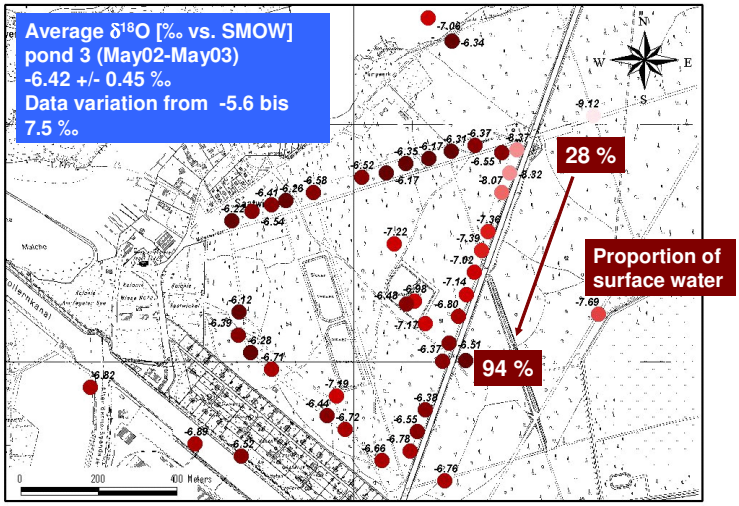

a)

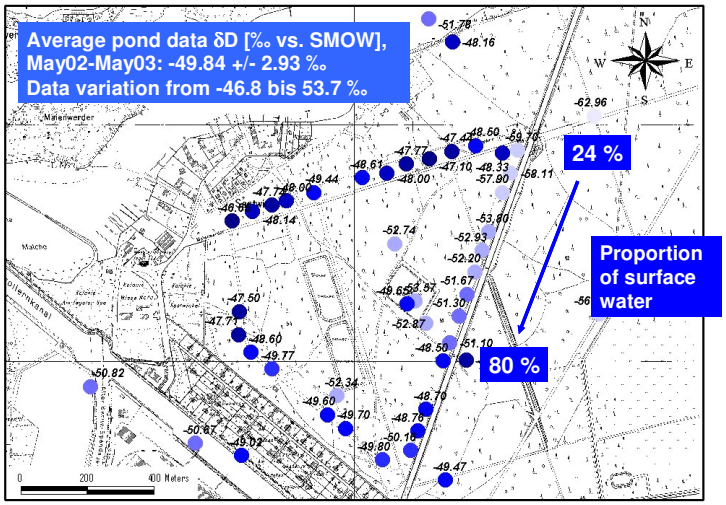

b)

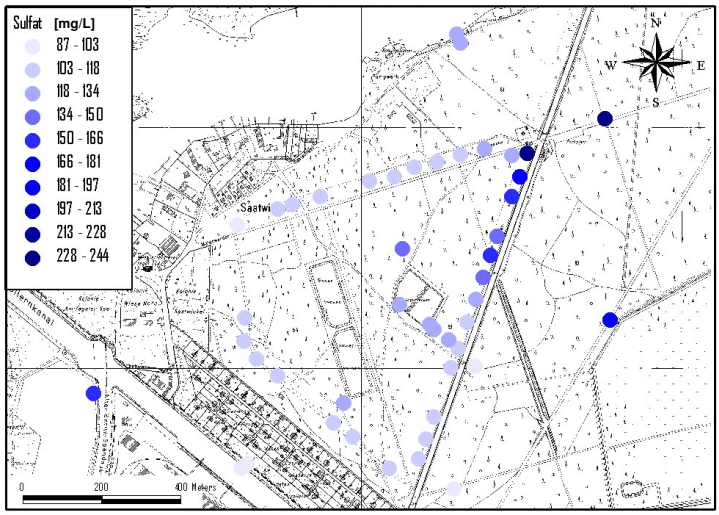

c)

Figure 125: Influence from the NE: $\delta^{18}O$ (a) & δD (b) values [‰ vs. SMOW] and sulfate concentrations, March/May 2003.

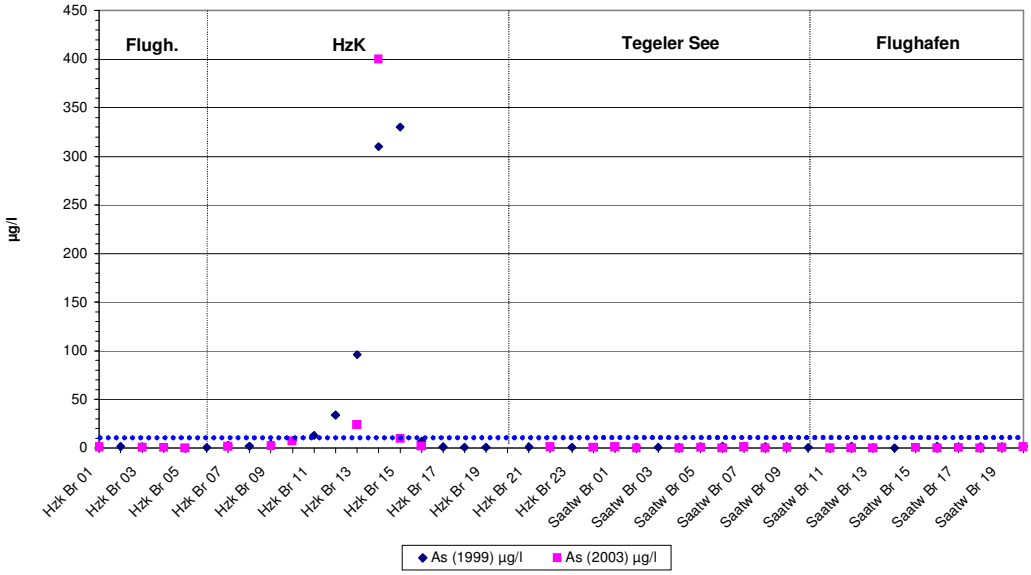

Figure 126: Arsenic concentrations in the production wells in 1999 and 2003. Blue-line: drinking water limit (data source: BWB).

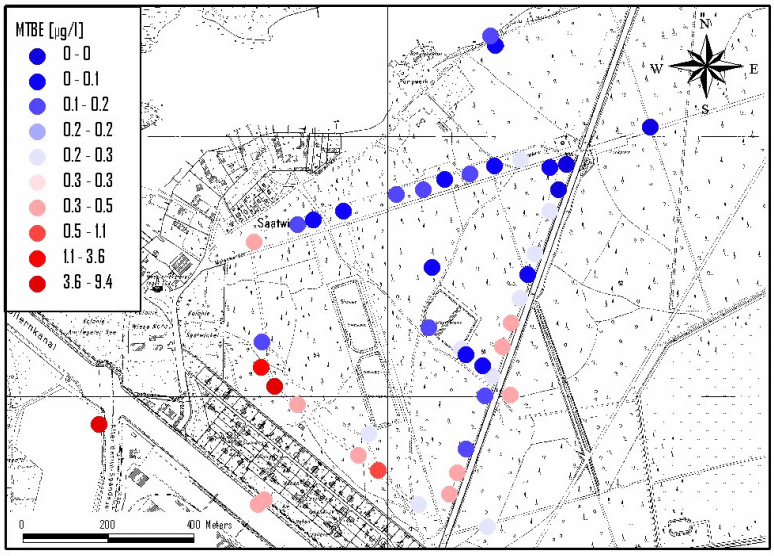

Figure 127: MTBE concentrations in samples wells in 2003 (data source: BWB).

The production wells in the south-west contain elevated concentrations of arsenic (Figure 126, exceeding the drinking water limit), MTBE (Figure 127), phenazone (Figure 128a), AMDOPH (Figure 128b) and EDTA, clearly originating from the south-western side of the Hohenzollernkanal, where highest concentrations are found in TEGAS2. As and MTBE originate from different contaminated industrial sites west of TEGAS2. The As pollution is known by BWB and As is removed during drinking water treatment (personal communication BWB).

While highest phenazone and AMDOPH concentrations are found in the south-west, highest propyphenazone (analgesic/anti-inflammatory) concentrations are found in the south-west and in the north, towards Lake Tegel. The phenazone-type pharmaceuticals and related substances originate from the surface water, where their presence is caused by their discharge from WWTP (Heberer, 2002) or from former production spills of a pharmaceutical plant near Oranienburg on the Upper Havel, which produced phenazone-type pharmaceuticals. Reddersen et al. (2002) suspected that spills of the plant released into the environment in the past, when regulations were less strict, are the cause of some of today's findings of PhAC residues. Because of the pharmaceutical plant, phenazone and dimethylaminophenazone (not detected) concentrations in the surface water of the Upper Havel were probably considerably higher in the past decades than they are today (exact values are not known). In addition, the production of dimethylaminophenazone was stopped in 1978 (Reddersen et al., 2002). Therefore, the high concentrations of phenazone and AMDOPH in the south-west indicate that the groundwater is probably older bank filtrate (similar to findings in greater depth at the bank filtration transects, where high phenazone and AMDOPH concentrations always corresponded to an older age of the bank filtrate). It infiltrated from the Upper Havel 1-2 km further west, passed the industrial contamination sites (thereby accumulating As, MTBE etc.) and is now abstracted by the production wells with a considerable time lag of a few years to a few decades. In addition, it appears that the share of "older" BF containing phenazone and, in particular, AMDOPH is getting larger with depth at all investigated sites (Figure 116 and previous BF chapters)

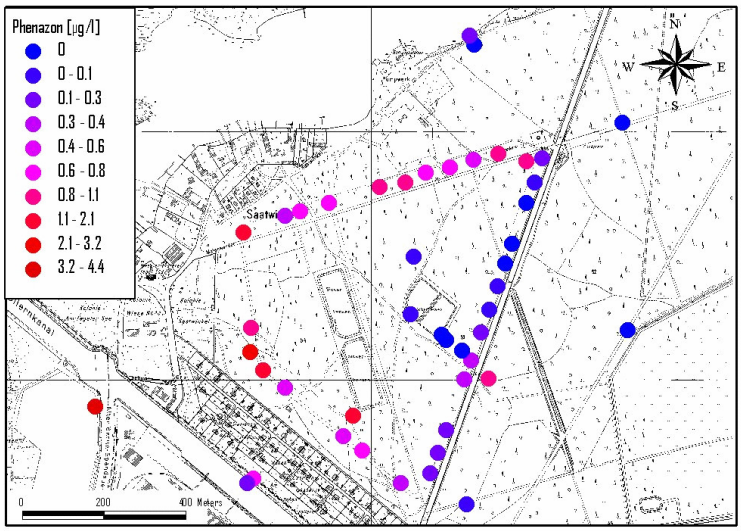

a)

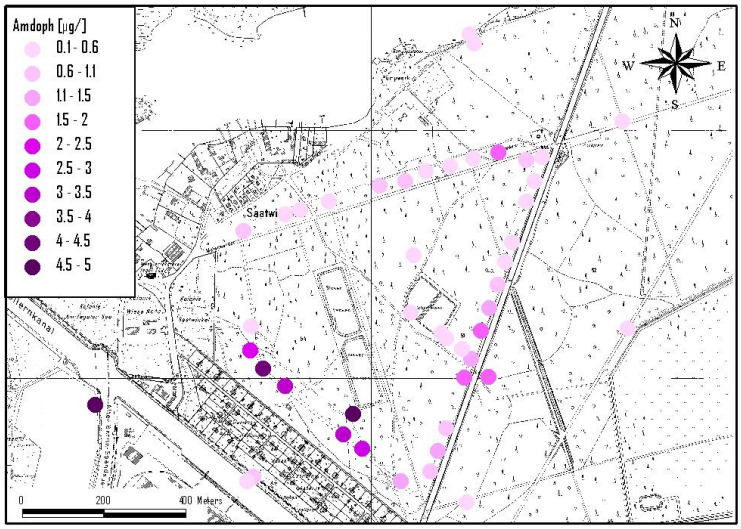

b)

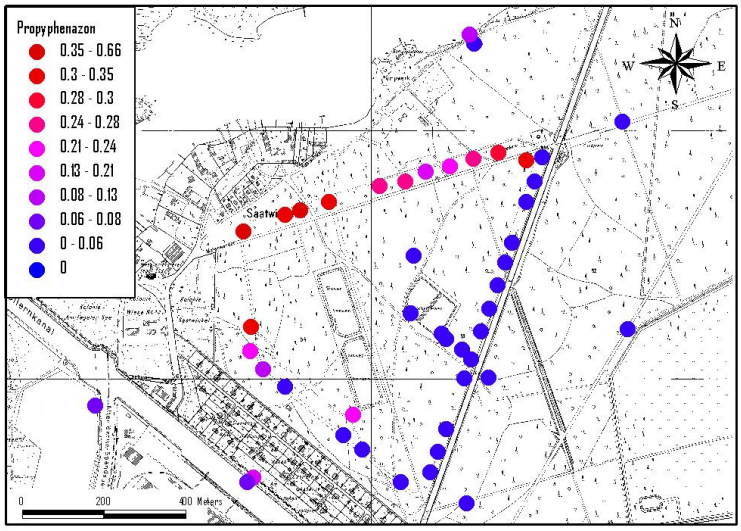

c)

Figure 128: Phenazone-type pharmaceuticals and residues phenazone (a), AMDOPH (b) & propyphenazone(c). Data source: BWB.

The higher propyphenazone concentrations towards Lake Tegel, where travel times should be in the order of magnitude of a few months suggest that it is presently brought in with the treated WW, thereby representing “younger” bank-filtrate. Approximate input pathways in the area are shown in Figure 129.

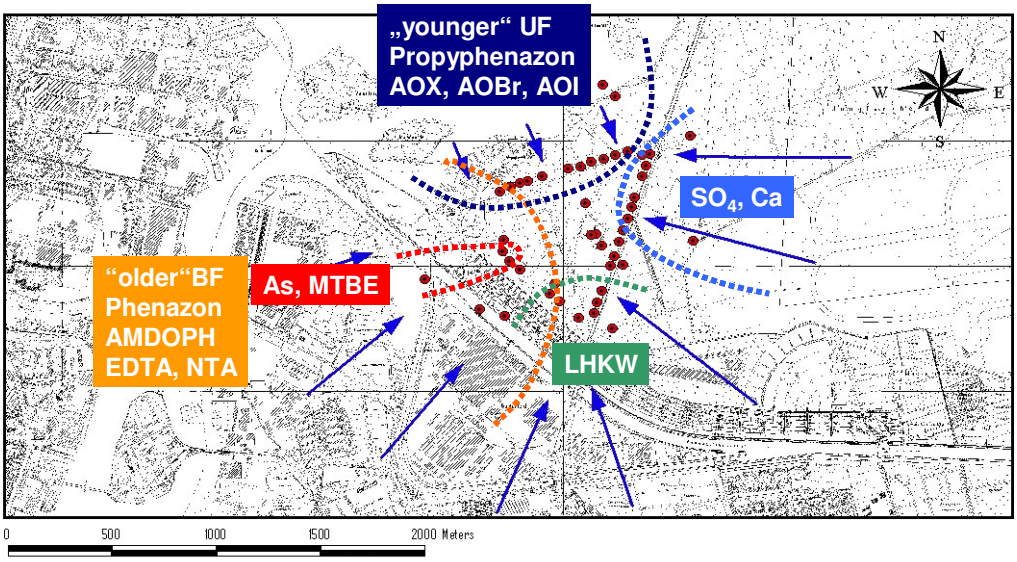

Figure 129: Summarising the major input paths for various water constituents in the area of the recharge ponds.

1.6.8 Major conclusions & summary of GWA Tegel Site

Operation/Clogging layer

- The hydraulic and hydrochemical conditions during artificial recharge are highly transient.
- The infiltration capacity varies in relation to the changes of the hydraulic conductivity of the pond bottom sediments.
- The pond bottom is covered with sand which are removed regularly and washed in order to restore the infiltration capacity by removal of finer grained material and algae.

Travel times/ age

Travel times from the pond to the observation well at the transect are short and vary between a few days to observation wells below the pond to ~ 50 days to production well 20.

None of the wells between the pond and production well 20 contain a share of “older” bank filtrate.

Mixing

The observation wells within the well triangle contain 100 % of artificially recharged water from the pond with a residence time of less than 50 days.

The production well 20 abstracts > 80 % BF.

Within the entire production well triangle proportions of BF vary largely between 25 % (north-eastern corner of the triangle) and 100 % in the west.

Hydrochemistry

- The redox conditions are influenced by seasonal temperature changes and changes between saturated and unsaturated conditions below the pond.
- The large temperature variations of ~ 25°C of the infiltrate have the greatest effect on the distribution of redox indicators in the groundwater. Above temperatures of approximately 14 °C, the redox conditions turn anoxic within hours to days of travel time, while oxic conditions prevail along the entire transect at temperatures below 14 °C.
- The hydraulic conditions (saturated/unsaturated below the pond) alternate at short time intervals and have a minor additional influence on the redox regime. A secondary effect of the cyclic operational changes is the oxidation of particulate organic matter caused by the presence of gaseous O_2 below the pond during unsaturated phases, which leads to calcite dissolution reflected by elevated concentrations of Ca^{2+} and HCO_3^-.
- The redox conditions, in turn, appear to affect the behaviour of a number of phenazone type PhACs. The removal of phenazone, and possibly also FAA and AAA is not complete at the absence of oxygen.
- The background groundwater variations are large, both in horizontal and in vertical direction.

In the SW, the concentrations of As and MTBE are very high, because of several old contamination sites south-west of the Hohenzollernkanal.

Elevated concentrations of phenazone and AMDOPH in the south–west originate from bank filtration at a time, when surface water concentrations of these substances were considerably higher (typical “old” bank filtrate).

1.7 Major differences between the artificial recharge site and the bank filtration sites

1.7.1 Differences

- At the AR site, the clogging layer is removed regularly; the natural lakes are covered with thick layers of low permeability laccustrine sappropels and clogged sands at the lake shores; unlike at the AR site, these layers are never removed artificially.
- At the BF sites infiltration takes place only at the clogged lake shores while at the AR site, infiltration occurs everywhere.
- At the AR site, the travel times are shorter; However, this may be site specific for our transects (even though the difference in the clogging layer suggests it could be a general trend).
- The most important difference is the lack of the vertical age stratification encountered at both BF sites, suggesting that this is a “real” difference and not only site specific for our transects (the suspected cause is the difference in the pond/lake base)
- Due to this stratification into 2 (or more, compare hydraulic models) BF types of different origin and age, the production wells themselves differ from each other with regard to their hydrochemistry.
- Overall and in average, the BF sites are more reducing, the infiltrate reaches ferrous / postoxic conditions before the production well at all times.
- The different redox conditions affect redox sensitive species, e.g. Phenazone, AOX and others.
- Depending on the substance, its elimination is favored at more anaerobic (AOX, BF site) or aerobic conditions (phenzone, AR site).

1.7.2 Similarities

- The artificial recharge site resembles the bank filtration sites with regard to the sediment characteristics. Production and observation wells are screened in the same Pleistocene glacio-fluvial porous aquifer with a thickness ~40 m (with the exception of the Wannsee site, where the production wells are also screened in deeper aquifers); the aquifer is partly divided by patches of glacial till, but the contact to deeper aquifer parts is never restricted.
- The surface water quality is similar.

- Both sites reveal a distinct and seasonally variable redox zoning, only because of the shorter travel times are conditions towards the production wells more reducing at the BF sites.

1.8 References

AG Boden,1996. Bodenkundliche Kartieranleitung, 4. Aufl., Nachd., 392 S., Hannover.

Appelo, C.A.J. and Postma, D., 1996. Geochemistry, groundwater and pollution. A.A. Balkema, Rotterdam.

Beyer. W. 1964. Zur Bestimmung der Wasserdurchlässigkeit von Kiesen und Sanden aus der Kornverteilungskurve. Wasserwirtschaft Wassertechnik 14. 165-168.

Beyerle, U., Aeschberg-Hertig, W., Hofer, M., Imboden, D. M., Baur, H. & Kipfer, R., 1999. Infiltration of river water to a shallow aquifer investigated with 3H/3He, noble gases and CFCs. J. of Hydr. 220, 169-185.

Berner, R. A., 1981. A new geochemical classification of sedimentary environments. J. of Sed. Petr. 51(2), 359-365.

Beyerle, U., Aeschberg-Hertig, W., Hofer, M., Imboden, D. M., Baur, H. & Kipfer, R., 1999. Infiltration of river water to a shallow aquifer investigated with 3H/3He, noble gases and CFCs. J. of Hydr. 220, 169-185.

Bourg A.C.M. and Bertin C., 1993. Biogeochemical processes during the infiltration of river water into an alluvial aquifer. Environ. Sci. Technol. 27, 661-666

Bouwer, H., 2002. Artificial recharge of groundwater: Hydrology and engineering. Hydrogeol. J., 10(1): 121-142.

Bouwer, E. J. and McCarty, P. L. 1983. Transformations of halogenated organic compounds under denitrification conditions. Appl. Environ. Microbiol., 45(4), 1295–1299.

Bresser, R., 1995. 1-Methyl-2-phenylacetohydracid als potentieller Metabolit der Pyrazolin-Analgetika. Verlag Dr. Köster, Berlin

Buß. 1994. KVS - Programm zur Auswertung und graphischen Darstellung von Kornverteilungen

Canfield, D.E, Raiswell, R., Westrich, J.T., Reaves. C.M., Berner. R., 1986. The use of chromium reduction in the analysis of reduced inorganic sulfur in sediments and shales. Chem. Geol. 54. 149–155.

Carrera, J., Vicent, T. Lafuente, F.J., 2003. Influence of temperature on denitrification of an industrial high-strength nitrogen wastewater in a two-sludge system. Water SA, 29: 11-16.

Champ, D.R., Gulens, J. and Jackson, R.E., 1979. Oxidation-reduction sequences in ground water flow systems. *Canadian Journal of Earth Sciences*, 16: 12-23.

Clark, I.D. and Fritz, P., 1997. Environmental Isotopes in Hydrogeology. Lewis Publishers, Boca Raton, New York.

Cornwell. J.C.. Morse. J.W. 1987. The characterization of iron sulfide minerals in anoxic marine sediments. Marine Chem. 22. 193–206.

David M.B., Gentry L. G., Smith K. M. and Kovacic D. A.,1997. Carbon, Plant, and Temperature Control of Nitrate Removal from Wetland Mesocosms. Transactions of the Illinois State Academy of Science, 90(3 and 4), 103-112.

Doussan C., Poitevin, G., Ledoux E., Delay M.,1997. River bank filtration: Modelling of the changes in water chemistry with emphasis on nitrogen species. J. of Cont. Hydrol. 25, 129-156)

Eichhorn 2000. Numerische Strömungsmodellierung der Uferfiltration am Tegeler See. Diplomarbeit Freie Universität Berlin.

Förster, U. & Wittmann, G.T.W., 1979. Metal pollution in the aquatic environment. 486 pp, Springer.

Faybishenko, B.A., 1986. Influence of entrapped air on soil permeability. Vod. Resur., 4: 48-60.

Faybishenko, B.A., 1995. Hydraulic behaviour of quasi saturated soils in the presence of entrapped air: Laboratory experiments. Water Resources Research, 31(10): 2421-2435.

Fritz, B., 2002. Untersuchungen zur Uferfiltration unter verschiedenen wasserwirtschaftlichen, hydrogeologischen und hydraulischen Bedingungen. Dissertation, Freie Universität Berlin, Berlin, 203 pp.

Fritz, B., Sievers, J., Eichhorn, S., Pekdeger, A., 2002. Geochemical and hydraulic investigations of river sediments in a bank filtration system. In: P.J. Dillon (Editor), 4th International symposium on artificial recharge of groundwater. A.A. Balkema, Adelaide, pp. 95-100.

Gagnon. C.. Mucci. A.. Pelletier. E., 1995. Anomalous accumulation of acid-volatile sulphides (AVS) in a coastal marine sediment. Saguenay Fjord. Canada. Geochim. et Cosmochim. Acta 59. 2663–2675.

Greskowiak, J. et al., 2005. The impact of variably saturated conditions on hydrogeochemical changes during artificial recharge of groundwater. Appl. Geochem., 20: 1409-1426.

Grünheid, S., Schittko, S., Jekel, M. (2004). Behavior of bulk organics abd tace pollutants during bank filtration and groundwater recharge of wastewater impacted surface waters. Proceedings of the annual meeting of the Water Chemical Society, Bad Sarow, 75-80.

Grünheid, S., Amy, G., Jekel, M., 2005. Removal of bulk dissolved organic carbon (DOC) and trace organic compounds by bank filtration and artificial recharge. Water Research, 39(14): 3219-3228.

Haeffner, H., Detay, M. and Bersillon, J.L., 1998., 1998. Sustainable groundwater management using artificial re-charge in Paris region. In: J.H. Peters (Editor), Artificial Recharge of Groundwater. A.A. Balkema, Amsterdam, pp. 9-14.

Hannappel, S., Asbrand, M., 2002. Entwicklung eines Hydrogeologischen Modells im unterirdischen Einzugsgebiet eines Wasserwerks im Lockergestein. *Schriftenreihe der Deutschen Geologischen Gesellschaft*, 24: 55-68.

Hazen. A., 1893. Some physical properties of sand and gravels with special reference to their use in filtration. Annual Report Mass. State Board of Health 24. 541-556.

Heberer, T., 2002. Tracking persistent pharmaceutical residues from municipal sewage to drinking water. Journal of Hydrology, 266(3-4): 175-189.

Heim, B., Fritz, B. & Pekdeger, A., 2002. Remote sensing techniques and investigations of surface water used for artificial recharge. In: P.J. Dillon (Editor), 4th International symposium on artificial recharge of groundwater. A.A. Balkema, Adelaide, pp. 557-560.

Heinrichs. H. 1989. Aufschlußverfahren in der Analytischen Chemie. Laborpraxis 12. 1–6.

Hinspeter, S. 2001. Geochemisch – Isotopenhydrogeologische Untersuchungen zur Uferfiltration am Wasserwerk Beelitzhof – Wannsee. Diplomarbeit Freie Universität Berlin

Hiscock, K. M., Grischek, T.,2002. Attenuation of groundwater pollution by bank filtration. J. Hydrol. 266, 139-144.

Holm J.V., Rügge K., Bjerg P.L., Christensen T.H., 1995. Occurrence and Distribution of Pharmaceutical Organic Compounds in the Groundwater Downgradient of a Landfill (Grindsted, Denmark). Environ. Sci. Technol. 29(5), 1415-1420.

Hoefs, J.,1997. Stable Isotope Geochemistry, Springer, Berlin, 201 p.

Hsieh. Y.P.. Yang. C.H., 1989. Diffusion methods for the determination of reduced inorganic sulfur species in sediments. Limnol. Oceanogr. 34. 1126–1130.

Jacobs L.A., von Gunten H.R., Keil R., Kuslys M.,1988. Geochemical changes along a river-groundwater infiltration flow path: Glattfelden, Switzerland. Geochim. et Cosmochim. Acta 52, 2693-2706.

Knappe, A., Hubberten, H.-W., Pekdeger, A., Dulski, P., Möller, P.: A multi-tracer study on bank filtration processes in Berlin. In: Dillon, P. (Ed.): Management of Aquifer Recharge for Sustainability, Balkema, Adelaide, Australia, 2002, pp 239-244.

Knappe, A., in prep. Das Verhalten der Seltenerd-Elemente -insbesondere Gadolinium als Abwasserindikation- in Oberflächen- und Grundwässern. Ph.D. diss. Department of Earth Science, Free University of Berlin, Berlin.

Kohfahl, C., 2004. The Influence of Water Table Oscillations on Pyrite Weathering and Acidification in Open Pit Lignite Mines, Column Studies and Modelling of Hydrogeochemical and Hydraulic Processes in the LOHSA Storage System, Germany, Dissertation, www.dissertation.de, in press.

Kretschmar, R.,1991. Kulturtechnisch-Bodenkundliches Praktikum, ausgewählte Laboratoriumsmethoden, eine Anleitung zum selbständigen Arbeiten an Böden. Christian-Albrechts-Universität Kiel, 7. Auflage.

Krouse, H.R., 1980. Sulphur isotopes in out environment. In: P.a.F. Fritz, J.CH. (Editor), Handbook of Environmental Isotope Geochemistry. The Terrestrial Environment. A. Elsevier, Amsterdam, pp. 435-471.

Langguth & Voigt, 2004. Hydrogeologische Methoden, Springer Verlag, D-Heidelberg

Lewandowski, J., Leitschuh, S., Koß, V., 1997. Schadstoffe im Boden - Eine Einführung in Analytik und Bewertung. 339 S, Springer

Limberg, A., Thierbach, J., 2002. Hydrostratigraphie von Berlin-Korrelation mit dem Norddeutschen Gliederungsschema. Brandenburgische Geowiss. Beiträge, 9(1/2): 65-68.

Massmann, G., Knappe, A., Pekdeger, A., Richter, D. (2004). Investigating the influence of treated sewage in ground- and surface water using wastewater indicators in Berlin, Germany. Acta Hydrochim. et Hydrobiol. 32 (4-5), 336-350.

Massmann, G. et al., subm. The impact of variable temperatures on the redox conditions and the behaviour of pharmaceutical residues during artificial recharge. J. Hydrol.

Mehra. O. P. and Jackson. M. L.. 1960. Iron oxide removal from soils and clays by a dithionite-citrate system buffered with sodium bicarbonate. Clays Clay Mineral. 5. 317-327

Meyer H., S.L., Wand U., Hubberten H.-W., and Friedrichsen H., 2000. Isotope Studies of Hydrogen and Oxygen in Ground Ice-Experiences with the Equilibration Technique. Isotopes Environ. Health Stud., 36: 133-149.

Nogeitzig, A., 2005. Processes During Infiltration At The Water-Sediment Interface. Diplomarbeit Institut für Geologische Wissenschaften, Freie Universität Berlin (unpublished).

Okubo, T. and Matsumoto, J., 1983. Biological clogging of sand and changes of organic constituents during artificial recharge. Water Res., 17(7): 813-821.

Olivie-Lauquet, G. et al., 2001. Release Of Trace Elements In Wetlands: Role Of Seasonal Variability. Wat. Res., 35(4): 943-952.

Ogata, A., 1970. Theory of dispersion in granular medium. U.S. Geol. Surv. Prof. Paper, 411(I)

Ogata, A. and Banks, R.B., 1961. A solution of the differential equation of longitudinal dispersion in porous media, US Geological Survey.

Pekdeger, A. Sommer.-von Jarmerstedt, C., 1998. Einfluß der Oberflächenwassergüte auf die Trinkwasserversorgung Berlins, Forschungspolitische Dialoge in Berlin - Geowissenschaft und Geotechnik, Berlin, pp. 33-41.

Prommer H. and Stuyfzand,2005. Identification of temperature dependent water quality changes during a deep well injection experiment in a pyritic aquifer. Environ. Sci. And Technol., in press

Rafter, T.A., 1967. Oxygen isotopic composition of sulfates. Part 1: a method for the extraction of oxygen and its quantitative conversion to carbondioxide for isotopic ratio measurements. New Zealand J. Sci. 10, 493–510.

Reddersen, K., Heberer, T. and Dünnbier, U., 2002. Identification and significance of phenazone drugs and their metabolites in ground- and drinking water. Chemosphere, 49: 539-544.

Richter, D. 2003. Untersuchung des Gewässersystems von Spree und Havel im Berliner Westen mit Hilfe verschiedener Tracer. Diplomarbeit Freie Universität Berlin.

Richters L., Eckert P., Teermann I., Irmscher R.,2004. Untersuchung zur Entwicklung des pH-Wertes bei der Uferpassage in einem Wasserwerk am Rhein. Wasser Abwasser 145(9), 640-645.

Rümmler, 2003. 2-dimensionale-horizontal-ebene Simulation der grundwasserströmungsverhältnisse unter Uferfiltratbedingungen. Diplomarbeit Humboldt-Universität zu Berlin.

Schuh, W.M., 1990. Seasonal variation of clogging of an artificial recharge basin in a northern climate. J. Hydol., 121: 193-215.

Schumacher, Skripalle, 1999. Arge Uferfiltration Detailbericht 1: Ermittlung der Uferfiltratanteile über die Abflussverhältnisse sowie die Durchflussaufteilung und Abwasseranteile im Berliner Gewässersystem bei Niedrigwasser für verschiedene Ableitungsvarianten der Klärwerke.- Abschlußbericht Uferfiltration Berlin: S 31

Senstadt, 2003. Öffentlichkeitsarbeit, Wasserwirtschaftliche Monatsberichte.

Sievers, J. 2001. Geochemische, hydrochemische und hydraulische Untersuchungen an Sedimentkernen aus dem Tegeler See.Diplomarbeit Freie Universität Berlin

Sommer-von Jarmersted, C., Kösters, E. & Pekdeger, A., 1998. Die Sulfat- und Chloridgehalte des Berliner Grundwassers.- Terra nostra 98/3: V341 - V342, Alfred- Wegener-Stiftung, Köln

Stute, M., Deák, J., Révész, K., Böhlke, J. K., Deseö, É., Weppernig, R. & Schlosser, P., 1997. Tritium /3He Dating of River Infiltration: An Example from the Danube in the Szigetköz Area, Hungary. Ground Water 35(5), 905-911.

Sültenfuß, J. and Massmann, G., 2004. Datierung mit der 3He-Tritium Methode am Beispiel der Uferfiltration im Oderbruch. Grundwasser, 9(4): 221-234.

Tolstikhin, I. N. & Kamenskiy, I. L., 1969. Determination of groundwater ages by the T-3He method. Geochemistry International 6, 810-811.

van Cappellen, P. and Wang, Y., 1996. Cycling of iron and manganese in surface sediments: A general theory for the coupled transport and reaction of carbon, oxygen, nitrogen, sulfur, iron, and manganese. American Journal of Science, 296: 197-243

Yanagisawa, F., Sakai, H., 1983. Preparation of SO_2 for sulphur isotope ratio measurements by the thermal decomposition of $BaSO_4$–V_2O_5–SiO_2 mixtures. Anal. Chem. 55, 985–987.

1.9 Publications

Fritz, B., G. Massmann, A. Knappe, A. Pekdeger (2003).“ Process studies in a bank filtration system in Berlin using environmental tracers”, Hydroplus

Fritz, B., Massmann, G., Grünheid, S., Heberer, T., Pekdeger, A., Jekel M. (2004)." Cleaning capacity of bank filtration and artificial recharge with influence of treated waste water", Chemrawn XV, Paris, June 2004

Fritz, B., H. Dizer, J. Greskowiak, S. Grünheid, G. Grützmacher, Th. Heberer, E. Holzbecher, G. Massmann (2007)." Naturnahe Grundwassergewinnung - Ergebnisse eines umfangreichen, interdisziplinären Forschungsvorhabens zur künstlichen Grundwasseranreicherung und Uferfiltration", wwt

Knappe, A., Massmann, G., Dulski, P., Pekdeger, A. (2006). Exploring surface- and groundwater interactions with the help of environmental tracers and wastewater indicators in Berlin/Germany. In: Unesco (2006), Recharge systems for protecting and enhancing groundwater resources. Proceedings of the 5th International Symposium on Management of Aquifer Recharge ISMAR5, Berlin, Germany, 11–16 June 2005. IHP-VI, Series on Groundwater No. 13: 297-303.

Massmann , G., Knappe , A., Richter, D. and Pekdeger, A., (2004). Investigating the influence of treated sewage in ground- and surface water using wastewater indicators in Berlin, Germany. Acta hydrochimica et hydrobiologica, 32(4-5): 336-350.

Massmann, G., Dünnbier, U., Greskowiak, J., Knappe, A. and Pekdeger, A. (2004). Investigating surface water - groundwater interactions with the help of sewage indicators in Berlin, Germany; Groundwater Quality 2004, Waterloo, Canada.

Massmann, G., Dünnbier, U., Heberer, T., Taute, T. (2008). Behaviour and redox sensitivity of pharmaceutical residues during bank filtration - Investigation of phenazone-type residues; Chemosphere **71**: 1476 – 1485.

Massmann, G., Greskowiak, J., Dünnbier, U., Knappe, A., Pekdeger, P. (2006). The impact of variable temperatures on the redox conditions and the behaviour of pharmaceutical residues during artificial recharge; J. of Hydrol. 328 (1-2): 141-156.

Massmann, G., Greskowiak, J., Dünnbier, U., Zuehlke, S., Pekdeger, A. (2006). In: Unesco (2006), In: The impact of alternating redox conditions on groundwater chemistry during artificial recharge in Berlin; Unesco (2006), Recharge systems for protecting and enhancing groundwater resources. Proceedings of the 5th International Symposium on Management of Aquifer Recharge ISMAR5, Berlin, Germany, 11–16 June 2005. IHP-VI, Series on Groundwater No. 13: 535-540.

Massmann, G., Greskowiak, J., Kohfahl, C., Knappe, A., Ohm, B., Pekdeger, A., Sültenfuß, J., Taute, T. (2006). Evaluation of the hydrochemical conditions during bank filtration and artificial recharge in Berlin; In: Unesco (2006), Recharge systems for protecting and enhancing groundwater resources. Proceedings of the 5th International Symposium on Management of Aquifer Recharge ISMAR5, Berlin, Germany, 11–16 June 2005. IHP-VI, Series on Groundwater No. 13: 61-66.

Massmann, G., Heberer, T., Grützmacher, G., Dünnbier, U., Knappe, A., Meyer, H., Mechlinski, A., Pekdeger, A. (2007). Trinkwassergewinnung in urbanen Räumen – Erkenntnisse zur Uferfiltration in Berlin; Grundwasser 12: 232-245.

Massmann, G., Knappe, A., Richter, D., Sültenfuß, J., Pekdeger, A. (2003). Application of different tracers to evaluate the flow regime at riverbank-filtration sites in Berlin, Germany. In: Melin, G. (Editor). Riverbank Filtration - The Future is Now. Conference Proceedings, Cincinnati Ohio, USA, National Water Institute: 49-56.

Massmann, G., Nogeitzig, A., Taute, T., Pekdeger, A. (in press). Seasonal and spatial distribution of redox zones during lake bank filtration in Berlin, Germany; Environm. Geol.,, DOI 10.1007/s00254-007-0792-9

Massmann, G., Sültenfuß, J., Dünnbier, U., Knappe, A., Taute, T., Pekdeger, A. (2007). Investigation of groundwater residence times during bank filtration in Berlin – a multi-tracer approach; Hydrol. Proc., in press, DOI 10.1002/hyp.6649

Massmann, G., Sültenfuß;, J., Knappe, A., Pekdeger, A. (2003). Using the Tritium/Helium Age Dating Method to characterise two river recharged aquifer systems in Germany. I-UGG Conference 2003, Sapporo, Japan.

Appendix

Table 9: Age dating results from all sites, analysed at the Institute for Environmental Physics, University of Bremen.

Well ID	Site	T [TU]	$^3He_{tri}$ [TU]	"stable" T [TU]	T/He age [years]
BR20	GWA Tegel	10.69	1.52	12.21	2.39
BR20	GWA Tegel	10.69	1.40	12.09	2.21
TEG342	GWA Tegel	12.12	43.45	55.58	27.30
TEG342	GWA Tegel	12.12	44.10	56.22	27.51
TEG3690P	GWA Tegel	10.54	-0.03	10.51	-0.05
TEG369UP	GWA Tegel	10.91	-0.04	10.87	-0.06
TEG369UP	GWA Tegel	10.91	0.10	11.01	0.17
TEG3700P	GWA Tegel	11.09	0.85	11.94	1.32
TEG3700P	GWA Tegel	11.09	1.25	12.34	1.91
TEG370UP	GWA Tegel	10.00	2.69	12.69	4.28
TEG368	GWA Tegel	8.47	0.16	8.63	0.34
TEG368	GWA Tegel	8.47	0.22	8.69	0.46
TEG373	GWA Tegel	9.29	7.90	17.19	10.93
TEG373	GWA Tegel	9.29	6.65	15.94	9.60
BR13	TS Tegel	12.12	12.49	24.61	12.71
BR13	TS Tegel	12.12	12.52	24.64	12.73
3301	TS Tegel	11.17	1.04	12.21	1.59
3301	TS Tegel	11.17	1.20	12.37	1.83
3303	TS Tegel	10.95	-0.17	10.78	-0.28
3304	TS Tegel	12.64	12.07	24.70	12.02
3304	TS Tegel	12.64	11.81	24.44	11.83
TEG3710P	TS Tegel	10.05	-0.13	9.93	-0.23
TEG3710P	TS Tegel	10.05	0.32	10.37	0.56
TEG374	TS Tegel	10.60	32.51	43.11	24.94
TEG374	TS Tegel	10.60	32.31	42.91	24.85
OFWBEE	TS Wannsee	10.64			0.00
3332	TS Wannsee 1	0.02	0.00	0.02	100.00
3334	TS Wannsee 1	0.03	1.08	1.11	65.53
3335	TS Wannsee 1	11.12	0.00	11.05	0.00
3336	TS Wannsee 1	0.02	4.48	4.49	99.40
3337	TS Wannsee 1	10.75	0.00	10.78	0.00
3338	TS Wannsee 1	10.94			
3339	TS Wannsee 1	11.15	0.00	11.15	0.00
BR4	TS Wannsee 1	2.41	8.01	10.42	26.23
BR4	TS Wannsee 1	2.41	6.65	9.07	23.73
3332	TS Wannsee 1	0.02	0.26	0.28	47.73
BEE202UP	TS Wannsee 2	9.39	8.27	17.66	11.33
BEE202UP	TS Wannsee 2	9.48	8.27	17.75	11.25
BEE202UP	TS Wannsee 2	9.39	7.16	16.55	10.16
BEE202UP	TS Wannsee 2	9.48	7.15	16.64	10.08
BEE203	TS Wannsee 2	9.24	-0.79	8.45	0.00
BEE203	TS Wannsee 2	8.78	-0.78	8.00	0.00
BEE204UP	TS Wannsee 2	13.97	15.76	29.73	13.54
BEE204UP	TS Wannsee 2	13.97	17.36	31.34	14.48
BEE202OP	TS Wannsee 2	8.99	-1.75	7.24	0.00
BEE202OP	TS Wannsee 2	8.80	-1.75	7.06	0.00
BEE202OP	TS Wannsee 2	8.99	-1.98	7.01	0.00
BEE202OP	TS Wannsee 2	8.80	-1.97	6.83	0.00
BEE202MP1	TS Wannsee 2	9.16	2.02	11.18	3.58
BEE202MP1	TS Wannsee 2	9.16	1.34	10.50	2.45
BEE202MP2	TS Wannsee 2	9.18	6.20	15.38	9.25
BEE202MP2	TS Wannsee 2	9.10	6.20	15.30	9.32
BR3	TS Wannsee 2	7.63	9.03	16.66	14.00
BR3	TS Wannsee 2	7.63	8.29	15.93	13.19

Table 10: Data of $\delta^{34}S$ (‰ vs. CDT) and $\delta^{18}O$ (‰ vs. V-SMOW) of sulfate at all sites, analysed at the Institute of Mineralogy of the Technical University Bergakademie Freiberg.

Well ID	Origin	Date	$\delta^{18}O_{V\text{-}SMOW}$ ‰	$\delta^{34}S_{CDT\ DELTA\ PLUS}$ ‰
TEG 365	GWA Tegel	July 2004	8.0	4.9
TEG 366	GWA Tegel	July 2004	8.9	4.9
OFWGWA	pond 3 water	July 2004	8.0	4.8
OFWTEG	surface water Lake Tegel	21.07.04	7.8	5.0
OFW-WS-11	surface water Lake Wannsee	17.03.04	6.6	4.2
OFW-WS 6	surface water Lake Wannsee	17.03.04	8.0	4.1
OFWBEE	surface water Lake Wannsee	15.03.04	7.4	4.1
3304	TS Tegel	20.07.04	7.6	4.1
TEG371OP	TS Tegel	20.07.04	8.6	5.4
3301	TS Tegel	20.07.04	8.9	3.5
3302	TS Tegel	20.07.04	8.5	5.8
3303	TS Tegel	21.07.04	7.8	3.8
TEG374	TS Tegel	21.07.04	12.5	8.4
BR13	TS Tegel	20.07.04	8.8	4.7
3337	TS Wannsee	16.03.04	7.5	3.9
3336	TS Wannsee 1	16.03.04	17.3	49.5
3334	TS Wannsee 1	16.03.04	not enough sulfate	not enough sulfate
3332	TS Wannsee 1	18.03.04	not enough sulfate	not enough sulfate
BR4	TS Wannsee 1	16.03.04	15.0	18.0
BEE200UP	TS Wannsee 2	16.03.04	0.9	-5.3
BEE204UP	TS Wannsee 2	16.03.04	3.5	-2.7
BEE204OP	TS Wannsee 2	16.03.04	0.8	-6.1
BEE201UP	TS Wannsee 2	16.03.04	9.5	7.4
BEE202UP	TS Wannsee 2	18.03.04	9.5	7.3
BEE202OP	TS Wannsee 2	18.03.04	7.3	4.3
BEE205	TS Wannsee 2	21.07.04	8.3	7.5
BEE206	TS Wannsee 2	21.07.04	11.7	12.6
BR3	TS Wannsee 2	18.03.04	7.3	3.3